



University  
of Glasgow

<https://theses.gla.ac.uk/>

Theses Digitisation:

<https://www.gla.ac.uk/myglasgow/research/enlighten/theses/digitisation/>

This is a digitised version of the original print thesis.

Copyright and moral rights for this work are retained by the author

A copy can be downloaded for personal non-commercial research or study,  
without prior permission or charge

This work cannot be reproduced or quoted extensively from without first  
obtaining permission in writing from the author

The content must not be changed in any way or sold commercially in any  
format or medium without the formal permission of the author

When referring to this work, full bibliographic details including the author,  
title, awarding institution and date of the thesis must be given

Enlighten: Theses

<https://theses.gla.ac.uk/>  
[research-enlighten@glasgow.ac.uk](mailto:research-enlighten@glasgow.ac.uk)

THE STRUCTURE AND FUNCTION OF THE LIGHT-HARVESTING ANTENNA  
COMPLEXES FROM PURPLE PHOTOSYNTHETIC BACTERIA

by

MARK B EVANS

A thesis submitted for the degree of Doctor of Philosophy

University of Glasgow  
Department of Botany  
February 1989

© Mark B Evans

ProQuest Number: 10999241

All rights reserved

INFORMATION TO ALL USERS

The quality of this reproduction is dependent upon the quality of the copy submitted.

In the unlikely event that the author did not send a complete manuscript and there are missing pages, these will be noted. Also, if material had to be removed, a note will indicate the deletion.



ProQuest 10999241

Published by ProQuest LLC (2018). Copyright of the Dissertation is held by the Author.

All rights reserved.

This work is protected against unauthorized copying under Title 17, United States Code  
Microform Edition © ProQuest LLC.

ProQuest LLC.  
789 East Eisenhower Parkway  
P.O. Box 1346  
Ann Arbor, MI 48106 – 1346

### **DECLARATION**

This thesis is an original composition which describes work performed entirely by myself unless otherwise cited or acknowledged. Its contents have not previously been submitted for any other degree. The research for this thesis was performed between October 1985 and October 1988.

signed.

Mark B Evans

Date: February 10 1989

TO MUM AND DAD

## SUMMARY

The structure and function of the B800-850 light-harvesting antenna complexes from *Rps. palustris*, strain French, have been extensively characterised. The B800-850 complexes isolated from high light (HL) grown cells have a normal Type I antenna spectrum. The complexes isolated from low light (LL) grown cells, however, have an 850nm absorption band of much lower intensity than the 800nm absorption band. This implies that there are significant structural differences between the two complexes. A comparative study was therefore undertaken to investigate the relationship between the structure and the near-infrared spectra. This was combined with a functional study to compare the energy transfer efficiencies of the two complexes.

The ratio of BChl to carotenoid was determined to be 2:1 for the HL B800-850 complexes and 3:1 for the LL complexes. Linear dichroism measurements detected the presence of an additional BChl chromophore with a different Q<sub>x</sub> dipole orientation to the other BChls in the complexes. Picosecond energy transfer kinetics measurements on the LL complexes imply the presence of an extra BChl chromophore which absorbs at about 800nm and which acts as an intermediate in the transfer of energy from B800 to B850. The extra BChl does not improve the efficiency of energy transfer from carotenoid to BChl and it is suggested that it acts solely as an additional light-harvesting pigment. The efficiency of energy transfer from carotenoid-to-BChl was measured to be 36% for both the HL and LL complexes. The efficiency is therefore not affected by the structural differences between the complexes.

Nine antenna polypeptides have been isolated from both the high light and low light grown cells. Two of these are the B875 complex  $\alpha/\beta$ -

polypeptide pair. The N-terminal sequences of these polypeptides have been determined. The sequences of the remaining seven antenna polypeptides, which are almost completed, are also presented. Four of these are B800-850- $\alpha$  polypeptides and three are B800-850- $\beta$  polypeptides. This is the first report of an antenna complex from a purple bacterium containing more than three different polypeptides. Hydropathy analysis suggests that the polypeptides all contain a central membrane-spanning region. Three of the  $\alpha$ -polypeptides are 52-54 amino acids long, the fourth is about 10 residues longer. This polypeptide contains an alanine-rich, C-terminal tail which possibly turns and inserts back into the membrane as a short stretch of  $\alpha$ -helix. Two of the  $\beta$ -polypeptides are also 52-54 amino acids long. The third is 5-6 amino acids shorter at the N-terminus. The  $\alpha$ - and  $\beta$ -polypeptides contain conserved histidine residues, at positions 31 and 40 respectively, which are believed to ligand the B850 chromophore BChl dimers. Interaction between the BChl molecules and conserved aromatic amino acids may partly determine the position of the near-infrared absorption maxima of the antenna complexes. Both the  $\alpha$ - and  $\beta$ -polypeptides contain amino acids which are capable of liganding the additional BChl chromophore in the LL complexes. Liquid chromatography has demonstrated a difference in the stoichiometry of the HL and LL B800-850 complex polypeptides. It remains uncertain, however, whether the complexes contain different combinations of polypeptides or whether they contain the same polypeptides but in a different stoichiometry.

Crystals of the LL B800-850 complexes from *Rps. palustris* have been grown using the vapour diffusion method, with ammonium sulphate as the precipitant, and the small amphiphile benzamidine hydrochloride. The crystals represent the first stage in the determination of the three-dimensional structure of the complexes by x-ray diffraction analysis. A systematic study of the ratios of BChl to carotenoid in a range of

antenna complexes is also reported. The ratio of 1:1 for the B875 complexes from *Rb. sphaeroides* agrees with the published value. However, the ratios for the B800-850 Type I complexes from *Rb. sphaeroides*, *Rps. palustris*, *Chr. vinosum* and *Rps. acidophila* were all determined to be 2:1 which contradicts the generally accepted value of 3:1 for this complex type. The ratio for the B800-850 Type II complexes from *Chr. vinosum* was also determined to be 2:1 in contrast to the published value of 3:1. The ratio for the B800-820 complexes of *Rps. acidophila*, strain 7750, was measured, for the first time, to be 2:1. This contradicts the belief that all B800-820 complexes have BChl-to-carotenoid ratios of 3:1. The ratios for the B800-850 Type II and B800-820 complexes from *Rps. acidophila*, strain 7050, were determined to be 2.7:1 and 3.5:1 respectively. But because of a possible inaccuracy in the absorption coefficient of cis-rhodopinal, it is proposed that the true ratios for these complexes are 2:1 and 3:1.

Steady state fluorescence measurements were used to determine the quantum efficiency of energy transfer from the carotenoid to the long-wavelength absorbing BChl chromophore in several antenna complexes. An efficiency of 70% was measured for the B800-820 complexes from *Rps. acidophila*, strain 7750, which agrees with the 70-75% value previously measured for the equivalent complexes from strain 7050. As the carotenoid compositions of the two complexes are very different it suggests that energy transfer efficiency is not strongly dependent on the carotenoid type. The efficiencies measured for the B800-850 Types I and II complexes from *Chr. vinosum* were 20 and 29% respectively. This substantiates a previous suggestion that Type II complexes are synthesised under low light conditions because they are inherently more efficient at light-harvesting than the Type I complexes.

The energy transfer efficiencies were measured at each of the carotenoid vibrational bands. In all of the complexes tested, the efficiency was highest for the longest-wavelength absorbing band and lowest for the shortest-wavelength absorbing band. This can be explained by stronger coupling between the longest-wavelength absorbing carotenoid and the ground state of the BChl acceptor, possibly mediated through the optically forbidden  $1A_g$  energy state. This assumes a Dexter electron-exchange mechanism of energy transfer.

## ACKNOWLEDGEMENTS

I would like to acknowledge the many people who have offered me help, guidance and friendship during the last three years. Firstly I would like to sincerely thank my supervisor, Prof Richard Cogdell, for both guiding me through a varied and interesting PhD and for helping to finance conferences and laboratory visits abroad.

I am very grateful to Dr René Brunisholz and Prof Herbert Zuber of the ETH University, Zürich, for giving me the opportunity to work in their laboratory during the spring of 1987. I would especially like to thank Franz Suter for his expert assistance with the protein sequencing, Miriam Wirth for operating the amino acid analyser and Eva Niederer for looking after me and for sharing her fine wine cellar. I would also like to extend my thanks to everyone at the ETH for their friendship and for taking the time to show me something of Swiss life.

I would like to acknowledge the role of the Zürich group in the work presented in chapter six. The initial characterisation of the antenna polypeptides, sequencing of the B800-850- $\alpha_4$  polypeptide, and partial sequencing of two  $\beta$ -polypeptides were performed by myself under the guidance of Dr Brunisholz. The remaining antenna polypeptide sequences must be entirely credited to the hard work and expertise of Dr Brunisholz and his laboratory.

I would like to give a special thanks to Dr George Britton and the Liverpool Lads for their patience, insanity and friendship during both my undergraduate and postgraduate training. Thank you for always keeping the door ajar and a warm welcome inside.

I would like to give a big thank you to Dani Graf, of the Zürich-ETH, for being my mentor during the final stages of my experimental

work, and for his help, particularly with the polyacrylamide gels and replicate quantitative measurements. I wish a successful future to a promising scientist.

I would also like to acknowledge Frank van Mourik, of The Free University, Amsterdam, for performing the linear dichroism measurements, and Dr Villy Sundström, of the University of Umeå, Sweden, for performing the picosecond energy transfer measurements on *Rps. palustris*. I am also very grateful to Tony Ritchie for his expertise and perserverence with the mass spectroscopy, Eoin Robertson for the electron microscopy and general enlightenment, and Norman Tate for his careful photography, and advice on presentation. I would also like to thank Dr Gordon Lindsay for the occasional use of his laboratory, Dr Joel Milner for ensuring the smooth operation of the computer facilities, and Dr Peter Dominy for his help and advice on many occasions.

I would like to acknowledge the SERC for funding my PhD and my attendance at the 8th International Symposium on Carotenoids, Boston, USA, and the British Photobiology Society for funding my attendance at the VI International Congress on Phototrophic Prokaryotes, Noordwijkerhout, The Netherlands.

Finally I would like to thank Jane for her constant encouragement and support, and for always being my best friend.

## TABLE OF CONTENTS

PAGE

### SUMMARY

### ACKNOWLEDGEMENTS

### TABLE OF CONTENTS

<b><u>CHAPTER ONE: Introduction</u></b>	1
1.1 Taxonomic and phylogenetic classifications of purple photosynthetic bacteria	2
1.2 Ecology and metabolic requirements of purple photosynthetic bacteria	5
1.3 Overview of photosynthesis in purple bacteria	7
(i) Introduction	7
(ii) Energy trapping by the photochemical reaction centre	9
(iii) Energy flow and the synthesis of ATP and NADH	12
1.4 Light absorption by photosynthetic pigments	14
1.5 The biosynthesis of photosynthetic pigments	16
1.6 The role of carotenoids in photoprotection	18
1.7 The light-harvesting antenna complexes of purple photosynthetic bacteria	20
(i) Introduction	20
(ii) The molecular structure of antenna complexes	22
(iii) Bathochromicity of the <i>in vivo</i> BChl Qy absorption bands	25
(iv) Antenna polypeptide sequence homology	29
(v) Pigment stoichiometry	30
(vi) Pigment orientation	30
(vii) The arrangement of antenna polypeptide aggregates	32
1.8 The mechanisms of energy transfer within antenna complexes	33
(i) Introduction	33
(ii) Fluorescence measurements in antenna complexes	34
(iii) Energy transfer between carotenoid and BChl	35
(a) Förster mechanism	
(b) Dexter electron-exchange mechanism	
<b><u>CHAPTER TWO: Materials and methods</u></b>	41
2.1 Culture storage	42
2.2 Cell culture	42
2.3 Cell counting and measurement of growth	43

	PAGE
2.4	Isolation of photosynthetic membranes 43
2.5	Solubilisation of photosynthetic membranes and isolation of crude antenna preparations 44
2.6	Separation of B890, B800-850 and B800-820 antenna complexes 45
(i)	Sucrose density-gradient centrifugation 45
(ii)	DEAE anion-exchange chromatography 46
(iii)	Ammonium sulphate precipitation 46
2.7	Pigment isolation, separation, purification and identification 47
(i)	General precautions 47
(ii)	Extraction of photosynthetic pigments 48
(iii)	Preparation of a total pigment extract 49
(iv)	Alumina column chromatography of pigment extracts 50
(v)	Thin-layer chromatography of pigments 51
(vi)	Isolation and separation of carotenoid glucosides 52
(vii)	Identification of carotenoids 52
2.8	Determination of the BChl-to-carotenoid ratios of light-harvesting antenna complexes 53
(i)	HPLC method 53
(ii)	Carotenoid partition method 55
(iii)	Difference spectroscopy method 56
(iv)	Simultaneous equation method 56
	(a) <i>determination of the carotenoid composition of an antenna complex</i>
	(b) <i>determination of an average absorption coefficient for the total carotenoid of an antenna complex</i>
	(c) <i>determination of the BChl absorption coefficient in acetone/methanol at the wavelength maximum of the total carotenoid</i>
	(d) <i>calculation of the BChl-to-carotenoid ratio</i>
	(e) <i>estimation of the absorption coefficient of cis-rhodopinal</i>
2.9	Isolation, purification and sequencing of antenna polypeptides 60
(i)	Isolation of antenna protein 60
(ii)	Separation of $\alpha$ - and $\beta$ -polypeptides 61
(iii)	FPLC analysis of antenna polypeptides 62
(iv)	Polypeptide amino acid analysis 62
(v)	N-terminal amino acid sequence determination 63
	(a) <i>automated sequential Edman degradation</i>
	(b) <i>conversion to PTH-amino acids</i>
	(c) <i>identification of PTH-amino acids</i>
2.10	Determination of the singlet-singlet, carotenoid-to-BChl energy transfer efficiencies of antenna complexes 65

	PAGE
2.11	Crystallisation of B800-850 antenna complexes from low light grown <i>Rps. palustris</i> 68
(i)	Sample preparation 68
(ii)	crystallisation 68
	(a) crystallisation with ammonium sulphate
	(b) crystallisation with polyethylene glycol
2.12	SDS polyacrylamide gel electrophoresis 70
(i)	Gel assembly 70
(ii)	Sample assembly 71
2.13	Tannin protein assay 72
2.14	Statistical analysis of data 72
(i)	Introduction 72
(ii)	t-test for comparison of sample means 74
(iii)	Analysis of variance 76
(iv)	Linear regression analysis 77
<b><u>CHAPTER THREE: The effect of growth conditions on cell culture and the synthesis of variable light-harvesting antenna complexes</u></b>	79
3.1	Introduction 80
3.2	Growth of <i>Rhodopseudomonas palustris</i> , strain French, under high and low light intensities, and a spectral characterisation of the cells and antenna complexes 80
3.3	A spectral characterisation of 30°C and 40°C grown <i>Chromatium vinosum</i> , strain D, and their antenna complexes 82
3.4	Temperature dependence of the near-infrared spectra of <i>Chr. vinosum</i> , strain D, cells and antenna complexes 83
3.5	A spectral characterisation of cells and antenna complexes from <i>Rhodopseudomonas acidophila</i> , strains 7050 and 7750, and the effect of light intensity and temperature 85
<b><u>CHAPTER FOUR: Determination of the BChl-to-carotenoid ratios of the B890 antenna complexes from <i>Rhodospirillum rubrum</i> and the B800-850 complexes from <i>Rhodobacter sphaeroides</i></u></b>	88
4.1	Introduction 89
4.2	HPLC method 90
4.3	Carotenoid separation method 95
4.4	Difference spectroscopy method 95
4.5	Summary 95

	PAGE
<b><u>CHAPTER FIVE: Determination of the BChl-to-carotenoid ratios of antenna complexes from <i>Rhodobacter sphaeroides</i>, <i>Rhodopseudomonas palustris</i>, <i>Chromatium vinosum</i> and <i>Rps. acidophila</i>, and a possible correlation with the results of linear dichroism and picosecond energy transfer measurements on <i>Rps. palustris</i></u></b>	96
5.1 Introduction	97
5.2 BChl-to-carotenoid ratios of the B800-850 and B875 complexes from <i>Rb. sphaeroides</i>	97
5.3 BChl-to-carotenoid ratios of the B800-850 complexes from high and low light grown <i>Rps. palustris</i> , strain French	98
(i) Carotenoid identification	98
(ii) Carotenoid composition	100
(iii) BChl-to-carotenoid ratio determinations	100
5.4 BChl-to-carotenoid ratios of the B800-850 complexes from 30°C and 40°C grown <i>Chr. vinosum</i> , strain D	102
5.5 BChl-to-carotenoid ratios of B800-850 and B800-820 complexes from <i>Rps. acidophila</i> , strains 7050 and 7750	103
(i) Introduction	103
(ii) Identification of the carotenoids from the B800-850 Type II, and B800-820 complexes from <i>Rps. acidophila</i> , strain 7050	106
(iii) Carotenoid compositions and BChl-to-carotenoid ratios of B800-850 Type II and B800-820 complexes from <i>Rps. acidophila</i> , strain 7050	108
5.6 Summary discussion of BChl-to-carotenoid ratio determinations and results of linear dichroism and picosecond energy transfer measurements on the B800-850 complexes from <i>Rps. palustris</i>	112
<b><u>CHAPTER SIX: Isolation and primary sequencing of the light-harvesting polypeptides from low and high light grown <i>Rps. palustris</i>, strain French</u></b>	118
6.1 Introduction	119
6.2 SDS polyacrylamide gel electrophoresis	120
6.3 Isolation of antenna protein	121
6.4 Separation of antenna protein into $\alpha$ - and $\beta$ -polypeptides	122
6.5 Liquid chromatography of antenna polypeptides	123
6.6 Amino acid analysis of antenna polypeptides	125

	PAGE
6.7	N-terminal amino acid sequence analysis 127
(i)	Introduction 127
(ii)	B875 antenna polypeptides 128
(iii)	B800-850- $\alpha$ polypeptides 129
(iv)	B800-850- $\beta$ polypeptides 134
6.8	Locating the position of the photosynthetic membrane 137
6.9	Stoichiometry of the polypeptides in the B800-850 complexes from high light and low light grown cells 140
6.10	Summary 142
<b><u>CHAPTER SEVEN: Determination of the singlet-singlet, carotenoid-to-BChl energy transfer efficiencies of antenna complexes from <i>Rhodopseudomonas palustris</i>, <i>Chromatium vinosum</i> and <i>Rps. acidophila</i></u></b>	144
7.1	Introduction 145
7.2	Results and discussion 147
7.3	Summary 155
<b><u>CHAPTER EIGHT: Crystallisation of the B800-850 complexes from low light grown <i>Rhodopseudomonas palustris</i>, strain French</u></b>	158
<b><u>CHAPTER NINE: Summary discussion</u></b>	166
<b><u>APPENDIXES</u></b>	178
A:	Semi-systematic names of carotenoids
B:	Chemical structures of carotenoids
C:	Absorption spectra of spirilloxanthin series carotenoids recorded in light petroleum 40-60 °C bp.
D:	Mass spectra of spirilloxanthin series carotenoids
E:	Compositions of growth media
F:	Compositions of solutions for polyacrylamide gel electrophoresis
G:	Compositions of buffers and other solutions
<b><u>REFERENCES</u></b>	

## CHAPTER ONE: INTRODUCTION

## 1.1 Taxonomic and Phylogenetic Classifications of Purple Photosynthetic Bacteria

Living organisms are classified to provide an unambiguous system of nomenclature (taxonomy) for clarity in communication, and to indicate how closely related different organisms are. The current system of taxonomic classification is founded on morphological similarity. But with the advent of gene sequencing it became evident that there is considerable discord between the taxonomic and phylogenetic relationships of bacteria [Pfennig, 1977; Floodgate, 1962].

The living world was originally divided into Plant and Animal Kingdoms. With the development of the light microscope, a myriad of micro-organisms were discovered which did not naturally fall into either of these [Stanier et al., 1976]. In 1866, Haeckel proposed the inclusion of a third kingdom to incorporate the micro-organisms; the Kingdom Protistae [Woese, 1987]. Later the protists were further classified, according to their internal cellular morphology, into eukaryotes and prokaryotes [Stanier et al., 1976; Ragan and Chapman, 1978]. The prokaryotes were divided into three groups on the basis of their cell wall structure. These were the mycoplasmas, the gram positive bacteria and the gram negative bacteria. The photosynthetic prokaryotes are all members of the latter group.

The prokaryotes now constitute a separate kingdom and the gram stain test is no longer used as a basis for taxonomic classification. With the exception of the cyanobacteria, prokaryotes contain no internal membrane-bordered organelles. According to "Bergey's Manual of Determinative Bacteriology" [Buchanan and Gibbons, 1974], the Kingdom Prokaryotae is taxonomically classified into: Division I the cyanobacteria, and Division II the bacteria. The bacteria are further

divided into nineteen "parts", of which Part I comprises the phototrophic bacteria. These belong to the order Rhodospirillales. Rhodospirillales has two sub-orders: the Rhodospirillineae (purple photosynthetic bacteria) and the Chlorobiineae (green photosynthetic bacteria) [Truper and Pfennig, 1978]. In 1984, the taxonomic classification of the purple phototrophic bacteria was revised after considering recent advances in our knowledge of their macromolecular structure [Imhoff et al., 1984; Imhoff, 1984; Imhoff, 1988]. The current classification of phototrophic bacteria is summarised in Fig. 1.1.

There are three families of purple phototrophic bacteria. The Chromatiaceae and Ectothiorhodospiraceae between them contain thirty species of purple sulphur bacteria. Before 1984, the *Ectothiorhodospira* species were included in the family Chromatiaceae but they have now been given their own family on the basis of their unique requirement for saline and alkaline growth conditions and various phylogenetic considerations (see below). There are twenty-five species of purple nonsulphur bacteria (Rhodospirillales) which are divided into six genera. The genus *Rhodocyclus* was created in 1984 during the re-classification. The taxonomic classification of the purple photosynthetic bacteria is now more consistent with their proposed phylogenetic classification.

Phylogenetic classifications are compiled by comparing the sequences of macromolecules which play equivalent roles in different organisms (i.e. protein amino acid sequences, and DNA and RNA nucleotide sequences) [Woese, 1980; Woese, 1987]. The nucleotide sequences of 16S ribosomal ribonucleic acids (rRNAs) have been determined for over five hundred species. Their sequence homology is reasoned to be a measure of their true phylogenetic relationships and is very similar to the sequence homologies of other important macromolecules such as cytochromes

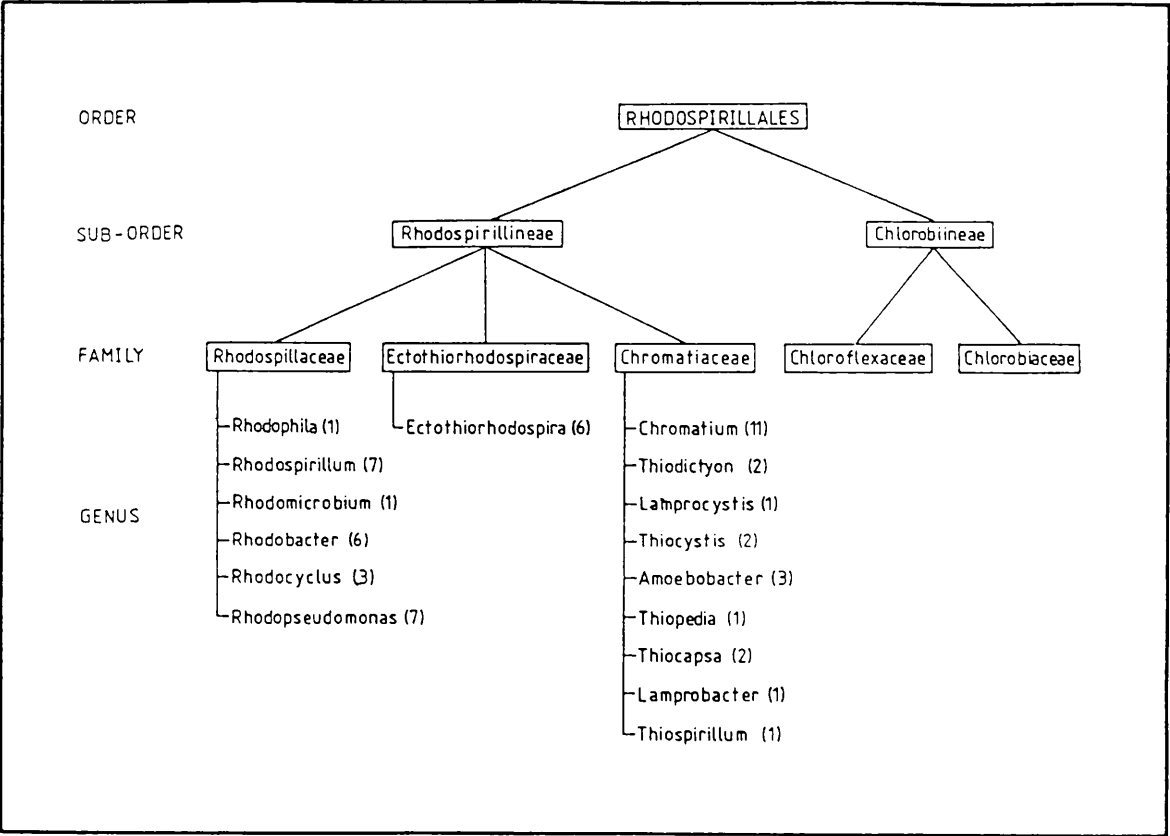


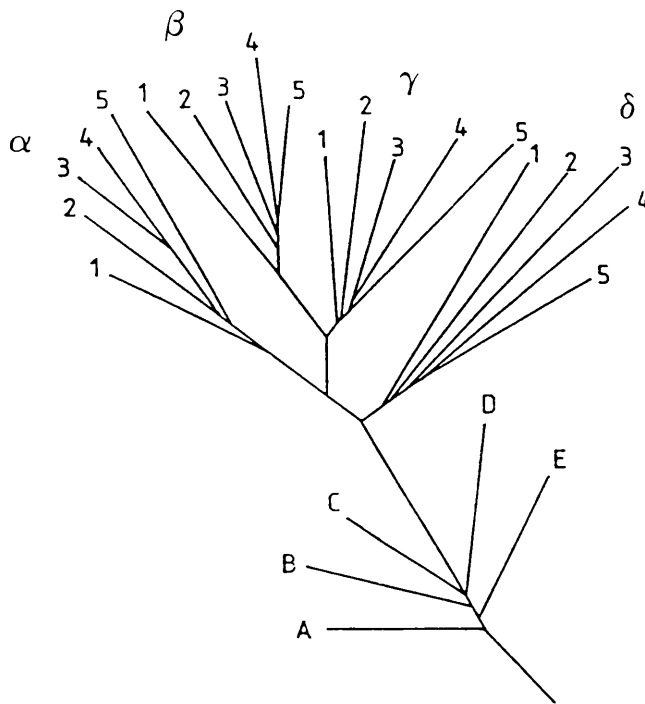
Fig. 1.1 Current classification of the phototrophic bacteria (genera of the green bacteria excluded). The number of species within each genus are given in brackets.

c. Sequence comparison of rRNAs infers that photosynthetic bacteria are not genealogically distinct from the nonphotosynthetic bacteria which is implied by determinative taxonomy. To illustrate this a phylogenetic tree which includes the purple bacteria is depicted in Fig. 1.2. The purple bacteria are divided into four subdivisions:  $\alpha$ ,  $\beta$ ,  $\gamma$  and  $\delta$ . The subdivisions  $\alpha$ ,  $\beta$  and  $\gamma$  contain both photosynthetic and nonphotosynthetic organisms. The nonphotosynthetic organisms are thought to have lost their photosynthetic capability during their evolution. The new genus *Rhodocyclus* is in a different phylogenetic subdivision ( $\beta$ ), to the other purple nonsulphur bacteria ( $\alpha$ ). Members of the  $\alpha$  subdivision have been further divided into four subgroups (not shown). One group includes the two *Rhodobacter* species, another includes all of the *Rhodospirillum* species, and *Rhodophila globoformis* and a third includes the remaining *Rhodopseudomonas* species and *Rhodomicrobium vanielii*. The purple sulphur bacteria are all contained within one subgroup of the  $\gamma$  subdivision.

The morphologies of the species used in the following studies [Buchanan and Gibbons, 1974] are summarised below. Line drawings of representative species are illustrated in Fig. 1.3 and electron micrographs of *Chr. vinosum* and *Rps. palustris* are presented in Figs 3.3 and 3.9.

#### *Rhodospirillum rubrum*

Cells are vibrio- (comma) or spiral-shaped, with up to one complete spiral turn. They are 1.5-2.5  $\mu\text{m}$  wide and, like the other species described below, are motile by means of polar flagella. They contain vesicular photosynthetic membranes (see section 1.3(i)) and are coloured red.



**Fig. 1.2** A phylogenetic tree compiled for a selection of purple bacteria. Phylogenetic relationships are inferred from 16S rRNA sequence homologies.

A: *Thermotoga*, B: flavobacteria, C: cyanobacteria, D: gram-positive bacteria, E: green nonsulphur bacteria.

**purple bacteria**

$\alpha$	$\beta$
1. <i>Rhodospirillum rubrum</i>	<i>Nesseria gonorrhoeae</i>
2. <i>Agrobacterium tumefaciens</i>	<i>Spirillum volutans</i>
3. <i>Rhodopseudomonas palustris</i>	<i>Nitrosolobus multiformis</i>
4. <i>Rhodopseudomonas acidophila</i>	<i>Rhodocyclus gelatinosus</i>
5. <i>Rhodobacter capsulatus</i>	<i>Rhodocyclus purpureus</i>
$\gamma$	$\delta$
1. <i>Chromatium vinosum</i>	<i>Myxococcus xanthus</i>
2. <i>Legionella pneumophila</i>	<i>Desulfovibrio desulfuricans</i>
3. <i>Pseudomonas aeruginosa</i>	<i>Bdellovibrio stolpii</i>
4. <i>Acinetobacter calcoaceticus</i>	<i>Desulfobacter postgatei</i>
5. <i>Escherichia coli</i>	<i>Desulfuromonas acetoxidans</i>

*Rhodobacter sphaeroides*

The cells are 0.7-4.0 $\mu$ m in diameter. They have vesicular photosynthetic membranes and are brown in colour.

*Rhodopseudomonas palustris*

The cells are rod-shaped to ovoid, 0.6-0.9 $\mu$ m wide. They have lamellar-type photosynthetic membranes and form red cultures which turn brown with age. This is the species of purple nonsulphur bacterium most commonly found in nature.

*Rhodopseudomonas acidophila*

The cells are rod-shaped to elongate-ovoid, slightly curved and 1.0-1.3 $\mu$ m wide. They are optimally cultured in acidic media (pH 5.2). They have polar flagella, lamellar photosynthetic membranes and are orange-brown or purple depending on the growth conditions.

*Chromatium vinosum*

The cells are round, 2.0 $\mu$ m in diameter and are brown-red in colour. They contain globules of elemental sulphur within the cytoplasm which are conspicuous in electron micrographs.

## 1.2 Ecology and Metabolic Requirements of Purple Photosynthetic Bacteria

Photosynthetic bacteria thrive in anaerobic areas of aquatic environments such as moist muddy soils, ditches, ponds, lakes, sulphur springs and marine habitats [Pfennig, 1967]. Purple nonsulphur bacteria are never present in the large red or green blooms which are common for sulphur bacteria. In the anaerobic depths of aquatic environments, organic matter is fermented by various microbes which release carbon dioxide and fermentive end products e.g. hydrogen, propionate, lactate

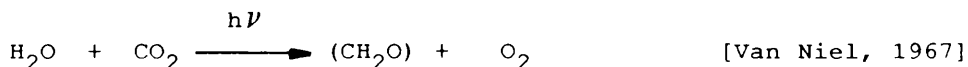
and butyrate. Purple photosynthetic bacteria use the carbon dioxide and fermentation products to perform anaerobic photosynthesis. To enable this they have evolved light-harvesting pigment protein complexes which absorb in the near-infrared region of the electromagnetic spectrum. The upper strata of a lake are occupied by oxygen-requiring cyanobacteria, algae and higher plants which do not absorb light in this region. Near-infrared wavelengths can therefore penetrate to the anaerobic layers below where they are absorbed by purple bacteria [Van Gemerden and Beeftink, 1983].

Purple nonsulphur photosynthetic bacteria are facultative aerobes which can either operate photosynthetically under anaerobic conditions or non-photosynthetically using oxygen, and deriving energy from aerobic respiration. Purple sulphur bacteria, with one exception (*Thiocapsa roseopersicina*) are strict photosynthetic anaerobes [Buchanan and Gibbons, 1974]. To perform photosynthesis purple bacteria require a source of electrons and a source of carbon. It has been demonstrated that most purple bacteria can grow photolithoautotrophically, obtaining carbon from  $\text{CO}_2$ , and electrons from molecular hydrogen [Ormerod and Gest, 1962]. Purple sulphur bacteria can also grow photoautotrophically using  $\text{CO}_2$  and reduced inorganic sulphur compounds such as hydrogen sulphide and thiosulphates. This is the nutritional mode usually used to culture *Chromatium*. In addition most purple bacteria can grow photoheterotrophically using reduced organic compounds to provide both carbon and electrons. This is the nutritional mode used to culture the nonsulphur bacteria.

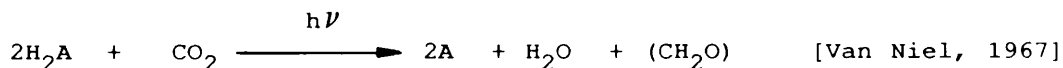
### 1.3 Overview of Photosynthesis in Purple Bacteria

#### 1.3(i) Introduction

Photosynthesis is a complex series of biochemical reactions in which light is converted into forms of energy which can then be used by the cell in the metabolic processes required for the maintenance of life. De Saussure first characterised photosynthesis in oxygen-evolving plants by the equation:



The metabolism of anaerobically grown purple photosynthetic bacteria was systematically studied for the first time by C.B. van Niel. He established that purple sulphur bacteria were performing anaerobic photosynthesis when they were supplied with bicarbonate and sulphide. In 1929, he perceptively proposed that photosynthesis is better considered to be a light-dependent reaction in which different substances, specific for different kinds of photosynthetic organisms, serve as H-donors for the reduction of  $\text{CO}_2$ . This can be expressed by a more general equation:



We now know that this equation represents an extremely complex process which can be divided into those reactions which require light to generate "high energy" compounds, and those reactions which subsequently use the compounds to drive light-independent reactions; essentially those of carbon metabolism. Some of the energy can however be "siphoned off" for other uses. The light-dependent reactions are performed within the photosynthetic membranes of purple bacteria. They involve the

transfer of energy between carrier molecules which must be highly organised within a membrane to ensure efficient energy transfer. The light-independent enzymic reactions of carbon metabolism are performed in the cytosol.

The cytoplasmic membrane of purple photosynthetic bacteria is considerably more complex than that of eukaryotic cytoplasmic membranes. It contains the electron transport machinery necessary to perform photosynthesis and the electron transport machinery for aerobic respiration. Under anaerobic conditions in the light, the membrane grows and invaginates into the cytoplasm. The invaginations become packed with the pigments and proteins necessary for the cell to adopt a photosynthetic mode of nutrition. Whether the photosynthetic membranes also contain aerobic respiratory electron transfer chains is unknown but it is clear that the photosynthetic, and cytoplasmic membranes are compositionally different [Kaplan and Arntzen, 1982]. The morphologies of photosynthetic membranes are species-specific. They can be tubular, lamellar, or vesicular in shape [Sprague and Varga, 1986; Imhoff, 1988] (Fig. 1.3). Electron micrograph studies indicate that photosynthetic membranes are continuous with the cytoplasmic membrane [Drews, 1978; Drews and Oelze, 1981; Lascelles, 1968] although this is disputed by Holmqvist (1979). The proposed arrangement of lamellar-type photosynthetic membranes is depicted in Fig. 1.4.

Photosynthetic membranes were first isolated by Schachman et al. (1952). Detailed procedures for the isolation of photosynthetic membranes are reviewed by Niederman and Gibson (1978). The membranes of most purple photosynthetic bacteria contain the pigment BChl a. Exceptions are the BChl b-containing *Rhodopseudomonas viridis*, *Ectothiorhodospira halochloris*, *E. abdelmalekii* and *Thiocapsa pfenningii* [Imhoff, 1988].

Fig. 1.3 Cartoons of various purple bacteria illustrating the cell shapes and the different forms of the intracytoplasmic membrane. (From Sprague and Varga, 1986.)

Fig. 1.4 Suggested arrangement of lamellar-type intracytoplasmic membranes. The cytoplasmic membrane (CM) invaginates to form stacks of intracytoplasmic membranes which contain the photosynthetic apparatus. The photosynthetic electron transport chain, pumps protons across the membrane into the periplasmic and lumenal spaces. This creates an electric potential and pH gradient which drives the formation of ATP and NADH (see section 1.3(iii)). (From Sprague and Varga, 1986.)

# PURPLE BACTERIA (INTRACYTOPLASMIC MEMBRANES)

*Rhodospirillum* sp  
*Rhodopseudomonas* sp

*Thiocapsa pfennigii*

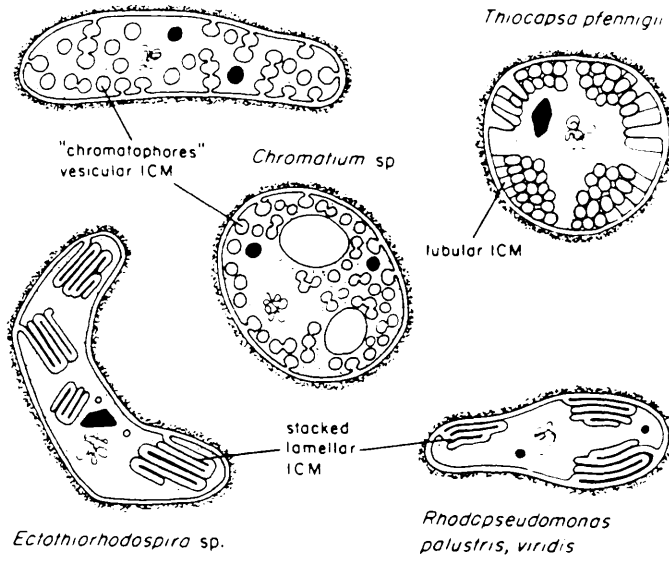


Fig. 1.3

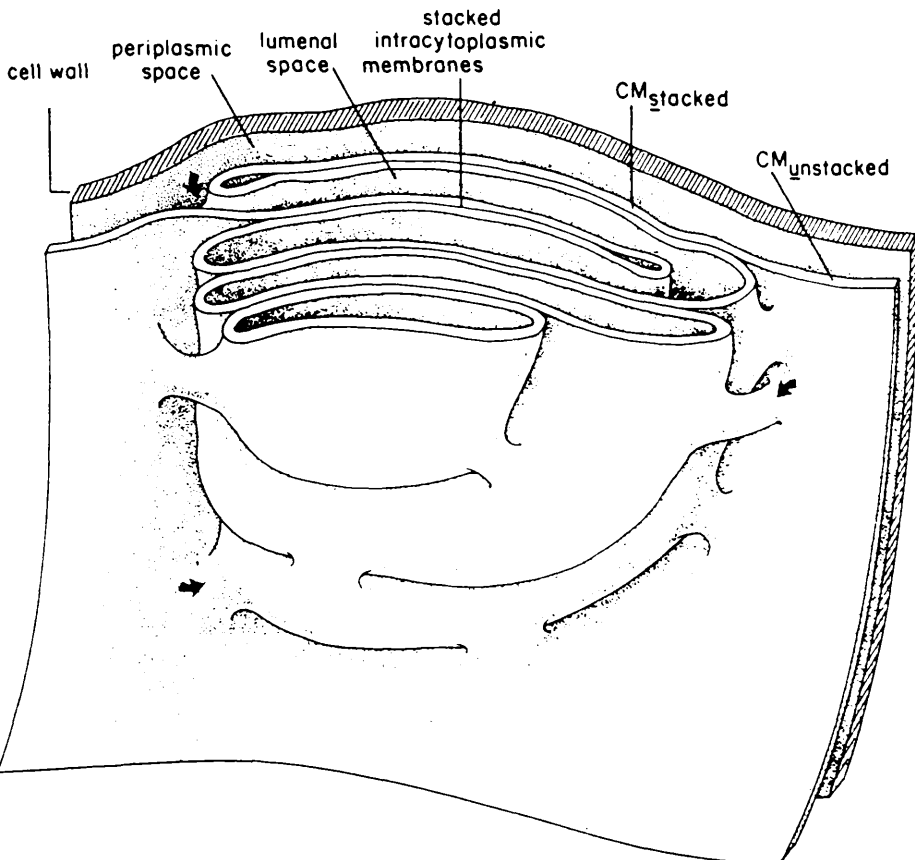
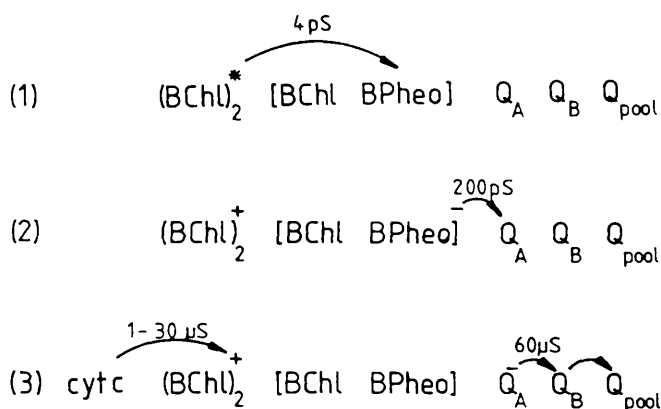


Fig. 1.4

The light reactions of photosynthetic bacteria comprise several steps: light harvesting, energy trapping, electron transfer and the generation of a membrane potential, and finally the formation of chemical bond energy (ATP) and reducing power (NADP). In 1951, Duysens proposed that only 5% of the membrane BChl is directly involved in energy trapping [Duysens, 1951]. The remaining BChl is bound to the light-harvesting pigment-protein complexes. These absorb light energy and transfer the resulting electronic excitation energy to the reaction centres where it is trapped [Sauer, 1975; Ames, 1978; Zanker, 1978]. The structure and function of antenna complexes will be described in detail after a brief discussion of other processes important in bacterial photosynthesis.

### 1.3(ii) Energy trapping by the photochemical reaction centre

Reaction centres were first isolated from photosynthetic membranes in 1968 [Reed and Clayton, 1968]. They contain three transmembrane proteins labelled heavy (H), medium (M), and light (L) [Okamura et al., 1982] which in *Rps. viridis* and (*Rb. sphaeroides*), have: 307 (258), 260 (320) and 281 (274) amino acid residues respectively [Williams et al., 1983; Michel et al., 1986]. The reaction centre of *Rps. viridis* has in addition a closely associated cytochrome c molecule. Reaction centres of purple bacteria also contain one carotenoid molecule, four bacteriochlorophylls (BChl), two bacteriopheophytins (Bphea), one non-haem iron and two quinone molecules. Two of the reaction centre BChls form an exciton-coupled "special-pair" which receives the excitation energy from the antennas [Norris et al., 1973; McElroy et al., 1969; Norris et al., 1971; Netzel et al., 1973]. The excitation energy induces a transition of the special-pair to its lowest excited singlet state. In about 4 picoseconds the excited special-pair donates an



**Fig. 1.5** The primary, (1) and (2), and secondary, (3), charge transfer reactions - the first photochemical steps of photosynthesis. The excitation energy received by the special-pair BChls is used to drive an electron across the reaction centre resulting in a stabilised charge separation. The charge separation must be very fast to compete with non-radiative deexcitation of the pigments and to minimise the probability of a wasteful back reaction.

electron to the "primary" electron acceptor, Bpheo (Fig. 1.5) [Leigh, 1978; Prince and Dutton, 1978; Parson and Holten, 1986]. Although a BChl molecule lies between the dimer and the Bpheo it doesn't appear to be an electron acceptor. It may however facilitate electron transfer in some way [Kirmaier and Holten, 1987]. A transient charge separation occurs between the BChl dimer and the Bpheo [Parson and Holten, 1986]. Within 200 picoseconds the electron is transferred further across the membrane to a quinone molecule ( $Q_A$ ). A cytochrome c molecule then donates an electron to the electron-depleted dimer which stabilises the charge separation, and the electron on  $Q_A$  is transferred to the membrane quinone pool via a second reaction centre quinone  $Q_B$ . Light therefore initiates a redox reaction which results in a charge separation and the formation of reduced quinone.

In a landmark in photosynthesis research, the structures of the

reaction centres of two species of purple bacteria, *Rps. viridis* [Deisenhofer et al., 1984; Deisenhofer et al., 1985; Michel and Deisenhofer, 1986] and *Rb. sphaeroides*, strain R-26, [Allen et al., 1987a; Allen et al., 1987b; Yeates et al., 1987] have been determined to less than 3Å resolution by X-ray diffraction analysis of reaction centre crystals. The crystals remarkably retain the ability to perform primary photochemistry. The orientations of the reaction centre cofactors and proteins are illustrated in Figs 1.6 and 1.7. The shape of the reaction centre is illustrated by the filled models in Fig. 1.8.

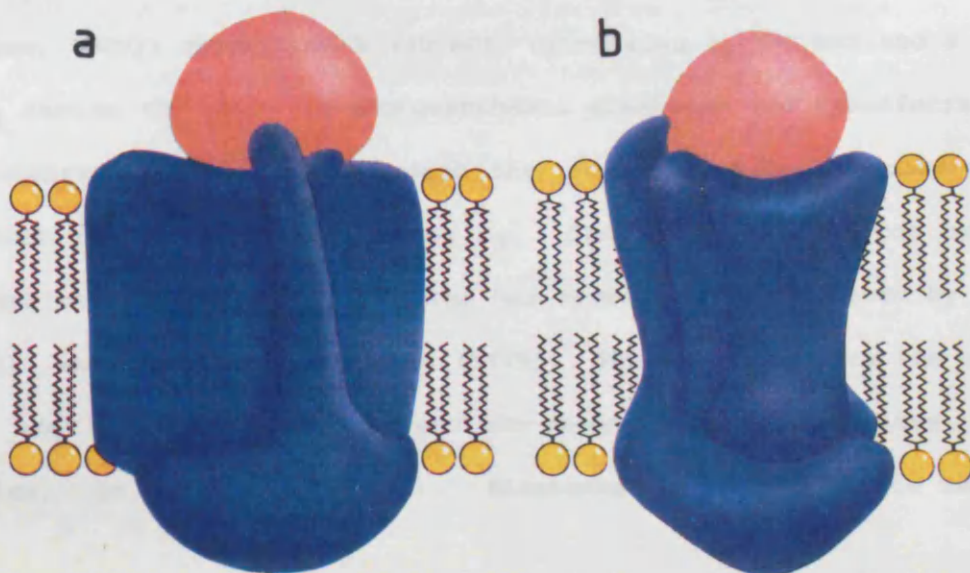
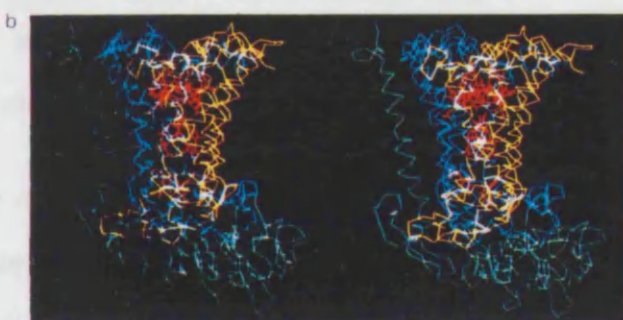
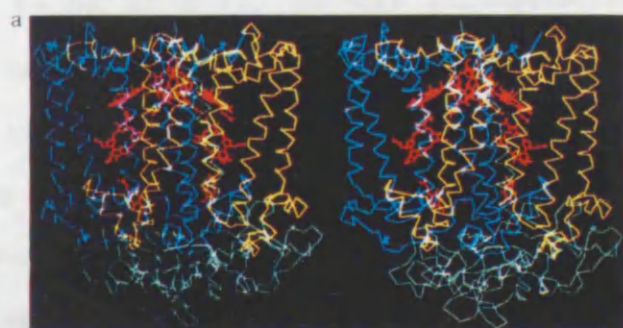
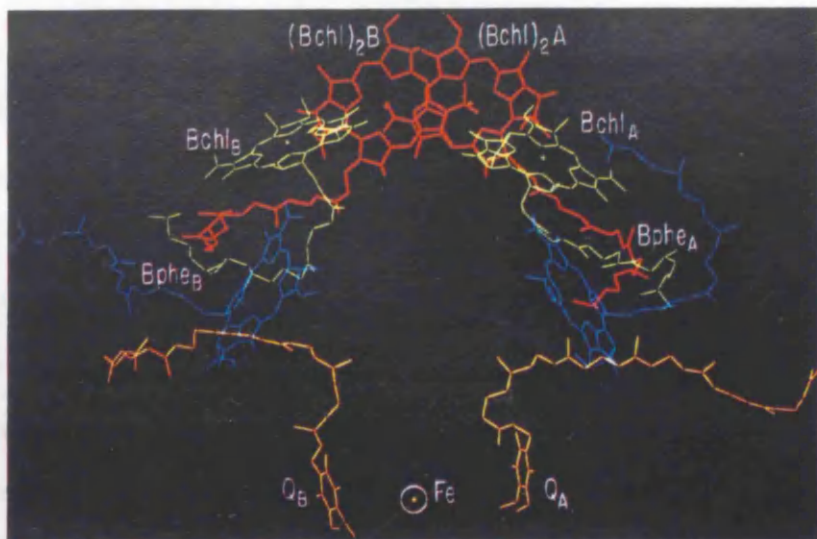
The reaction centre has a two-fold vertical symmetry. The L and M subunits each contain five transmembrane  $\alpha$ -helices, and have additional small  $\alpha$ -helices in the turns near the surfaces of the membrane. The L and M subunit transmembrane helices are labelled A-E. The central D and E helices from each protein, cross each other and form a core complex around the pigments which appears to be analogous to the D1/D2 protein core of photosystem II in plants [Michel and Deisenhofer, 1986]. The H subunit has a single transmembrane  $\alpha$ -helix positioned outside the LM complex and a large globular, polar domain on the cytoplasmic side of the membrane. This protein does not bind any of the cofactors and is not required for the primary photochemistry. But it may be involved in electron transfer from the primary to the secondary quinone, or it may help to stabilise the reaction centre, or bind antenna complexes, or act as a target site in the cytoplasmic membrane for the synthesis of new photosynthetic units [Michel and Deisenhofer, 1986].

The pigments are arranged within the core, in two almost symmetrical branches labelled A and B, which are co-ordinated to the L and M polypeptide subunits respectively [Allen et al., 1987b]. The cytochrome on the periplasmic side of the membrane feeds electrons to the special-pair, BChl dimer. Electrons travel across the membrane via the A branch

Fig. 1.6 Computer graphic showing the arrangement of the pigments, quinones and non-haem iron in the reaction centre of *Rb. sphaeroides*. Excitation energy is fed from the light-harvesting antenna complexes to the special-pair BChls (red). The planar BChl chromophores of the special-pair overlap so that the excitation energy is spread across both molecules. Electrons are transferred from the special pair on the periplasmic side of the membrane to quinone  $Q_A$  on the cytoplasmic side of the membrane and then to  $Q_B$ . When  $Q_B$  has received two electrons it dissociates from the reaction centre and reduces the membrane quinone pool. (From Allen et al., 1987a.)

Fig. 1.7 Stereoviews of the reaction centre cofactors and proteins. The L (yellow) and M (blue) proteins each contain five transmembrane  $\alpha$ -helices which enclose the cofactors. The heavy protein (green) contains a single transmembrane helix and a large polar domain on the cytoplasmic side of the membrane. The two views are related by  $90^\circ$ . (From Allen et al., 1987b.)

Fig. 1.8 Models showing the shape of the reaction centre. The L, M, and H subunits are pictured in blue. The cytochrome c molecule, which reversibly associates with the periplasmic side of the reaction centre, and donates electrons to the special-pair BChls, is coloured red. The left-hand model corresponds to the upper stereoview in Fig. 1.7. The right-hand model corresponds to the lower stereoview. (From Hunter, 1988).



pigments to the primary quinone  $Q_A$  (Fig. 1.6) and pass around the nonhaem iron as they are transferred to the B branch quinone ( $Q_B$ ). When  $Q_B$  has accepted two electrons it dissociates from the reaction centre and reduces a ubiquinone in the large, membrane quinone pool. The role of the nonhaem iron is still uncertain. Its removal does not affect the rate of electron transfer from  $Q_A$  to  $Q_B$ . But it does form six coordinate bonds with surrounding amino acids which may help to stabilise the reaction centre.

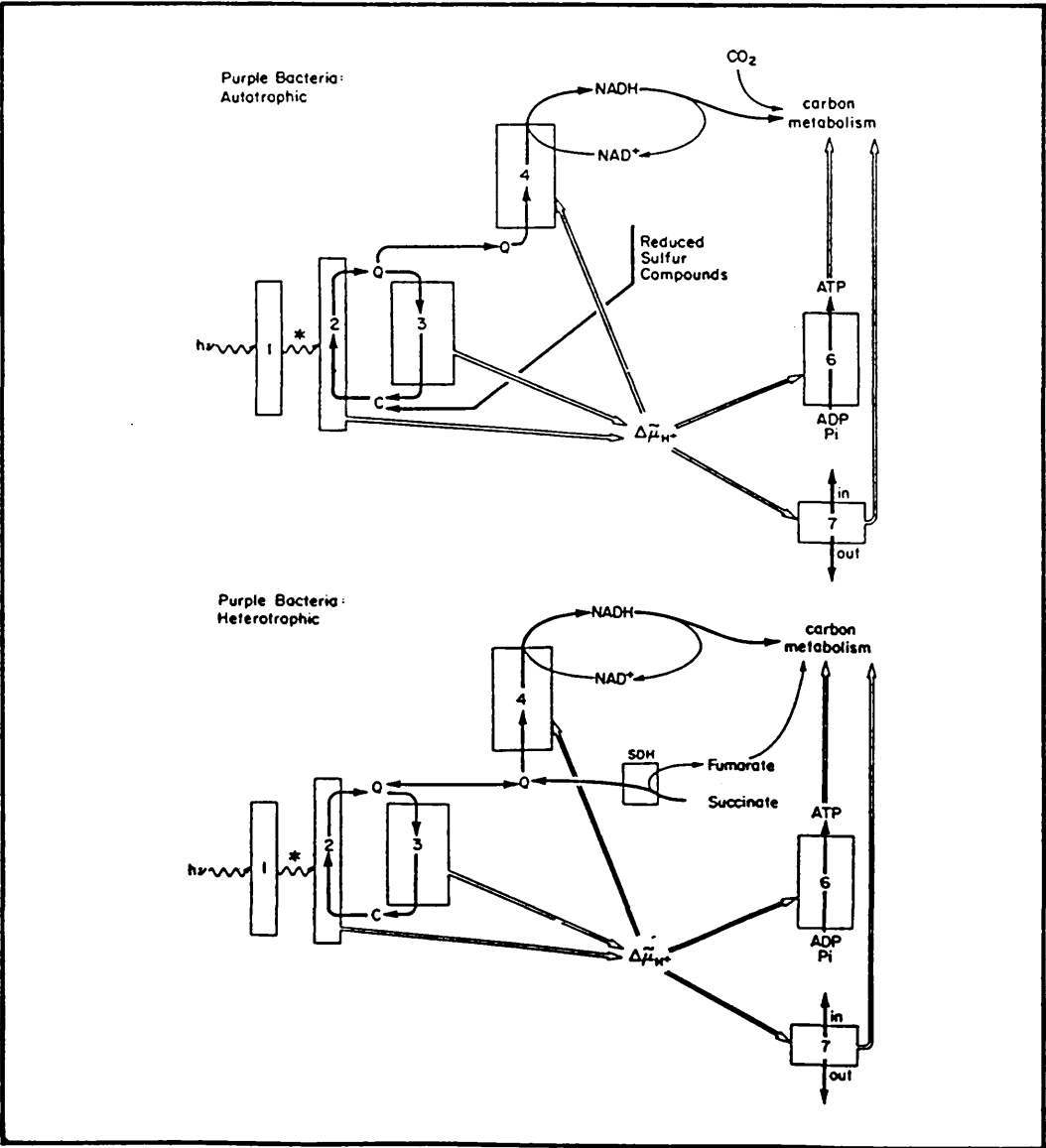
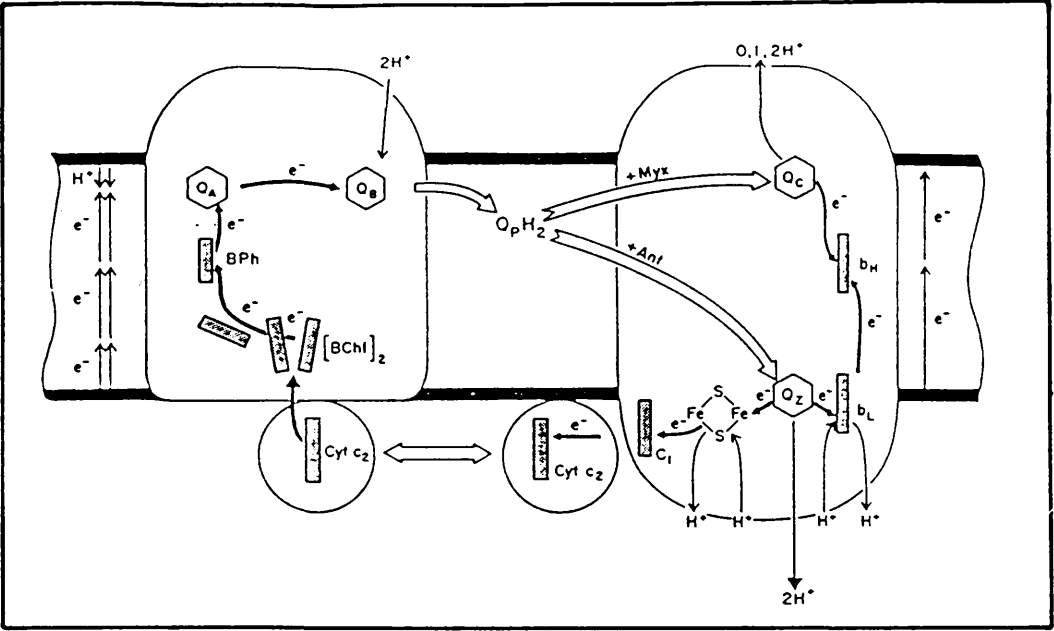
Resonance Raman spectroscopy has determined the carotenoid in the reaction centre to be in a 15, 15'-cis configuration [Lutz et al., 1978]. There has, however, been some difficulty in locating the position of the carotenoid in the reaction centre. This has recently been achieved by comparing the crystal diffraction patterns of *Rps. sphaeroides* wild-type and the carotenoidless mutant strain R26 [Allen et al., 1988]. It appears to lie just outside the BChl and Bpheo molecules on the B branch of the reaction centre. This allows it to quench any triplet BChl which forms.

### 1.3(iii) Energy flow and the synthesis of ATP and NADH

The membrane quinol pool supplies electrons to the transmembrane cytochrome  $bc_1$  complex [Gabellini et al, 1982] which is used in both photosynthesis and respiration. It has three transmembrane proteins [Hauska, 1986]: cytochrome b (40 kD), cytochrome  $c_1$  (34 kD) and a Reiske  $Fe_2S_2$  centre (25 kD). In photosynthesis electrons are transferred from the membrane quinone pool through the cytochrome  $bc_1$  complex to the reaction centre donor cytochrome  $c_2$ . The route of electron transfer through the cytochrome  $bc_1$  complex has recently been reviewed by Dutton (1986), and Robertson and Dutton (1988). The electrons from the quinone pool are transferred to two protein-associated quinone sites in the complex,  $Q_c$  and  $Q_z$  (Fig. 1.9). Electrons from the  $Q_c$  site and some

Fig. 1.9 Cyclic electron flow between the reaction centre (left) and the cytochrome  $bc_1$  complex (right). Membrane pool quinones reduce two quinones in the cytochrome  $bc_1$  complex ( $Q_c$  and  $Q_z$ ). Electrons then flow to cytochrome  $b_H$  and back to the membrane quinone pool, or to cytochrome  $c_2$  in the periplasmic or lumenal space. Cytochrome  $c_2$  then donates electrons to the reaction centre special-pair to complete the cycle. The cyclic electron flow results in a net transport of protons across the membrane. (From Robertson and Dutton, 1988.)

Fig. 1.10 Electron flow and energy transfer in autotrophic and heterotrophic nutritional modes in purple bacteria. (1) light-harvesting antenna complexes, (2) reaction centre, (3) cytochrome  $bc_1$  complex, (4) NADH-quinone oxidoreductase, (6) ATP synthase complex, (7) transmembrane metabolite transporters, (Q) membrane pool quinone, (c) cytochrome  $c_2$ , (SDH) succinate dehydrogenase. (From Dutton, 1986.)



from the Qz site reduce the cytochrome  $b_h$  which is then thought to reduce the membrane quinone pool. The remaining electrons from the Qz site reduce soluble cytochrome  $c_2$  in the periplasmic space, which then diffuses across and donates electrons to the reaction centre. Overall there is a net oxidation of one quinol and a net reduction of two cytochromes  $c_2$ . The diffusion of cytochrome  $c_2$  through the periplasm to the reaction centre is difficult to envisage in *Chr. vinosum* and *Rps. viridis* however, because unlike in other organisms the reaction centres have been shown to bind the cytochrome quite tightly by hydrophobic interactions. This is why the cytochrome was crystallised with the reaction centre in *Rps. viridis*.

The cyclic electron flow through the cytochrome  $bc_1$  and reaction centre complexes results in a net transfer of protons across the membrane, and hence a net electric potential and pH difference. As electron flow proceeds the combined  $\Delta pH$  and  $\Delta\psi$  ( $\Delta\mu_{H^+}$ ) increases and can be used to drive three processes: (1) the reduction of nicotinamide adenine dinucleotide (NAD) to NADH in an energy-linked reversed transfer process, by membrane-bound NADH-quinone oxidoreductase enzymes (2) the synthesis of adenosine triphosphate (ATP) by proton flow across the membrane through the ATP synthase complex (chemiosmotic hypothesis) [Mitchell, 1961; Nicholls, 1982; Jackson and Crofts, 1969], and (3) active transport of metabolites across the cytoplasmic membrane.

With an autotrophic nutritional mode, reduced inorganic compounds feed electrons into the cyclic electron flow by reducing soluble cytochrome  $c$  (Fig. 1.10). This also adds to the  $\Delta\mu_{H^+}$ . With a heterotrophic mode of nutrition, succinate for example, is oxidised to fumarate by a membrane bound succinate dehydrogenase complex. This is coupled with the reduction of the membrane quinone pool which then feeds electrons into either the cyclic electron flow, or NAD reduction pathway. Fumarate is then used in carbon metabolism. Carbon metabolism

in phototrophic bacteria has been reviewed by Ormerod and Sirevag (1983).

#### 1.4 Light Absorption by Photosynthetic Pigments

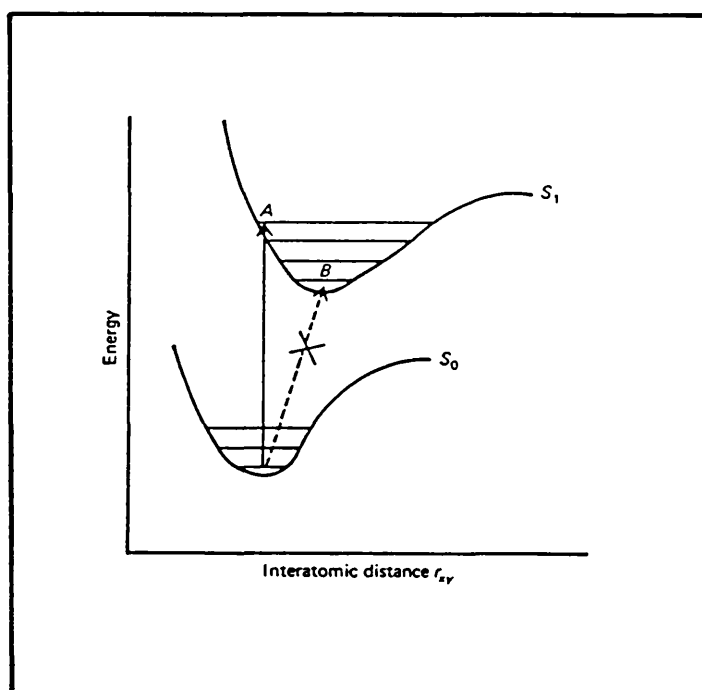
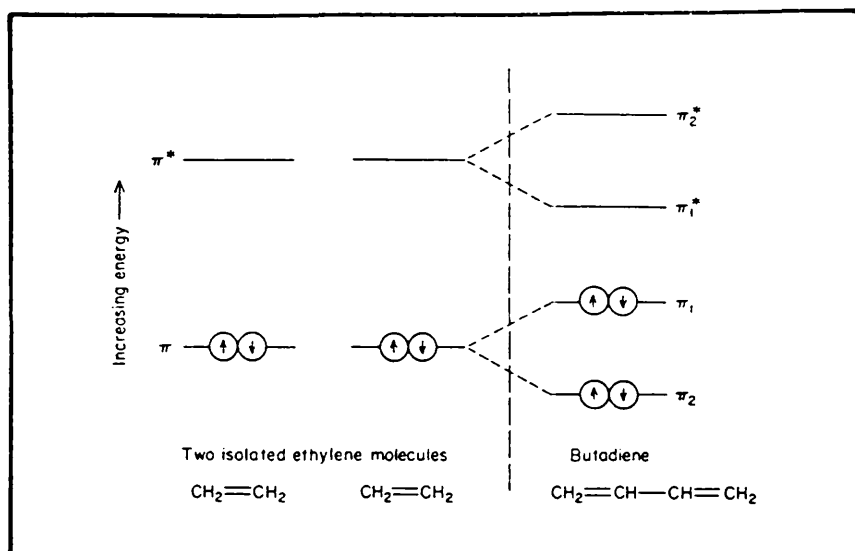
When light is absorbed by a pigment molecule an electron undergoes a transition into a higher energy state. This is unstable and the electron returns to the ground state giving up its energy either by radiative emission, or by radiationless heat loss to the environment.

In organic molecules there are three types of molecular electron orbitals: single bond orbitals ( $\sigma$ ), double bond orbitals ( $\pi$ ) and lone pair orbitals ( $n$ ). The energies of these orbitals increase in the sequence  $\sigma < \pi < n < \pi^* < \sigma^*$ , where  $*$  represents the excited state antibonding orbitals. Photosynthetic pigments contain regions of alternating single and double bonds across which the electrons are delocalised. The effect of delocalisation on the molecular orbital energy levels is demonstrated in Fig 1.11. The  $\pi$ - $\pi^*$  transition of ethene is energetically, relatively large. When two ethene molecules are bonded to form butadiene, the bonding and antibonding orbitals split. The lowest energy  $\pi$ - $\pi^*$  transition now requires less energy and light of longer wavelength is absorbed. With increasing conjugation, the energy of the first  $\pi$ - $\pi^*$  transition decreases further so that conjugation of at least seven double bonds results in visible absorption. When the electron spins of an energy state are oppositely paired the energy state is said to be singlet. When the electrons are spin-parallel the energy state is said to be triplet. Hund's rule of multiplicity decrees that triplet states have lower energies than their corresponding singlet states [Cowan and Drisko, 1976].

Whether an electronic transition between two energy states is allowed or forbidden is governed by theoretical selection rules. One selection rule for upward electronic transitions forbids a change in the

Fig. 1.11 The effect of delocalisation on  $\pi$ -bonding molecular orbitals. (From Brown, 1980.)

Fig. 1.12 Morse curves for an electronic transition of a diatomic molecule into the first excited singlet state. The transition occurs into the highest vibrational energy level. Subsequent vibrational relaxation results in an increase in the interatomic distance. (From Cowan and Drisko, 1976.)



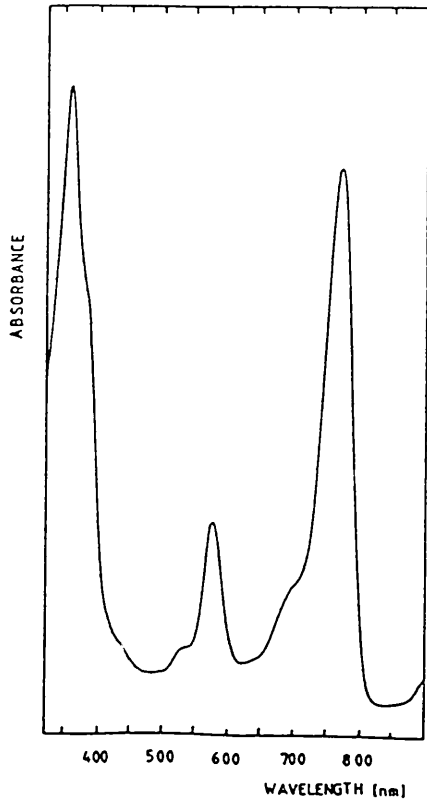
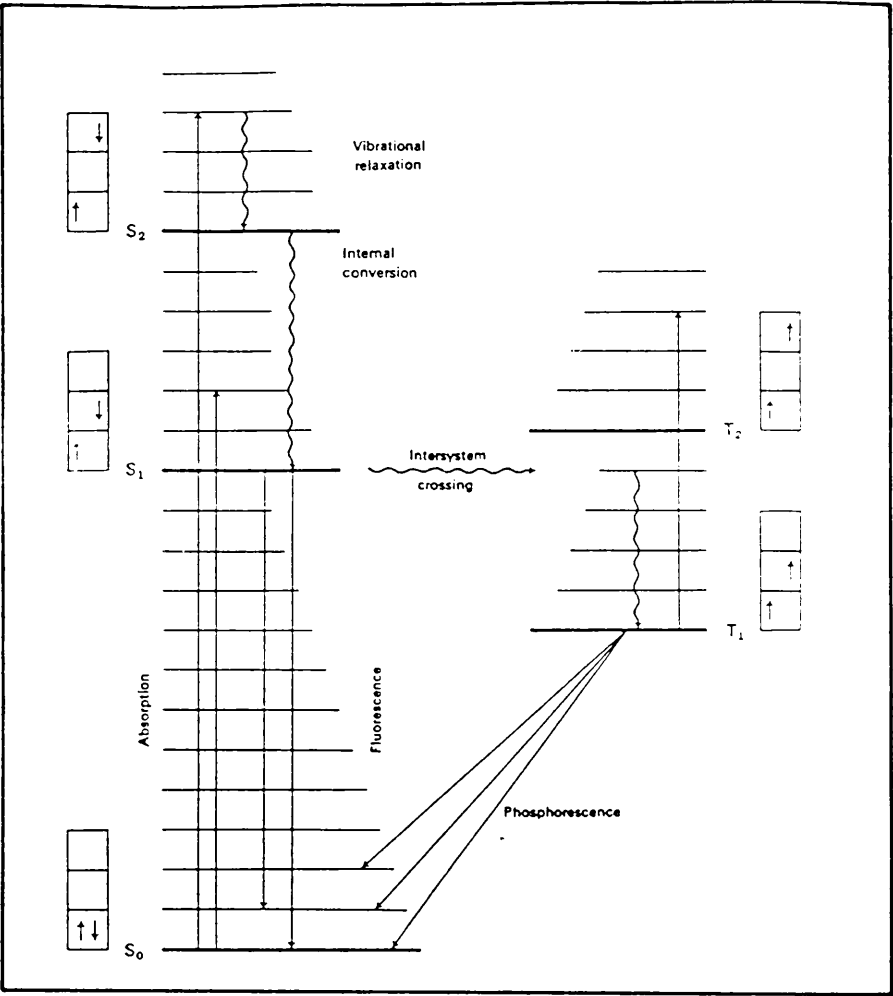
quantum spin number. Under normal conditions triplet states cannot therefore be formed directly by light absorption but can be formed by intersystem crossing from an excited singlet state. Pigment triplets play no role in normal light-harvesting energy transfer processes but are important for the photoprotective function of carotenoids (section 1.5). A second selection rule forbids energy transitions between bonding and antibonding orbitals of incompatible symmetry (e.g.  $n-\pi^*$  transitions). However, in reality, electronic states are never pure and contain some mixing with other states so that weak absorption due to symmetry-forbidden transitions can be observed.

The potential energy of an electron is defined by its electronic, vibrational, rotational and spin states. Electronic transitions involve the greatest energy changes. They occur very rapidly, more rapidly than the time required for a molecular vibrational transition (vibrational relaxation) [Cowan and Drisko, 1976]. According to the Frank-Condon principle, upward electronic transitions occur into the highest vibrational energy level (Fig. 1.12). During the vibrational relaxation which follows the symmetry of the excited state changes and the internuclear distance increases. Allowed electronic transitions can occur between any vibrational level in the ground state and any vibrational level of the excited state. The energy required to effect an electronic transition therefore varies within a limited range and gives rise to an absorption band rather than an absorption line. The various intermolecular energy transitions initiated by light absorption are illustrated in Fig. 1.13.

The absorption spectrum of BChl (Fig. 1.14) shows three main absorption bands. The Soret, UV band results from an electronic transition to the second excited singlet state. The Qx absorption band at 590nm and the Qy absorption band at about 770nm result from

Fig. 1.13 Jablonski diagram illustrating allowed electronic transitions. Upward transitions occur into first and second excited, spin antiparallel energy states. Relaxation into lower vibronic states can then occur. Internal conversion can also occur from higher to lower excited states, with concomitant heat loss (e.g. BChl Soret to Q<sub>y</sub> energy states). Energy can be lost from first excited singlet states by radiative fluorescence emission. Alternatively deexcitation can occur by intersystem crossing to spin-parallel triplet states and subsequent phosphorescence. (From Cowan and Drisko, 1976.)

Fig. 1.14 Electronic absorption spectrum of BChl, in acetone.



excitations into the first excited singlet state. After excitation into the Soret band, rapid internal conversion to the first excited singlet state occurs. The Q<sub>y</sub> and Q<sub>x</sub> bands arise from two different, perpendicular transition dipoles across the porphyrin ring. Light absorption into the Q<sub>x</sub> band at  $\sim 590\text{nm}$  induces a different molecular orbital electron distribution, and hence a different orientation compared to the Q<sub>y</sub> dipole.

The lowest  $\pi^*$  energy state of polyenes, including carotenoids, has been named the 2Ag state [Birge, 1986]. The upward transition of an electron into this state is symmetry-forbidden [Thrash et al, 1979; Razi Naqvi, 1980]. The first optically allowed transition is into the 1Bu state. Internal conversion to the 2Ag state may then occur. In carotenoids the energy, and hence absorption wavelength corresponding to the 2Ag state is not yet known. An absorption spectrum of a carotenoid is presented in Fig. 1.15. Carotenoids typically have three main absorption bands. These correspond to transitions into three different vibrational energy levels of the first electronic excited singlet state. The vibrational absorption bands are labelled 0-2, 0-1 and 0-0 from short-wavelength to long-wavelength absorption respectively. Carotenoids also have less intense bands in the ultra violet region known as cis-peaks. These result from excitation into the second excited singlet state. Cis-peaks, as the name suggests, are more intense in the absorption spectra of cis-carotenoids.

### 1.5 The Biosynthesis of Photosynthetic Pigments

The biosynthetic pathways of BChl and the carotenoids of purple bacteria are shown in Fig. 1.16. The key intermediate in the biosynthesis of porphyrins is  $\delta$ -aminolevulinic acid (ALA). This can be synthesised from glycine and succinyl CoA using the regulatory enzyme

Fig. 1.15 Electronic absorption spectrum of a typical carotenoid with labelled vibrational absorption bands. The bands between 400 and 520nm are a result of excitation into the first excited singlet state. The cis-peak is due to excitation into the second excited singlet state.

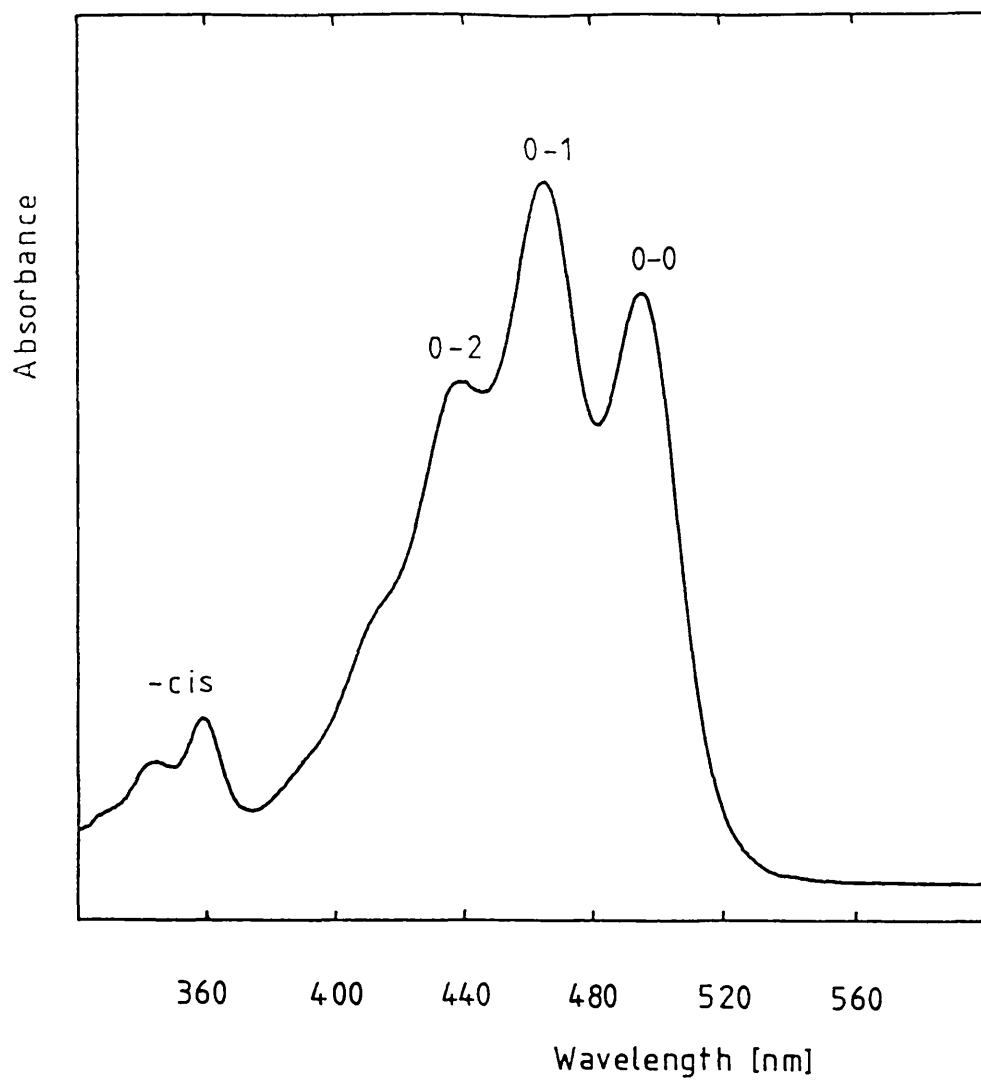
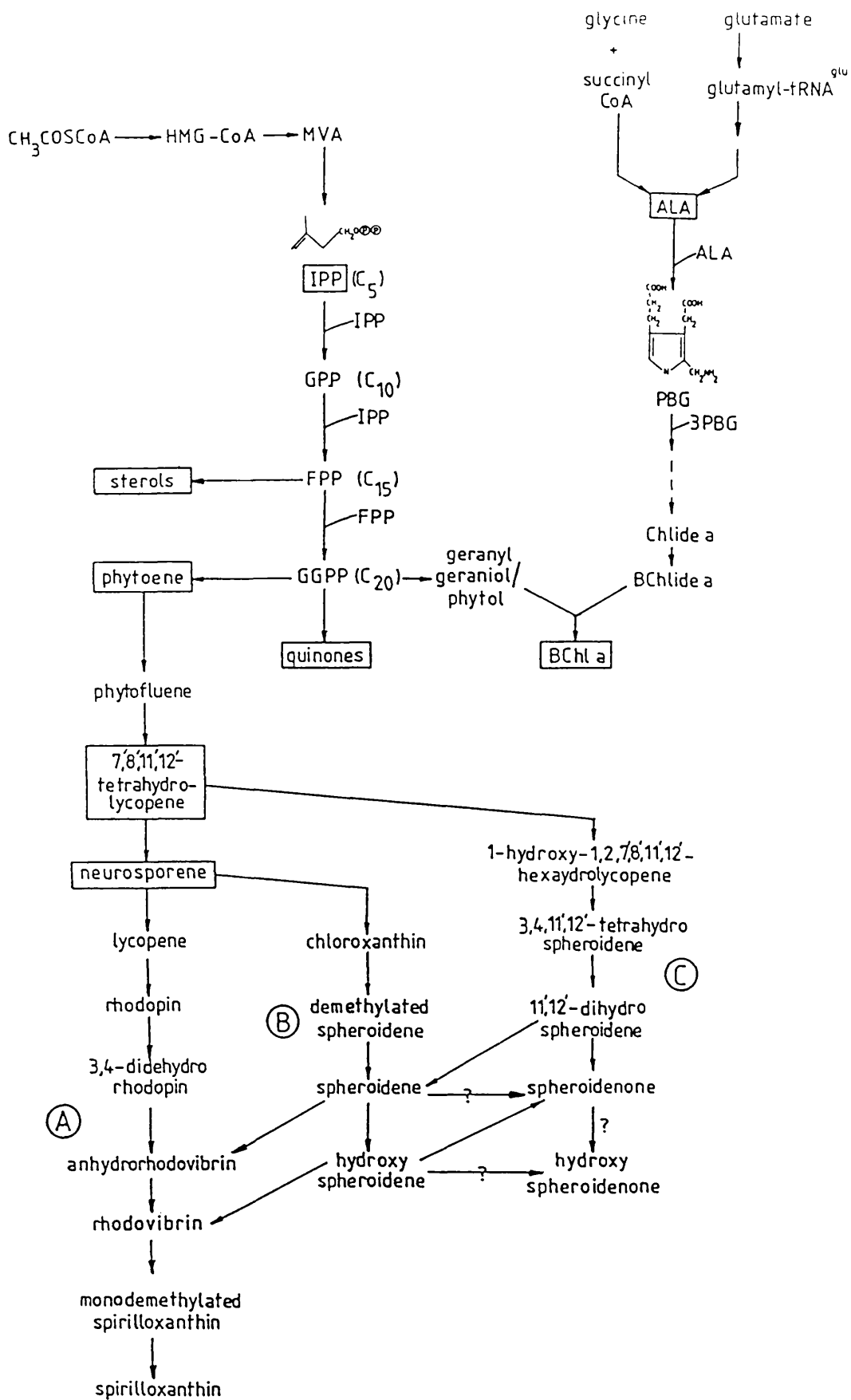


Fig. 1.16 Partial biosynthetic pathways of BChl and carotenoids. The macrocyclic chromophore of chlorophylls is made by the haem biosynthetic pathway. Carotenoids and the hydrocarbon tails of chlorophylls are made by the isoprenoid biosynthetic pathway. See text for details. (From Goodwin (1980) and Liaaen Jensen (1965)).



ALA synthetase which is inhibited by protoporphyrin feedback [Bogorad, 1965]. Recently a second pathway for ALA synthesis has been discovered [Kannangara et al., 1988] in an unusual reaction involving a glutamate-specific tRNA molecule. This reaction pathway is present in *Chromatium* spp. but *Rb. sphaeroides* uses the long-established ALA synthetase pathway. Two ALA molecules combine to form porphobilinogen (PBG) which is the basic five-membered ring of the porphyrin molecule. The pathway then proceeds through numerous intermediates to bacteriochlorophyllide a. This is a BChl molecule without the hydrocarbon tail. The BChl tail, and carotenoid molecules are synthesised via the isoprenoid biosynthetic pathway. The isoprenoid pathway [Goodwin, 1965] synthesises many important molecules such as steroids, quinones and plant growth hormones. The common precursor of these molecules is acetyl CoA. The reaction pathway proceeds through hydroxymethylglutaryl CoA (HMG-CoA) and mevalonic acid (MVA) to the isoprene building block, isopentenyl pyrophosphate (IPP). These C<sub>5</sub> units combine, through geranylpyrophosphate and farnesylpyrophosphate, to form C<sub>20</sub> geranyl-geranylpyrophosphate. This is used to synthesise the hydrocarbon tail of BChl. Two GGPP molecules combine to form the first carotenoid, phytoene. A series of desaturation reactions follows in which the chromophore is increased by two double bonds at each step. The wavelength at which the carotenoid absorbs therefore also increases. i.e. phytoene (3 db's) 297nm; phytofluene (5) 350nm; 7',8',11',12'-tetrahydrolycopene (7) 400nm; neurosporene (9) 440nm; lycopene (11) 470nm, in light petroleum. The first desaturation reaction forms 7',8',11',12'-tetrahydrolycopene. This is an isomer of  $\zeta$ -carotene (7,8,7',8'-tetrahydrolycopene) which is found in higher plants. (See Appendix A for semi-systematic names of carotenoids.)

Many purple bacteria contain carotenoids which are synthesised by the "normal spirilloxanthin" pathway [Imhoff, 1988]. These include

*R. rubrum*, *Rps. palustris* and *Chr. vinosum*. The biosynthetic pathway from phytoene to spirilloxanthin was studied by Liaaen Jensen et al. (1958; 1961) (Fig. 1.16A). Spheroidene is a major carotenoid in the *Rhodobacter* genus species [Imhoff, 1988]. A biosynthetic pathway from neurosporene and via chloroxanthin to spheroidene was proposed by Goodwin et al. (1955) (Fig. 1.16B). The coexistence of spirilloxanthin and spheroidene, and the absence of rhodopin in *Rc. gelatinosus* has led to the proposal that the above pathway is linked to the normal spirilloxanthin pathway between spheroidene and anhydrorhodovibrin Liaaen [Eimhjellen and Jensen, 1964]. Experimental evidence later confirmed the existence of this "alternative" biosynthetic pathway [McDermott et al., 1973].

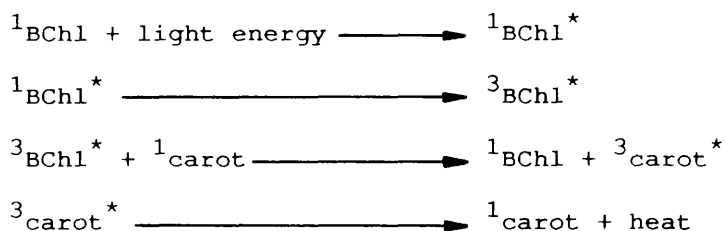
The presence of 11',12'-dihydrospheroidene in *Rb. sphaeroides* has led to the suggestion of an alternative biosynthetic pathway to spheroidene from 7',8',11',12'-tetrahydrolycopene [Malhotra et al., 1969] (Fig. 1.16C).

The biosynthetic pathways of carotenoids in purple photosynthetic bacteria have been reviewed by Liaaen Jensen (1965; 1978) and Goodwin (1980).

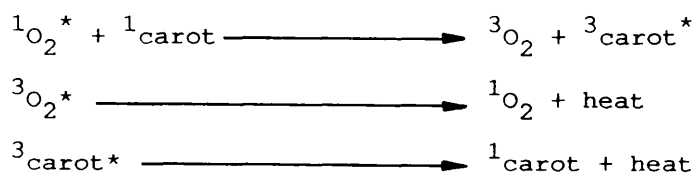
## **1.6 The Role of Carotenoids in Photoprotection**

When BChl absorbs light a proportion of the molecules undergo intersystem crossing to the triplet state [Cogdell and Frank, 1987]. Triplet BChl can interact with ground state molecular oxygen to form singlet oxygen, a strong oxidant which can react with any membrane pigments, proteins or lipids in its vicinity [Halliwell and Gutteridge, 1985]. This causes the breakdown of membrane function and cell death. If electronic excitation reaches the reaction centre special pair before the completion of a previous photochemical reaction cycle, the

excited state will be long-lived and the probability of BChl triplet formation will increase. Carotenoids protect against the formation of singlet oxygen by direct quenching of the BChl triplet in a reaction which can be described as follows:



Carotenoids are able to do this because they possess lower first excited triplet states than BChl. The resulting carotenoid triplet loses its energy by harmless radiationless decay. If close enough it is possible that carotenoids are also able to quench singlet oxygen itself by the reaction:



Carotenoids also transfer energy to the special-pair BChls in reaction centres [Cogdell *et al.*, 1976] but the importance of this role is insignificant compared to the energy transferred to the dimer from the antenna. The main role of the reaction centre carotenoid is to act as a photoprotector [Cogdell and Frank, 1987].

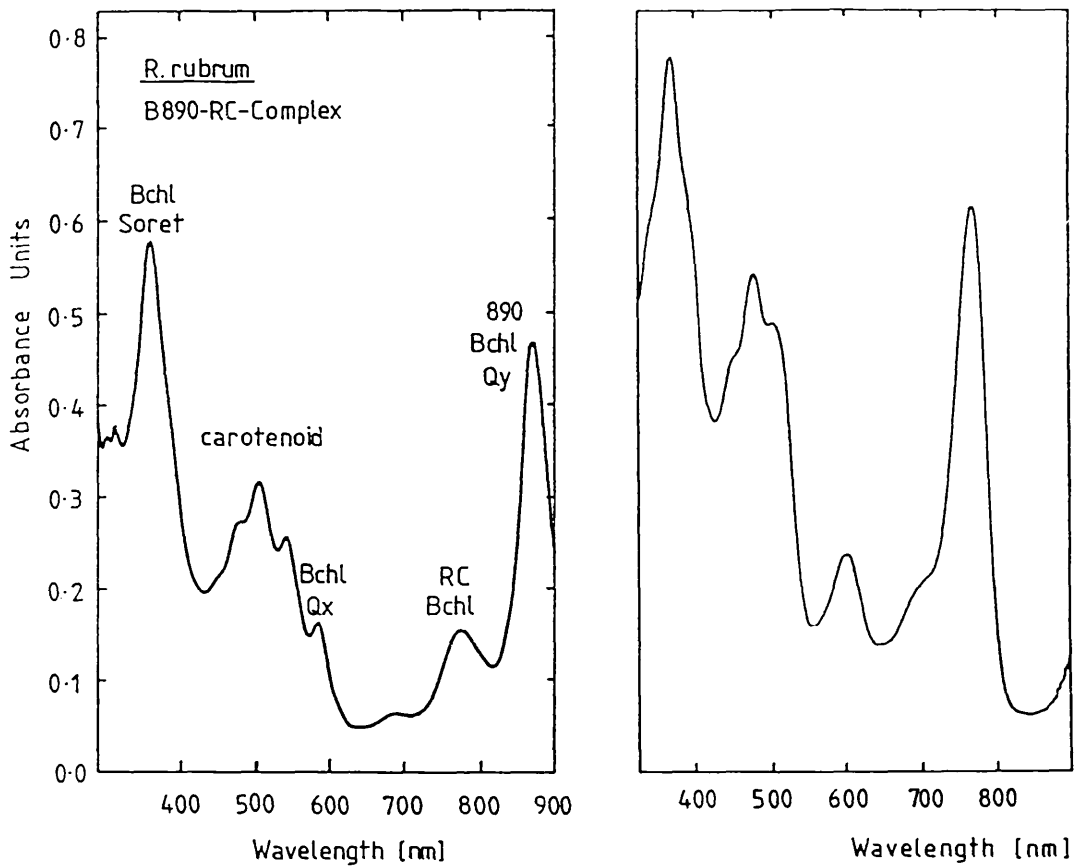
## 1.7 The Light-harvesting Antenna Complexes of Purple Photosynthetic Bacteria

### 1.7(i) Introduction

Light-harvesting antenna complexes contain more than 95% of the total pigment in the photosynthetic membrane [Duysens, 1951]. Antenna complexes can be isolated by solubilising photosynthetic membranes with a suitable detergent followed by differential centrifugation and protein fractionation techniques (see section 2.5). Several distinct types of antenna complexes have so far been isolated from purple bacteria. They are named according to the pattern of their absorption spectra. Fig. 1.17A is an absorption spectrum of the native B890 antenna complex from *R. rubrum*. Fig 1.17B is a spectrum of an acetone/methanol extract of the complex. The Qy band and carotenoid bands are positioned further to the red in the native complex. This suggests that the chromophores are involved in specific interactions with other molecules.

*R. rubrum* contains only one type of antenna complex, which because of the position of the near-infrared BChl band is termed a B890 complex (B=Bulk pigment). Equivalent complexes are found in *Rps. viridis*, *Rps. acidophila* and *Chr. vinosum* [Cogdell, 1987]. The exact wavelengths of their Qy maxima do vary slightly but they are grouped together as B890 complexes for convenience. Other species of purple photosynthetic bacteria (e.g. *Rps. palustris* and *Rb. sphaeroides*) contain similar antenna complexes which have near-infrared maxima at 875nm. B890/B875 complexes are closely associated with the reaction centre and if required they can be isolated together as a B890/B875-reaction centre "core" complex. Unless otherwise stated B890 or B875 is used as a generic term to describe the core antenna complexes.

Another type of antenna complex can be isolated from the photosynthetic membranes of most species (*R. rubrum* and *Rps. viridis*



**Fig. 1.17** Absorption spectra of the B890 antenna complex from *R. rubrum* (left) and its organic solvent extract (right). In the intact antenna complex the carotenoid absorbs at about 20nm further to the red than in the extract. The BChl Soret and Qx peaks absorb at roughly the same wavelengths but the BChl Qy band is red-shifted in the intact complex by about 120nm.

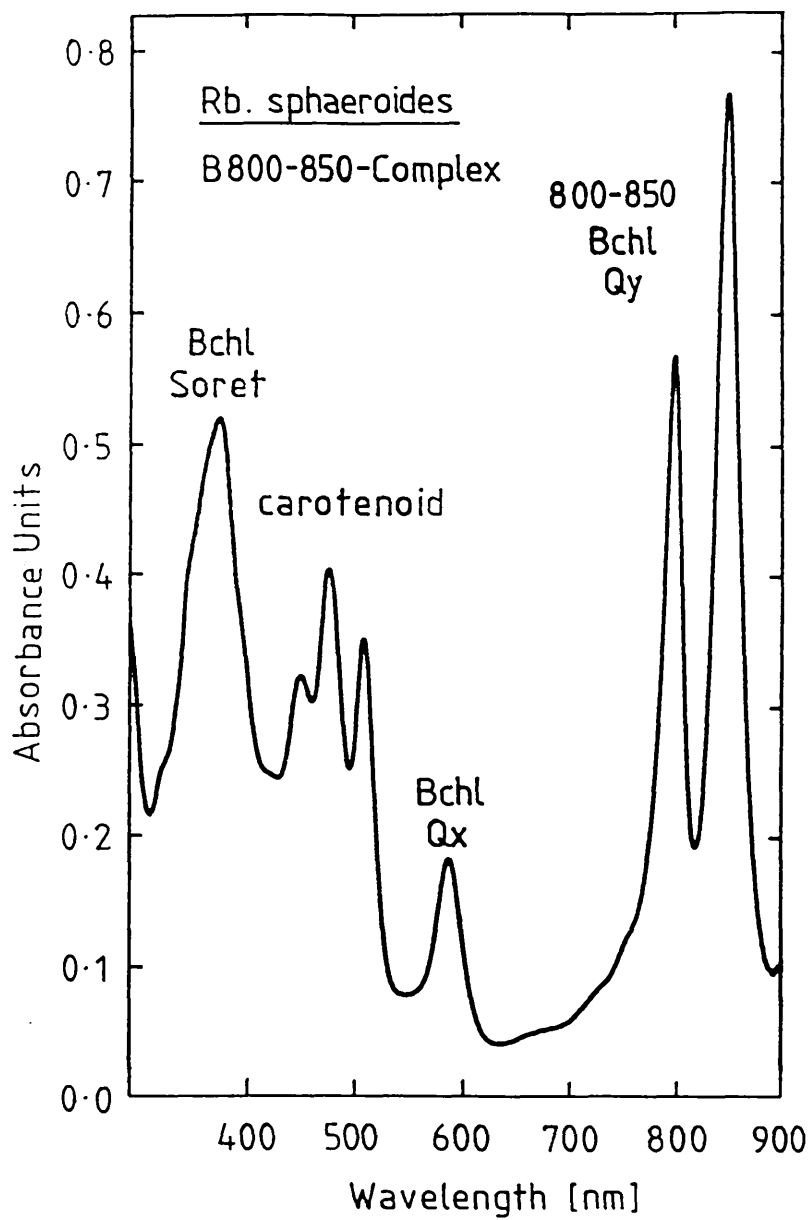


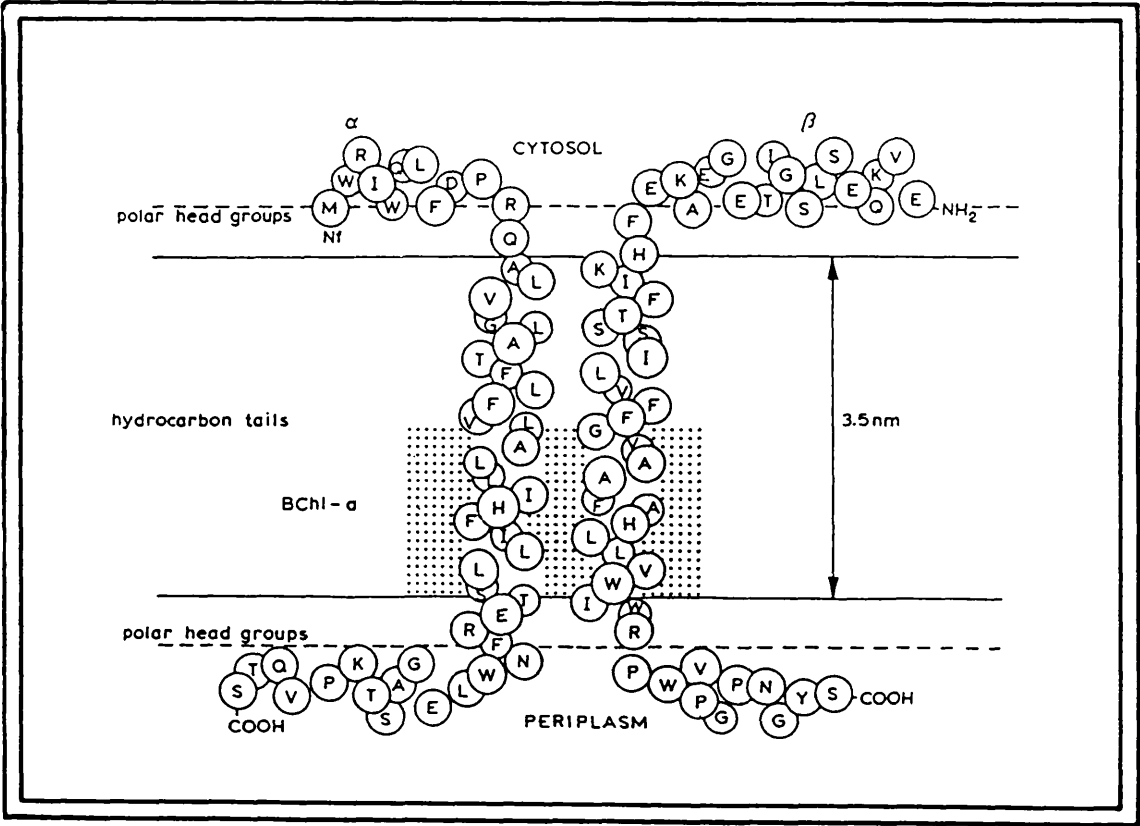
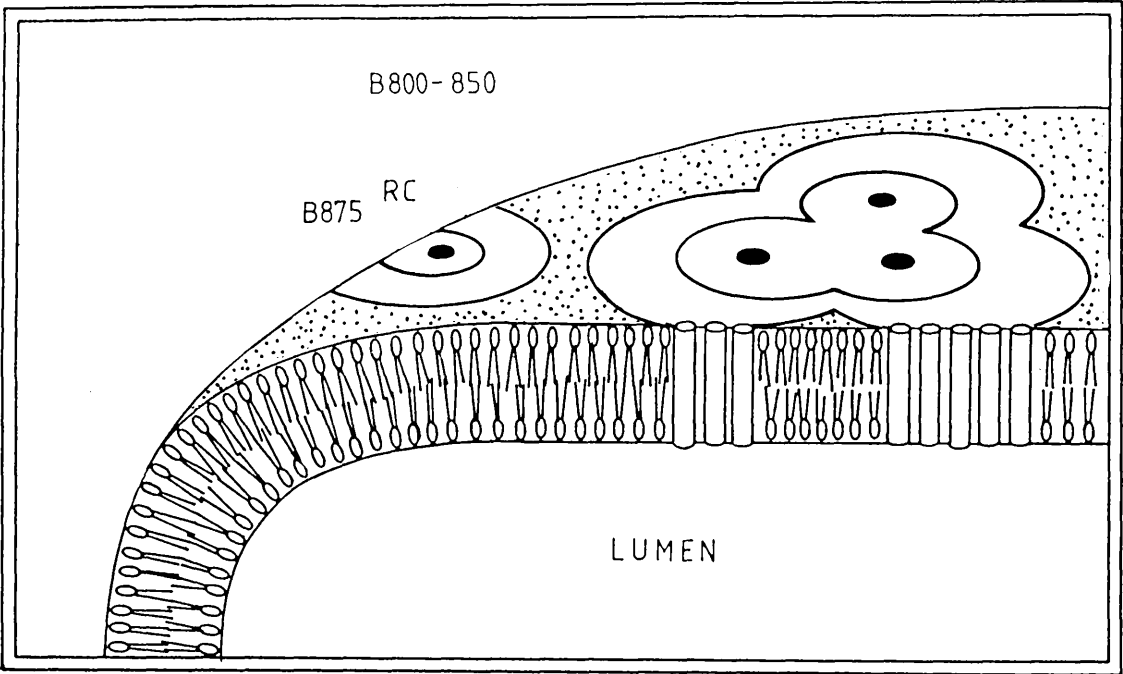
Fig. 1.18 Absorption spectrum of B800-850 antenna complexes from *Rb. sphaeroides*.

are some exceptions). An absorption spectrum of this type of complex has two Qy BChl bands positioned at about 800nm and 850nm (Fig. 1.18). "B800-850" antenna complexes are arranged peripherally around the core B890 complexes and deliver excitation energy to them. Fluorescence studies have demonstrated that excitation energy within a B800-850 complex can be delivered to any one of several reaction centres in what has become known as the "lake model" [Monger and Parson, 1977]. The photosynthetic unit (i.e. minimal functional unit of light-harvesting and trapping) therefore consists of several reaction centre cores surrounded by a shared B800-850 antenna (Fig. 1.19). This may improve the efficiency of light trapping because if an "exciton" of energy reaches a reaction centre which is already performing photochemistry and therefore "closed", it may be able to migrate to a neighbouring reaction centre.

Purple photosynthetic bacteria respond to a reduction in light intensity in several ways: (1) by the synthesis of additional photosynthetic membrane (2) by increasing the density of photosynthetic units within the membrane, and (3) by expansion of the B800-850 complex relative to the core [Clayton, 1980; Firsow and Drews, 1977]. *Chr. vinosum*, strain D, [Thornber, 1970] and *Rps. acidophila*, strain 7050, [Cogdell et al., 1983; Thornber et al., 1984], additionally respond to low light intensities by incorporating new types of complexes into the membrane and by possibly changing the conformations of existing ones. The "low light" (LL) B800-850 complexes have an 850nm BChl absorption band (B850 chromophore) equal to, or lower than the 800nm band (B800). These complexes have been named B800-850 Type II complexes [Thornber, 1986] (see chapter three for details). The normal "high light" (HL) complexes have an 850nm band about one and half times as intense as the 800nm band. These complexes are called the B800-850 Type I complexes (Fig. 1.18). At low light intensities these two species also synthesise

Fig 1.19 "Lake model" for the arrangement of the photosynthetic unit. Reaction centres are interconnected by a lake of B875 complexes. Energy is donated to the B875 complexes by peripheral B800-850 complexes.

Fig. 1.20 Model for the arrangement of antenna apoproteins of the B890 complex of *R. rubrum*. proposed by Brunisholz et al. (1986).  $\alpha$ - and  $\beta$ -subunits traverse the membrane as an  $\alpha$ -helix, and polar domains protrude on either side. The BChl dimer is co-ordinated to two histidine residues in the periplasmic leaflet of the membrane. (For a key to the one-letter amino acid codes see Fig. 1.21.)



an entirely new type of complex with BChl Qy absorption maxima at 800 and 820nm. These are called B800-820 complexes. It is not yet known whether B800-850 Type II complexes are structurally different to B800-850 Type I complexes or if these are a mixture of existing Type I complexes and another component such as B800-820 complexes which have not been separated by the isolation methods employed. This can only be determined by investigating the polypeptide compositions of the different complexes. The B890 complexes are present in a fixed stoichiometry of 20-40 BChls per reaction centre, irrespective of the growth conditions [Aagard and Sistrom, 1972; Dawkins et al., 1988]. The B800-850 and B800-820 "variable" complexes are thought to contain 50-300 BChls per reaction centre depending on the growth conditions.

Some evidence has been presented for the presence of a proportion of special "trapping", long-wavelength absorbing components in the B890 antenna type. Fluorescence polarisation and low temperature circular dichroism (CD) measurements on *R. rubrum* chromatophores detect the presence of an antenna component absorbing at about 905nm which forms an integral part of the antenna and which can accept energy from the main B890 pigments [Borisov et al., 1977; Kramer et al., 1984b; Razjivin et al., 1978]. A similar conclusion was drawn By Sebban et al., (1984) and Kramer et al., (1984b) for *Rb. sphaeroides*. This high-wavelength antenna component is purported to constitute 15% of the total B890 antenna complex of *R. rubrum*.

#### 1.7(ii) The molecular structure of antenna complexes

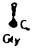
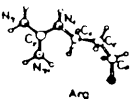

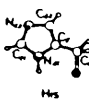
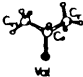
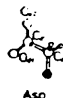

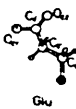
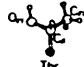
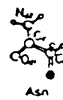
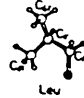
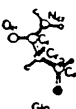
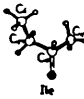
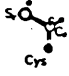
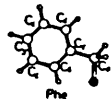
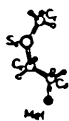
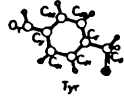
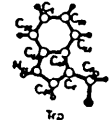
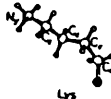
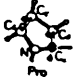
Near-infrared CD measurements on isolated antenna complexes indicate that the 890nm absorption band of B890 complexes results from excitation of an exciton-coupled (i.e. energy shared) BChl dimer [Vredenberg and Ames, 1967; Miyazaki and Morita, 1981; Sauer and

Austin, 1978; Cogdell and Scheer, 1985]. B800-850 antenna complexes are shown to contain an exciton-coupled dimer which is the 850nm chromophore, and a monomeric BChl which is the 800nm chromophore.

During the last eight years many light-harvesting antenna polypeptides have been sequenced. Comparison of their conserved amino acid sequences has invited speculation about the binding sites and amino acid environments of the BChl molecules which may play an important part in determining the magnitude of the Qy band red shift. The first antenna apoprotein to be sequenced was a B890 complex polypeptide from *R. rubrum* [Brunisholz et al., 1981; Gogel et al., 1983]. A second apoprotein was isolated and sequenced later [Brunisholz et al., 1984] confirming reports that the complex contains two different polypeptides [Oelze and Golecki, 1975; Moskalenko et al., 1978]. The apoproteins proved to be smaller than was suggested by SDS polyacrylamide gel electrophoresis (10-14 kD) with molecular weights of 6097 and 6101 g.mol<sup>-1</sup> [Brunisholz et al., 1984; 1986]. Hydropathy plots (see chapter six) suggest that antenna apoproteins can be divided into three domains: a central hydrophobic domain of 20-23 amino acids, a polar N-terminal domain and a polar C-terminal domain. Protease digestion experiments have confirmed that the N-terminal region of the antenna polypeptides lies on the cytoplasmic side of the photosynthetic membrane and that the C-terminal region extends into the periplasm [Brunisholz et al., 1986]. The antenna polypeptides therefore span the membrane with the hydrophobic domain lying within the lipid interior. From ultra violet circular dichroism (CD) and infrared (IR) spectroscopy it is predicted that the hydrophobic stretch is in the form of an  $\alpha$ -helix, 31-34 Å long [Cogdell and Scheer, 1985]. Breton and Navedryk (1984) have suggested from IR dichroism studies that the  $\alpha$ -helices lie at 30-35° to the membrane normal. Combining some of this data a model for the B890 complex of *R. rubrum* has been proposed by Brunisholz et al. (1986) (Fig.

1.20). The one-letter amino acid codes are given in Fig. 1.21. By comparing the antenna apoprotein sequences of *R. rubrum* with those of *Rps. viridis* [Brunisholz et al., 1985], *Rb. sphaeroides* [Theiler et al., 1984], *Rb. capsulatus* [Tadros et al., 1983], *Rc. gelatinosus* [Brunisholz et al., 1982] and *Rps. acidophila* [Bissig et al., 1988; Youvan and Ismail, 1985; Youvan, 1984] regions of homology can be determined. (For discussions of the comparative analysis of antenna polypeptides see: Zuber, 1986; Zuber et al., 1985; Zuber, 1987; Zuber, 1985.) One striking feature is the occurrence of conserved histidine residues within the hydrophobic stretch of the membrane. Histidines are rarely found within hydrophobic domains of proteins. One of the antenna polypeptides in the pair, designated  $\alpha$ -, contains one conserved histidine residue near the periplasmic side of the membrane. The other polypeptide in the pair, designated  $\beta$ -, contains two histidine residues, one in a similar position to the  $\alpha$ -subunit histidine and the other near the cytosolic surface of the membrane. The presence of the conserved histidine residues has led to the suggestion that the BChl dimer is non-covalently liganded between the two adjacent histidines and that the monomer interacts with the second histidine on the  $\beta$ -subunit. The inferred positioning of the BChl molecules in B800-850 complexes is corroborated by fluorescence measurements which suggest a separation of 21Å [van Grondelle, 1982]. The presence of coordinate bonds between the central magnesium atom of BChl and a nitrogen atom orbital of histidine amino acids has been demonstrated by high resolution diffraction pattern analysis of crystals of the water-soluble BChl a-protein complex of the green bacterium *Prosthecochloris aestuarii* [Fenna and Matthews, 1975; Fenna et al., 1977; Pearlstein, 1987].

Resonance Raman spectroscopy has been used to probe the vibrational interactions of the BChl chromophores in isolated antenna complexes

	glycine	[G]		arginine	[R]
	alanine	[A]		histidine	[H]
	valine	[V]		aspartate	[D]
	serine	[S]		glutamate	[E]
	threonine	[T]		asparagine	[N]
	leucine	[L]		glutamine	[Q]
	isoleucine	[I]		cysteine	[C]
	phenylalanine	[F]		methionine	[M]
	tyrosine	[Y]		tryptophan	[W]
	lysine	[K]		proline	[P]

**Fig. 1.21** Key to the one-letter, and two-letter amino acid codes [IUPAC-IUB Joint Commission on Biochemical Nomenclature (1984)]

[Robert and Lutz, 1985]. The data were interpreted as evidence that ground state dimers of BChl are not found in antenna complexes, whether formed directly or via hydration. The concept of B890/B850 chromophores being dimers is therefore a concept of their electronically excited states so there is no physical bond between them. The data confirmed that the magnesium atom of the BChls has five ligands, four of which are presumably coordinated to the dihydrophorbin ring. The fifth ligand is therefore coordinated to an external structure. By comparing the Raman spectra of imidazole-BChl models with those of the antenna complexes, Robert and Lutz concluded that the B890/B850 chromophores are liganded to histidine residues. However, a different Raman spectrum was found for the B800 chromophores which has been interpreted as meaning that the B800 BChls are not coordinated to histidine residues as has been suggested.

#### **1.7(iii) Bathochromicity of the *in vivo* BChl Q<sub>y</sub> absorption bands**

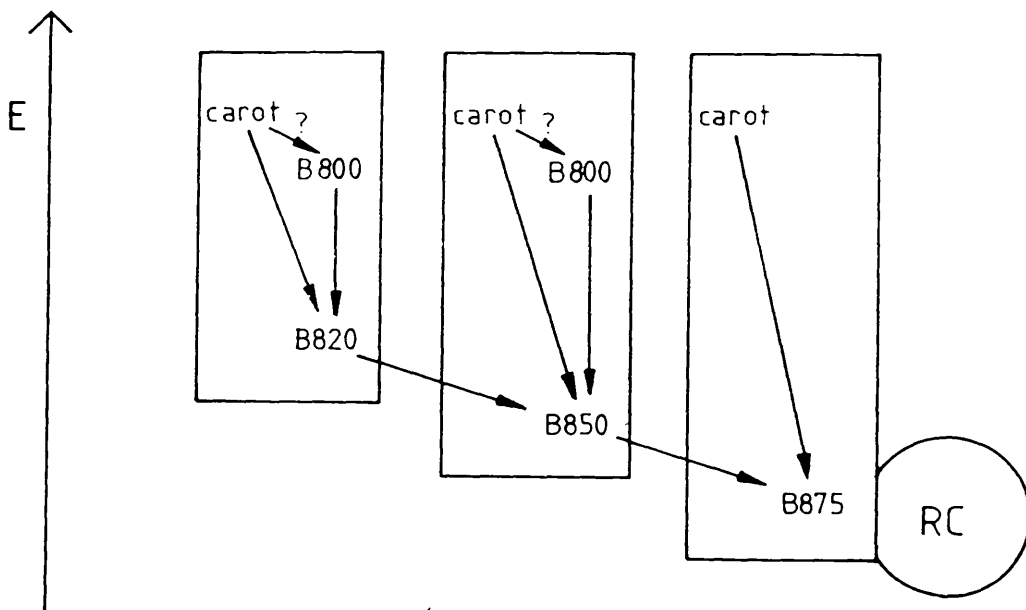
Katz and Wassink (1939) first reported that different species of purple bacteria have different near-infrared absorption spectra. It was originally believed that the different near-infrared absorption bands were due to absorption by different antenna complexes [Wassink, 1939], but we now know that a single antenna type can have multiple near-infrared absorption maxima.

In different complexes the same BChl a molecule can absorb at almost any wavelength between 800 and 890nm. Those species containing BChl b have Q<sub>y</sub> absorption bands typically at 800, 830 and 1020nm [Englehardt et al., 1983]. The *in vivo* near-infrared maxima observed in detergent-solubilised antenna complexes are a property of the specific interactions of the BChl with its native environment. The presence of pigment-protein complexes which absorb at different wavelengths is of functional importance in the transfer of energy to the reaction centre.

The route of BChl energy transfer within a photosynthetic unit of low light grown *Rps. acidophila*, strain 7050, is shown in Fig. 1.22. Because the energy of an electronic transition is inversely proportional to the absorption wavelength, the transfer of energy from the outermost, B800-820 complex to the reaction centre is an energetically downhill, favourable process. The mechanism of energy transfer within, and between antenna complexes will be discussed in section 1.8.

Many factors can alter the wavelength at which the Qy bands absorb e.g. the strain of bacterium, the carbon and electron sources, growth conditions and the age [Thornber et al., 1978]. Wavelength shifts have also been noted during detergent solubilisation of antenna complexes e.g. 5nm and 12nm blue shifts in LDAO extracts from *Rb. sphaeroides*, wild-type, and R-26 carotenoidless mutant respectively [Clayton and Clayton, 1972; Reed 1970].

*In vitro*, BChl and Bpheo oligomers have been formed in small Triton X-100 and LDAO detergent micelles [Gottstein and Scheer, 1983; Scherz and Parson, 1984; Scherz et al., 1986; Cotton et al., 1978]. The oligomers have Qy bands which can absorb at wavelengths as high as 880nm. It is thought that their pyrrole rings III overlap, giving rise to exciton coupling, and inducing the red shift. However, in very dry, non-nucleophilic solvents aggregation does not occur [Cotton et al., 1978; Katz et al., 1977]. It has been proposed that during aggregation nucleophiles, such as solvent hydroxyl groups, form lone-pair coordinate bonds with the central magnesium atom of one of the chlorophylls. The solvent can then hydrogen-bond the keto group on ring V of the second chlorophyll to form the aggregate. Hanson and Hofrichter (1985) formed water-free phaeophorbide a crystals which had red shifts high enough to account for the *in vivo* Qy BChl forms, by just  $\pi - \pi$  orbital interactions.



**Fig. 1.22** Pathway of energy transfer to the reaction centre in the photosynthetic unit of low light grown *Rps. acidophila*, strain 7050. "E" refers to the energy required for an electronic transition into the first excited singlet state.

Although this evidence demonstrates that *in vitro* BChl molecules can form oligomers resulting in a red shift, resonance Raman spectroscopy has indicated that such oligomerisation does not occur *in vivo* (section 1.7(ii)). This does not however dismiss the overlap of excited state wavefunctions of closely positioned molecules.

There is some evidence to suggest that interactions with carotenoids can effect a bathochromic shift in the Q<sub>y</sub> maximum [Griffiths et al., 1955]. The wild-type *R. rubrum* antenna complex has a Q<sub>y</sub> maximum at 881nm whereas the G9<sup>+</sup> carotenoidless mutant strain absorbs maximally at 873nm [Parkes-Loach et al., 1988]. The  $\alpha$ - and  $\beta$ -apoproteins of these complexes have identical amino acid sequences [Brunisholz et al., 1984], so the wavelength difference seems to be associated with the carotenoid, assuming that the wavelengths were recorded accurately.

Finally it is also possible that the bathochromicity is partly due to BChl-protein interactions, especially with charged or aromatic amino acids. The evidence for BChl-histidine ligation has already been discussed. With rare exceptions both the N-terminal and C-terminal polar domains of antenna polypeptides contain clusters of two to four conserved aromatic residues. The B800-850 Type I complexes from strains 7050 and 7750 have identical absorption spectra. Although there are some differences in primary structure, there is a conserved cluster of aromatic amino acids in the C-terminals of the  $\alpha$ -apoproteins. i.e. Tyr<sub>44</sub>-Trp<sub>45</sub> [Brunisholz and Zuber, 1987]. When strain 7050 is grown under low light intensity it synthesises a B800-820 complex, which has a different aromatic cluster: Phe<sub>44</sub>-Leu<sub>45</sub>. In the B800-820 complex of low temperature grown 7750 cells, the cluster is replaced by Phe<sub>44</sub>-Thr<sub>45</sub>. As these are the only major differences in the C-terminal regions of the polypeptides it is suggested that the aromatic amino

acids are specifically responsible for the variation in the Qy band absorption maxima of these complexes.

An interesting explanation for the variation in the wavelength at which the core antenna complexes absorb (i.e. at either 875 or 890nm) has been suggested from comparison of the primary sequences of the polypeptides. The B890 antenna complexes have strong near-infrared CD spectra [Thornber, 1986; Cogdell and Scheer, 1985]. These complexes also have an aromatic phenylalanine residue on the C-side of the conserved histidine of the  $\alpha$ -apoprotein (Fig. 1.23A). The C-terminal ends of the  $\beta$ -subunits contain pairs of "extreme turn" proline residues which may interact with nearby tyrosine/tryptophan residues (Fig. 1.23B). B875 complexes exhibit weak Qy band CD spectra in the near-infrared region. The  $\alpha$ -apoproteins of these complexes do not have aromatic residues adjacent to the histidines, and the  $\beta$ -chains are eight or more residues shorter and so do not contain the proline turns found in the complexes with strong CD spectra.

In the water-soluble BChl a-binding protein complex of *Prosthecochloris aestuarii*, which is the only antenna complex structure determined to atomic resolution [Fenna and Matthews, 1975], both BChl-BChl and BChl-aromatic amino acid interactions are present. This complex is however quite different to the hydrophobic antenna complexes of purple bacteria.

Parkes-Loach et al. (1988) have described a remarkable experiment in which they separated the  $\alpha$ - and  $\beta$ -apoproteins of the carotenoidless mutant, *R. rubrum*, strain G9<sup>+</sup> by organic solvent extraction, and then reconstituted the BChl-protein complex into detergent-lipid micelles. The Qy absorption spectra and CD spectra of the reconstituted complexes were identical to those of the native complex. Using this technique it may be possible to study the effects of the protein environment on the

<u>B880-<math>\alpha</math></u>									
			*						
1	...	A	L	L	I	H	F	I	L
2	...	A	L	L	I	H	F	G	L
3	...	A	L	I	I	H	F	I	A
4	...	A	V	L	I	H	L	M	L
5	...	A	V	M	I	H	L	I	L
6	...	A	V	L	I	H	L	I	L
<u>B 880-<math>\beta</math> C-end</u>									
1	..	R	P	W	V	(P)	G	(P)	N
2	..	R	P	W	I	A	(P)	I	(P)
3	..	R	P	W	I	(P)	G	(P)	K
4	..	R	P	W	L				
5	..	R	P	W	F				
6	..	R	P	W	F				

) STRONG NIR-  
 CD SIGNAL  
 ) WEAK NIR-  
 CD SIGNAL  
 ) STRONG NIR  
 CD SIGNAL  
 ) WEAK NIR-  
 CD SIGNAL

Fig. 1.23 C-terminal sequences of  $\alpha$ - and  $\beta$ -polypeptides from a representative selection of species. (From Brunisholz et al. (1988)).

BChl absorption spectrum by reconstituting antenna complexes from different polypeptide mixes.

In summary, the observed bathochromicity of the BChl Qy bands is probably due to a combination of different BChl interactions. The BChl-BChl interaction in the B850 dimer will induce a red shift of unknown magnitude. The coordinate ligation of both the dimer and monomer to histidine residues will alter the first excited state wavefunctions of the BChl and induce a red shift. And finally, the presence of aromatic amino acids in the environment of the antenna BChls may play a role in "fine tuning" the near-infrared absorption maxima.

#### 1.7(iv) Antenna polypeptide sequence homology

An overall comparison of the sequences of antenna polypeptides shows low homology (7-13%) between  $\alpha$ - and  $\beta$ -subunits indicating an early separation of their genes during the course of evolution [Zuber, 1986]. The homology between  $\alpha$ -subunits of the B890/875 and B800-850 complexes is higher (13-28%), the same being true for the  $\beta$ -subunits. Equivalent polypeptides in different species show a homology of 32-78%. Three antenna complexes are reported to contain a third non-pigmented  $\gamma$ -polypeptide. They are the B1015 complex of *Rps. viridis* [Brunisholz et al., 1985], the analogous complex in *Ectothiorhodospira halochloris* and the B800-850 complex of *Rb. capsulatus* [Bolt et al., 1981; Feick and Drews, 1978]. The  $\gamma$ -polypeptide of *Rps. viridis* is only 36 amino acids long and is more hydrophobic than the  $\alpha$ - or  $\beta$ -subunits. The  $\gamma$ -polypeptide of *Rb. capsulatus* has an apparent molecular weight of 14000 g.mol<sup>-1</sup>. The role of non-pigmented polypeptides is uncertain. It has been suggested, with particular reference to the BChl *b*-containing species, that they act as linker polypeptides between adjacent  $\alpha/\beta$ -subunit pairs. This may account for the observation of ordered

hexameric arrays seen in electron micrographs of some BChl b-containing species [Englehardt et al, 1983].

The B800-820 complex of low temperature grown *Rps. acidophila*, strain 7750, unusually contains two  $\beta$ -type polypeptides [Brunisholz et al., 1987]. This will be discussed in chapter six, in relation to the B800-850 complex of *Rps. palustris*, strain French, which also has an unusual polypeptide composition.

#### 1.7(v) Pigment stoichiometry

B890/875 complexes contain one BChl dimer per  $\alpha/\beta$ -polypeptide pair whereas B800-850 complexes contain a dimer and a monomer giving a stoichiometry of 3 BChls per polypeptide pair [Sauer and Austin, 1978; Broglie et al., 1980; Picorel and Gingras, 1988]. The ratio of BChl to carotenoid appears to be antenna-type specific. B875 complexes are believed to have ratios of 1:1 [Broglie et al., 1980; Bachman et al., 1983] but B890 complexes are believed to have ratios of 2 BChl a to 1 carotenoid [Picorel et al., 1983; Ueda et al., 1985; Cogdell et al., 1982]. B800-850 Types I and II, and B800-820 complexes are reported to have ratios of 3:1 [Thornber, 1970; Cogdell et al., 1983]. The pigment ratios of these complexes have been reassessed and will be discussed in detail in chapters four and five where it is proposed that some of the accepted ratios are incorrect.

#### 1.7(vi) Pigment orientation

The position of the carotenoid molecules in antenna complexes is unknown. They are non-covalently bound and can be reconstituted into complexes isolated from carotenoidless mutants, to reinstate both the energy transfer and photoprotective functions [Davidson and Cogdell, 1981]. To act as photoprotectors the carotenoids must be positioned

$\leq 0.5\text{nm}$  from the BChl molecules. Zuber et al. (1985) suggest that the carotenoid may be located within short  $\alpha$ -helical regions of the  $\alpha$ - and  $\beta$ -polypeptides at the N-terminal side of the membrane. Brunisholz et al. (1986) found differences in the action of proteases on the N-terminal domains of the apoproteins of *R. rubrum* wild-type and the carotenoidless mutant strain G9<sup>+</sup>, which they suggest indicates that the carotenoid may lie in this region.

From fluorescence polarisation and linear dichroism studies, Breton et al. (1984) have proposed a model in which the porphyrin ring of the BChl 800nm-absorbing monomer lies almost parallel to the plane of the membrane, and perpendicular to the carotenoid. The porphyrin rings of the 850nm-absorbing BChls also lie perpendicular to the plane of the membrane and it is proposed that they are orientated so that their Qy transition moments are mutually perpendicular. Fluorescence polarisation measurements indicated that the Qy transition moments of B850 BChls are circularly degenerate within the plane of the membrane. Kramer et al. (1984a) repeated some of these measurements on the B800-850 complex of *Rb. sphaeroides* and measured a positive fluorescence polarisation upon excitation into the Qx band. From this they envisage energy transfer between at least two B800 chromophores and describe a model in which the "minimal unit" of the antenna complex comprises two  $\alpha/\beta$ -polypeptide pairs, 2 BChl B850 dimers and 2 BChl B800 monomers (Fig. 1.24). From a number of theoretical assumptions (e.g. the rate constant of B800-B800 energy transfer) they calculated a monomer-monomer distance of 18-19 Å. Their fluorescence polarisation measurements indicate that some of the carotenoid lies approximately parallel to the membrane and that some is orientated in the plane of the membrane normal. In the same study Kramer et al. measured the efficiency of energy transfer from carotenoid to BChl in the B800-850 complexes of *Rb. sphaeroides* and compared it to that of complexes treated with lithium

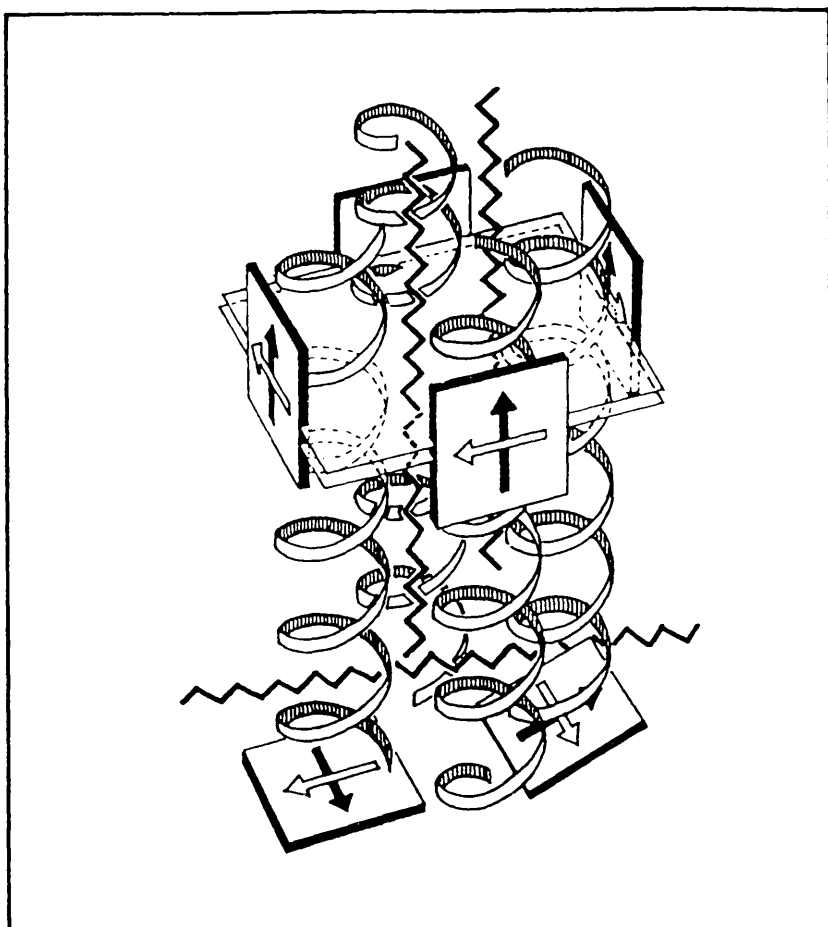


Fig. 1.24 Model of the minimal aggregate of the B800-850 complex of *Rb. sphaeroides* proposed by Kramer et al. (1984a). Two BChl B850 dimers are positioned in a square, orientated parallel to the membrane. Qy dipoles are represented by open arrows and Qx dipoles are represented by block arrows. Two BChl monomers lie approximately perpendicular to the plane of the membrane. A BChl-to-carotenoid stoichiometry of 2:1 was used for the model. Two carotenoids (zig-zags) lie perpendicular to the plane of the membrane and deliver energy to the BChl dimer. A third carotenoid lies in the plane of the membrane and delivers energy to the BChl monomer. The periplasmic side of the model is at the top of the diagram.

dodecyl sulphate (LDS). LDS causes a reversible hypochromic shift (reduction) of the 800nm absorption band, and a 15% reduction in energy transfer efficiency. This has also been demonstrated for B800-850 complexes from *Rps. acidophila*, strain 7750 [Chadwick et al., 1987]. From the reduction in  $A_{800}$  and the reduction in energy transfer efficiency, it was calculated that one third of the energy is transferred to B800, purportedly from a carotenoid pool orientated in the membrane normal, and that the remaining two thirds is transferred to the dimer from a separate pool of carotenoid positioned parallel to the plane of the membrane. Unfortunately it seems as though it will be difficult to validate the Kramer et al. hypothesis by other experimental methods. Recently the rates of energy transfer from carotenoid to B820, and from B800 to B820, have been measured for the B800-820 antenna complex of *Rps. acidophila*, strain 7750 [Gillbro, T., Cogdell, R.J. and Sundstrom, V., unpublished]. The transfer time from carotenoid to B820 was determined to be about 3ps and the transfer time from B800 to B850 was an order of ten faster. This means that the concentration of excited B800 will always be very low so it will be difficult to detect B800\* as an intermediate in the transfer of energy to B820.

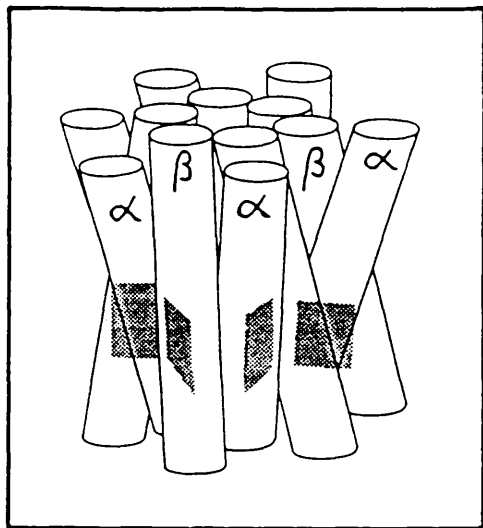
#### 1.7(vii) The arrangement of antenna polypeptide aggregates

Electron microscopy and image processing, of photosynthetic membranes from *Rps. viridis* suggest that the B1015 complex has a hexagonal arrangement around the reaction centre [Stark et al, 1984; Englehardt et al, 1983]. Assuming a 30° tilt of the  $\alpha$ -helices [Breton and Navedryk, 1984] a speculative model for the circular arrangement of  $\alpha/\beta$ -apoprotein pairs has been proposed [Zuber, 1986; Zuber et al., 1985] (Fig. 1.25). The model envisages an aggregate which forms a left-handed superhelix; the individual apoproteins interacting at the centre.

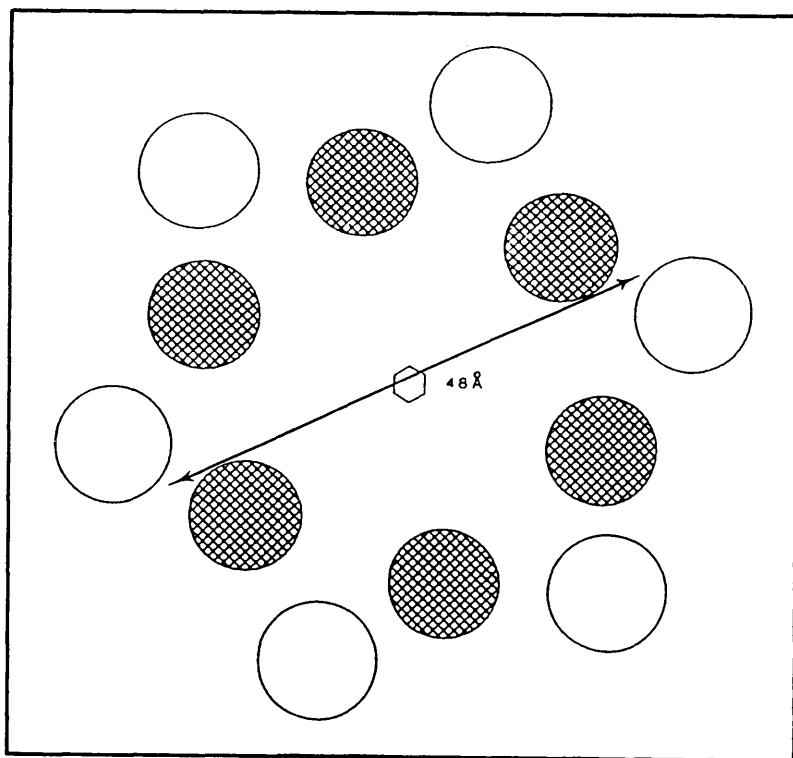
Fig. 1.25 Speculative model of the arrangement of  $\alpha/\beta$ -polypeptide aggregates proposed by Zuber (1986). The  $\alpha$ -helices of the polypeptides are tilted about  $30^\circ$  to the membrane normal, and are arranged in a hexameric aggregate.

Fig. 1.26 The arrangement of the minimal intact structural unit of the B800-850 antenna complex of *Rps. acidophila*, strain 10050, from x-ray diffraction data with a resolution of  $12\text{\AA}$ . The polypeptides are arranged in a hexameric aggregate. Blank circles represent  $\alpha$ -polypeptides, hashed circles represent  $\beta$ -polypeptides. The diameter of the aggregate is  $48\text{\AA}$ . The helices are positioned approximately perpendicular to the membrane.

de  
es  
a



he  
ay  
re  
/-  
of  
ly



Preliminary x-ray diffraction data, with a resolution of 12Å, supports a cyclic, hexameric arrangement for the minimal functional unit of antenna complexes (Fig. 1.26) [Papiz, M., Hawthornthwaite, A., Lindsay, J.G. and Cogdell, R.J., unpublished]. Such a hexameric aggregate would have a molecular weight approximately equal to the 84kD which is close to that estimated from density-gradient centrifugation.

From exciton theory, Pearlstein and Zuber (1985) have proposed that such a regular arrangement of structural units is not necessary for efficient Förster energy transfer. In two dimensions, the Förster mechanism appears to be "rather insensitive to the details of regular structure" [Knox, 1977]. Pearlstein and Zuber speculate that the ordered pigment clustering proposed for the light-harvesting complexes may have a function other than to maximise the efficiency of Förster migration. They suggest that this may be a mechanism of storing excitons within the hexameric units.

## **1.8 The Mechanism of Energy Transfer Within Antenna Complexes**

### **1.8(i) Introduction**

When an antenna pigment absorbs a photon the pigment becomes excited. It then returns to its ground state giving up its energy in one of four ways: (1) by transfer to a neighbouring pigment molecule (2) by radiative fluorescence emission (3) by intersystem crossing and radiative phosphorescence, and (4) by non-radiative heat loss. These processes compete with each other and the proportion of energy dissipated by each mechanism is dictated by the chemistry and geometry of the pigments. At any instant the intensity of the fluorescence emitted from a particular pigment type within a photosynthetic unit indicates the proportion of excited molecules in that pigment type [Clayton, 1980]. This is because each excited molecule has a certain

probability per unit time of emitting a quantum of fluorescence. By measuring the fluorescence at different wavelengths which correspond to the different pigment types, the distribution of excitation can be determined either in steady state under constant illumination, or on a transient timescale using picosecond flash photolysis. Time-resolved studies can be used to investigate the rates of each of the above competing processes and by implication, provide information about the mechanisms of energy transfer.

### 1.8(ii) Fluorescence measurements in antenna complexes

When a population of  $N$  pigment molecules is excited, the rate of de-excitation is given by:

$$\frac{dN}{dt} = - (k_f + k_{nr} + k_{et})N \quad (1)$$

where,  $k_f$ ,  $k_{nr}$ , and  $k_{et}$  are the rate constants (probabilities) of de-excitation by radiative fluorescence emission, non-radiative decay and energy transfer to another molecule respectively [Clayton, 1980; Cowan and Drisko, 1976]. The actual observed lifetime of an excited population is denoted by:

$$\tau = \frac{1}{(k_f + k_{nr} + k_{et})} \quad (2)$$

A lifetime is the time taken for a population of  $N$  molecules to become de-excited to  $N/e$  excited molecules, where  $e$  is the base number of natural logarithms. A high rate constant for one of the pathways of de-excitation means that the probability of this pathway being chosen is high compared to the probabilities of the competing pathways.

The quantum yield of fluorescence [Clayton, 1980; Cowan and Drisko,

1976] i.e. the proportion of molecules decaying by the fluorescence route is given by:

$$\phi_f = \frac{k_f}{(k_f + k_{nr} + k_{et})} \quad (3)$$

Correspondingly the energy transfer efficiency is given by:

$$\phi_{et} = \frac{k_{et}}{(k_f + k_{nr} + k_{et})} \quad (4)$$

If fluorescence emission is the only route available for deexcitation, the lifetime, known as the intrinsic fluorescence lifetime [Clayton, 1980], is represented by:

$$\tau_f = 1 / k_f \quad (5)$$

Combining equations (2), (3) and (5), a linear relationship is obtained which describes how the actual, and the fluorescence lifetimes are proportional to the fluorescence yield:

$$\phi_f = \tau / \tau_f \quad (6)$$

The quantum efficiency of energy transfer between two chromophores can be determined either by picosecond flash photolysis experiments or by measuring fluorescence under constant illumination (i.e. a steady state of excitation-deexcitation). The use of steady-state fluorescence measurements to determine the efficiencies of energy transfer from carotenoid to BChl in several types of antenna complexes is described in chapter seven.

### 1.8(iii) Energy transfer between carotenoid and BChl

The rate of energy transfer between two pigments is governed by a matrix element ( $U_{DA}$ ) which is itself defined by the initial ( $\phi_i$ ) and final ( $\phi_f$ ) wavefunctions, and the coulombic interaction between them ( $V_{DA}$ ):

$$U_{DA} = \langle \phi_i | V_{DA} | \phi_f \rangle$$

$U_{DA}$  has two contributions [van Grondelle, 1985]. One of these, called the Coulomb term is labelled  $U_{DA}^C$ . The other, electron-exchange term is labelled  $U_{DA}^{ex}$ . These two contributions represent two different mechanisms of energy transfer for which there are different geometric constraints. When the Coulombic term for two chromophores is large energy transfer between them is described by the Förster equation [Förster, 1948]. When the electron-exchange term for two chromophores is large the energy transfer can be described by the Dexter electron-exchange equation [Dexter, 1953].

Energy transfer between carotenoid and BChl can proceed with quantum efficiencies approaching 100% [Cogdell et al., 1981]. To obtain such high efficiencies the carotenoid and BChl molecules must be orientated in very specific way so that the carotenoid dipole lies parallel to the plane of the porphyrin ring at a distance of  $\leq 4\text{\AA}$  [Moore et al., 1980; Dirks et al., 1980]. At this distance the mechanism of energy transfer can be either that described by Förster or Dexter. The different constraints for each mechanism will be described below followed by a discussion of the current opinion regarding which of these mechanisms actually operates to transfer energy from carotenoid to BChl.

#### (a) Förster Mechanism

Förster energy transfer is envisaged when vibronic coupling between the donor and acceptor energy states is very weak [van Grondelle, 1985].

An electron in the donor molecule is excited into a high vibrational energy state (Frank-Condon overlap) and then relaxes into a low vibronic state before energy transfer occurs. A Coulombic interaction between the excited state of the donor molecule and the acceptor molecule induces the transfer of energy between the two, and an electron in the acceptor becomes excited simultaneously with the donor returning to its ground state (Fig. 1.27). The rate of Förster energy transfer between the donor (D) and acceptor (A) [Förster, 1948] can be simplified to the following form [Knox, 1975; 1986]:

$$k_{DA} = \frac{1}{\tau} \cdot \left( \frac{\bar{R}_O}{R_{DA}} \right)^6$$

The equation describes how the rate varies inversely with the observed donor lifetime ( $\tau$ ). This can be measured directly by picosecond absorption spectroscopy. The rate also varies with the sixth power of the separation of the donor and acceptor molecules ( $R_{DA}$ ). Finally the rate varies with the sixth power of  $\bar{R}_O$ . This is in turn determined by four factors:

- (1) The fluorescence yield of the donor molecule.
- (2) The orientations of the two molecules: it is proportional to the cosine of the angle between the dipoles. This is maximal for parallel dipoles and zero for mutually perpendicular dipoles. It is also proportional to the cosine of the angle each dipole makes with a line joining their centres. These angles can be measured by linear dichroism or polarised fluorescence spectroscopy.
- (3) The refractive index of the medium.
- (4) The overlap of donor fluorescence emission, and acceptor absorption spectra: If the absorption spectrum of the acceptor pigment is re-plotted as the molar absorption coefficient against wavenumber

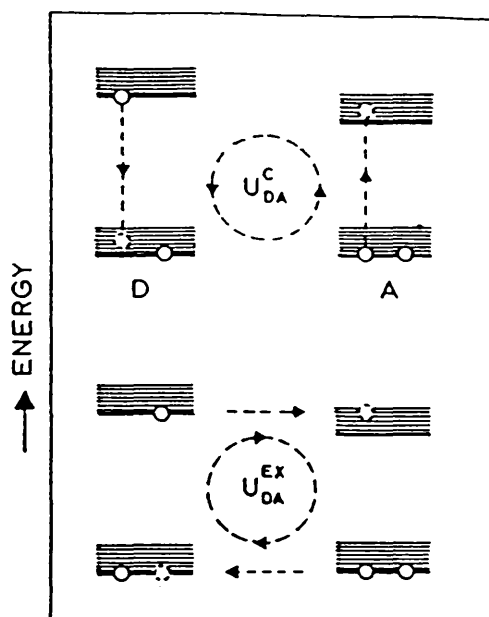


Fig. 1.27 Diagram illustrating the two mechanisms of pigment-pigment energy transfer. Förster transfer (upper) results from a strong coulombic interaction. An excited electron in the donor molecule returns to its ground state while simultaneously an electron in the acceptor undergoes an upward transition. With Dexter transfer (lower) electrons are exchanged between the donor and acceptor molecules. (From van Grondelle, 1985.)

(k) ( $k = \text{wavelength}^{-1}$ ) and the normalised fluorescence emission spectrum of the donor is added to the plot, the integrated area of overlap of the two spectra can be calculated. The value  $\bar{R}_O$  is proportional to this area so the greater the area of overlap the higher is the probability that the transition will take place.

(b) **Dexter electron-exchange mechanism** The Dexter energy transfer mechanism operates when there is strong vibronic coupling between the donor and acceptor molecules. i.e. vibrational relaxation of the donor may be incomplete before energy transfer takes place. Förster energy transfer may operate over distances as great as 100 Å. In contrast the Dexter mechanism can only operate when the excited state electron orbitals of the donor molecule physically overlaps with the ground state orbitals of the acceptor molecule [Cowan and Drisko, 1976]. This means that the two molecules must lie very close together ( $R_{DA} \leq 0.5\text{nm}$ ) [Dexter, 1953]. The rate constant of electron-exchange energy transfer is given by:

$$k_{et} = \left( \frac{2\pi}{\hbar} \right)^2 (U_{DA})^2 \int F_D(\nu) \epsilon_A(\nu) d\nu$$

where  $\hbar = \text{Planck's constant}/2\pi$ , and the integral expression describes the overlap integral of the donor fluorescence ( $F_D(\nu)$ ) and acceptor absorption ( $\epsilon_A(\nu)$ ) spectra on a wavenumber scale [van Grondelle, 1985]. The value of  $U_{DA}$  decreases exponentially with the donor-acceptor distance and depends on the orientation of the donor-acceptor dipoles but is independent of their dipole strengths.

As the name implies, in Dexter exchange energy transfer electrons are actually exchanged between the donor and acceptor molecules (Fig. 1.27). The distance between the B800 monomers and B850 dimers of B800-

850 complexes has been estimated by fluorescence measurements to be 21Å which is consistent with their proposed polypeptide binding sites [van Grondelle, 1982]. The distances between the BChls of neighbouring antenna units are probably even larger suggesting that the Förster mechanism is used for BChl-BChl excitation transfer.

Which of these mechanisms actually operates to transfer energy from the carotenoid to the BChl in antenna complexes is still uncertain, although some recent evidence has swayed the argument in favour of the Dexter mechanism. Experimental evidence for a Dexter transfer mechanism between carotenoids and BChl comes from estimation of the distance-dependence of the energy transfer efficiency. The distance-dependence of Förster transfer was confirmed experimentally by Stryer and Haugland (1967) for two chromophores linked by a polymer which could be synthesised in various lengths. The energy transfer efficiency from one chromophore to the other was measured as a function of distance (Fig. 1.28). The distance-dependence was calculated to be  $d^{-5.9}$  which agrees extremely well with that described by the Förster equation.

The distance-dependence of energy transfer between carotenoids and chlorophyll derivatives in model systems has been estimated by experiment. Liddell and coworkers (1982) reported that unless the carotenoid and chlorophyll were in close proximity the energy transfer between them is insignificant. Wasielewski et al. (1986) synthesised model caroteno-pyropheophorbide molecules with different distances between the  $\pi$ -orbitals of the two chromophores. With a distance of 5Å the carotenoid to pyropheophorbide energy transfer efficiency, measured by picosecond flash photolysis, was found to be less than 5%. With a distance of 2Å the efficiency was 53%. A comparison with the distance-dependence plot for Förster transfer implies that the distance-dependence is too strong for a Förster mechanism to operate between

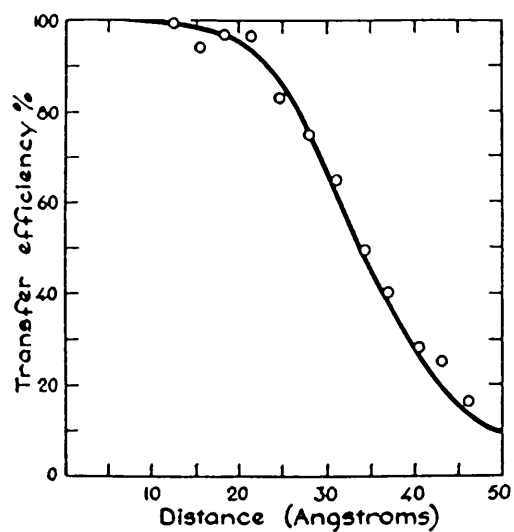


Fig. 1.28 The relationship between energy transfer efficiency and intermolecular distance for Förster energy transfer. (From Stryer and Haugland, 1967)

carotenoid and BChl. The measurements indicate that as soon as the  $\pi$ - $\pi$  donor-acceptor orbitals no longer overlap the energy transfer falls off rapidly.

Triplet-triplet energy transfer by the Förster mechanism is doubly forbidden by selection rules [Cowan and Drisko, 1976] so for carotenoids to offer photoprotection to antenna BChls, a triplet-triplet electron-exchange mechanism must operate [van Grondelle, 1985; Razi-Naqvi, 1981]. As electron-exchange already operates for transfer from BChl to carotenoid, it seems likely that it can also operate for singlet-singlet transfer in the other direction.

It is also argued that the very low fluorescence yields of carotenoid give reason to doubt whether carotenoids can efficiently transfer energy by the Förster mechanism [Razi-Naqvi, 1980; Cogdell and Frank, 1987, van Grondelle, 1985]. The fluorescence yield of  $\beta$ -carotene has recently been determined to be  $6 \times 10^{-5}$  [T Gillbro and R J Cogdell, unpublished]. In contrast the fluorescence yield of Chl a has been measured to be 0.33 [Clayton, 1980]. Whether this argument is accepted or not depends upon the exact interpretation of the Förster equation as different photophysical parameters can be exchanged into the equation. The rate equation for electron-exchange transfer does not contain an expression for the fluorescence yield of the donor so the low fluorescence yields of carotenoids would not disqualify them from this mechanism of energy transfer.

## **MATERIALS AND METHODS**

## 2.1 Culture Storage

Cell cultures were maintained in agar stabs at room temperature and under low light. Additional stock cultures were prepared in 50% (w/v) glycerol, which acts as a protein stabiliser [Scopes, 1982], and were maintained at -70°C.

## 2.2 Cell Culture

*R. rubrum*, strain S1, *Rb. sphaeroides*, strain 2.4.1 and *Rps. palustris*, strain French, were grown photoheterotrophically at pH 6.8 with sodium succinate as the sole carbon source [Bose, 1963]. *Rps. acidophila*, strains 7750 and 7050, were grown photoheterotrophically at pH 5.2, in Pfennig's medium [Pfennig, 1969]. *Rps. palustris* was grown from a culture of unknown lineage obtained from Dr Bruno Robert, Saclay, France, and was termed strain "French". *Rb. sphaeroides* mutant strain M2192 cells were provided by Dr Neil Hunter, University of Sheffield.

*Chr. vinosum*, strain D, was grown photoautotrophically at pH 7.8, with sodium hydrogen carbonate as the carbon source and sodium thiosulphate as the electron donor [Pfennig, 1967]. For the chemical compositions of growth media see Appendix E.

Liquid starter cultures were prepared from agar stabs and grown in 25ml McCartney bottles positioned between arrays of 100 and 150 Watt incandescent electric light bulbs in a temperature controlled growth room. Cells were routinely grown with a local temperature of 30°C and illuminance flux of about 16000 lux. After 1-2 days, during the log phase of growth, the cultures were transferred to 500ml flat-sided, screw capped bottles. If large quantities of cells were required, the bottle cultures were transferred to 10 litre stoppered flasks. Cells

grown at low light intensities were illuminated by a single 40W incandescent light bulb providing an illuminance flux of about 400 lux. Cells cultured above 30°C were grown in thermostatically controlled waterbaths. Cells cultured below 30°C were grown in a cool room illuminated by fluorescent strip lights, and with a stream of cold air directed onto the bottles.

Axenic cell cultures were maintained by aseptic transfer techniques [Stanier, 1976] and their purity was checked by occasionally selecting single colonies grown on agar plates for subsequent transfer into liquid culture.

### 2.3 Cell Counting and Measurement of Growth

Calibration curves of cell concentration versus absorbance measured at 650nm (where light scattering is proportional to cell number) were first plotted. A dilution series of freshly harvested cells were prepared in a solution of glycerol/iodine 1:1 (v/v). Cell concentrations were estimated by counting on a haemocytometer slide.

A fresh inoculum of cells was transferred aseptically to an ethanol-washed quartz spectrophotometer cuvette which was air-sealed with a tightly fitting stopper and sealing film. The absorbance at 650nm was measured against a blank of distilled water and the cuvette was transferred to a growth room. Absorbance measurements were recorded at intervals over several days. For direct comparison of high and low light grown cells, starter inocula were prepared with approximately equal cell concentrations. A small air gap was left in the cuvettes to mimic normal culture conditions.

## 2.4 Isolation of Photosynthetic Membranes

Cells were harvested from liquid culture during the log phase of growth by centrifugation at 2000xg for 100min, at 4°C. After resuspending in MES/KCl buffer, pH 6.8 (Appendix G), the cells were either used immediately or stored at -20°C until required. After addition of a little bovine pancreas DNAase I (Sigma) and magnesium chloride, the cells were broken open by a single passage through a French pressure cell at 154 MPa [French and Milner, 1955; Van der Rest and Gingras, 1974; Frenkel and Nelson, 1971]. For those species with lamellar-type photosynthetic membranes the procedure continued as follows [Cogdell et al., 1983]: The broken cell suspension was centrifuged at 12000xg for 15 min, and the supernatant further centrifuged at 180000xg for 1h. The pellets from both spins were combined and resuspended in 20mM Tris-HCl, pH 8.0.

For those species with vesicular photosynthetic membranes, chromatophores were prepared as follows. The broken cell suspension was centrifuged at 12000xg for 15min to pellet unbroken cells and cell wall debris which were discarded. The chromatophores were then harvested from the supernatant by centrifugation at 180000xg for 1h.

## 2.5 Solubilisation of Photosynthetic Membranes and Isolation of Crude Antenna Preparations

Vesicular-type photosynthetic membranes were solubilised with lauryl dimethylamine N-oxide (LDAO). The membranes were diluted to give a near-infrared absorption maximum of 50 cm<sup>-1</sup> for *Rb. sphaeroides* or 37.5 cm<sup>-1</sup> for *R. rubrum*. LDAO was then added to a concentration of 0.25% (v/v). After a dark incubation at room temperature for 30 min the membranes were centrifuged at 12000xg for 15 min. The pellets were kept and the supernatants centrifuged at 180000xg for 1h. Electronic

absorption spectra of the second supernatants were recorded to ensure the presence of reaction centres. The reaction centre-depleted pellets were combined with those of the first centrifugation and resuspended in 20mM Tris-HCl, pH 8.0, to give a near-infrared maximum of  $50 \text{ cm}^{-1}$ . LDAO was then added to a concentration of 1% and the preparation was incubated at room temperature for 10 min. Finally unsolubilised material was removed by centrifuging at 12000xg for 15 min and the LDAO concentration in the supernatant antenna preparation was reduced tenfold by dialysis.

A slightly different procedure was used to isolate crude antenna preparations from those species with lamellar-type intracytoplasmic membranes. The membrane suspension was adjusted to give a near-infrared maximum of  $50 \text{ cm}^{-1}$  by dilution with Tris-HCl, pH 8.0. It was then made to a final LDAO concentration of 1%. After a 20 min incubation at room temperature, unsolubilised material was removed by centrifugation at 12000xg for 15 min. The supernatant antenna preparation was then dialysed against 0.1% LDAO before storage.

## **2.6 Separation of B890, B800-850 and B800-820 Antenna Complexes**

Several methods were used for the purification of individual antenna complexes from a crude isolate. Because of the variation in properties of different complexes, not all of these methods work for every complex type.

### **2.6(i) Sucrose density-gradient centrifugation**

Sucrose density-gradient centrifugation is a universal method of separating a crude pigment-protein, detergent-stable preparation into B800-850 and reaction centre-B890 complexes [Garcia et al., 1966]. Sucrose gradients were prepared in 28ml polycarbonate centrifuge bottles

(Du Pont), in 6ml steps of 0.6, 0.4, 0.3 and 0.2 molar sucrose for *Rps. palustris* and 1.0, 0.5, 0.3 and 0.2 molar sucrose for *Rps. acidophila*. The sucrose solutions were prepared in Tris-HCl, pH 8.0, 0.2% LDAO. The gradients were centrifuged at 180000xg and 4°C, in a fixed angle rotor (Du Pont, Sorvall T 865) for at least 16 h. During the centrifugation the complexes separated into two bands as they move into the region of the gradient of equivalent density (see Fig. 3.5). The RC-B890-detergent-lipid micelles resolve from the less dense B800-850-detergent-lipid micelles. The individual bands were removed with a pasteur pipette and dialysed against Tris-HCl, 0.1% LDAO buffer. For further purification the individual bands were subjected to a second gradient run.

## 2.6(ii) DEAE anion-exchange chromatography

This method was used to separate individual antenna complexes from *Rb. sphaeroides* and *Rps. acidophila*. Whatman DE52 diethylethyl-aminoethylcellulose (DEAE) exchanger was prepared in 10mM Tris-HCl, pH 8.0, and slowly poured into a sintered glass column to a height of 3-8cm. Several column volumes of buffer were run through the column to equilibrate the exchanger at the desired pH. The mixed antenna preparation was carefully loaded onto the column and followed by a further wash. Individual antenna complexes were eluted with increasing, stepwise concentrations of sodium chloride (e.g. 50, 100, 150, 200, 250mM), prepared in 0.1% LDAO buffer. Complexes elute in the order B875, B800-850 and B800-820. Separation of the different complexes can be followed by eye. Eluted complexes were collected in 1-2ml fractions, their electronic absorption spectra were recorded and spectrally pure fractions were pooled.

### 2.6(iii) Ammonium sulphate precipitation

Pigment-protein complexes from sodium dodecyl sulphate (SDS)-solubilised *Chr. vinosum* membranes were separated by ammonium sulphate precipitation [Green and Hughes, 1955; Scopes, 1982]. The precipitation was performed in a series of "cuts" according the following equation (adapted from Scopes, 1982) which includes a correction for the volume change incurred on addition of the salt:

$$\text{grams to add} = \frac{\text{vol (ml)} \times 1000(100 - 0.3S_2)}{533 (S_2 - S_1)}$$

$S_1$  and  $S_2$  are the initial and final ammonium sulphate % saturation concentrations respectively. Ammonium sulphate saturates at approximately  $4.05 \text{ mol.l}^{-1}$  at room temperature.

The precipitations were performed in 50mM Tris-HCl, pH 8.0, to buffer the slight acidifying action of the salt. After each salt addition the solubilised membranes were stirred slowly in the dark for 15-20 min and were then centrifuged for  $10^5 \text{ xg} \cdot \text{min}^{-1}$  (i.e. 10000 xg for 10 min), to pellet any precipitate. The required precipitates were redissolved in 20mM Tris-HCl, pH 8.0, and their absorption spectra were recorded. Finally samples were dialysed immediately into 1% deoxycholate for storage.

## 2.7 Pigment Isolation, Separation, Purification and Identification

### 2.7(i) General precautions

Photosynthetic pigments can be chemically altered in many ways. The correct procedures for handling carotenoids and chlorophylls to minimise the formation of unwanted alteration products are described by Goodwin (1965) and Britton (1985). Briefly, BChls were protected from high temperatures which can cause epimerisation to BChl a', and from the

presence of acid which causes phaeophytinisation, and from light which allows the photosensitisation of singlet oxygen. Carotenoid manipulations were performed in dim light to protect against cis-trans isomerisation and photooxidation. Where possible chromatographic procedures were carried out in total darkness. Pigments are most susceptible to photooxidative damage when they are adsorbed to a chromatographic material. All samples were stored under oxygen-free nitrogen, even for short periods. For longer periods of storage pigments were evaporated to dryness under nitrogen and stored at  $-20^{\circ}\text{C}$  in the dark. Home-made silica thin-layer chromatography (TLC) plates were made slightly alkaline by the addition of a pellet of potassium hydroxide.

For the preparation of samples for mass spectroscopy special precautions were taken. All solvents were doubly redistilled. Diethyl ether was redistilled over iron (II) sulphate to remove traces of peroxide radicals, and methanol was redistilled over potassium hydroxide. Redistilled solvents were further purified by passage through a column of activated alumina. Care was taken to prevent contact between solvents and plastics, which would otherwise result in contamination of the solvents with plasticisers.

## **2.7(ii) Extraction of photosynthetic pigments**

Pigments from whole cells and complexes were extracted with acetone and methanol, either used separately to extract carotenoids or BChl respectively, or together in a 7:2 (v/v) ratio to extract both. 1-3 ml of solvent was mixed with the preparation, which was then centrifuged in a low speed bench centrifuge. For qualitative work the supernatant of the first centrifugation, with a high water content, was normally discarded. Otherwise the total supernatant was pipetted into a snap-cap glass vial and stored under nitrogen in the dark. A second

volume of solvent was then mixed with the pellet and the process repeated two or three more times until the supernatant was colourless. For careful quantitative work a final extraction with warm ethanol was performed in an attempt to dislodge any polar carotenoids still bound to the pellet.

The total pigment extract was filtered through a pasteur pipette, plugged tightly with absorbent cotton wool to remove any particulate matter. This step is important if absorption spectra are to be recorded without scatter. The extraction of pigments from *Chr. vinosum* cells and complexes is particularly difficult because of the presence of a glutinous floc in the supernatant which can retain some of the pigment. This is revealed on filtering. The pigments can then be extracted properly from the filter with warm ethanol. The total extracts were either evaporated to dryness and stored, or used immediately.

### 2.7(iii) Preparation of a total pigment extract

An acetone/methanol total pigment extract was transferred to a separating funnel and a small volume of light petroleum (40-60°C bp) / dichloromethane 9:1 (v/v) was added along with a volume of distilled water twice that of the extract. The aqueous hypophase was removed and in quantitative work was further back extracted with light petroleum/dichloromethane and finally a volume of diethyl ether. The total carotenoid-containing epiphase was then washed several times with water. Water/organic emulsions at the interface were dispersed with either a few drops of acetone or a wash with warm saline solution.

A crude separation of BChl from carotenoid was achieved by partitioning with 90% methanol/water [Davies, 1965]. The BChl-containing aqueous hypophase was backwashed with light petroleum/dichloromethane and the combined carotenoid epiphase was

further partitioned to remove more BChl. The total carotenoid extract was then dried in a rotary evaporator and transferred to a glass vial.

## **2.7(iv) Alumina column chromatography of pigment extracts**

Stepwise elution alumina column chromatography was used as a first step in the purification of individual carotenoids from a total carotenoid extract [Goodwin, 1965]. The carotenoid sample, prepared by the above method was firstly dried by storage overnight with anhydrous sodium sulphate. 5-10g neutral alumina was mixed in a beaker with light petroleum and deactivated to grade III by the addition of 6% water (i.e. 600 $\mu$ l to 10g alumina). The alumina was ground with a glass rod and left for 10 min to ensure even distribution of the water. The alumina was then poured as a slurry into a sintered column and washed with light petroleum. 40-mesh glass beads were then added to the column surface to a height of about 0.5cm (see later) and the column was allowed to run almost dry before a small volume of concentrated sample was loaded. This was followed by a small volume (2-3 ml) of light petroleum. With concentrated samples some crystallisation occurs on the top of the column resulting in very diffuse bands and poor chromatography. Crystal formation was detected by the coloration of the glass beads, which do not adsorb carotenoids. The crystals were dissolved by the dropwise addition of dichloromethane to the top of the column. Chromatography was initiated by adding one or more column volumes of light petroleum followed by light petroleum/dichloromethane (9:1) and increasing proportions of diethyl ether (1%, 2%, 5%, 10%, 15% etc.). The dichloromethane was added because it dissolves carotenoids efficiently and prevents crystallisation on the column. The adsorption affinities of carotenoids on alumina increase with their increasing polarity, giving an elution order of: hydrocarbons, monomethoxy-, dimethoxy-, monohydroxy-, monohydroxymonomethoxy- and dihydroxy-carotenoids.

Polarity also increases slightly with increasing desaturation. The addition of carbonyl groups further increases the adsorption affinity, as does the presence of glucose residues in the special cases of carotenoid glucosides. Bacteriopheophytin (Bpheo) has an adsorption affinity which is approximately equal to that of monomethoxymonohydroxy carotenoids. BChl remains at the origin. Cytochromes have varying adsorption affinities and can easily be mistaken for carotenoids until their absorption spectra are recorded. Eluted carotenoid bands were evaporated to dryness and stored for further purification by thin-layer chromatography.

## **2.7(v) Thin-layer chromatography of pigments**

Whatman AL SIL G 0.25mm thin-layer silica gel plates were used for high resolution separation of small samples of carotenoid. For separation of larger samples 0.5mm home-made silica gel plates were prepared using 40g Kieselgel G (Merck), 80ml water and one pellet of potassium hydroxide. The plates were dried for at least an hour before use.

For a preliminary investigation of a carotenoid extract a TLC plate was first chromatographed in light petroleum (40-60 °C bp.) to detect the presence of hydrocarbons. The plate was then dried and run successively in 5%, 10%, 25%, 50% and 100% diethyl ether/light petroleum to estimate the polarities of the individual carotenoids [Goodwin, 1965]. For routine analysis of the spirilloxanthin series carotenoids a solvent system of light petroleum/dichloromethane/diethyl ether, 8:1:1 provided suitable resolution. To purify carotenoids for mass spectroscopy a further chromatographic step was employed with home-made TLC plates and an adsorbant of magnesium oxide/Kieselguhr (Merck) 1:1 (w/w). This adsorbant separates on the basis of the number of double

bonds in a molecule [Britton and Goodwin, 1971].

Carotenoids were recovered from TLC plates by quickly and carefully scraping off each individual band into a glass vial and eluting with one of, or a combination of diethyl ether, dichloromethane and warm ethanol. Samples were finally filtered through a pasteur pipette plugged with cotton wool.

#### **2.7(vi) Isolation and separation of carotenoid glucosides**

Carotenoid extracts from *Rps. acidophila* contain varying proportions of polar, water-soluble carotenoid glucosides [Heinemeyer and Schmidt, 1983; Schmidt et al., 1971]. These remained with BChl at the origin during thin-layer chromatography. To separate carotenoid glucosides the hydroxyl groups on the glucose residue were acetylated and the less polar carotenoid peracetates were chromatographed as before. The dry carotenoid was dissolved in 2-4ml dry pyridine with 0.1ml acetic anhydride/ml pyridine [Davies, 1976]. The vial was sealed under nitrogen and left in the dark at room temperature overnight. The acetylated sample was then transferred to a separating funnel and small volumes of water and diethyl ether were added. The aqueous hypophase was removed and backwashed quantitatively with diethyl ether. The ether epiphases were then combined and washed free of pyridine with water. The sample was evaporated to dryness aided by the addition of a few drops of ethanol. After redissolving in dichloromethane the sample was loaded onto a silica gel TLC plate and developed in 50% diethyl ether/ light petroleum. The carotenoid peracetates separated according to their polarities.

#### **2.7(vii) Identification of carotenoids**

Carotenoids were tentatively identified by their adsorption affinities on silica TLC and the shape and absorption maxima of their

electronic absorption spectra [Davies, 1965]. The identifications of the spirilloxanthin series carotenoids from *Rps. palustris* were confirmed by mass spectroscopy. An MS 902S high resolution double focusing spectrometer was used to provide mass spectra and elemental compositions. The carotenoid was delivered by direct probe insertion. The probe temperature was increased slowly from 180-250 °C to remove any volatile contaminants prior to carotenoid vaporisation. An electron beam energy of 70eV was used. Ten mass spectra were recorded over time and an average spectrum was calculated. Because the diagnostic carotenoid peaks appear above m/e 200, the spectra were normalised above this value before being plotted.

The spirilloxanthin series carotenoids from *R. rubrum*, *Chr. vinosum* and *Rps. acidophila* were positively identified by co-chromatography with the isolated carotenoids from *Rps. palustris*. The carotenoids from *Rb. sphaeroides* were identified from their absorption spectra and adsorption affinities during both silica TLC and reversed phase C<sub>18</sub> HPLC. The carotenoid glucosides were identified by reference to Schmidt et al. (1971).

## **2.8 Determination of the BChl-to-Carotenoid Ratios of Light-Harvesting Antenna Complexes**

### **2.8(i) HPLC method**

Aliquots (100-200 µl) of antenna complex (with near infra-red maxima = approx. 30cm<sup>-1</sup>) were extracted exhaustively with approximately 5ml acetone/methanol 7:2 (v/v) as previously described, and evaporated to dryness. The extracts were completely dissolved in 100-400 µl HPLC grade dichloromethane and 20 µl samples (containing approx. 10<sup>-9</sup> mol pigment) were injected immediately onto the column. The HPLC equipment

comprised Kontron LC-T414 pumps, Hewlett-Packard 85B interface and 1040A diode array detector. Suitable pigment separation was achieved with a Zorbax ODS (Du Pont) reversed phase  $C_{18}$  column (25 x 0.46cm) [Britton et al., 1987], and a 1ml/min flow rate and linear gradient of 0-100% B over 25min (A= Acetonitrile/water, 0.5% triethylamine; B= ethyl acetate). The triethylamine formed ionic bonds with any uncapped silyl groups in the column packing material preventing the opportunity for ion-exchange chromatography which would result in pigment band broadening. The time taken to prepare and run each extract was approximately 45 min.

To calculate the molar concentrations of each pigment eluted from the column it was necessary to first determine the absorption coefficients of each pigment in the eluting HPLC solvent mixture. The concentration of BChl used in the ratio determination was calculated from its Qx absorption band. Its millimolar absorptivity in acetone/methanol 7:2 (v/v) was first calculated from its peak height relative to that of the Qy band and the  $\epsilon_{772}$  value of  $76\text{mM}^{-1}\cdot\text{cm}^{-1}$  [Clayton, 1966]. Several absorption spectra of different BChl extractions were recorded and an average  $\epsilon_{590}$  value was determined to be  $18.5 \pm 2.0 \text{ mM}^{-1}\cdot\text{cm}^{-1}$  ( $\bar{x} \pm s$ ,  $n=3$ ). The millimolar absorption coefficient of BChl in the eluting HPLC solvent was then determined by recording the  $A_{\text{max}}$  of several samples in acetone/methanol, evaporating them to dryness, redissolving them in the same volume of eluting HPLC solvent and then by calculating the coefficient from the changes in  $A_{\text{max}}$ .

The millimolar absorptivities of the main carotenoids at their absorption maxima were similarly calculated from the following published  $\epsilon_{\text{1cm}}^{1\%}$  values: spirilloxanthin (at 499nm) 2500 in light petroleum [Liaaen-Jensen et al., 1971]; spheroidene (at 455nm), 2630 and spheroidenone (at 482nm), 2065 in acetone [Goodwin et al., 1956]. The final absorption coefficients used in the ratio determinations were:

BChl  $\epsilon_{580} = 17.4 \text{ mM}^{-1}.\text{cm}^{-1}$ ; spirilloxanthin  $\epsilon_{497} = 149 \text{ mM}^{-1}.\text{cm}^{-1}$ ; spheroidene  $\epsilon_{453} = 149 \text{ mM}^{-1}.\text{cm}^{-1}$  and spheroidenone  $\epsilon_{485} = 120 \text{ mM}^{-1}.\text{cm}^{-1}$ .

The diode array detector was programmed to monitor simultaneously the absorption at the absorbance maxima of each carotenoid and at the Qx band of BChl. The absorbance area of each pigment peak in the chromatogram was automatically integrated to give the total absorbance for each pigment. The molar concentrations of each pigment in the sample were then calculated using their millimolar absorptivities. For each ratio determination 10-27 different antenna extracts, prepared from more than one batch of cells, were used.

Before the final BChl-to-carotenoid ratios were calculated, the HPLC system was calibrated for pigment losses. BChl and carotenoids were isolated and spectrophotometrically-determined known amounts of each pigment were separately injected onto the column. The molar amounts of each pigment eluted from the column, according to the HPLC analysis, were then compared to the actual amounts injected and the apparent pigment losses were calculated. This was repeated 10-15 times for each major pigment.

## 2.8(ii) Carotenoid partition method

This method was used for the B890 complexes of *R. rubrum* and the B800-850 complexes of *Rb. sphaeroides*. Samples of antenna complex (0.5-3ml) were extracted into acetone/methanol as previously described. The concentration of BChl was determined spectrophotometrically at 772nm where there is no interference from carotenoid absorption. The total carotenoid was then isolated and dried overnight by the addition of anhydrous sodium sulphate, and a quantitative absorption spectrum was recorded in acetone/methanol 7:2 (v/v). Average absorption coefficients for the total carotenoid of a complex were calculated from the

carotenoid compositions, previously determined by HPLC, and the absorption coefficients of the individual carotenoids at the wavelength maximum of the total carotenoid spectrum. The calculation of average absorption coefficients is described in section 2.8 (iv).

The concentration of carotenoid was calculated using the spectrophotometric data and the average millimolar absorptivities determined to be: *R. rubrum*  $\epsilon_{497} = 158\text{cm}^{-1}$  and *Rb. sphaeroides*  $\epsilon_{455} = 145\text{cm}^{-1}$  in acetone/methanol.

### 2.8(iii) Difference spectroscopy method

This method was used for the B800-850 complexes of *Rb. sphaeroides* and the B890 complexes of *R. rubrum*. Samples of antenna complex (0.2-1ml) were extracted as before, filtered, dried and redissolved in dry acetone/methanol 7:2 (v/v). Absorption spectra were recorded to determine the molar concentration of BChl. A spectrum of BChl from an extract of the carotenoidless mutant, *Rb. sphaeroides*, R-26 was then recorded over the first spectrum. Increasing amounts of BChl were added to the sample cuvette until the absorption maxima at 772 and 590nm were identical to those in the extract of the antenna spectrum. The molar concentration of carotenoid was then determined from the antenna extract minus BChl extract, difference spectrum, at the carotenoid wavelength maximum, using average absorption coefficients determined in acetone/methanol.

### 2.8(iv) Simultaneous equation method

This method was used for B800-850 complexes from *Chr. vinosum*, *Rps. palustris* and *Rps. acidophila*, and for B800-820 complexes from *Rps. acidophila*. 0.2-1ml antenna complex was extracted and a quantitative absorption spectrum recorded in acetone/methanol. The molar concentration of BChl was determined spectrophotometrically from

the absorbance at its Qy band. The molar concentration of carotenoid was calculated after a number of steps to determine an average absorption coefficient for the total carotenoid complement of the complex and to correct for some BChl absorption at the wavelength maximum of the carotenoid:

(a) *determination of the carotenoid composition of an antenna complex.* 1-3ml of concentrated antenna complex were extracted and the carotenoid quantitatively isolated as previously described. The individual carotenoids were then separated by preparative TLC. Each band was scraped off, eluted with diethyl ether and filtered, and its absorption spectrum was quantitatively recorded. The amounts of each pigment were then determined from their published absorption coefficients and the percentage carotenoid composition calculated.

(b) *determination of an average absorption coefficient for the total carotenoid of an antenna complex.* The published absorption coefficients for each carotenoid were determined at specific wavelengths and in specific solvents. For the ratio calculations, an average coefficient in acetone/methanol 7:2 (v/v) and at the specific wavelength maximum of the total carotenoid was first required. Quantitative spectra of each individual carotenoid were recorded in the solvent used for the published value. The sample was then evaporated to dryness and redissolved in an equal volume of acetone/methanol. A second spectrum was then recorded. The new coefficient was calculated from the absorbance differences. This was repeated at least twice to obtain an average value. The average absorption coefficient in acetone/methanol was then calculated from:

$$(\sum (\% \text{ carotenoid}_i \times \epsilon_i \text{ at absorption max. in Ac/MeOH}) ) \div 100$$

Care was taken to record the absorbance values at the correct

wavelengths. A shift in wavelength of only 5nm can alter the calculated coefficient by as much as 10%.

(c) *determination of the BChl absorption coefficient in acetone/methanol at the wavelength maximum of the total carotenoid complement.* BChl was extracted from *Rb. sphaeroides*, R-26 and quantitative spectra were recorded in dry acetone/methanol. The absorption coefficient at the wavelength maximum of the total carotenoid was then calculated for several species, from the  $\epsilon_{772}$  value of  $76\text{mM}^{-1}.\text{cm}^{-1}$ , and the difference in peak heights. This was repeated nine times to obtain an average value of  $4.4 \pm 0.82$  ( $\bar{x} \pm s$ ) which was used for all antenna complex pigment ratio calculations.

(d) *calculation of the BChl-to-carotenoid ratio.* Simultaneous equations can be used to calculate the concentrations of each chromophore in a multicomponent absorption spectrum [Barnes and Waring, 1970; Segal, 1976]. With two chromophores and a cuvette path length of 1cm, the simultaneous equation is written:

$$A_1 = (\epsilon^{A1} \times C_{m_A}) + (\epsilon^{B1} \times C_{m_B})$$

$$A_2 = (\epsilon^{A2} \times C_{m_A}) + (\epsilon^{B2} \times C_{m_B})$$

where:  $A^1$  and  $A^2$  are the absorbances at wavelengths 1 and 2, and  $\epsilon^{A1}$  is the millimolar absorption coefficient of chromophore A at wavelength 1 etc.  $C_{m_A}$  is the millimolar concentration of chromophore A.

Carotenoids do not absorb at 772nm. Therefore for a mixture of BChl with an  $A_{\text{max}}$  at 772nm and total carotenoid with an absorption maximum at 500nm, the equation can be rearranged to read:

$$\frac{A_{772}}{\epsilon_{772} (\text{BChl})} \div \left[ \frac{A_{500} - \frac{A_{772}}{\epsilon_{772} (\text{BChl})} \times \epsilon_{500} (\text{BChl})}{\epsilon_{500} (\text{carot})} \right]$$

(e) *estimation of the absorption coefficient of cis-rhodopinal.*

The published absorption coefficient for cis-rhodopinal of 2300 [Aasen and Liaaen Jensen, 1967] is unreliable (see section 5.4 (ii)). An attempt to determine this coefficient from the more reliable coefficient of 3100 for trans-rhodopin [Aasen and Liaaen Jensen, 1967] was therefore made. Cis-rhodopinal was quantitatively reduced to cis-rhodopinol and then quantitatively isomerised to cis-rhodopinal. The absorption coefficient of trans-rhodopinol should also be 3100, so by measuring the absorbance changes, a back calculation should give the absorption coefficient for cis-rhodopinal.

The absorption coefficient of trans-rhodopinal was first determined by quantitative reduction of rhodopin to rhodopinol (see chapter five). A sample of rhodopinal was dissolved in a known volume of light petroleum and a quantitative absorption spectrum was recorded. This was evaporated to dryness and redissolved in the same volume of absolute ethanol. A few grains of sodium borohydride were added to the stoppered cuvette and after approximately 10 min when the effervescence had stopped and the colour change apparently complete, a repeat spectrum was recorded. Further spectra were recorded over short time intervals to ensure that the reaction was complete. On reduction the rounded spectrum of the carotenal molecule undergoes a large hypsochromic shift with an increase in absorbance and an increase in the degree of vibrational structure. Care was taken to ensure that the concurrent hyperchromic shift was due to the conversion to rhodopinol and not due to the evaporation of the solvent. On completion of the reaction the ethanol was evaporated and the sample redissolved in the same volume of acetone/methanol. A further spectrum was recorded over the first, and the absorption coefficient of cis-rhodopinal at 500nm (the wavelength used for quantitating *Rps. acidophila* carotenoid) in acetone/methanol

was calculated from peak height differences. The millimolar absorption coefficient of trans-rhodopinol is the same as that of trans-rhodopin. The  $\epsilon_{1\text{cm}}^{1\%}$  values were determined to be 2740 in ethanol and 2283 in acetone/methanol. For conversion to millimolar absorptivities the molecular weight of rhodopin ( $554 \text{ g.mol}^{-1}$ ) was used, giving average values of  $152 \text{ mM}^{-1}.\text{cm}^{-1}$  in ethanol and  $127 \text{ mM}^{-1}.\text{cm}^{-1}$  in acetone/methanol.

An attempt was made to estimate the absorption coefficient of cis-rhodopinal by measuring the absorbance change during quantitative isomerisation of trans-rhodopin. A quantitative spectrum was first recorded in acetone/methanol. A small iodine crystal was added to the sample in a stoppered vial which was sealed under nitrogen and left in direct sunlight for at least one hour. The carotenoid was then separated by silica TLC and the amounts of the cis- and trans-isomers were then determined quantitatively. This method proved unsatisfactory, however, because recovery from silica TLC was incomplete.

## **2.9 Isolation, Purification and Sequencing of Antenna Polypeptides**

### **2.9(i) Isolation of antenna protein**

B800-850 complexes from high and low light grown *Rps. palustris* cells were prepared by sucrose gradient centrifugation, and dialysis against distilled water. Whole cells and isolated antenna complexes were lyophilised and the total protein was extracted with dichloromethane/methanol 1:1 (v/v), made to 0.1M ammonium acetate, 5mM octadecathiol or dithiothreitol. The cell material was ground in a glass homogeniser and pelleted by a short, low speed centrifugation. The supernatant was pipetted off and the extraction repeated until the supernatant was colourless. For the complete extraction of more polar polypeptides 10% acetic acid must be added to the extraction buffer and

used throughout the separation [Brunisholz et al., 1981]. This was shown not to be necessary for *Rps. palustris* antenna extraction.

A sephadex LH60 gel filtration column (150 x 2.5cm) was prepared in dichloromethane/methanol 1:1 (v/v), 0.1 M ammonium acetate. 10ml extract was loaded evenly across the gel surface. The eluate was monitored by absorption at 280nm by an LKB Uvicord UV monitor and was collected in fractions. The extract components were eluted in the order: reaction centre M and L protein subunits, antenna apoproteins and finally carotenoid/BChl/lipid molecules. Samples of protein were stored for short periods under nitrogen at 4°C. For longer periods they were dialysed against distilled water in Spectra/Por 3 dialysis tubing, MW cut-off 3500 g.mol<sup>-1</sup> (Spectrum Medical Instruments Inc.). A precipitate forms at the interface between the water and the organic solvent phases which can then be scooped out of the dialysis tubing and lyophilised. The precipitate actually comprises a white precipitate and a yellow fatty precipitate. Both of these should be taken.

## 2.9(ii) Separation of $\alpha$ - and $\beta$ -polypeptides

Whatman DE32 anion exchange column packing material was prepared for chromatography as follows:

- 1) 50g DE32 was shaken with 100% ammonium acetate for 30min in a 1 litre stoppered bottle.
- 2) Ammonium acetate was removed by filter-washing with water to pH 7.0.
- 3) DE32 was shaken for 30min with 25% ammonia and washed to pH 7.0 as before.
- 4) DE32 was shaken with methanol for 10min and washed three times with dichloromethane/methanol 1:1.
- 5) One volume of dichloromethane/methanol 1:1, 0.1M ammonium acetate was added. The DE32 was allowed to settle and the fines were removed.

The DE32 was packed under nitrogen pressure into a sintered column (13 x 1.5cm). Extra care was taken not to let this packing material run dry. Antenna protein eluted from the LH60 column was loaded onto the DE32 column and  $\alpha$ -polypeptides were eluted with dichloromethane/methanol, 0.1M ammonium acetate buffer. Elution was monitored at 280nm as before. The  $\beta$ -polypeptides were eluted with 5% acetic acid added to the above buffer.

### **2.9(iii) FPLC analysis of antenna polypeptides**

Protein samples from the LH60 or DE32 columns were concentrated in a rotary evaporator and injected onto a reversed phase C<sub>8</sub> pro RPC column attached to a "Fast Protein Liquid Chromatography" system (Pharmacia). The separation was based on the principle of reversed phase ion-pair chromatography [Snyder and Kirkland (1979); Hancock et al., 1978]. With normal reversed phase chromatography, highly hydrophobic proteins such as antenna polypeptides are strongly retained with poor resolution. A hydrophilic counter-ion (e.g. trifluoroacetic acid, TFA) is added in low concentration (0.1%) to form ion-pairs with -NH<sub>3</sub> groups on basic amino acids. This leads to a net increase in charge on the protein and therefore a decrease in retention. TFA is recommended because it is volatile and is easily removed from protein samples by lyophilisation [Dunlap, et al., 1978]. Polypeptides were eluted with a 30-100% B linear gradient over 30 min (A= H<sub>2</sub>O, 0.1% TFA; B= CH<sub>3</sub>CN, 0.1% TFA). Elution was monitored at 280nm. Individual protein peaks were collected as separate fractions and lyophilised for quantitative amino acid analysis and sequencing.

### **2.9(iv) Polypeptide amino acid analysis**

200-250 $\mu$ g polypeptide in a small glass test tube was hydrolysed by

the addition of 6M HCl. The HCl was frozen by immersion in liquid nitrogen and degassed as it melted, by attachment of the test tube to a vacuum pump. The tubes were then sealed under vacuum with a hot flame and incubated at 110°C for 24 hr. The amino acid hydrolysate was then applied to a sulphonated styrene-divinylbenzene cation exchange resin in an automated amino acid analyser [Benson, 1975]. Amino acids were eluted from the column in the order of most acidic to most basic, using successive sodium citrate buffers of varying pH and concentration: asp, thr, ser, glu, pro (eluted with 0.2M citrate, pH 3.25), gly, ala, cys, val, met, ile, leu (eluted with 0.2M citrate, pH 4.25), tyr, phe, lys, his, arg (eluted with 0.35M citrate, pH 5.28). (For a list of the names of amino acids and their one-letter and three-letter codes see Fig. 1.21).

Eluted amino acids were reacted with ninhydrin reagent in a heated coil and detected by light absorption at 440nm and 570nm [Eveleigh, 1970]. The amount in nmol of the yellow, ninhydrin-proline complex in the sample was determined from the  $A_{570\text{nm}}$ . The amounts of the remaining blue, ninhydrin-amino acid complexes were determined from their  $A_{440\text{nm}}$  values. The analysis was calibrated by injection of a standard solution containing 10 nmol of each amino acid and by comparing the integrated absorbance areas with those of the sample. The amounts of amino acid were not corrected to zero time hydrolysis.

## 2.9(v) N-terminal amino acid sequence determination

(a) *automated sequential Edman degradation.* 0.5-1.0 mg purified antenna protein was reacted with 1M HCl in methanol for 2h. This was a precaution in case the N-terminal residue was formylated, which would have prevented N-terminal cleavage. Automated N-terminal amino acid sequence analysis was then performed by sequential Edman degradation

(Beckman 890C liquid-phase sequenator) [Edman and Beg, 1967; Edman, 1970; Brunisholz et al., 1985].

The protein was layered onto the wall of the spinning-cup of the sequenator. Phenylisothiocyanate, introduced to the spinning-cup, reacts with the N-terminal amino group of the polypeptide. The phenylthiocarbamyl derivative was then cleaved by the action of a strongly acid medium to form a thiazolinone derivative which was then collected in a test tube labelled with the amino acid residue number. The automated cycle of reagent additions to the spinning cup was repeated through seventy cycles and each thiazolinone derivative was collected separately.

(b) *conversion to PTH amino acids.* Each thiazolinone derivative was manually converted into its phenylthiohydantoin (PTH) amino acid derivative. 0.5ml of 1M HCl was pipetted into each thiazolinone-containing test tube. The tubes were then sealed under nitrogen and incubated at 90°C for 15 min. The PTH-amino acids (except water-soluble PTH-arg, PTH-his and PTH-cys) were extracted into a 0.5ml addition of ethyl acetate. The aqueous-ethyl acetate mixture was separated into two phases by a short centrifugation in a bench centrifuge. The ethyl acetate epiphase was pipetted into a screw-capped vial and the extraction was repeated. The total ethyl acetate extract was dried in a dessicator under high vacuum. The aqueous hypophase fractions were stored at room temperature.

(c) *identification of PTH-amino acids.* PTH-amino acids were identified by their HPLC retention times using a detection wavelength of 269nm. Each derivative was dissolved in 50-150  $\mu$ l HPLC solvent. An aliquot of each was chromatographed with two different isocratic solvent systems:

- 1) For the separation of all non-polar amino acids except arginine and histidine: Whatman P-5PAC stationary phase; mobile phase prepared

with 2.5l dichloromethane, 100ml methanol, 20ml dimethylsulphoxide, 5-100  $\mu$ l TFA (depending on the required pH adjustment).

- 2) For the separation of polar amino acids: Lichrosorb SI60 (Merck) stationary phase, isocratic mobile phase prepared from 2.5l dichloromethane, 100ml methanol, 20-30ml of 200g isopropanol/3g dimethylsulphoxide.

Each HPLC run took approximately 5min. If no PTH-amino acid was detected in the ethyl acetate epiphase fraction of the conversion reaction, the aqueous hypophase was then dried. Any protein in the fraction was redissolved in the following solvents: 2l dichloromethane, 100ml methanol, 5g ammonium acetate and 50ml 1,4-dioxan. An aliquot was then injected onto a Whatman P-5PAC HPLC column to look for the presence of water-soluble PTH-cys and PTH-arg.

Confirmation of the presence of the labile derivatives PTH-ser and PTH-thr was obtained by repeating the HPLC with solvent system (2) and a detection wavelength of 323nm which detects the PTH-amino acid degradation products.

#### **2.10 Determination of the Singlet-Singlet, Carotenoid-to-BChl Energy Transfer Efficiencies of Antenna Complexes**

Singlet-singlet, carotenoid-to-BChl energy transfer efficiencies were determined using a home-made scanning fluorescence spectrometer (Fig. 2.1). B800-850 complexes from 30°C and 40°C grown *Chr. vinosum* were prepared in Tris-HCl buffer, pH 8.0, 0.3% (w/v) sodium dodecyl sulphate (SDS). Low and high light grown *Rps. palustris* B800-500 and B880 complexes were prepared in Tris-HCl, pH 8.0, 0.05% LDAO. Quantitative absorption spectra of the antenna complexes from 400-600nm were first recorded, in a quartz fluorescence cuvette. The cuvette was

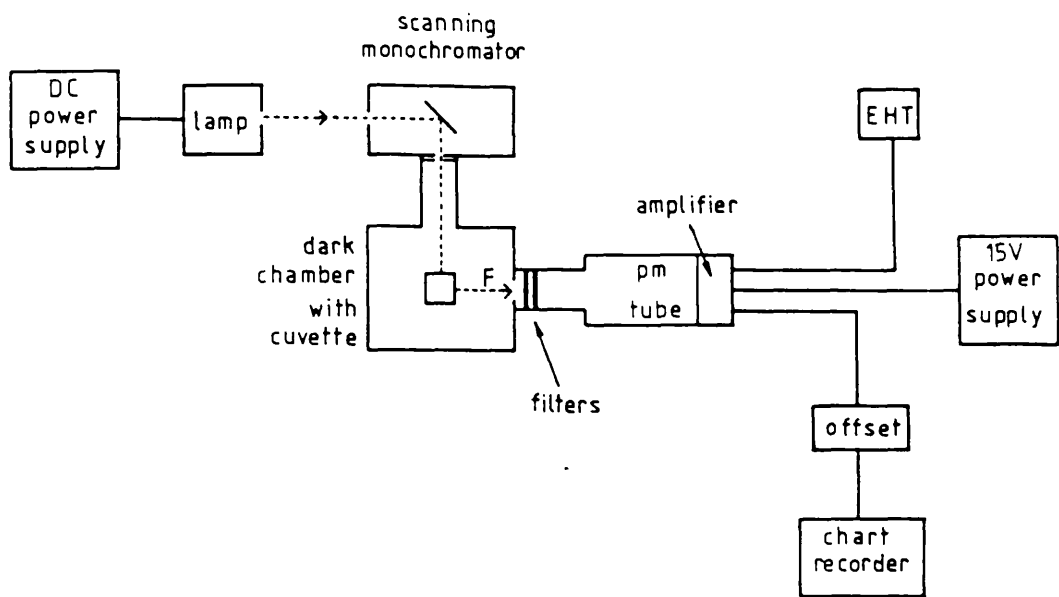


Fig. 2.1 Block diagram of the home-built fluorescence spectrometer.

then positioned in the dark chamber. The scanning monochromator was switched on to deliver a scan of exciting light from 400-620nm. The relative fluorescence emission, expressed in millivolts, was recorded during the 400-620nm scan for which the x-axis wavelength scale was calibrated to be identical to that of the initial absorption spectrum ( $20\text{nm}\cdot\text{cm}^{-1}$ ). BChl Qy band fluorescence was detected by an EMI 9659QB photomultiplier with a S20 window, positioned perpendicular to the incident light. A 700nm high pass red filter, and either a 858nm (for B800-850 complexes) or 913nm (for B890 complexes) interference filter (Balzer) was positioned at the photomultiplier tube window to ensure that only true BChl fluorescence was recorded. 1000-2000V EHT (Brandenberg power supply) was supplied to the photomultiplier which was also connected to a 15V stabilised operational amplifier.

Blank baseline spectra were recorded without the light source after each run. The carotenoid-to-BChl energy transfer efficiency was then calculated in a number of steps (see chapter seven for theory):

- 1) The absorption spectrum from 400-620nm was plotted at 5nm intervals as a fractional absorption spectrum.  
i.e. y-axis =  $100 - \% \text{ transmission}$ .  
( $\% \text{ transmission} = (1/\text{antilog } A) \times 100\%$ )
- 2) The exciting lamp emission spectrum was recorded from 400-620nm by a light meter and a radiometric, flat-response diode detector positioned at the cuvette holder. The spectrum was then tabulated as height against wavelength at 5nm intervals.
- 3) The relative fluorescence emission spectrum of the antenna complex was recorded and tabulated as in (2). The height at each 5nm interval was then divided by the height in (3) to normalise the fluorescence spectrum.
- 4) The height of the fractional absorption maximum at the BChl Qx band

was divided by the Qx maximum value calculated in (3).

- 5) Each value obtained in (3) was then multiplied by the result of (4) to normalise the fluorescence emission and fractional absorbance spectra.
- 6) Normalising the fluorescence emission spectrum and the lamp emission spectrum means that the excitation energy effectively remains constant throughout the fluorescence emission wavelength scan. As a result excitation at 590nm results in more quanta being absorbed than with excitation at the carotenoid wavelengths. In turn the number of quanta absorbed by the three carotenoid vibrational peaks increases from lower to higher wavelength. Corrections must therefore be used to calculate the final efficiency measurements. The correction factor is proportional to the energy of an electronic transition (E) at each wavelength and is calculated from  $E = (hc)/\lambda$ . Correction factors for *HL Rps. palustris* B890 were calculated to be -18% and -0 for the carotenoid absorption maximum and the Qx band maximum respectively. For the *Chromatium* complexes the corrections were -26%, -19% and -14% for carotenoid peaks from short to long wavelength respectively. For the remaining complexes the corrections were -26%, -19% and -12% respectively.
- 7) The final efficiency measurements were then calculated for each of the three carotenoid vibrational bands from the fractional absorbance spectrum using the equation:

$$\frac{\text{height of fluorescence}}{\text{height of absorbance}} \times (100 - \text{correction})\%$$

A range of concentrations of antenna preparations was used for each complex type with Qy band  $A_{\text{max}}$  of  $0.5\text{--}1.8\text{cm}^{-1}$ .

## 2.11 Crystallisation of the B800-850 Complexes from Low Light Grown *Rps. palustris*

### 2.11(i) Sample preparation

B800-850 complexes from low light grown *Rps. palustris* cells were isolated and purified by sucrose density-gradient centrifugation followed by dialysis and a repeat density-gradient centrifugation. The complexes were further purified by sephacryl S-200 gel permeation chromatography [Ackers, 1975] at 4°C. Absorption spectra of fractions eluted from the column were recorded and their pigment / protein ratios were calculated ( $A_{800}/A_{280}$ ) to serve as a purity index. Damaged antenna preparations contain more free pigment, and hence less 800nm-absorbing BChl. This gives a low pigment/protein ratio. Preparations with a purity index of 0.9-1.2 were used for crystallisation trials.

### 2.11(ii) Crystallisation

Protein crystallisation was performed by the vapour diffusion method, in a "sandwich box" apparatus [Davies and Segal, 1971; McPherson, 1982]. This consists of a sealed plastic container within which lies a raised platform with a sample well which holds approximately 50  $\mu$ l sample.

(a)-crystallisation with ammonium sulphate. 8ml ammonium sulphate (1.8-3.0M) were added to the crystallisation reservoir [Gilliland and Davies, 1984]. The small amphiphile benzamidinium hydrochloride hydrate (Aldrich) or heptane-1,2,3-triol (Sigma), was weighed into 3ml eppendorf vials to give a final concentration of 3%. The antenna preparation was exchanged from LDAO into 1% dimethyldecylamineoxide (DDAO) (Oxyl 8903-Bobingen), using a pasteur pipette mini-column of DEAE-cellulose anion exchanger. The complexes were eluted with either 1.8M ammonium sulphate

(for heptane-triol crystallisations) or 0.9M potassium phosphate (for benzamidine hydrochloride crystallisations), previously corrected to the desired pH. A separate column was used for each pH. A volume of eluted complexes was then added to the amphiphile in the eppendorf allowing 50 $\mu$ l for each crystallisation trial plus an additional 50 $\mu$ l. The sample was mixed until the amphiphile dissolved, and was centrifuged at the high speed setting in a MSE microcentaur centrifuge to pellet any denatured, unsolubilised material. The final pH was then recorded and 50 $\mu$ l of mother liquor was pipetted into each crystallisation well. The lid was air-sealed with plastic sticky tape and the apparatus was incubated at 20°C. Protein concentrations in the range 2-5mg/ml were required [McPherson, 1978; McPherson, 1982].

(b) *crystallisation with polyethylene glycol.* 8ml polyethylene glycol (PEG) (18-25%) was pipetted into the crystallisation dish. Isolated complexes were transferred into 1% DDAO in 20mM Tris-HCl, pH9.5, on a DE52 mini-column. Magnesium chloride and PEG 4000 were added to the antenna preparation to final concentrations of 20mM and 9% (w/v) respectively, and the samples were adjusted to the required pH. After centrifugation in a microcentrifuge the supernatant was applied to the wells of the crystallisation apparatus.

The pH of both the polyethylene glycol and ammonium sulphate reservoir solutions was adjusted to equal that of the crystallisation material sample. The crystallisation dishes were incubated at 20°C and monitored at weekly intervals until either crystal growth was complete or protein denaturation occurred. The crystals were not subjected to x-ray diffraction analysis.

## 2.12 SDS polyacrylamide gel electrophoresis

### 2.12(i) Gel assembly

Polyacrylamide gel electrophoresis was performed with a notched plate "Studier"-type apparatus [Studier, 1973] and a discontinuous buffer system after Laemmli [Laemmli, 1970]. A polyacrylamide concentration gradient of 6-25% provided a good resolution of low molecular weight polypeptides whilst maintaining a reasonable resolution of the remaining membrane proteins over quite a wide range of molecular weight. Bis-acrylamide was used as the cross-linker in a proportion of 2.5% of the total acrylamide monomer. The buffers used in the electrolyte, stacking gel and resolving gel were: Tris(25mM)-glycine(193mM), pH8.3, 0.1% SDS; 0.5M Tris-HCl, pH6.8, 0.4% SDS and 1.5M Tris-HCl, pH8.8, 0.4% SDS respectively. Two thick glass plates (one notched) were cleaned thoroughly. Three nylon "spacers", 1mm thick, were lightly greased with petroleum jelly and positioned along the two sides and bottom of the un-notched plate, leaving room to fit the stacking gel comb. The notched plate was gently laid on top and the two plates clamped together with spring clips. A 1% liquid agarose solution was syringed into the gap around the outside of the plate edges to provide a seal. An SDS-resistant sealing tape was sometimes used as an extra precaution against leakage. A 25% acrylamide mixture was prepared using ammonium persulphate and TEMED (N,N,N',N'-tetramethylethylenediamine) as polymerising catalysts, was poured between the plates to a depth of approximately 1cm. This was left to polymerise forming a plug capable of withstanding the weight of the liquid resolving gel to be poured on top. A gradient mixer was used to pour a linear gradient of 25% to 6% acrylamide, stopping approximately 3.5cm from the notch. A small volume of methanol was layered onto the acrylamide surface to aid the formation of a flat surface and the gel

was allowed to polymerise. The methanol was then poured off and the 4.5% acrylamide stacking gel was layered on top. The well-forming comb was slipped between the gel plates and the stacking gel was allowed to polymerise.

The bottom spacer was removed from the gel which was then clipped onto the perspex Studier apparatus. The upper and lower reservoirs were filled with electrolyte and any air trapped underneath the gel was removed. The correct volume of the solubilised protein solution was added to each well with a micro-syringe to give protein loadings of 10-15  $\mu\text{g}$ . 20  $\mu\text{l}$  standard protein/ boiling solution 1:1 (v/v) were used to give a protein loading of 5  $\mu\text{g}$  per marker. A constant current of 10-20mA was applied until the ion front reached the polyacrylamide plug (10-15 h). The apparatus was then disassembled and the gel was stained overnight with Brilliant Blue R 140-5, stain (Aldrich Chem. Co. Ltd). This was followed by a period of destaining lasting 1-2 days.

#### 2.10(ii) Sample preparation

A standard protein solution containing 5mg.ml<sup>-1</sup> horse heart cytochrome c (11 700 g.mol<sup>-1</sup>), horse heart myoglobin (16950 g.mol<sup>-1</sup>), horse liver alcohol dehydrogenase (41000 g.mol<sup>-1</sup>) and bovine serum albumin (68000 g.mol<sup>-1</sup>) was prepared to run as molecular weight markers alongside the sample proteins. Protein concentrations of antenna complexes, whole cells and membranes were determined by tannin protein assays. An equal volume of boiling solution (see Appendix F) was added to the sample in an eppendorf vial and heated for 2min in a boiling waterbath. Crude membrane preparations or whole cells were centrifuged in a microcentrifuge at the high speed setting to pellet any unsolubilised material prior to the electrophoresis.

### **2.13 Tannin Protein Assay**

The addition of tannin reagent (Appendix G) to a protein sample results in the formation of tannic acid-protein complexes which are turbid in solution [Mejbaum-Katzenellenbogen and Drobyszzycka, 1959]. With 10-100 $\mu$ g protein in solution the relationship between absorbance at 500nm and the amount of protein is linear.

A series of dilutions of standard protein (e.g. bovine serum albumin) of known concentration was prepared in Tris-HCl buffer, pH 8. 1ml volumes were equilibrated at 30°C and 1ml volumes of tannin reagent at the same temperature were added. After incubation for 10 min, 1ml gum acacia (0.2% w/v) was added to stabilise the reaction and a calibration curve of  $A_{500}$  versus  $\mu$ g protein was constructed. The assay was then repeated with the protein samples of unknown concentration (i.e. antenna complexes, membranes and whole cells), and the concentration of the protein stock solution was estimated from absorbance measurements at 500nm and interpolation of the calibration curve.

### **2.14 Statistical Analysis of Data**

#### **2.14(i) Introduction**

A brief description of the statistical methods used in the results chapters will be given here. A lucid introduction to elementary statistics is presented in McCormick and Roach (1987).

If for example the value of the efficiency of energy transfer from carotenoid to BChl in a particular antenna complex is required, an experiment would be designed in which replicate measurements would be performed on samples of antenna complexes taken from a population of that type of complex. The arithmetic mean of the measurements ( $\bar{x}$ ) is assumed to be the best estimate of the true population mean ( $\mu$ ). All

experimental measurements are subject to random error, which results in a spread of data about the arithmetic mean. The magnitude of random error, or "precision" of a measurement, is described by the sample standard deviation ( $s$  or  $\sigma_{n-1}$ ):

$$s = \sqrt{\frac{(x_i - \bar{x})^2}{n-1}}$$

where,  $x_i$  = value of an individual measurement

$n$  = number of replicate measurements

If  $n$  is very large the sample standard deviation approaches the value of the population standard deviation ( $\sigma$ ).

It is unlikely that an experimental mean is identical to the true population mean. If a series of sample means are determined they too will have a standard deviation, centred around the true population mean. Their standard deviation (standard error) is given by,  $\sigma/\sqrt{n}$ , and the distribution of the means follows a normal distribution curve (central limit theorem). Experimental sample means can therefore be related to true population means by examination of the normal distribution curve. The total area under a normal distribution curve is always equal to 1. The area lying outside a range  $\mu \pm \sigma$ , can be determined by reference to a statistical table. For a distribution of sample means these areas are also the probabilities of an experimentally determined sample mean value falling outside  $\pm\sigma$ . In a "standardised normal distribution table", the value  $z$  is equal to one population standard deviation. So, for example, reference to the table shows that when the tail areas under the curve represent 5% of the total area, the  $z$  value is 1.96.  $\bar{x}$  and  $\mu$  can then be related by saying that  $\mu$  lies between  $\bar{x} \pm (z\sigma)/\sqrt{n}$ . It is therefore 95% certain that  $\mu$  lies within  $\bar{x} \pm 1.96 \sigma/\sqrt{n}$ . However, because the

number of individual measurements taken to obtain a sample mean is usually small,  $\sigma$  is usually unknown. The sample standard deviation is an erratic parameter and becomes an increasingly unreliable estimate of  $\sigma$  as the number of replicate measurements becomes smaller. A t-distribution curve, which is dependent on sample size, is used to compensate for this. For arithmetic means calculated from over 120 measurements the t-distribution is identical to the normal distribution. But when  $n$  is small the value of  $t$  (which replaces  $z$  in the t-distribution) becomes large, reflecting the larger uncertainty. For a given probability ( $p$ ) and sample size ( $n-1$  "degrees of freedom") a value of  $t$  is determined from a t-table. For the chosen probability (e.g. 5% or  $p = 0.05$ ),  $\mu$  lies between  $\bar{x} \pm (ts)/\sqrt{n}$ .

#### **2.14(ii) t-test for comparison of sample means**

Experiments often involve measuring a certain parameter in samples treated in different ways, to study the effect of the treatment. In chapter 7 the efficiency of energy transfer from carotenoid to BChl in B800-850 complexes isolated from high and low light grown cells were measured to determine whether light intensity affects the energy transfer efficiency. The arithmetic means of the efficiencies under the two growth conditions were different but the question arises, is this difference due to normal, random experimental error or does it reflect a real difference in their energy transfer efficiencies? The question can be answered by performing a t-test. A t-test compares the differences between the means of two sets of data, with the spread of data about the means described by the sample standard deviation. For the purpose of the test it is assumed that the two sets of data arise from the same population and that the difference between the sample means is solely due to random error (i.e. a null hypothesis is set up). A value for  $t$

is calculated from the experimental data:

$$t_{\text{calc}} = \frac{(x_1 - x_2) - (\mu_1 - \mu_2)}{s_p \sqrt{(1/n_1 + 1/n_2)}}$$

The population means are assumed to be equal, so  $\mu_1 = \mu_2$  (null hypothesis).  $s_p$  is a value for the pooled standard deviation and is given by:

$$s_p = \sqrt{\frac{(n_1 - 1)s_1^2 + (n_2 - 1)s_2^2}{n_1 + n_2 - 2}}$$

The higher the value of  $t_{\text{calc}}$  the greater is the probability that the difference between the sample means is real and is not due to random error. A table is consulted for  $n_1 + n_2 - 2$  degrees of freedom to determine the probability of the difference being "real". For a chosen probability  $t_{\text{tab}}$  gives the  $\pm$  range within which  $t_{\text{calc}}$  must lie if the two sample means are from the same parent population. The  $t_{\text{calc}}$  value was matched up with  $t_{\text{tab}}$  values using a computer statistics program package (t-tables can be used but these are less accurate) and a probability value corresponding to  $t_{\text{calc}}$  was read off. This gives the decimal probability that the two sets of data are from the same parent population. If  $p < 0.05$  it is accepted, with a certainty of  $>95\%$  that there is a real difference between the sample means. If  $p > 0.05$  the evidence is assumed to be inconclusive.

t-tests can be performed on two sets of data. However when more than two sets of data are to be compared, analysis of variance must be used. These computations rely on the variance ratio distribution curve, which is a measure of variance (the square of the standard deviation) instead of the t-distribution curve.

**2.14(iii) Analysis of variance**

One way analysis of variance was performed on the measurements of the efficiency of energy transfer from carotenoid to BChl to test whether the efficiency of energy transfer is significantly different for excitation at different carotenoid vibrational bands. Analyses were performed manually and checked using the statistical computer package "Minitab". The method of manual computation will be described below using the data for the B800-820 complex of *Rps. acidophila*, strain 7750. Energy transfer efficiencies were measured at each of the carotenoid vibrational bands (0-2, 0-1 and 0-0), for two different samples. The results are tabulated below:

	% efficiency		
	0-2	0-1	0-0
sample 1	60	69	74
sample 2	64	72	78
$\bar{x}$	62	70	76
$s^2$	7.2	3.2	6.5

$\bar{x}$  = arithmetic mean       $s^2$  = variance

The random error of the experimental technique can be denoted by the sample standard deviation at each vibrational band. Because standard deviations are not additive and cannot be used directly in further calculations, the standard deviations are squared to give the variances for each column. For this data the best estimate of random error is given by a pooled value for the three variances. This is calculated by:

$$s_p^2 = \frac{(n-1)s_1^2 + (n-1)s_2^2 + (n-1)s_3^2}{(n_1 + n_2 + n_3) - k} = 9.99$$

where  $k$  is the number of data sets pooled (i.e. 3). The number of degrees of freedom is given by the denominator of the equation.  $sp^2$  is known as the within sample variance, and is a measure of random error.

There is another way of calculating the variance of this data. If the arithmetic means are calculated for each column, these can be further averaged to give a mean of the means ( $\bar{\bar{x}}$ ), and variance of the means ( $s_{\bar{x}}^2$ ). When this is multiplied by the sample number (i.e.  $n=2$ ) the value of  $ns_{\bar{x}}^2$  is calculated. For the data presented this is equal to 197.3. The value  $ns_{\bar{x}}^2$  has two contributions: variance due to any differences between the means of the columns, and variance due to random error. Therefore if the differences between the means of the columns can be accounted for by random error only,  $sp^2 = ns_{\bar{x}}^2$ .

To determine the probability of there being a genuine difference between the data sets 0-2, 0-1 and 0-0 the variance ratio ( $ns_{\bar{x}}^2/sp^2$ ) is first calculated. Variance ratio tables are consulted for the appropriate number of degrees of freedom and a significance level corresponding to the calculated variance ratio is read off. If the significance level is  $<0.05$  it is  $>95\%$  probable that the differences between the efficiencies measured at bands 0-2, 0-1 and 0-0 are genuine.

#### 2.14(iv) Linear regression analysis

Regression analysis was performed on the optical density versus cell number calibration curves for high and low light *Rps. palustris*. This method calculates the best fit for the calibration curve taking into account the random error associated with the cell counting procedure. The slope of the plot ( $m$ ) is also calculated along with its standard deviation ( $s_m$ ). With this data a t-test was performed to test the significance of the difference between the gradients of the low light and high light grown cell plots.

The equation for a straight line is  $y = mx + c$  where  $m$  is the slope of the line,  $y$  is the y-axis value,  $x$  is the x-axis value, and  $c$  is the value of  $y$  when  $x = 0$ .  $m$  is given by:

$$m = \frac{[(n\sum xy) - (\sum x \cdot \sum y)]}{[(n\sum x^2) - (\sum x)^2]}$$

To calculate the standard deviation of the y-values (cell counting procedure), the sum of the squares of the deviations of  $y$  on  $x$  from the regression line ( $d_i$ ) must first be calculated:

$$d_i^2 = \sum y^2 - [(\sum xy)^2 / \sum x]^2$$

Then the sample standard deviation of  $y$ ,  $s_y = \sqrt{(\sum d_i^2 / (n-2))}$ ,

and the sample standard deviation of the slope,

$$s_m = \frac{s_y}{\sqrt{((\sum x^2 - (\sum x)^2) / n)}}$$

**CHAPTER THREE:    The   Effect of Growth Conditions on Cell Culture and the  
Synthesis of Variable Light-Harvesting Antenna Complexes**

### 3.1 Introduction

All purple photosynthetic bacteria adapt to a reduction in light intensity by increasing the amount of the existing photosynthetic machinery. A few species respond to low light intensities by synthesising new types of antenna complexes; specifically B800-850 Type II and B800-820 complexes (section 1.7(i)). Curiously these complexes are also synthesised in some species in response to changes in temperature or the composition of the growth medium. The effect of growth conditions on the structure and function of variable antenna complexes will be discussed in some of the following results chapters. This introductory results chapter describes some of the effects of a changing environment on the growth and the synthesis of the variable antenna complexes of three species of purple bacteria.

### 3.2 Growth of *Rps. palustris*, strain French, Under High and Low Light Intensities and a Spectral Characterisation of the Cells and Antenna Complexes.

The growth of *Rhodospseudomonas palustris* was monitored by the increase in culture turbidity with time. Calibration curves of  $A_{650}$  versus cell number were plotted for cultures grown at 300 lux (low light; LL) and 16000 lux (high light; HL) (Fig. 3.1). The curves of best fit were determined by linear regression. The slopes of the two curves are notably different:  $m(\text{HL}) = 11.7 \times 10^7$ ;  $m(\text{LL}) = 10.0 \times 10^7$ . To determine whether this difference can be accounted for by the random error of the cell counting procedure, the sample standard deviations of the slopes of the fitted regression curves were first calculated. The standard deviations were  $1.1 \times 10^7$  and  $1.6 \times 10^7$  cells/ $\mu\text{l}$  for the curves of the LL and HL grown cells respectively. A t-test performed on this

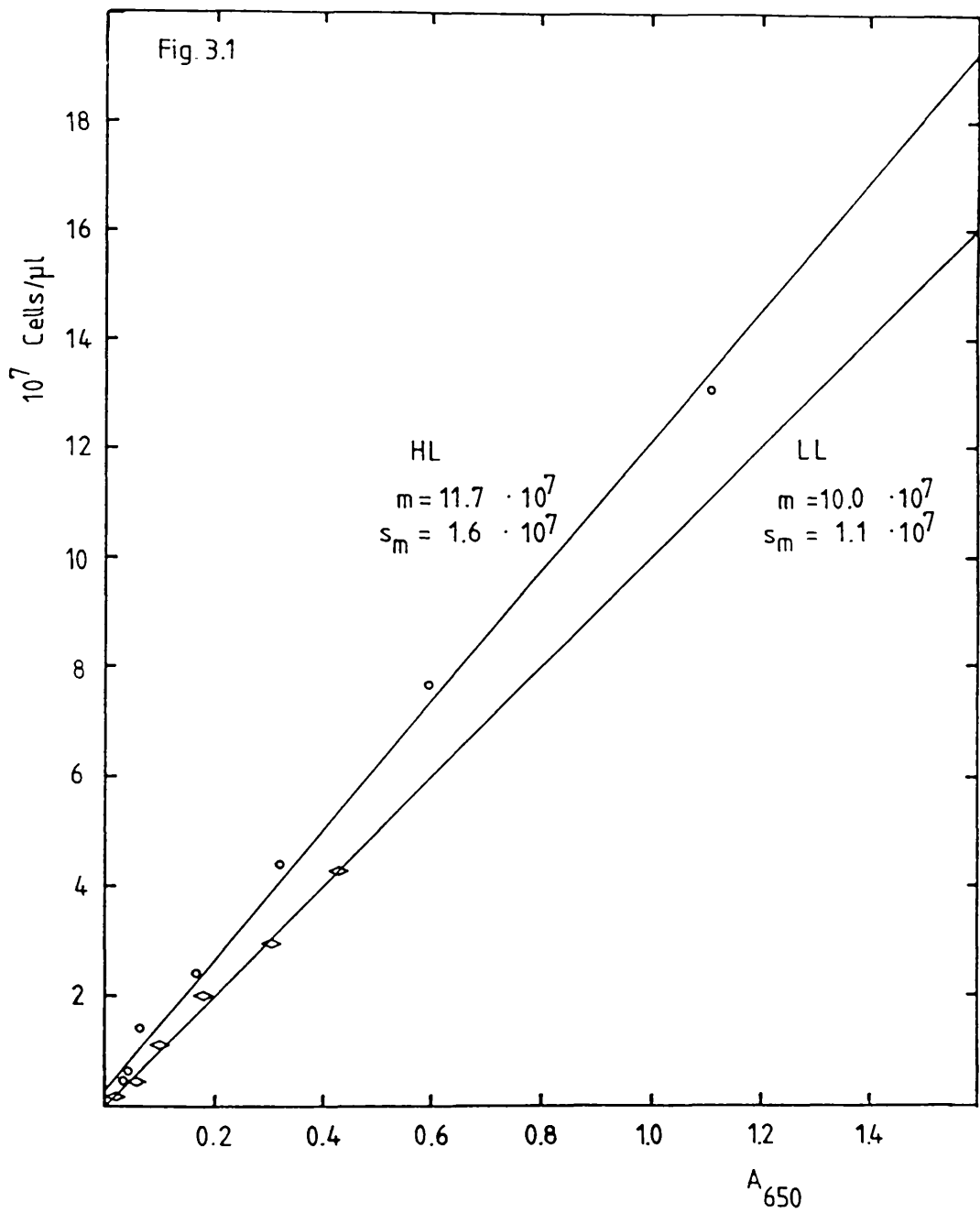


Fig. 3.1 Calibration curves of cell number versus absorbance at 650nm for low and high light grown *Rps. palustris* cells.

data indicates that the difference in the slopes cannot be attributed to random error in the cell counting procedure ( $t = 3.52$ ,  $p = 0.005-0.001$ ). The most likely explanation for this data is that under low light growth conditions the cells contain more photosynthetic membrane per cell and therefore have greater light-scattering properties compared to the high light grown cells.

Growth curves plotted for high and low light culture conditions have a form typical of microbial growth curves (Fig. 3.2) [Stanier et al., 1976]. There is an initial lag phase during which the cells accommodate to their new environment after inoculation. The lag phase of the low light grown cells is considerably longer than that of the high light grown cells, presumably because the supply of energy required for cell growth is limited by the light intensity. The lag phase is followed by a logarithmic phase. The doubling times of the cultures during the log phase were estimated from the growth curves to be approximately 6h for the high light grown cells and 29h for the low light grown cells. The doubling time for *Rps. palustris*, strain 1e5, has been reported to be 3.5h [Firsow and Drews, 1977], at an undisclosed light intensity. The doubling time for *Rps. sphaeroides* is reported to be 2.2h [Stanier et al., 1976]. For comparison the doubling times of most other microbes grown at optimal growth conditions are shorter e.g. *Escherichia coli* 0.35h. The effect of low light intensity on *Rps. palustris*, strain French, is obviously to retard the growth rate. The high light grown cells reach the stationary, nutrient-limiting, phase at a cell concentration of about  $278 \times 10^6$  cells/ $\mu$ l. The low light grown cells reach the stationary phase at a cell concentration of  $254 \times 10^6$  cells/ $\mu$ l. This difference of approximately 9% is less than the 95% confidence intervals associated with the slopes of the calibration curves and is therefore probably not significant.

Electron micrographs of high and low light grown *Rps. palustris*,

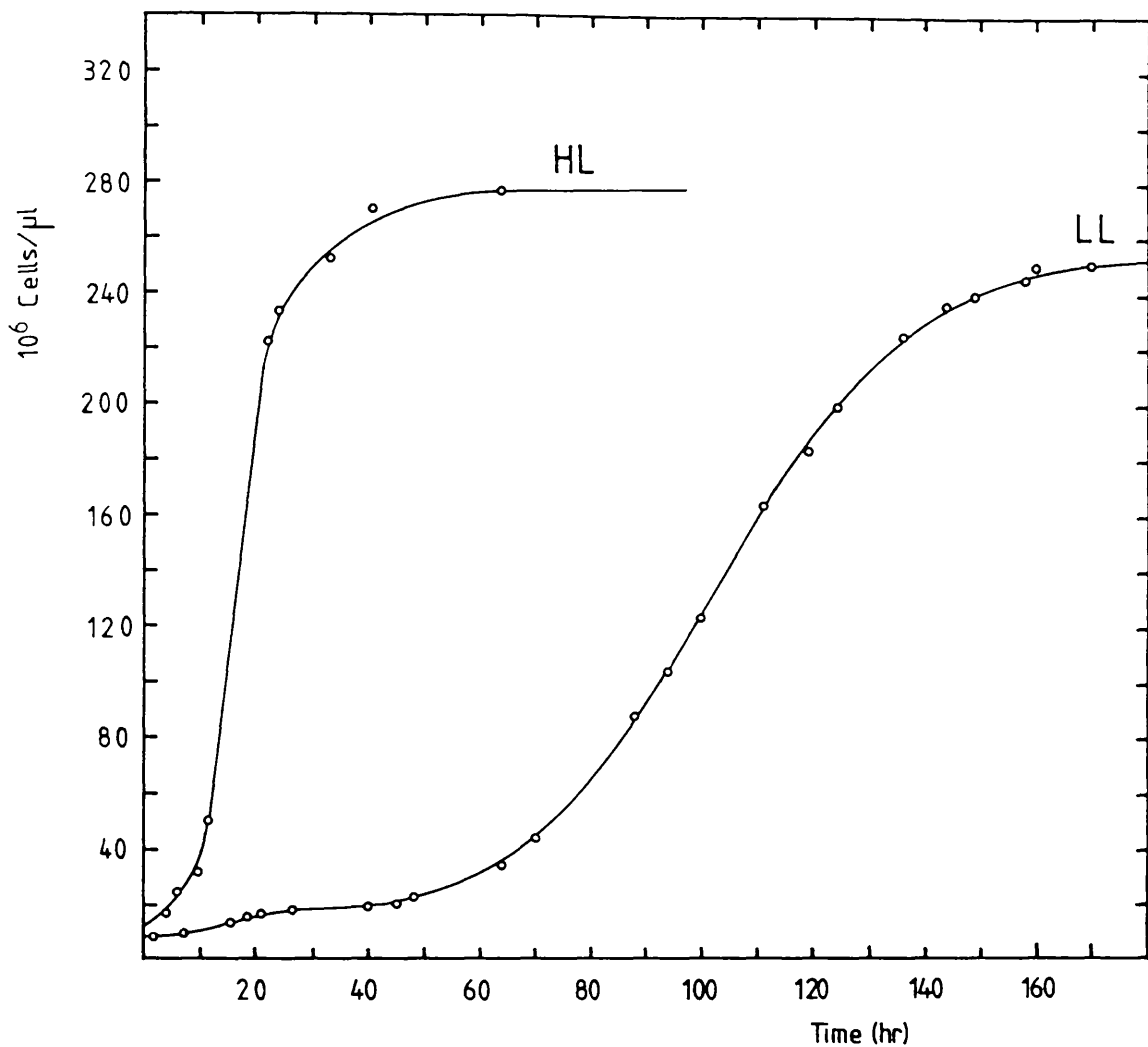


Fig. 3.2 Growth curves for high and low light grown *Rps. palustris* cells.  $m$  = gradient of slope,  $s_m$  = standard deviation of the gradient of the slope.

strain French, cells are presented and described in Fig. 3.3

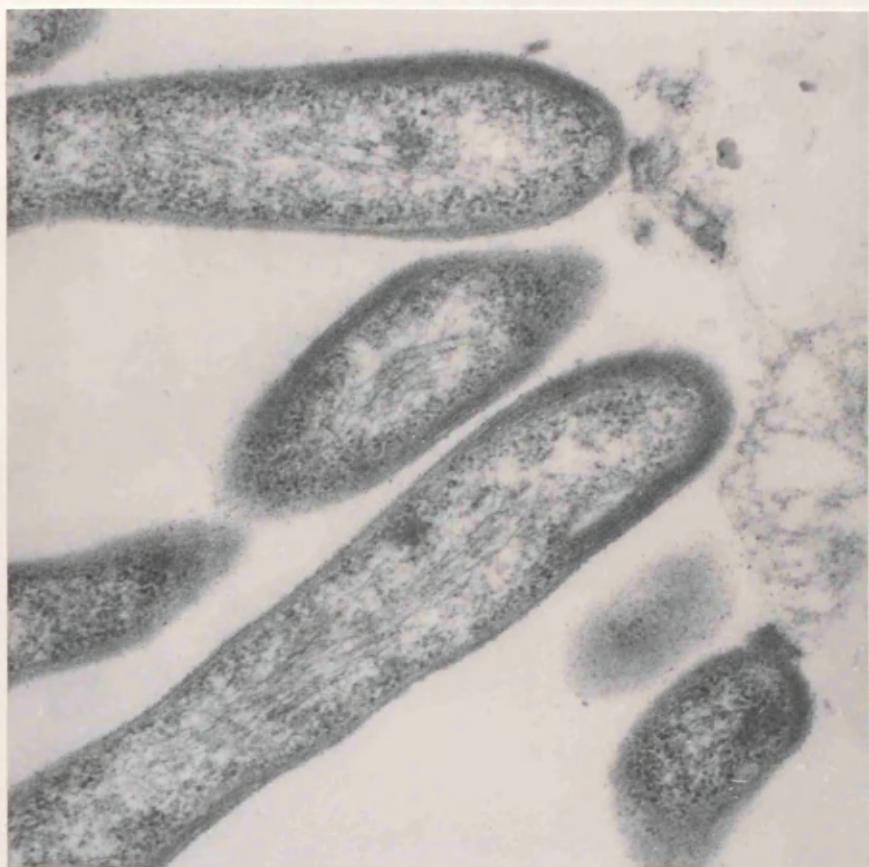
### 3.3 A Spectral Characterisation of 30°C and 40°C Grown *Chr. vinosum*, strain D, and Their Antenna Complexes

The shape of the near-infrared absorption spectrum of *Rps. palustris*, strain French, changes with the light intensity (Fig. 3.4). With high light grown cells the 850nm absorption intensity ( $A_{850}$ ) is greater than the 800nm absorption intensity ( $A_{800}$ ). In contrast under low light  $A_{850} < A_{800}$ . This phenomenon was previously reported by Hayashi et al., 1982(a)(b) and Miyazaki and Morita, (1981). However, near-infrared spectral changes with light intensity were not observed for strain 1e5 [Firsow and Drews, 1977], or for strain DSM (unpublished observations). This phenomenon is therefore strain-dependent.

The B875 and B800-850 complexes were isolated from *Rps. palustris*, strain French, cells by sucrose density-gradient centrifugation of LDAO-solubilised photosynthetic membranes (Fig. 3.5). The B875 complex preparation has some absorption at 800nm, in addition to the main BChl absorption band, due to the presence of reaction centres and possibly a small contamination with B800-850 light-harvesting complexes (Fig. 3.6). Absorption spectra of B800-850 complexes isolated from high and low light grown cells are presented in Fig. 3.7. In addition to spectral variation in the near-infrared region, the LL B800-850 complexes exhibit a Qx absorption maximum at about 3nm further to the blue than the Type I complexes. This was previously noted by Hayashi et al. (1982a) who also measured the fluorescence emission spectra of the two complexes and found little difference between them. The fluorescence emission maximum was centred at 890nm for both complexes. *large difference*

In an attempt to determine whether the low light B800-850 complex preparation contained more than one antenna component, a preparation was

Fig. 3.3 Electron micrographs of high light (top) and low light (bottom) grown *Rps. palustris*, strain French cells. The electron micrograph of the high-light grown cells shows the cell membrane and the presence of some stacked photosynthetic membranes near the edges of the cells. Dark, granular ribosomes can also be observed near the edges of the cells. Running through the centres of the cells are strand-like chromatin fibres. The main feature of the low light grown cells is the presence of densely stacked photosynthetic membranes which run along the length of the cells. The cell in the bottom left corner is cross-sectioned, rather than transverse-sectioned, and shows how the lamellar membranes are distributed around the cell edge.  $2\text{cm} \approx 1\mu\text{m}$ .



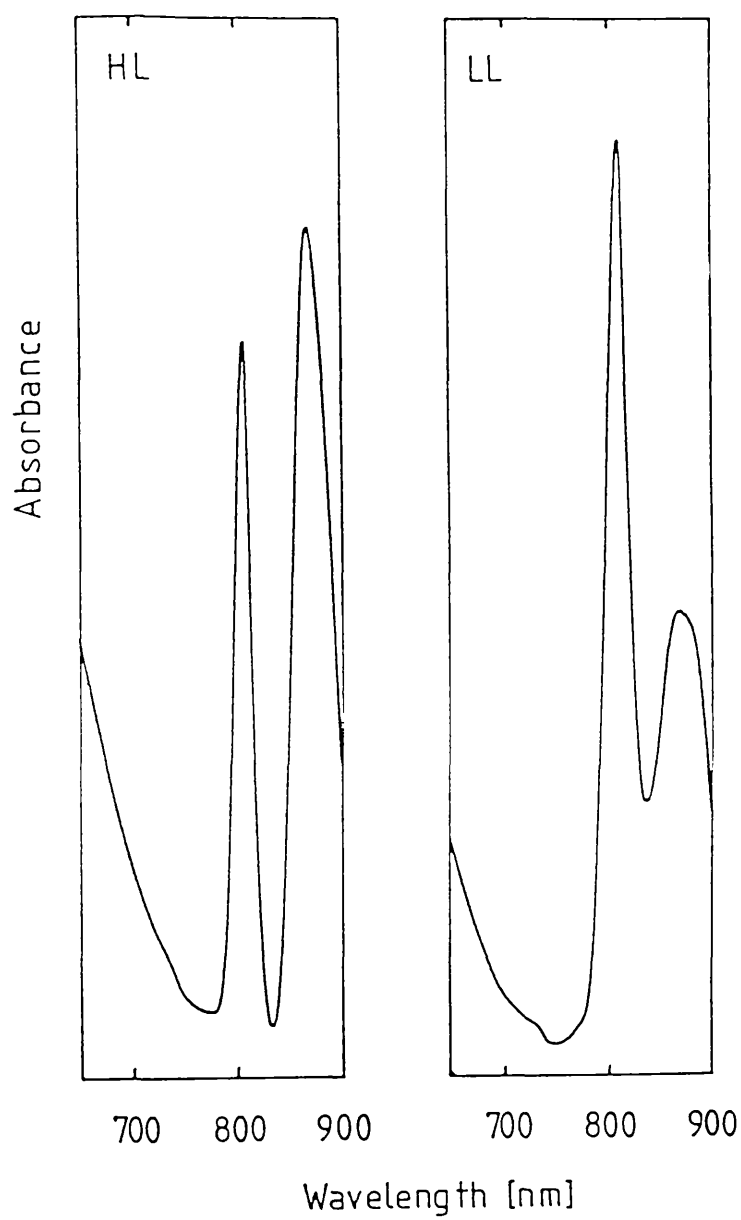
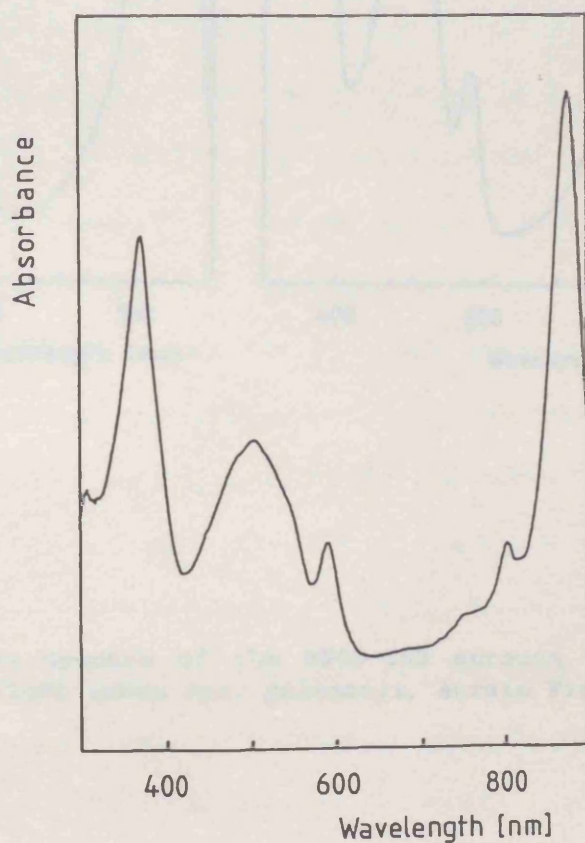
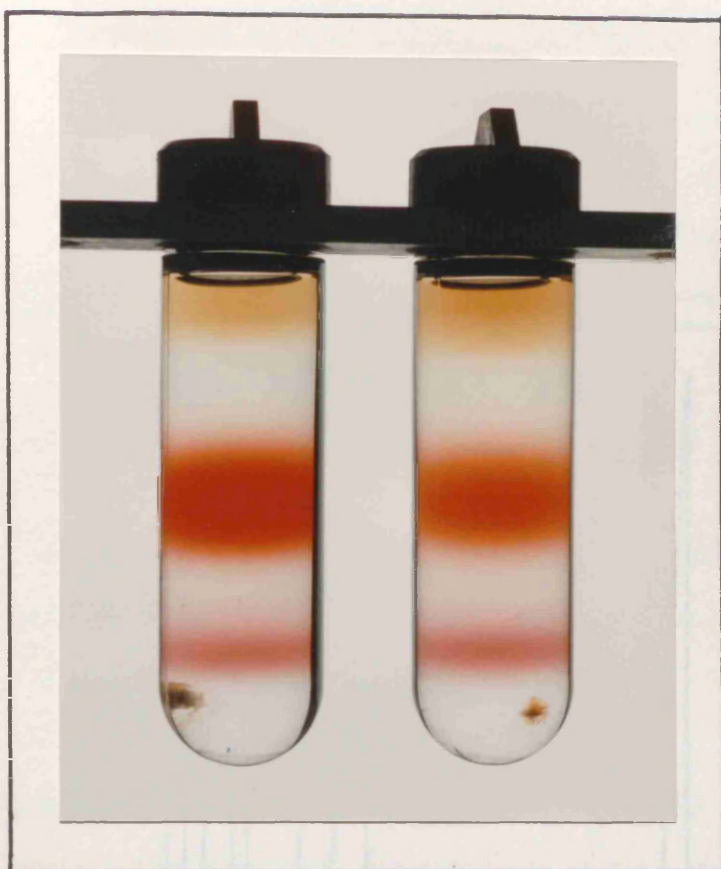


Fig. 3.4 Electronic absorption spectra of *Rps. palustris*, strain French, cells grown under low (300 lux) and high (16000 lux) illuminance flux.

Fig. 3.5 Sucrose density-gradients of detergent-solubilised photosynthetic membranes after centrifugation at 180000 xg for 16hr. The lower bands comprise B875-reaction centre pigment-protein complexes and the upper bands comprise B800-850 complexes. Some free pigment is present at the top of the gradient.

Fig. 3.6 Absorption spectrum of the B875-reaction centre complexes from *Rps. palustris*, strain French.



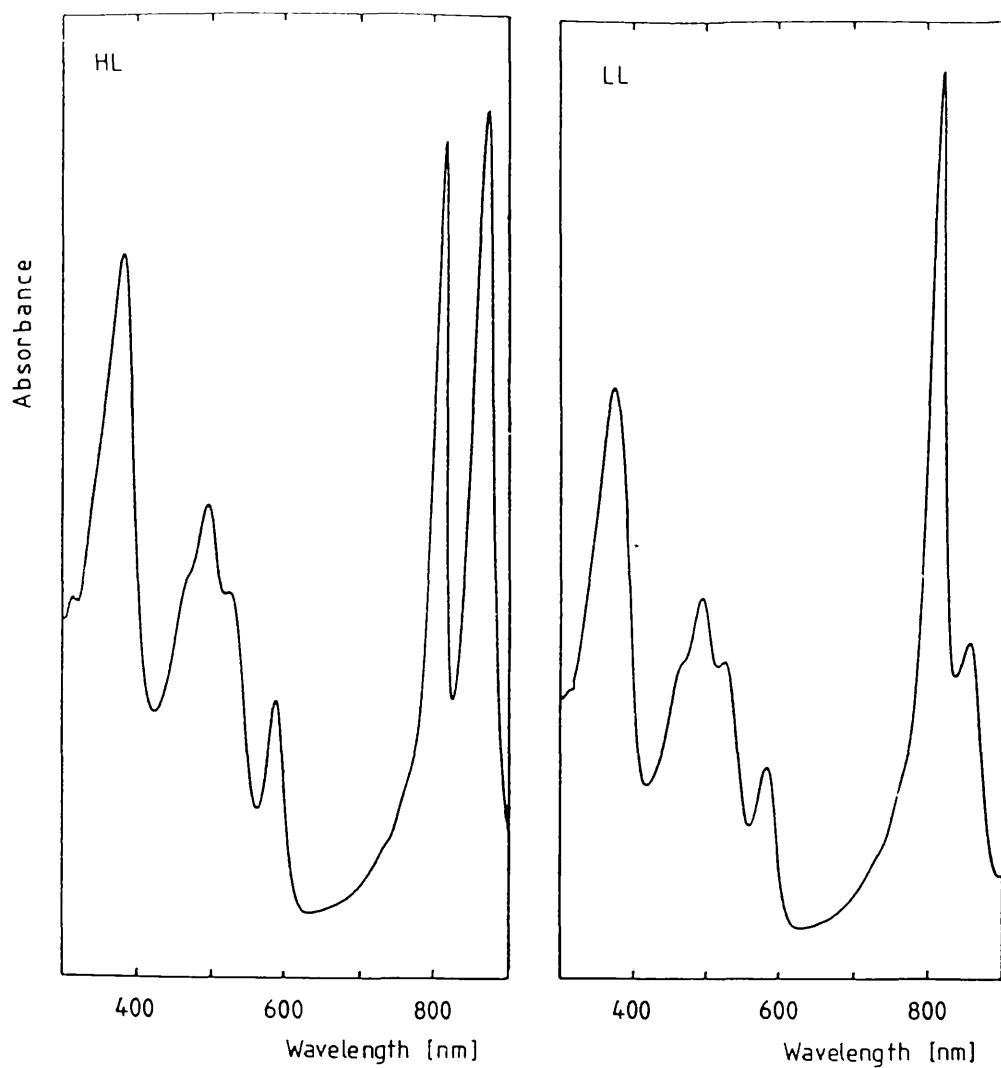


Fig. 3.7 Absorption spectra of the B800-850 antenna complexes from low light and high light grown *Rps. palustris*, strain French.

passed through a DEAE-cellulose anion-exchange column. An elution profile against the ratio of  $A_{800}/A_{850}$  is presented in Fig. 3.8. The first fractions gave a typical HL B800-850 near-infrared spectrum. With continuing elution the ratio of  $A_{800}/A_{850}$  increased to eventually give a typical LL B800-850 absorption spectrum. This suggests that low light grown cells contain both LL and HL extreme spectral forms of B800-850 complex, but with a predominance of the LL form. Intermediate absorbance ratios can probably be attributed to mixing of the two extreme spectral forms. It should be noted that the concentration of eluted antenna complexes was not constant, although the elution band was broad and the concentration range was not very great.

#### 3.4 Temperature dependence of the near-infrared spectra of *Chromatium vinosum*, strain D, cells and antenna complexes

Wassink et al., (1939) reported that the shape of the near-infrared absorption spectrum of *Chr. vinosum*, strain D, varies with growth under different light intensities. The ratio of  $A_{800}$  to  $A_{850}$  increases when the light intensity is reduced in a similar manner to that previously mentioned for *Rps. palustris*. Garcia et al. (1966) were able to partially separate the B800-850 component from the B890 component of *Chromatium* chromatophores using Triton X-100 detergent treatment and sucrose density-gradient centrifugation. They too noted the changes in the relative absorption intensities at 800 and 850nm. Thornber (1970) reported the first successful isolation of separate antenna complexes from *Chr. vinosum*, strain D. Under high light growth conditions a B800-850 Type I complex and a B890 complex were isolated. When the cells were cultured under low light intensities a B800-850 Type II complex, a B800-820 complex and a B890 complex were isolated.

Mechler and Oelze (1978a,b,c) further studied the effect of growth

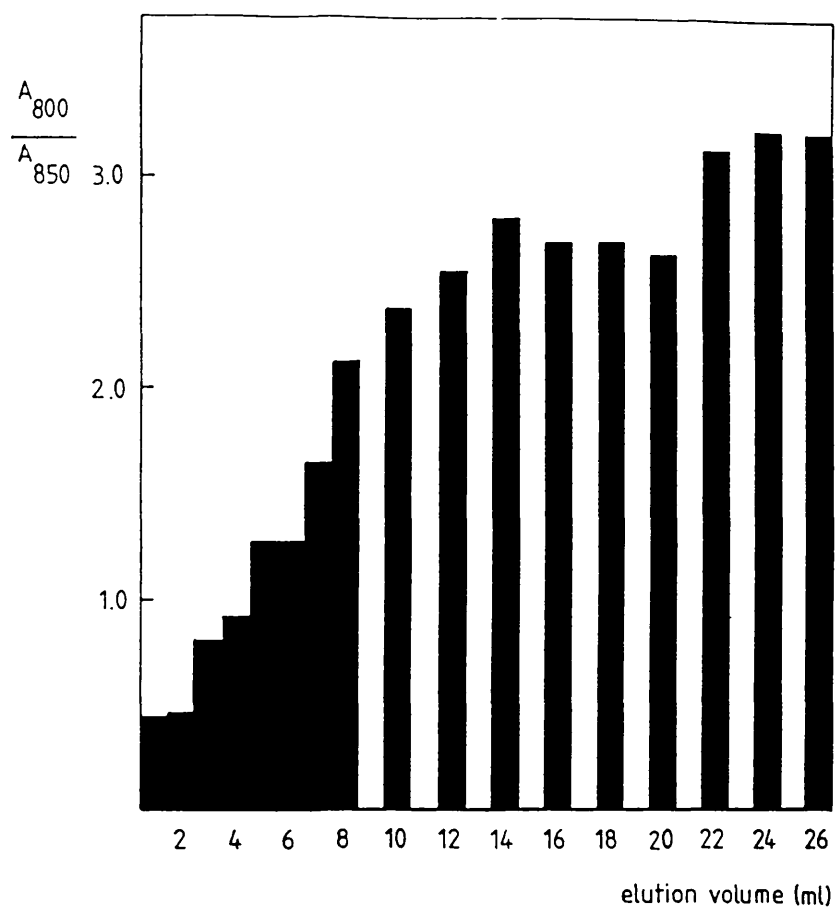


Fig. 3.8 An elution profile of LL B800-850 complexes from a DEAE-cellulose anion-exchange column, measured as  $A_{800}/A_{850}$  against elution volume.

conditions on the near-infrared absorption spectra of *Chr. vinosum*. They reported that with heterotrophic growth on malate, the spectral form was independent of light intensity. However, when cultured above 36.5°C the spectral form of the chromatophores was similar to that reported by Thornber for chromatophores isolated from low light cells. i.e.  $A_{800} > A_{850}$ . Under heterotrophic growth conditions, Mechler and Oelze also reported that the near-infrared spectral form is independent of temperature. And corroborating the findings of Thornber they reported that the spectral form is dependent on the light intensity. The situation is further complicated by the findings of Hayashi and Morita (1980), who reported that at the usual culture temperature (29-33°C) and at an apparent low light intensity (actual intensity was not reported), with autotrophic growth, the spectral form is dependent on the composition of the growth medium. In the presence of 0.1% sodium sulphide (also used by Thornber) the spectral form as expected is equivalent to that described by Thornber for low light growth conditions. But in the absence of sodium sulphide the spectra indicate the presence of a Type I B800-850 complex.

Despite extensive spectral characterisation of the pigment-protein complexes from *Chr. vinosum* the structural and functional characterisation of this species has been minimal. No antenna apoprotein sequence data is yet available, the carotenoid compositions and BChl-to-carotenoid ratios of the antenna complexes have only been crudely determined [Thornber, 1970] and the efficiency of energy transfer from carotenoid to BChl has not been measured for the isolated complexes. Some data on the BChl-to-carotenoid ratios and carotenoid-to-BChl energy transfer efficiencies will be presented in the following chapters.

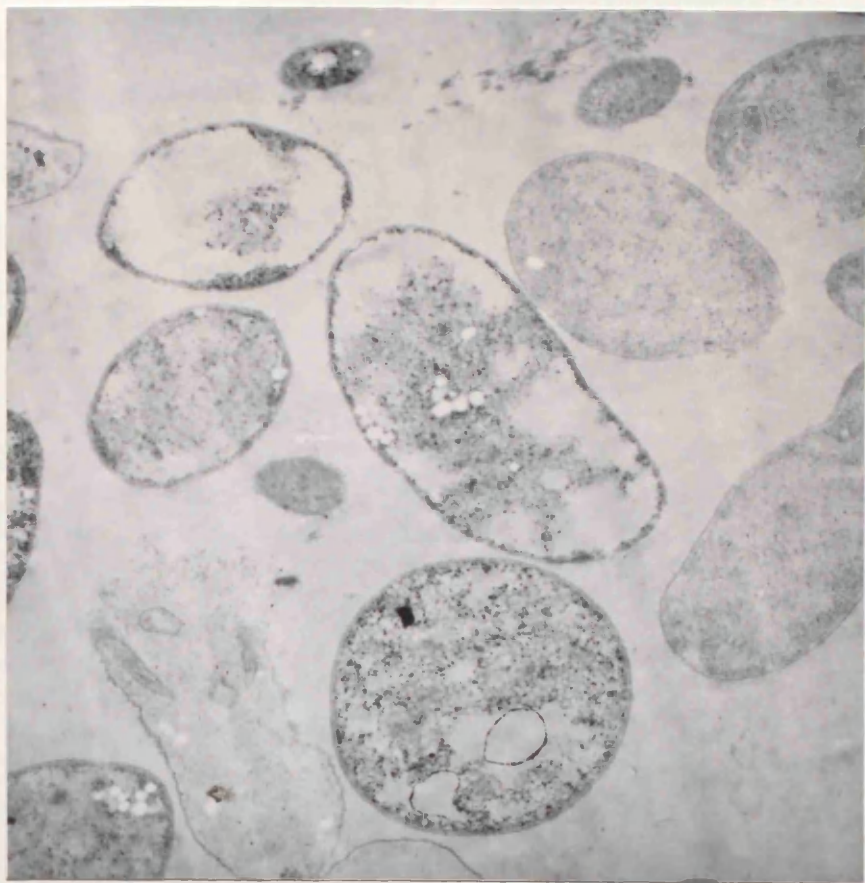
*Chr. vinosum* was cultured anaerobically and autotrophically under high light intensity. Electron micrographs of *Chr. vinosum* cells cultured at 30°C and 40°C are presented in Fig. 3.9. It was found that at 30°C the cells show near-infrared absorption spectra with  $A_{850} \sim A_{800}$  but at 40°C the cells had spectra with  $A_{850} < A_{800}$  containing a shoulder at around 830nm (Fig. 3.10). This contradicts the findings of Mechler and Oelze (1978) who reported that the spectral form of autotrophic cultures is temperature independent. This can only be explained by either an effect of small differences in composition of culture media or by spontaneous change in the strain D cells since distribution of the type-culture.

The variable light-harvesting antenna complexes were separated from the B890-RC core complexes by SDS-solubilisation of photosynthetic membranes and ammonium sulphate precipitation. Near-infrared spectra were recorded during the isolation procedure. Typical data are presented for 40 °C grown cells in Fig. 3.11. There is slight variation between different preparations in the shape of the shoulder of the LL B800-850 complex spectrum. Some preparations have a shoulder at 820nm. Despite this no B800-820 complexes could be isolated from the membranes. A spectrum of B800-850 Type I complexes isolated from cells grown at 30°C is presented in Fig. 3.12.

### 3.5 A Spectral Characterisation of Cells and Antenna Complexes from *Rhodopseudomonas acidophila*, strains 7050 and 7750, and the Effect of Light Intensity and Temperature

*Rhodopseudomonas acidophila* was first described by Pfennig [Pfennig, 1969]. The spectral characteristics of strains 7050 and 7750 were investigated by Cogdell et al. (1983). They reported the isolation of a B800-850 Type I complex from cells grown under high light

Fig. 3.9 Electron micrographs of *Chr. vinosum* cells, grown at 30°C (upper) and 40°C (lower). In contrast to *Rps. palustris*, *Chr. vinosum* cells are rounded in shape. Some of the cell walls of the 30°C grown cells have a wavy appearance which is characteristic of the outer cell walls of many gram negative bacteria [Stanier et al., 1976]. *Chr. vinosum* contains vesicular photosynthetic membranes which can be seen as small circles in the protoplasm. The small, black granules are probably storage products such as  $\beta$ -polyhydroxybutyrate. The grey granules are ribosomes. The light-grey membrane-bordered circular structures, which appear to be surrounded by dark storage products are possibly vacuoles or sulphur storage vesicles. The white circular structures are either sulphur storage vesicles or artefacts caused by holes in the resin mount of the section. For positive identification of these structures histochemical analyses would be required. The 40°C grown cells appear to be more densely packed with chromatophores than the 30°C grown cells and contain large aggregates of an electron dense material which is probably a storage polymer. 2cm  $\simeq$  1 $\mu$ m



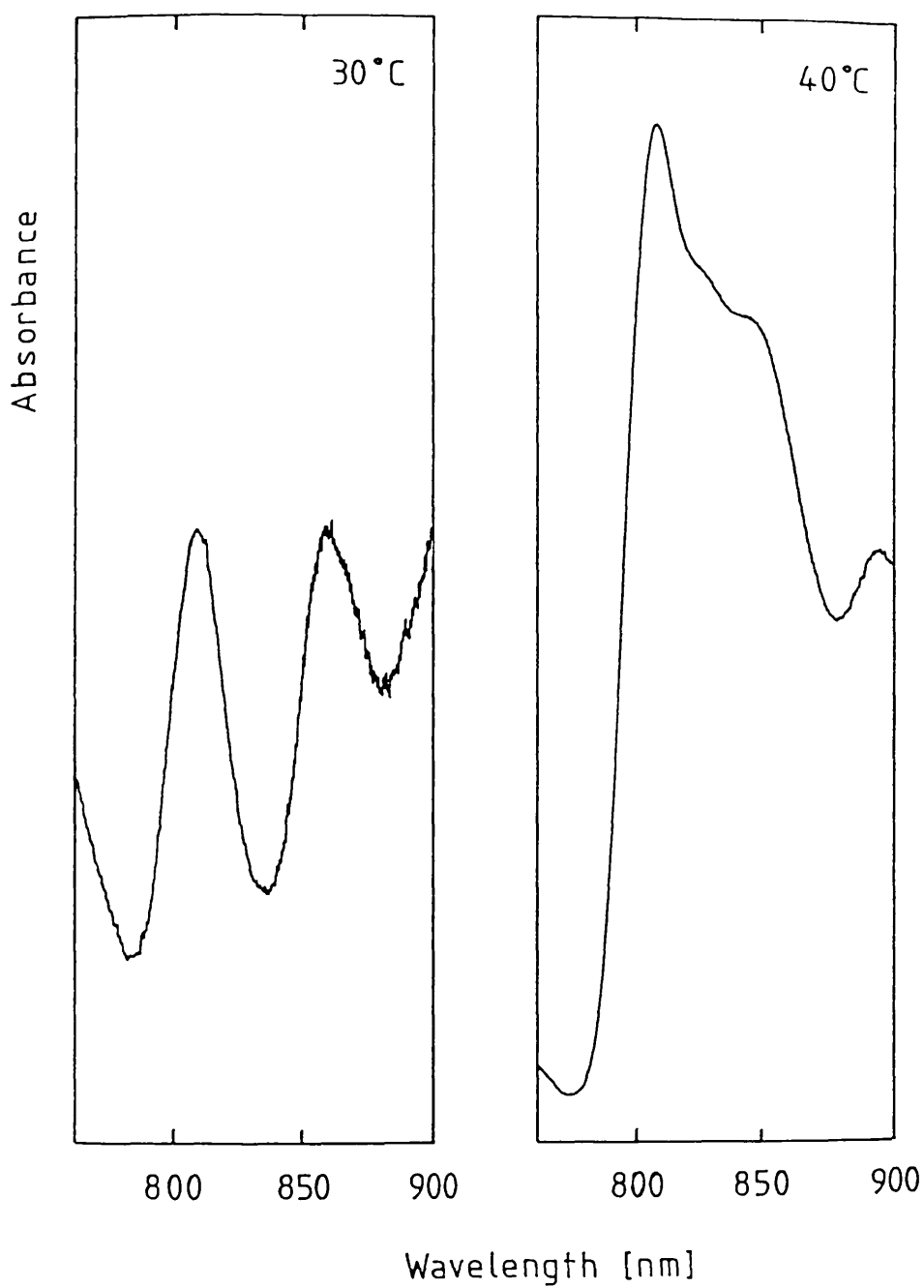
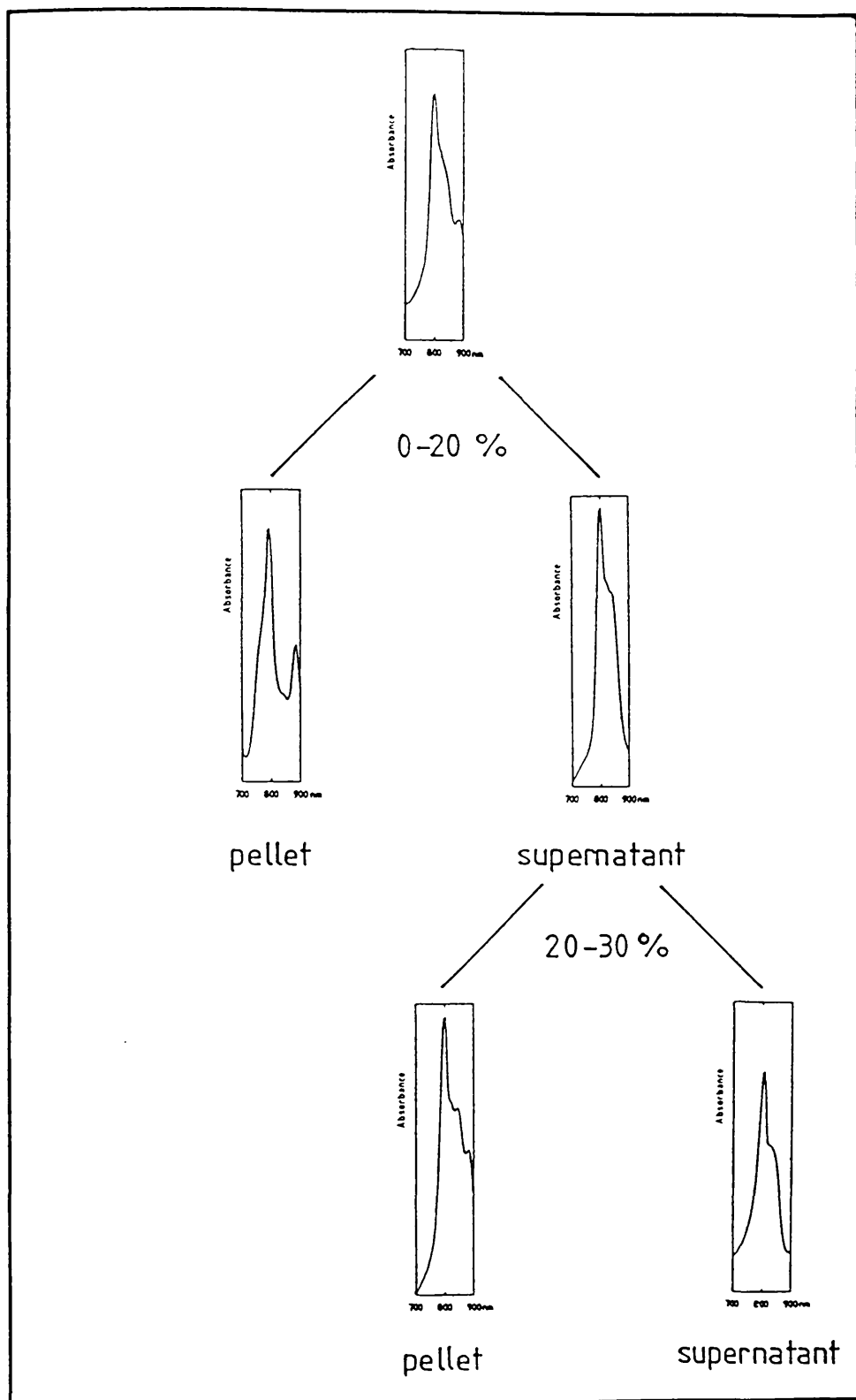


Fig. 3.10 Near-infrared absorption spectra of 30°C and 40°C grown *Chr. vinosum* cells.



**Fig. 3.11** Procedure for isolating B800-850 antenna complexes from solubilised membranes of 40°C *Chr. vinosum* cells. At the top is a near-infrared spectrum of solubilised membranes. Below are spectra of the pellets and supernatants from centrifugations of ammonium sulphate precipitation cuts of 0-20% saturation and 20-30% saturation.

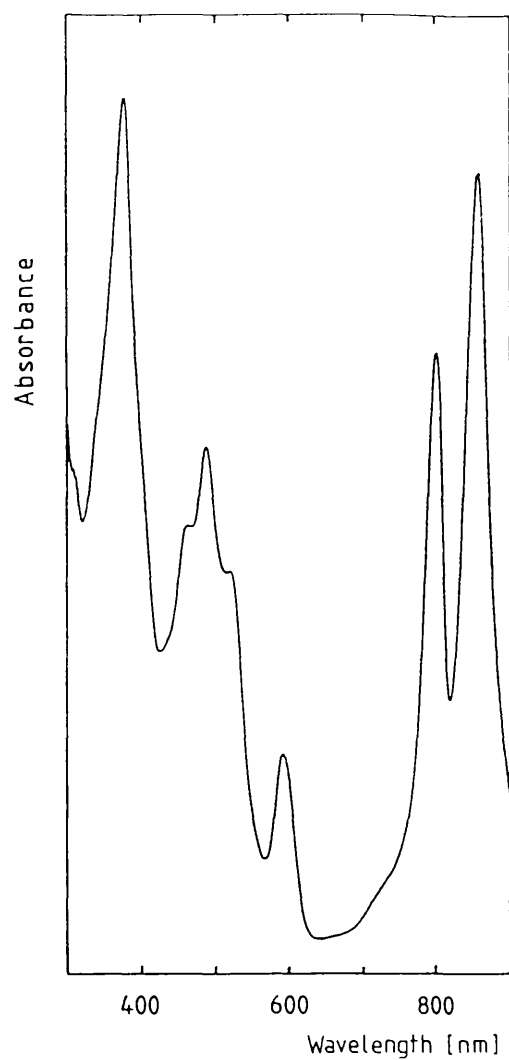


Fig. 3.12 Absorption spectrum of B800-850 antenna complexes from 30°C grown *Chr. vinosum* cells.

conditions and the isolation of B800-820 and B800-850 Type II complexes from low light grown cells, in addition to the core B890 complex. Brunisholz et al. (1987) reported that when strain 7750 is cultured at  $<23^{\circ}\text{C}$  it also synthesises a B800-820 complex. The antenna polypeptides from this complex, the polypeptides from the B800-850 Type I complex from strains 7750 and 7050, and the polypeptides from the B800-820 complex from strain 7050 have now been sequenced [Brunisholz et al, 1987]. The B800-820 complex from strain 7750 is particularly unusual because it contains one  $\alpha$ - and two  $\beta$ -polypeptides.

*Rps. acidophila*, strain 7750, was cultured at  $20-23^{\circ}\text{C}$  under high light intensity in an attempt to obtain a B800-820 complex which lacks the carotenoid cis-rhodopinal (see chapter five). Near-infrared absorption spectra of low light grown strain 7050 cells, low temperature grown strain 7750 cells, and  $30^{\circ}\text{C}$  grown strain 7750 cells are compared in Fig. 3.13. The spectrum of  $30^{\circ}\text{C}$  grown strain 7750 cells indicate the presence of B800-850 Type I complexes as judged by the high  $A_{850}/A_{800}$  ratio, and B890 complexes as judged by the high absorbance at 890nm. The near-infrared spectrum of strain 7750 cells grown at  $20^{\circ}\text{C}$  (b) is very different. Absorption at 850nm is replaced by absorption at 820nm, substantiating the report by Brunisholz et al. (1987), that a B800-820 complex is synthesised under these conditions. When this is compared to the low light grown cells of strain 7050 (a), a difference in intensity of the 850nm shoulder is noted, indicating that the complement of B800-850 complexes in  $20^{\circ}\text{C}$  grown strain 7750 is considerably less than in low light grown cells of strain 7050. In the low temperature grown strain 7750 cells the absorbance at 820nm is significantly higher than that at 800nm, which is unlike any other complex.

Membranes of strain 7750 cells grown at  $20^{\circ}\text{C}$  were prepared (Fig. 3.14a). B890, B800-850 and B800-820 complexes were isolated by DEAE-

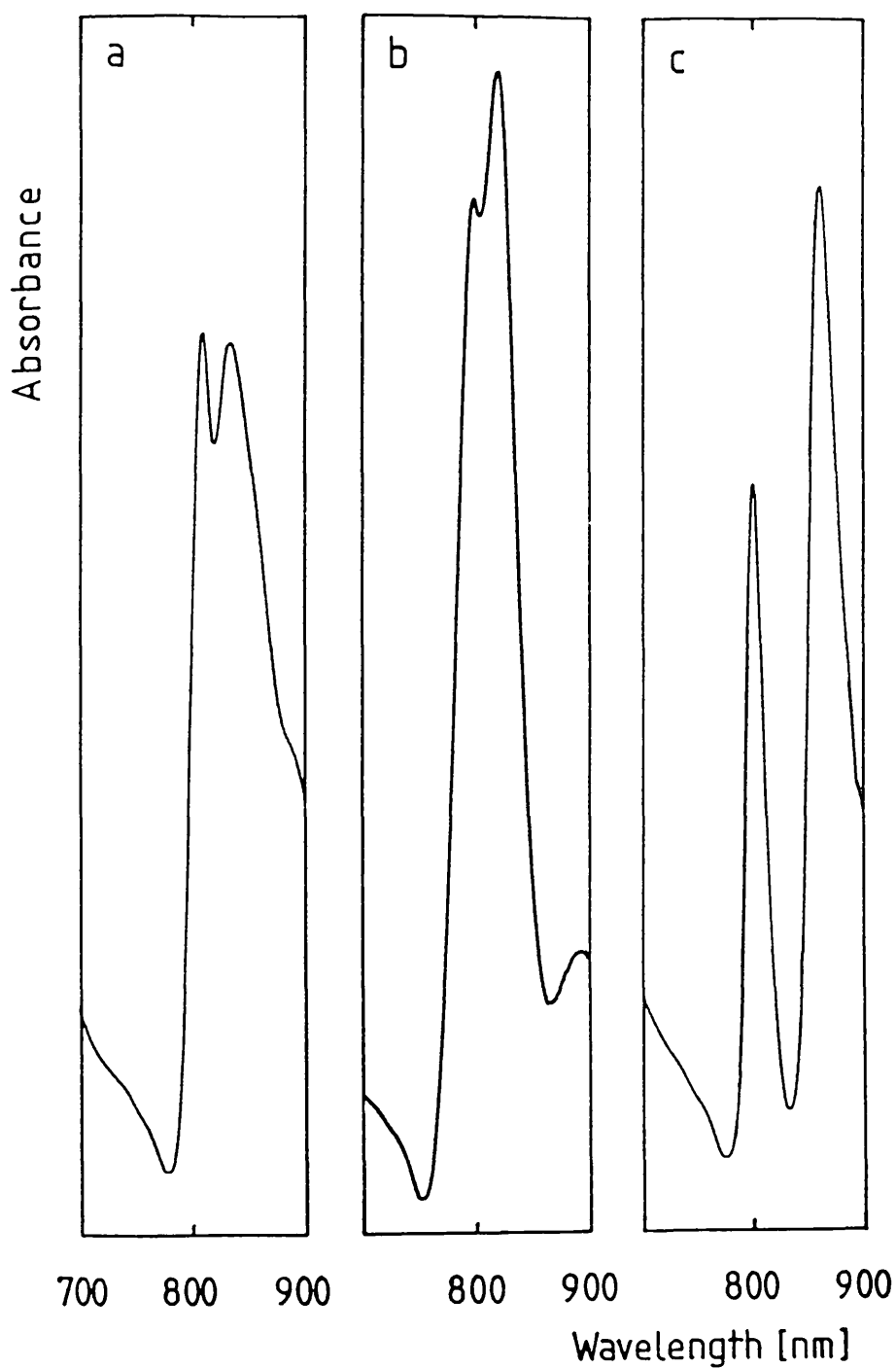
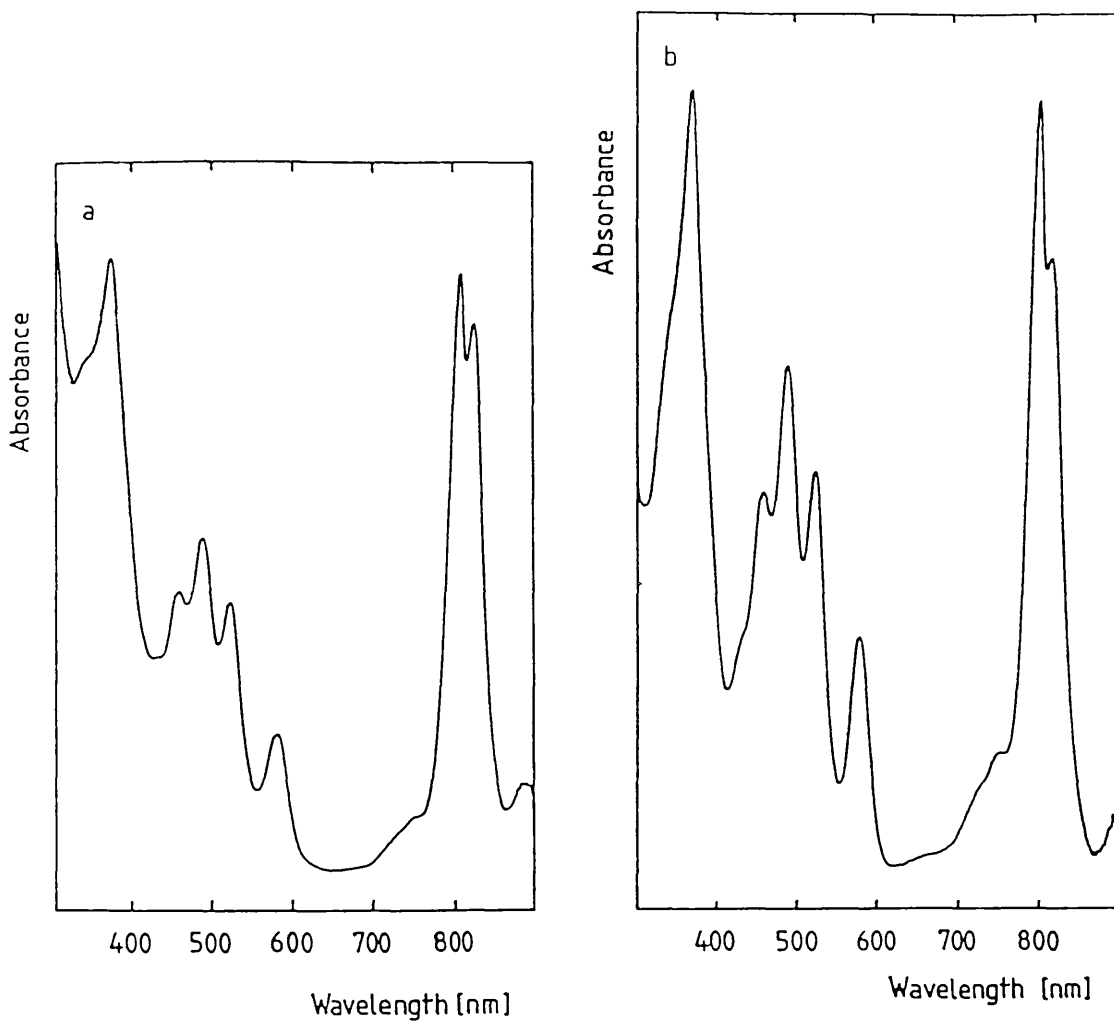


Fig. 3.13 Near-infrared absorption spectra of cells from *Rps. acidophila*: (a) low light grown strain 7050, (b) 20°C grown strain 7750 and (c) 30°C grown strain 7750.



**Fig. 3.14** Absorption spectra of: (a) photosynthetic membranes from *Rps. acidophila*, strain 7750, grown at 20°C and, (b) their isolated B800-820 antenna complexes.

cellulose anion-exchange chromatography. This confirmed the very small proportion of B800-850 complexes present in the cells, estimated to be <5% of the complement of B800-820 complexes. This is the first report of a purple bacterium containing almost exclusively B800-820 complexes as the variable light-harvesting antenna component. The spectra presented are from a second generation culture grown under these conditions. Perhaps with inoculation of further generations the B800-850 component will completely disappear. An absorption spectrum of the isolated B800-820 complex is presented in Fig. 3.14b.

A summary of the different variable antenna complexes synthesised under different growth conditions is presented below.

**Table 3.1**

species	LL/30°C	HL/30°C	HL/40°C	HL/20°C
<i>Rps. palustris</i> , French	B800-850 LL	B800-850 HL	nd	nd
<i>Chr. vinosum</i> , D	B800-850 II B800-820	B800-850 I	B800-850 II B800-820 ?	nd nd
<i>Rps. acidophila</i> , 7050	B800-850 II B800-820	B800-850 I	nd	nd
7750	B800-850 I	B800-850 I	nd	B800-820

**CHAPTER FOUR: Determination of the BChl-to-Carotenoid Ratios of the B890 Antenna Complexes from *Rhodospirillum rubrum* and the B800-850 Complexes from *Rhodobacter sphaeroides***

#### 4.1 Introduction

By investigating the light reactions of photosynthesis we aim to develop an understanding of the molecular organisation of the photosynthetic membrane, and its relation to photosynthetic function. The first objective of an investigation into the structure of the light-harvesting antenna complexes must be to determine their molecular compositions. The empirical ratios of the polypeptides, BChl and carotenoids provide the foundation for our attempts to build an accurate model of the molecular structures of these complexes.

The species *Rhodospirillum rubrum* and *Rhodobacter sphaeroides* have become "laboratory standards" for research into bacterial photosynthesis. *R. rubrum* contains only B890 complexes whereas *Rb. sphaeroides* has core B875 complexes, and B800-850 complexes. These complexes all contain  $\alpha$ - and  $\beta$ -polypeptide subunits in a ratio of 1:1 [Picorel, 1983]. In the B890 antenna type, each polypeptide pair binds two BChl molecules whereas three are bound in the B800-850 complexes [Broglie et al., 1980; Sauer and Austin, 1978]. The ratio of BChl to carotenoid in the B890 complex of *R. rubrum* has been consistently determined to be 2:1 [Picorel et al., 1983; Ueda et al., 1985; Cogdell et al., 1982]. However there have been conflicting reports about the ratio of the B800-850 antenna type. This ratio was originally determined in *Rb. sphaeroides* by Cogdell and Crofts, to be 3 BChl to 1 carotenoid [Cogdell and Crofts, 1978; Cogdell and Thornber, 1979]. Since then the ratio in the analogous B800-850 complexes of *Rb. capsulatus* has been determined to be both 3:1 [Shiozawa et al., 1982] and 2:1 [Feick and Drews, 1978] and Radcliffe et al. (1984) have reported a ratio of 2:1 in *Rb. sphaeroides*, although in the latter case no experimental data were given. Most recently the ratio in *Rb. sphaeroides* has been determined to be 3:1 [Ueda et al., 1985], and 2.5:1 [Picorel and Gingras, 1988]. Although Picorel and Gingras

determined the ratio to be 2.52:1 they concluded that the true stoichiometry is 3:1!

A controversial model for the B800-850 complex of *Rb. sphaeroides* was presented by Kramer et al. (1984a). For this model it was suggested that the basic unit of the complex comprises at least two  $\alpha/\beta$  polypeptide pairs, six BChls and three carotenoids. The controversy arises from two issues: (1) the conclusion that the complex contains two discrete pools of carotenoid (this will be discussed further in chapter seven), and (2) that the ratio of BChl to carotenoid was assumed to be 2:1. Using three different methods the BChl-to-carotenoid ratio of these complexes has been carefully determined to test the validity implied by the Kramer model. The accuracy of each method was checked by repeating the measurements for the B890 complexes of *R. rubrum* which are generally accepted to have a ratio of 2:1.

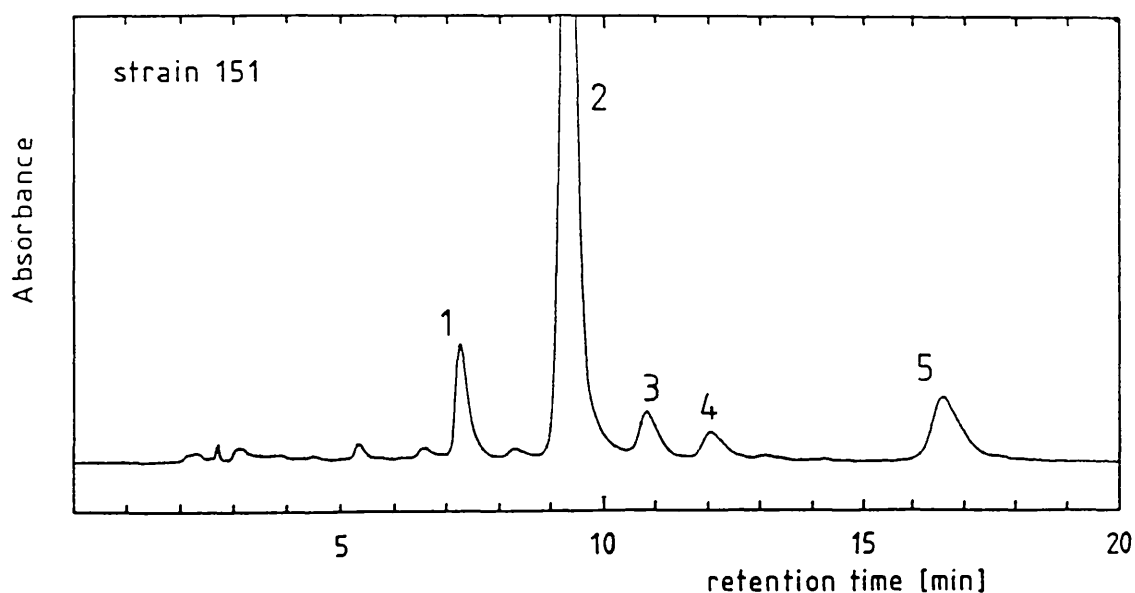
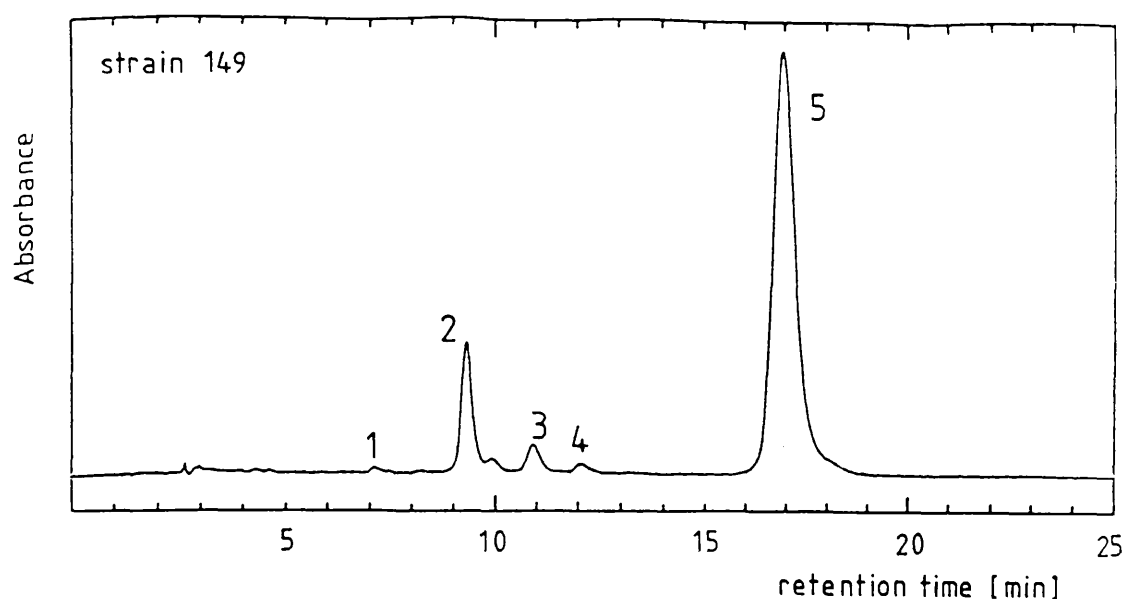
The concentration of BChl in an acetone/methanol pigment extract can be simply determined from an absorption spectrum using the well established absorption coefficient of  $76\text{mM}^{-1}\cdot\text{cm}^{-1}$ , at 772nm [Clayton, 1966]. The concentration of carotenoid is however more difficult to determine because wild-type antenna complexes contain a mixture of carotenoids which absorb at different wavelengths and have different absorption coefficients, and also because there is a small absorption by BChl in the carotenoid region. The three methods used to measure the ratios overcome these problems in different ways.

#### 4.2 HPLC Method

The above problems can be overcome by completely separating the extracts into their component pigments and by quantitating them individually. This can be achieved by reversed phase high performance liquid chromatography using a diode-array detector and automatic

integrator. The pigments are separated on the column, and the absorption spectra of the eluted pigments are recorded at 10ms time intervals. Each pigment can then be quantitated at the required wavelength by peak integration of the elution profiles. The time taken from starting the pigment extraction to obtaining the results is less than 45 min. Combined with minimal exposure to light and oxygen (the solvents are degassed) the opportunity for photodestruction of the pigments is minimal. While developing a solvent system for the separation of acyclic carotenoids, extracts of B800-850 complexes from *Rps. gelatinosus*, strains 149 and 151, were subjected to HPLC. It has been reported that *Rb. sphaeroides* accumulates mainly spheroidene whereas *Rc. gelatinosus* accumulates mainly hydroxyspheroidene [Van Niel, 1947; Goodwin et al., 1955; Eimhjellen and Liaaen-Jensen, 1964]. From the chromatograms of *Rc. gelatinosus* B800-850 complexes (Fig. 4.1) it is obvious that whilst strain 151 contains mostly hydroxyspheroidene as expected, strain 149 has a similar carotenoid composition to *Rb. sphaeroides*. This is probably true of the whole cells as well and it appears to be the first report of a strain of *Rc. gelatinosus* which accumulates mainly spheroidene.

*Rb. sphaeroides* and *Rc. gelatinosus* contain alternative spirilloxanthin series carotenoids. The pigment composition of *Rb. sphaeroides* is demonstrated by the multi-channel chromatogram of a total pigment extract (Fig. 4.2). For quantitative determination BChl was monitored at 580nm, spheroidene and hydroxyspheroidene were monitored at 453nm and spheroidenone was monitored at 485nm. The second, smaller component of the main BChl peak was assumed to be a BChl isomer, possibly the C-10 epimer, because its absorption spectrum was identical to that of the main peak. It was only noted in some extracts of *Rb. sphaeroides* cells and complexes and when it was found the contribution of its peak area



**Fig. 4.1** HPLC chromatograms of total pigment extracts of antenna complexes from *Rc. gelatinosus*, strains 149 and 151, monitored at 455nm: 1=spheroidenone or hydroxyspheroidenone (7.3min); 2=hydroxyspheroidene (9.3min); 3=spirilloxanthin (10.9min); 4=spheroidenone (12min); 5=spheroidene (16.6-16.9min). Note time axes have different scales. Zorbax ODS reversed phase column. Solvent system: 0-100% B over 25min (A= 90% acetonitrile/water, 0.5% triethylamine; B= ethyl acetate).

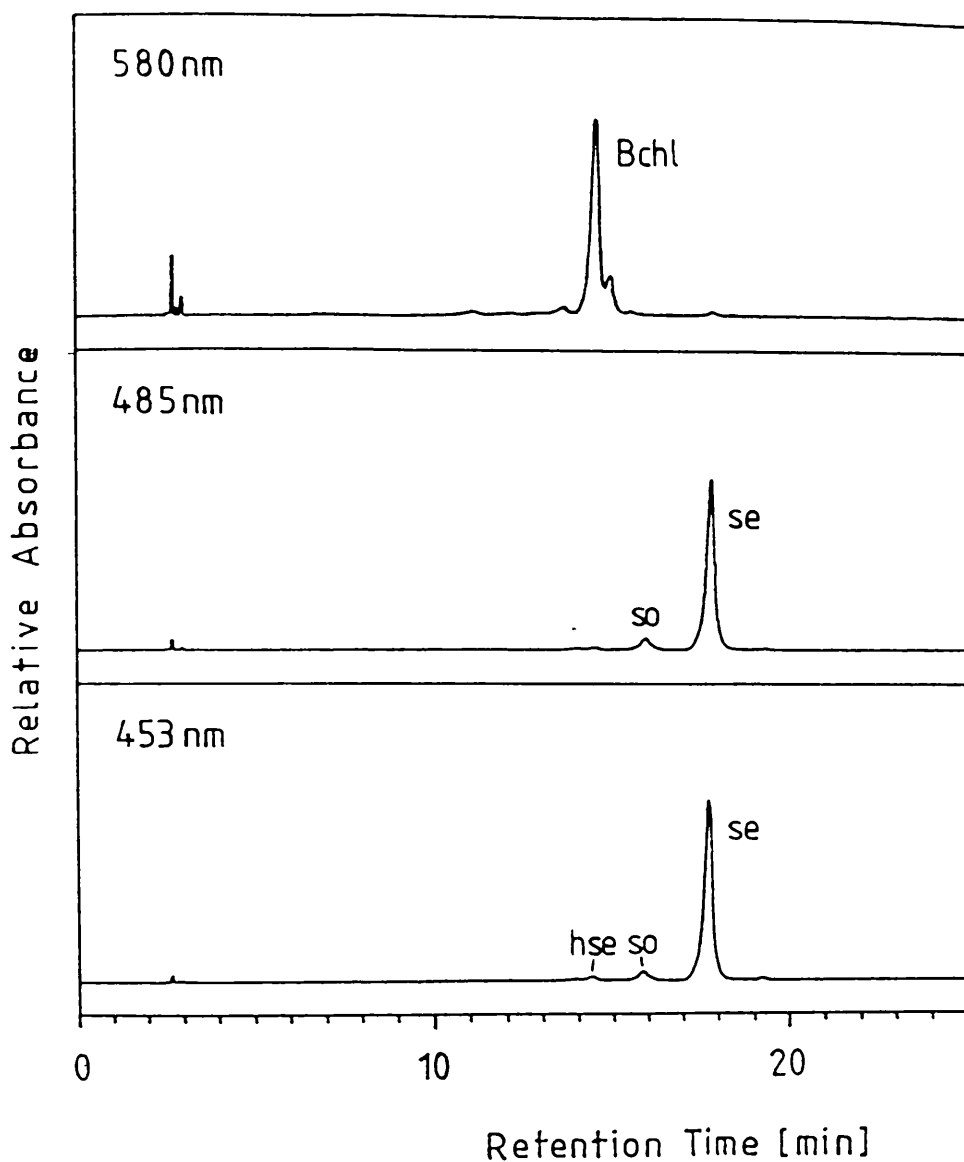


Fig. 4.2 "multi-channel" HPLC chromatogram of total pigment extract of the B800-850 complexes from *Rb. sphaeroides* (se= spheroidene; so= spheroidenone; hse= hydroxyspheroidene). Zorbax ODS reversed phase column. Solvent system: 35% B for 20min, 35-40% B over 10min (A and B as Fig. 4.1).

was included in the ratio calculations. Bacteriopheophytin which is a sensitive indicator of pigment degradation was not detected in any of the antenna complex extracts.

Chromatograms of the total pigment extracts of the B890 complexes from *R. rubrum* and the B800-850 complex of *Rb. sphaeroides*, monitored in the carotenoid absorption range, are illustrated in Figs 4.3 and 4.4. The average retention times in minutes ( $\bar{x} \pm s$ ) of each pigment were as follows:

spheroidene	17.7 $\pm$ 0.5,	spheroidenone	16.9 $\pm$ 0.3,
hydroxyspheroidene	15.8 $\pm$ 0.2,	hydroxyspheroidenone	12.5 $\pm$ 0.1,
anhydropheophytin	17.3 $\pm$ 0.3,	spirilloxanthin	15.4 $\pm$ 0.3,
rhodovibrin	14.0 $\pm$ 0.4,	BChl from <i>R. rubrum</i>	11.4 $\pm$ 0.2
		and from <i>Rb. sphaeroides</i>	15.2 $\pm$ 0.1.

It is interesting to note that the BChl from *Rb. sphaeroides* is significantly less polar than BChl from *R. rubrum*. This is consistent with the reports that the esterifying C<sub>20</sub> alcohol side-chain of *Rb. sphaeroides* BChl is phytol whereas that of *R. rubrum* is geranylgeraniol [Katz, 1982; Kunzler and Pfennig, 1973; Gloe and Pfennig, 1974]. Separation of the two BChls on reversed phase HPLC was demonstrated more clearly by extracting the BChls from the carotenoidless mutants *R. rubrum* G9 and *Rb. sphaeroides* R26, mixing them together and injecting them onto the HPLC column (Fig. 4.5). The absorption spectra, and therefore the chromophores of the two BChls were shown to be identical. The difference in polarity is then due to the structure of the isoprenoid side-chains. The structures of the two BChls are given in Fig. 4.6. A previous report of reversed-phase HPLC of pheophytins esterified with different alcohols has demonstrated that chlorophyll-type molecules can be separated on reversed-phase HPLC on the basis of the length of the isoprenoid side-chain [Schoch et al., 1978]

To quantitate the pigment losses during the chromatography, known amounts of each major pigment were injected and compared to the amounts

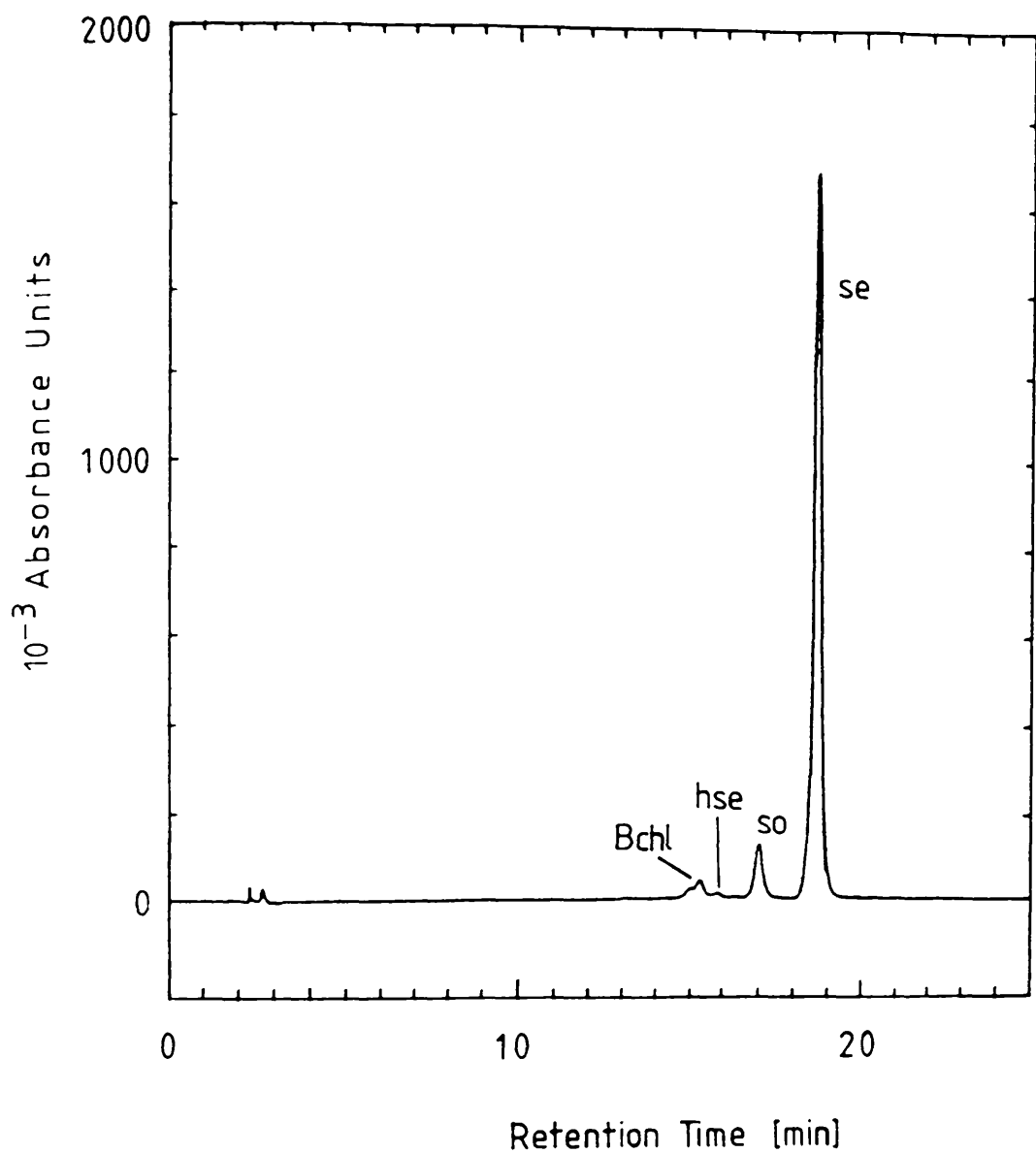


Fig. 4.3 HPLC chromatogram of total pigment extract of the B800-850 complexes from *Rb. sphaeroides* monitored at 453nm (se= spheroidene; so= spheroidenone; hse= hydroxyspheroidene). HPLC system as Fig. 4.1.

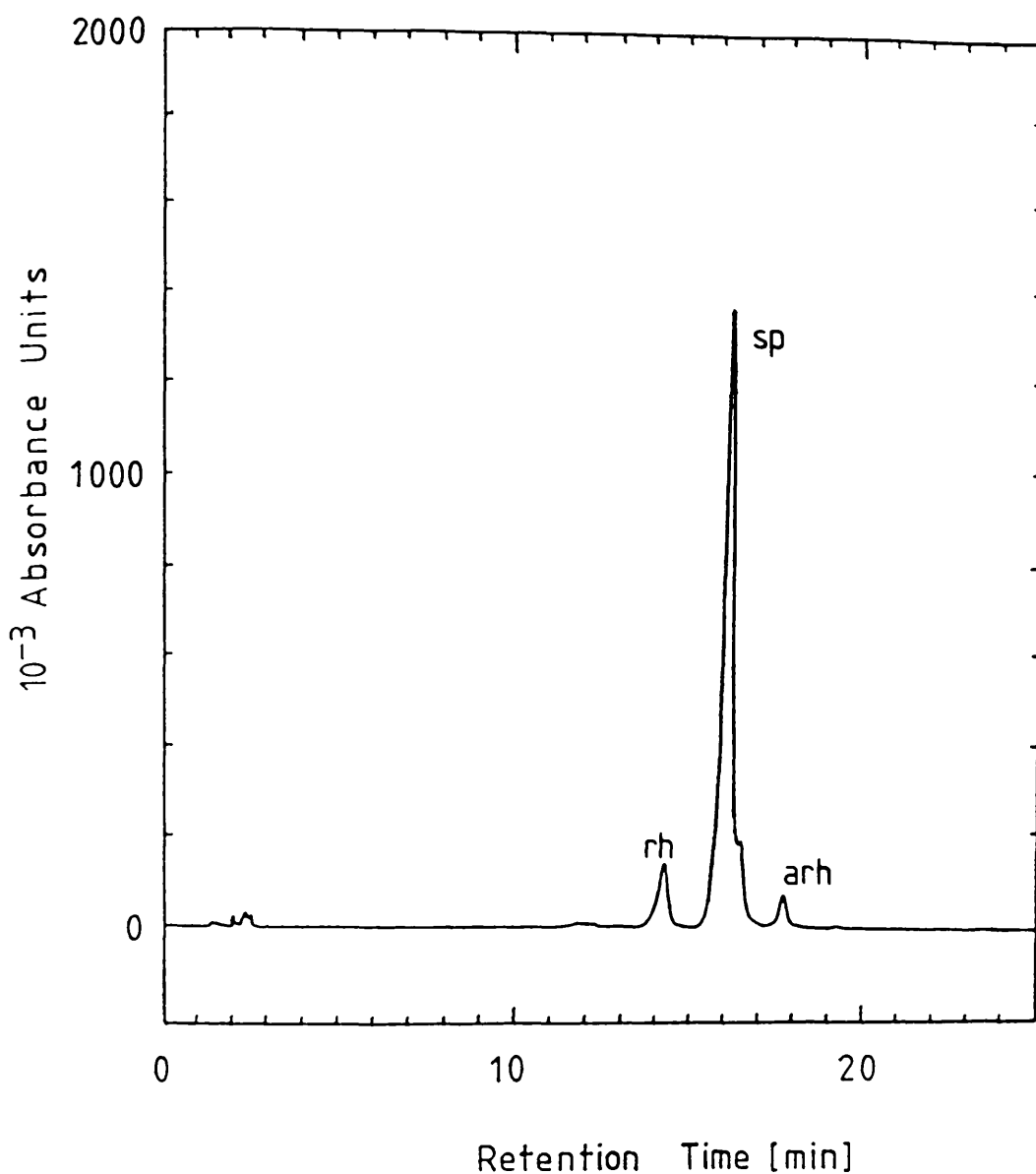
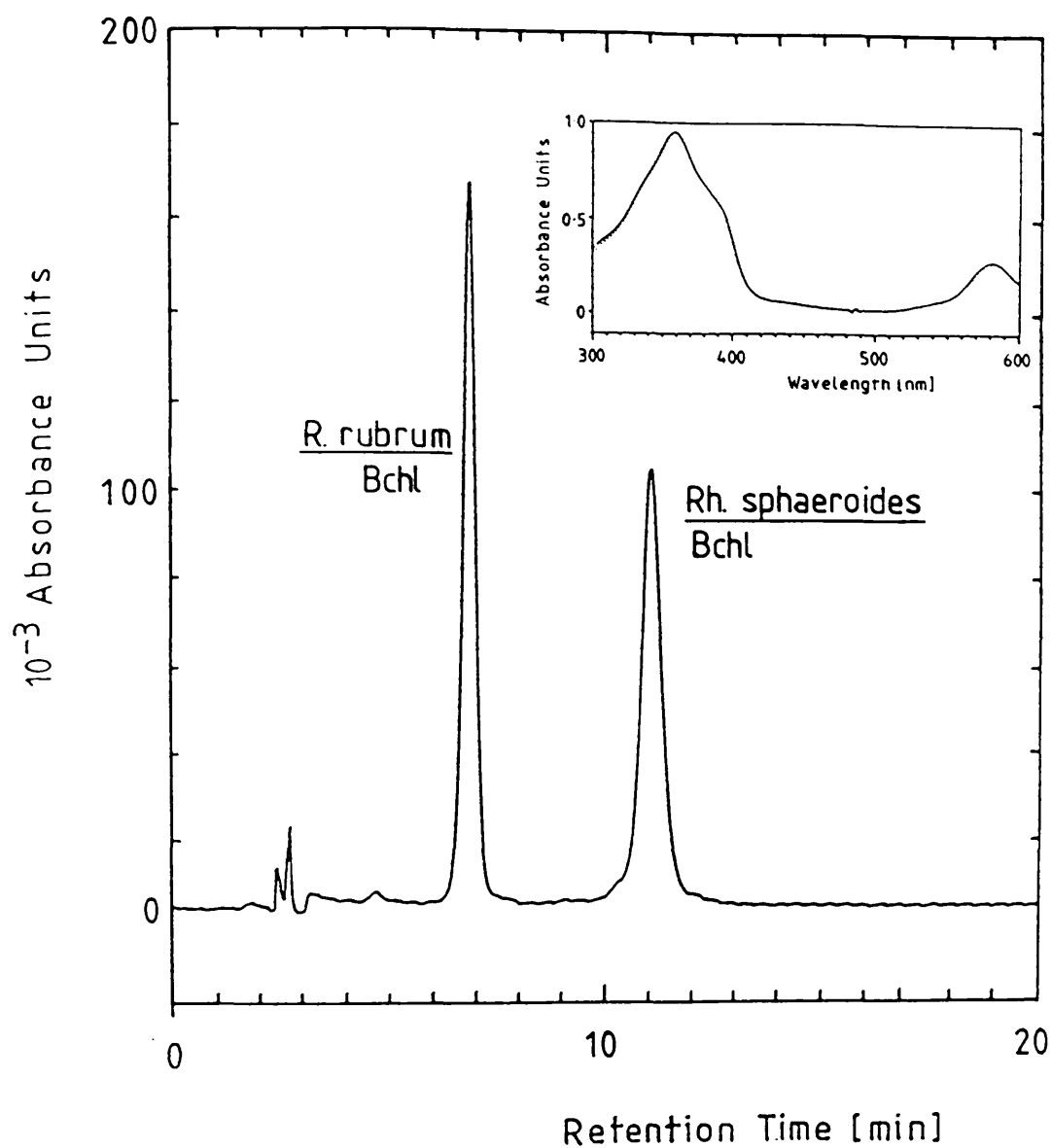


Fig. 4.4 HPLC chromatogram of total pigment extract of the B890 complex from *R. rubrum* monitored at 497nm (rh= rhodovibrin; sp= spirilloxanthin; arh= anhydrorhodovibrin). HPLC system as Fig. 4.1.



**Fig. 4.5** Chromatogram of mixed extracts of the carotenoidless mutants *R. rubrum*, strain G9 and *Rb. sphaeroides*, strain R26, monitored at 580nm. Inset: identical absorption spectra of BChls from *R. rubrum* and *Rb. sphaeroides*. HPLC system as Fig. 4.2.

Fig. 4.6

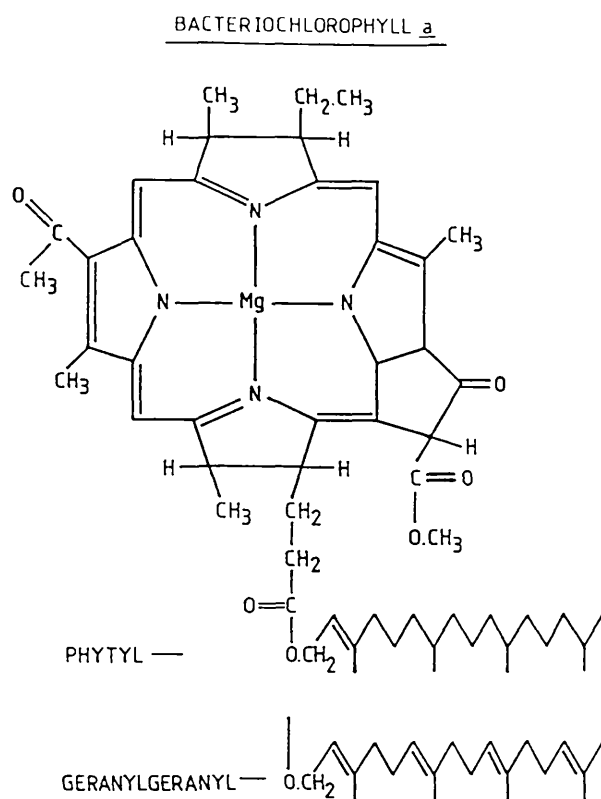


Fig. 4.6 The structure of Bacteriochlorophyll *a*

calculated from the elution peak integration. The averaged carotenoid recovery was determined to be 95% (Table 4.1). As 100% lies within the 95% confidence interval of this mean, it is consistent with the 100% recoveries determined for higher plant carotenoids on similar HPLC systems [Britton et al., 1987]. The carotenoid compositions of the complexes and of the whole cells were determined from the HPLC data (Table 4.2). The compositions of the whole cells were similar to those previously reported for *R. rubrum* (91% spirilloxanthin, 6% rhodovibrin, 2% anhydrorhodovibrin and 1% rhodopin) [Schmidt, 1978] and *Rb. sphaeroides* (90% spheroidene and 10% spheroidenone [Cogdell et al., 1986]. When *Rb. sphaeroides* cells are grown semi-aerobically most of the spheroidene is converted to spheroidenone giving a carotenoid composition of approximately 98% spheroidenone and 2% spheroidene [Goodwin, 1955]. Other minor carotenoids are also present in cells of both species.

The recoveries of the respective BChls of *Rb. sphaeroides* and *R. rubrum* were determined to be  $64 \pm 3\%$  and  $72 \pm 11\%$  (Table 4.1). The unexpectedly high losses were proportional to the sample size. The difference in the percent recoveries of the two BChls is perhaps a property of the different polarities of the molecules.

The BChl-to-carotenoid ratios of the total pigment extracts from *R. rubrum* B890 complexes and *Rb. sphaeroides* B800-850 complexes were both calculated to be 1.3:1. When corrected for BChl losses the values become 1.9 and 2.0 respectively. To confirm these results BChl and the total carotenoid from each species were isolated, mixed in a known 2:1 ratio and then injected onto the column. The ratios subsequently calculated from the integrated peak area were 1.5 and 1.3 respectively. When corrected for BChl losses these gave BChl-to-carotenoid ratios of 2.08:1 and 2.06:1.

**Table 4.1: BChl-to-carotenoid ratio results table**

	<i>R. rubrum</i>		<i>Rb. sphaeroides</i>	
	B890 complex		B800-850 complex	
	n	x ± s	n	x ± s
% recovery carotenoid	15	95 ±11	10	96 ±4
recovery BChl	10	72 ±11	10	64 ±3
BChl/carotenoid ratio by HPLC	17	1.3 ±0.2	15	1.3 ±0.1
Ratio corrected for losses <sup>*</sup>		1.9 ±0.2		2.0 ±0.1
Ratio of 2:1 mixtures by HPLC	11	1.5 ±0.3	10	1.3 ±0.1
Ratio by solvent extraction	9	1.7 ±0.4	10	2.2 ±0.4
Ratio by difference spectroscopy	3	2.0 ±0.3	3	2.0 ±0.2

x=arithmetic mean

s=sample standard deviation

n=sample number

<sup>\*</sup> assuming 100% carotenoid recovery**Table 4.2: Carotenoid composition of whole cells and complexes**

	complex		w/cells	
	n	x ±s%	n	x ±s%
<i>R. rubrum</i>		B890		
spirilloxanthin	7	89.4 ±0.2	3	83.4 ±0.3
rhodovibrin	7	7.4 ±0.5	3	9.6 ±0.1
anhydrorhodovibrin	7	3.2 ±0.3	3	7.0 ±0.2
<i>Rb. sphaeroides</i>		B800-850		
spheroidene	14	93.6 ±1.4	8	71.3 ±0.5
spheroidenone	14	4.5 ±1.4	8	16.0 ±0.1
hydroxyspheroidene	14	1.7 ±0.2	8	9.2 ±0.1
hydroxyspheroidenone	14	0.0	8	4.4 ±0.2

### 4.3 Carotenoid Separation Method

This method overcame the problem of BChl absorption in the carotenoid region by quantitatively separating the carotenoid from the BChl using methanol/water partitioning. The carotenoid compositions previously determined by the HPLC work were used to calculate an average carotenoid absorption coefficient. The ratios were determined to be 1.7:1 and 2.2:1 for the B890 and B800-850 complexes respectively. This method was the least accurate of those used because of the error inherent in the carotenoid isolation manipulations.

### 4.4 Difference Spectroscopy Method

In this method the concentrations of both BChl and carotenoid were determined directly from the absorption spectrum. Isolated BChl was added to the blank cuvette until BChl absorption was eliminated, allowing the true absorption due to carotenoid to be measured. In both complexes the ratios were determined to be 2:1. This method is the quickest of the three and is quite reliable.

### 4.5 Summary

In summary the 2:1 BChl-to-carotenoid ratio for the B800-850 complex of *Rb. sphaeroides* suggested by each of the three methods, agrees with the stoichiometry used in the Kramer model. There are therefore 3 BChl and  $1\frac{1}{2}$  carotenoid molecules per  $\alpha/\beta$ -polypeptide pair. This gives a stoichiometry of 18 BChl and 9 carotenoids per hexameric antenna complex aggregate (see section 1.7(vii)).

**CHAPTER FIVE:** Determination of the BChl-to-Carotenoid Ratios of Antenna Complexes from *Rhodobacter spheroides*, *Rhodopseudomonas palustris*, *Chromatium vinosum* and *Rhodopseudomonas acidophila*, and a Possible Correlation With the Results of Linear Dichroism and Picosecond Energy Transfer Measurements on *Rps. palustris*

## 5.1 Introduction

The careful study of the BChl-to-carotenoid ratios of antenna complexes was continued using a new method which proved to be reliable and more convenient than the methods used in the previous chapter. The pigment ratios were determined directly from the absorption spectra of the total pigment extracts using the simultaneous equation method described in section 2.8(iv).

## 5.2 BChl-to-carotenoid Ratios of the B800-850 and B875 Complexes from *Rb. sphaeroides*

The reliability of the simultaneous equation method was first assessed by performing a single ratio determination on the B800-850 complexes from *Rb. sphaeroides*. The ratio was calculated to be 2.07 which agrees well with the data already presented. The ratio for the B875 complexes from *Rb. sphaeroides* was then determined. Because these complexes are damaged by traditional LDAO and alkaline Triton X-100 treatment [Loach et al., 1970; Clayton and Clayton, 1972] methods for their isolation have only recently been reported. Broglie et al. (1980) reported a laborious method of isolating the complexes using gel electrophoresis. Very recently a method has been reported by Picorel and Gingras (1988) which uses SDS and Triton X-100. The BChl-to-carotenoid ratio of these complexes has previously been determined to be 1:1 [Broglie et al., 1980; Picorel and Gingras, 1988]. The B875 complexes for this work were obtained from a mutant strain of *Rb. sphaeroides* (strain M2192) which contains neither reaction centres nor B800-850 complexes. The mutant cells were acquired from Dr Neil Hunter, Sheffield University. They were obviously grown microaerobically because their carotenoid composition was determined to

be approximately 98% spheroidenone. Traces of spheroidene and other unidentified minor carotenoids were also found. The average millimolar absorption coefficient for the total carotenoid at the absorption maximum was calculated to be  $124\text{mM}^{-1}\cdot\text{cm}^{-1}$  in light petroleum. The BChl-to-carotenoid ratio measurements were: 0.87, 0.95, 1.05, 1.11, 1.24 and 1.13, giving an arithmetic mean of 1.06, sample standard deviation of 0.133 and 95% confidence limits of 0.92-1.20 (i.e. it is 95% certain that in the absence of systematic error the true population mean lies between these values). These results agree well with the published stoichiometry.

### 5.3 BChl-to-Carotenoid Ratios of the B800-850 Complexes from High and Low Light Grown *Rps. palustris*, strain French

The BChl-to-carotenoid ratios of B800-850 antenna complexes isolated from high and low light grown *Rps. palustris*, strain French, were determined to complement the studies on the polypeptide compositions of these complexes which are presented in the following chapter.

#### **5.3(i) Carotenoid identification**

The carotenoids of *Rps. palustris*, strain French, were identified by absorption spectroscopy, their adsorption affinities on silica TLC, mass spectroscopy and their elemental compositions. A thin-layer chromatogram of the major carotenoids, isolated from the "low light" (LL) complexes is pictured in Fig. 5.1. A summary of the data used to identify the carotenoids is presented in Table 5.1. With the exception of rhodopin, the carotenoid absorption maxima were all slightly lower than the published values of: lycopene 472nm; anhydroporphyrin 483nm; spirilloxanthin 510nm; rhodopin 470nm and rhodovibrin 483nm, when

Table 5.1.1 Summary of the data used to identify the carotenoids isolated from B800-850 complexes from *Rps. palustris*, strain French.

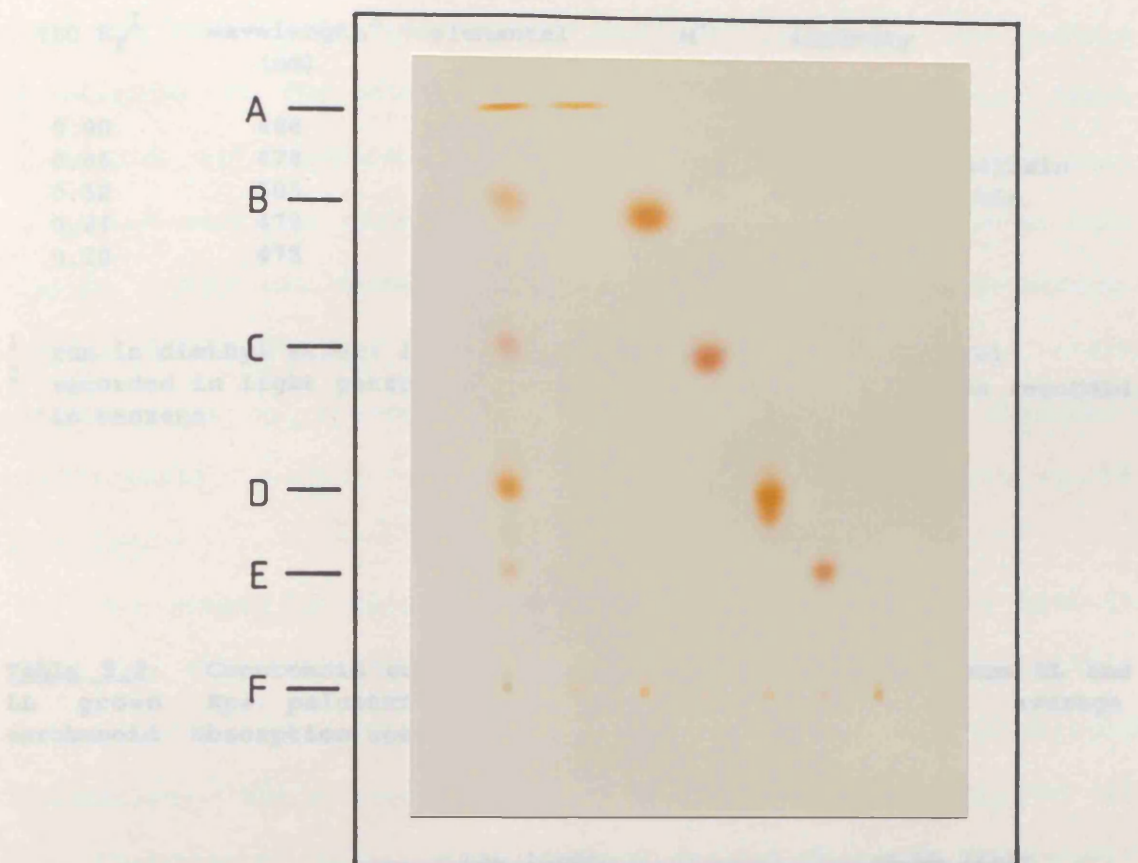


Table 5.1.2 Summary of the data used to identify the carotenoids isolated from B800-850 complexes from *Rps. palustris*, strain French.

Lycopene	25	154	2342	25	154	2342
Anhydrorhodovibrin	8	142	1712	8	142	1712
Spirilloxanthin	58	165	2342	58	165	2342
Rhodopin	8	158	245	8	158	245
Rhodovibrin	8	145	2342	8	145	2342
			[+16120]			[+16120]

Table 5.1.3 Summary of the data used to identify the carotenoids isolated from B800-850 complexes from *Rps. palustris*, strain French.

**Fig. 5.1** Silica thin-layer chromatogram of pigments extracted from B800-850 complexes from *Rps. palustris*, strain French. The leftmost column is a total pigment extract. The remaining columns demonstrate the purity of individual carotenoids isolated for identification by mass spectroscopy.

- A lycopene
- B anhydrorhodovibrin
- C spirilloxanthin
- D rhodopin
- E rhodovibrin
- F origin

The pigments were detected by a high resolution mass spectrometer in conjunction with the mass spectroscopic analysis.

**Table 5.1: Summary of the data used to identify the carotenoids isolated from B800-850 complexes from *Rps. palustris*, strain French**

TLC $R_f$ <sup>1</sup>	wavelength <sup>2</sup> (nm)	elemental composition	$M^+$	identity
0.90	468	$C_{40}H_{56}$	536	lycopene
0.86	478	$C_{41}H_{58}O$	566	anhydrorhodovibrin
0.52	505	$C_{42}H_{60}O_2$	596	spirilloxanthin
0.24	470	$C_{40}H_{58}O$	554	rhodopin
0.20	478	$C_{41}H_{60}O_2$	584	rhodovibrin

<sup>1</sup> run in diethyl ether: light petroleum 40-60°C bp (1:5, v/v)

<sup>2</sup> recorded in light petroleum except spirilloxanthin which was recorded in benzene

**Table 5.2: Carotenoid compositions of B800-850 complexes from HL and LL grown *Rps. palustris* and calculation of their average carotenoid absorption coefficients in acetone/methanol**

	Low light			High light		
	%	$\epsilon_{470}$	% x $\epsilon$	%	$\epsilon_{475}$	% x $\epsilon$
lycopene	25	116	2900	10	113	1130
anhydrorhodovibrin	8	142	1136	6	109	654
spirilloxanthin	55	169	9295	57	162	9232
rhodopin	6	158	948	6	134	804
rhodovibrin	6	145	870	20	118	2360
			$\Sigma = 15149$			$\Sigma = 14180$
			$\Sigma / 100 = 151 \text{mM}^{-1} \text{cm}^{-1}$			$\Sigma / 100 = 142 \text{mM}^{-1} \text{cm}^{-1}$

recorded in the same solvents [Davies, 1965]. Variation from the published wavelengths can be expected because of differences in solvent purity, water content etc. The wavelengths were recorded against a holmium reference filter to ensure accuracy. The mass spectra and their diagnostic interpretation are presented in Appendix D. The elemental compositions of the carotenoids were determined by a high resolution mass detector in conjunction with the mass spectroscopic analysis.

### 5.3(ii) Carotenoid composition

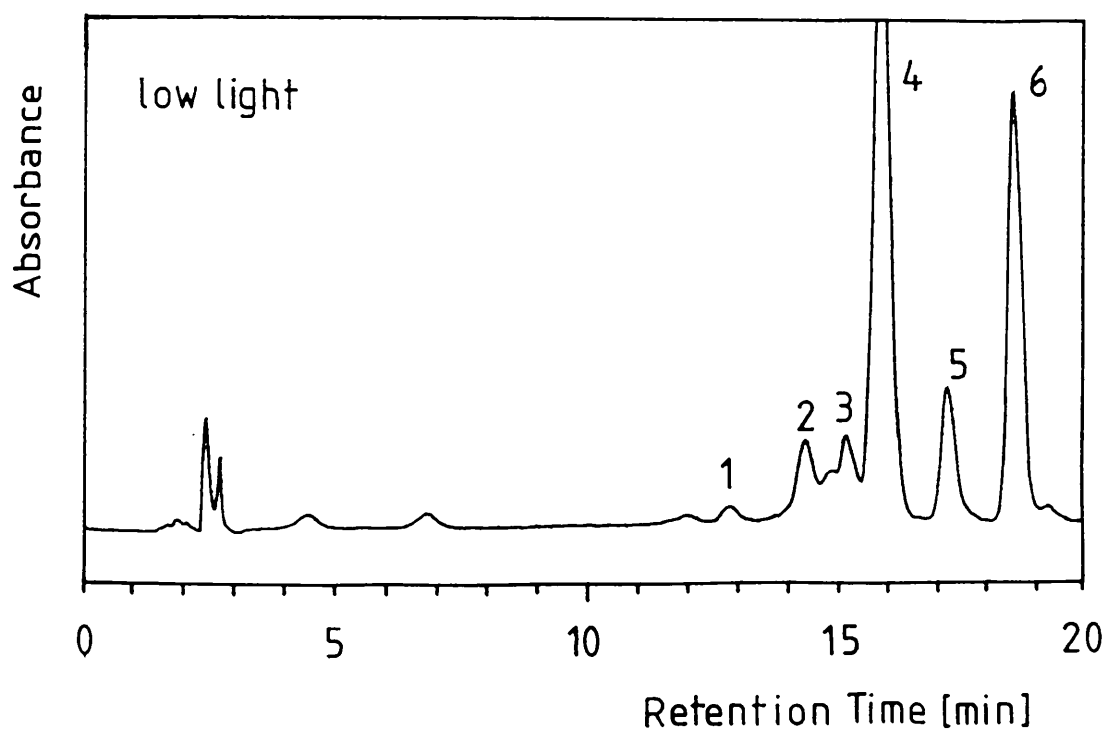
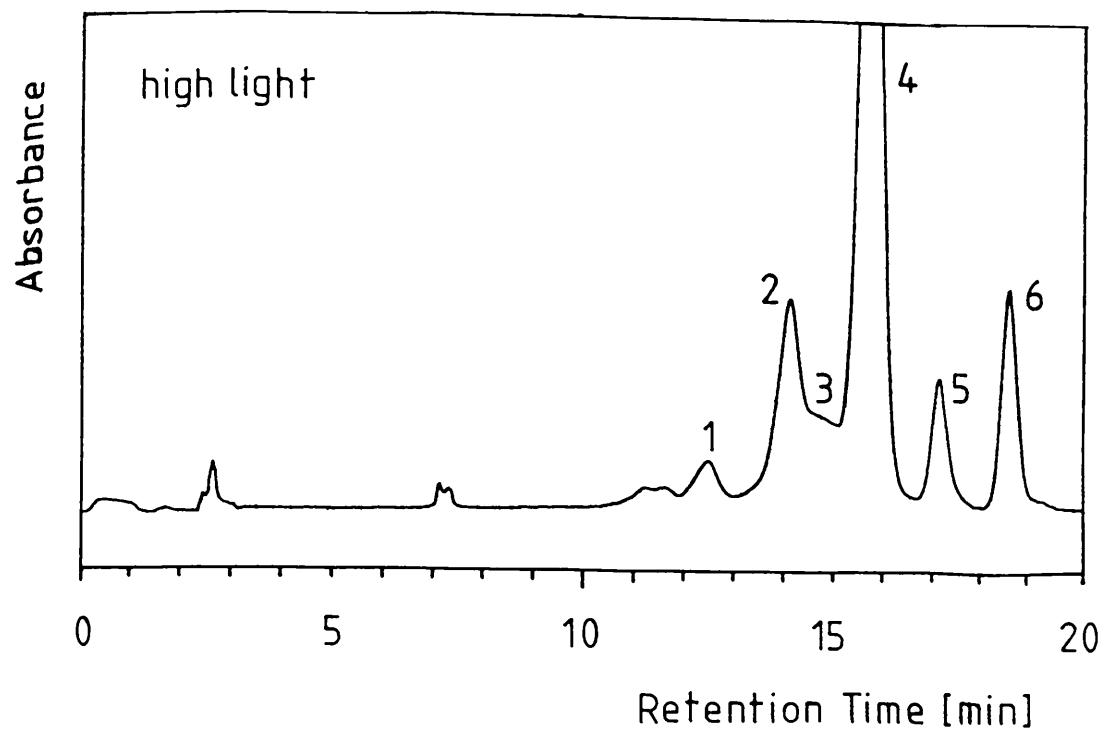
The carotenoid compositions of the B800-850 complexes from low light and high light grown *Rps. palustris* cells combined with example calculations of the average absorption coefficients for the total carotenoid, are presented in Table 5.2. The compositions were only determined once for these, and all other complexes analysed in this chapter. They can therefore only approximate the true compositions. Because the largest source of systematic error in these ratio determinations is probably the values of the published absorption coefficients, single compositional analyses were thought to be sufficient.

The absorption maxima of the total carotenoid extracts were at 470nm and 475nm for the LL and HL complexes respectively. This difference can be explained by comparison of their carotenoid compositions. The LL complex contains proportionately more lycopene and less rhodovibrin, giving an absorption maximum of lower wavelength. HPLC chromatograms of pigment extracts from high and low light grown cells are presented in Fig. 5.2. As in the B800-850 complexes, the low light grown cells contain proportionately more lycopene and less rhodovibrin than the high light grown cells.

### 5.3(iii) BChl-to-carotenoid ratio determinations

Absorption spectra of total pigment extracts of B800-850 complexes from LL and HL grown *Rps. palustris* cells are presented in Fig. 5.3. The ratios determined for the HL complex preparations were: 2.04, 1.93, 1.94, 2.36, 1.87, 1.82, 2.21, 1.76, 1.92, and 1.90. These give an arithmetic mean of 1.98, a sample standard deviation of 0.183 and 95% confidence limits of 1.84-2.11.

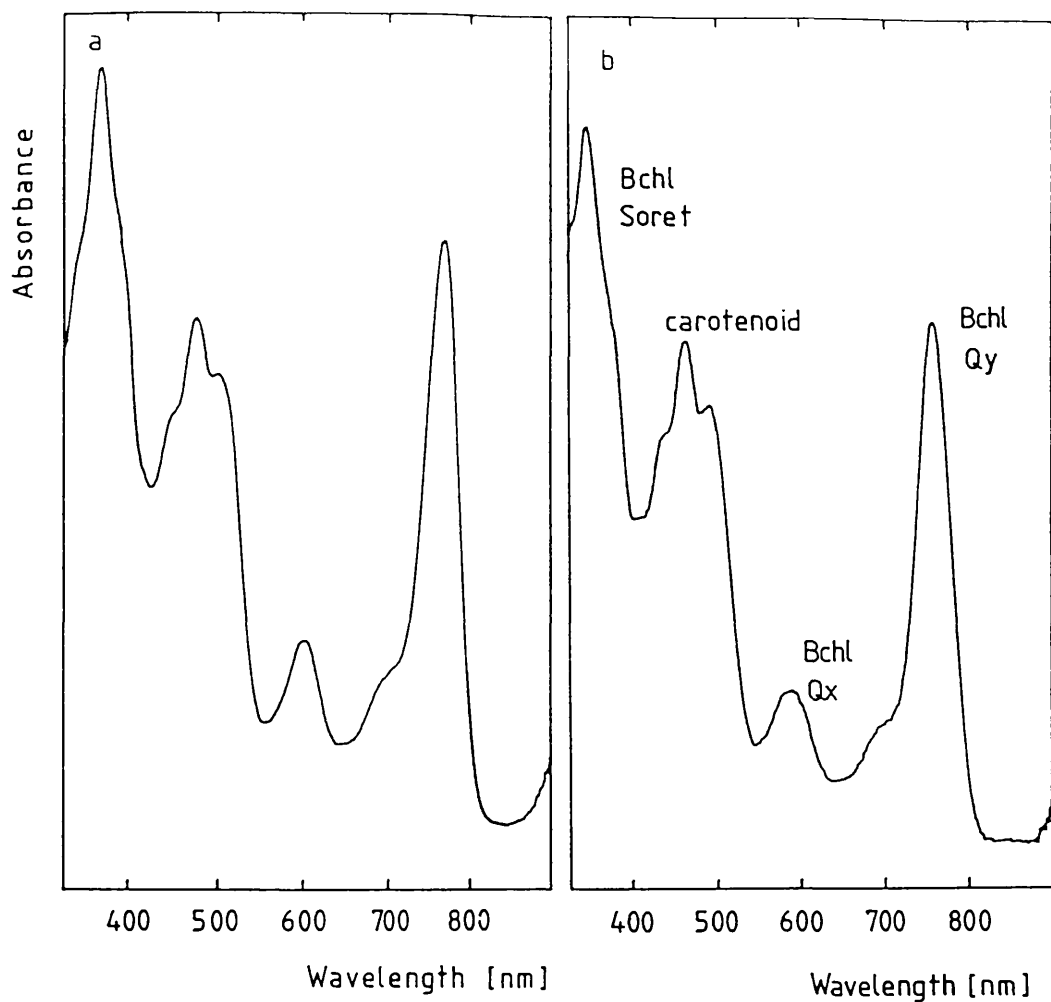
Initial BChl-to-carotenoid ratio determinations of the LL B800-850 complexes were rejected. The measurements were: 3.51, 2.51, 2.39, 3.97,



**Fig. 5.2** HPLC chromatograms of pigment extracts from high and low light grown *Rps. palustris*, strain French, cells, monitored at 455nm. 1=unknown, 2=rhodovibrin, 3=rhodopin, 4=spirilloxanthin, 5=anhydrorhodovibrin and 6=lycopene. Zorbax ODS reversed phase column. Solvent system: 0-100% B over 25 min. A= 90% acetonitrile/water, 0.5% triethylamine; B= ethyl acetate.

2.65, 4.23, 2.41, 2.06, 2.15, 2.94, 2.08, 2.82, 2.13, 2.17, 2.28 and 2.30. These give an arithmetic mean of 2.66, a standard deviation of 0.68 and standard error of 0.17. The standard error indicates a precision two-times lower than that expected from previous measurements for this method (see Table 5.7) and the 95% confidence interval of the mean (2.33-2.99) does not encompass a whole number. The measurements were all made on the same antenna complex preparation which was more dilute than normally used. Because the initial data was suspect, it was decided to repeat the measurements on two fresh preparations which were far more concentrated. Small volumes (100 and 200  $\mu$ l) were then extracted with a relatively large volume of dry solvent to minimise the water content of the extraction mixture. Previously, approximately 1ml of dilute complex was used. The new BChl-to-carotenoid ratios were: 3.00, 3.13, 2.91, 3.01, 2.99, 2.91, 2.91, 2.93, 3.28, 2.79, 3.21, 2.93, 2.91, 3.01, 3.05, 3.04, 4.36, 3.34, 2.75, 3.91, 2.97, 2.91, 2.90, 2.83, 2.67 and 2.76. These give an arithmetic mean of 3.05, a standard error of 0.05, sample standard deviation of 0.36 and 95% confidence limits of 2.90-3.20.

It is clear that for precise ratio measurements the water content of the extraction mixture must be minimised because it prevents the complete organic solvent solvation of the carotenoids. The carotenoids probably aggregate into unsolubilised lipid globules. Addition of water to a clear organic solvent carotenoid extract causes the sample to cloud. When extracts with high water content were filtered through a pasteur pipette plugged with cotton wool, a significant proportion of the carotenoid was adsorbed to the cotton wool. With dry extracts the pigments passed through with no adsorption. Water cannot be eliminated from the extracts by evaporation to dryness under nitrogen, because BChl dries into the proteins and lipids etc. which coat the glass vial, and



**Fig. 5.3** Absorption spectra of total pigment extracts of B800-850 complexes from low light (left) and high light grown *Rps. palustris* cells. Note the different  $A_{772}/A_{\text{carot}}$  ratios.

it cannot be quantitatively redissolved.

#### 5.4 BChl-to-Carotenoid Ratios of the B800-850 Complexes from 30°C and 40°C grown *Chromatium vinosum*, strain D

Thornber (1970) analysed the molar composition of antenna complexes isolated from *Chr. vinosum*, strain D. He reported that the carotenoid compositions of the B800-850 Type II complexes and B800-820 complexes are lycoxanthin and spirilloxanthin, in a ratio of 2:1. His identification of lycoxanthin (3-hydroxylycopene) was however incorrect. Subsequent analysis of the carotenoid composition of this species did not detect the presence of lycoxanthin but found the normal spirilloxanthin series carotenoids instead [Schmidt, 1978; Schmidt et al., 1965]. Thornber determined the BChl-to-carotenoid ratios for the above complexes to be 10:3 (i.e. 3.3:1). The BChl concentrations were determined spectrophotometrically without extraction into organic solvent. This, combined with an incorrect carotenoid composition analysis, suggests that the ratio data presented are unreliable. The ratios of the B800-850 Types I and II complexes isolated from *Chr. vinosum*, strain D, were therefore reassessed in the present study. The carotenoids from these complexes were identified by co-chromatography with carotenoids previously isolated from *Rps. palustris*. The carotenoid compositions determined for the B800-850 complexes are presented in Table 5.3. From these data, average absorption coefficients were calculated to be  $152\text{mM}^{-1}.\text{cm}^{-1}$  and  $147\text{mM}^{-1}.\text{cm}^{-1}$  for the 30°C and 40°C complexes respectively.

**Table 5.3: Carotenoid compositions of B800-850 complexes isolated from 30°C and 40°C grown *Chr. vinosum***

	30°C %	40°C %
lycopene	4.7	8.4
anhydrorhodovibrin	7.6	15.7
spirilloxanthin	6.2	14.3
rhodopin	78.6	59.9

The ratios determined for the 30°C complexes were: 2.31, 2.14, 1.83 and 1.97. These give an arithmetic mean of 2.06, a sample standard deviation of 0.208 and 95% confidence limits of 1.73-2.39. The ratio measurements for the 40°C complexes were: 2.00, 2.04, 2.52, 2.47, 1.66, 1.89 and 1.93, giving an arithmetic mean of 2.07, sample standard deviation of 0.313, and 95% confidence limits of 1.78-2.36.

### **5.5 BChl-to-carotenoid Ratios of the B800-850 and B800-820 Complexes from *Rps. acidophila*, strains 7050 and 7750**

#### **5.5(i) Introduction**

BChl-to-carotenoid ratios for antenna complexes isolated from *Rps. acidophila*, strains 7750 and 7050, have previously been determined by Cogdell et al. (1983), using the difference spectroscopy method (section 2.8(iii)). Their results, averaged from two determinations, were:

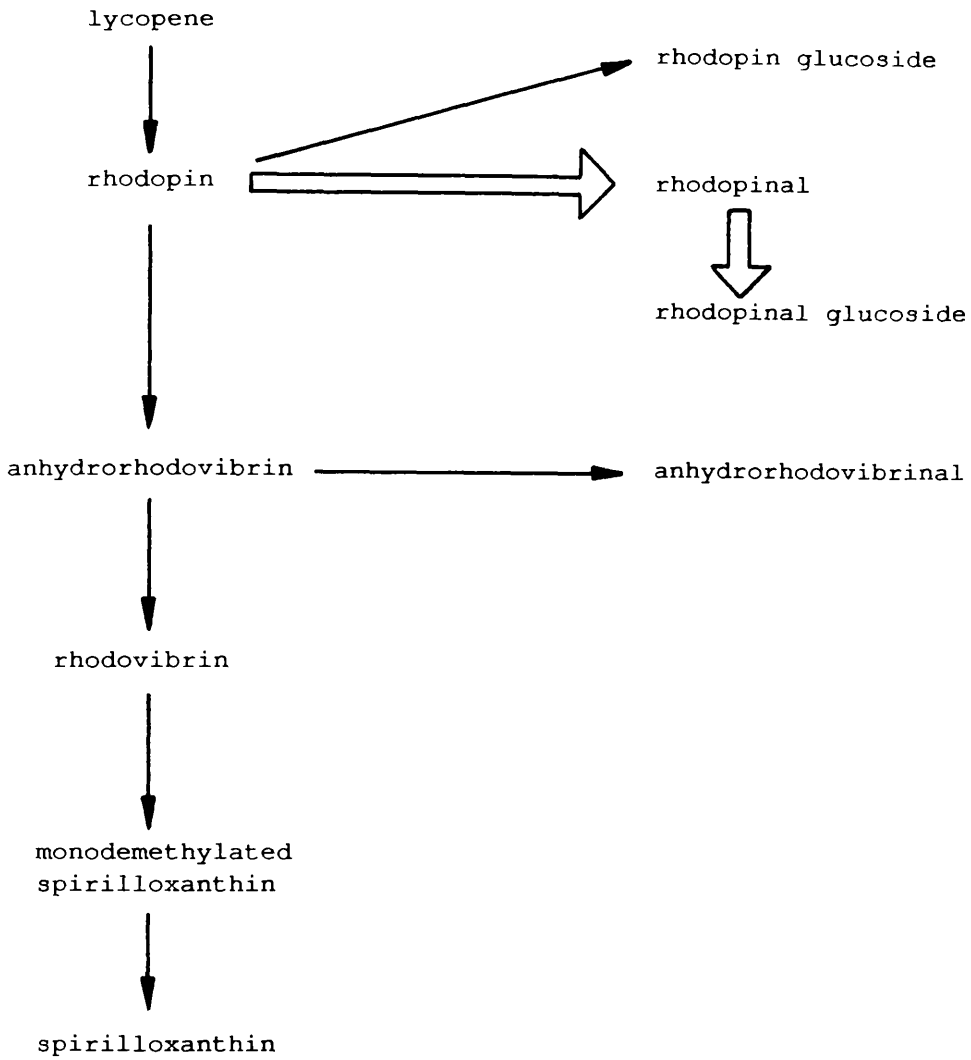
B800-850 Type I complexes, strain 7750	2.8:1
B800-850 Type II complexes, strain 7050	3.1:1
B800-820 complexes, strain 7050	3.2:1

The ratio for the Type I B800-850 complexes contradicts the 2:1 ratios presented for all complexes of this type, in this and the previous

chapter. The ratio for the B800-850 Type II complexes agrees with the published value for the equivalent complexes of *Chr. vinosum* which was however disputed in the previous section.

BChl-to-carotenoid ratios have previously been determined for low and high light grown whole cells of *Rps. acidophila*, strain 7050, to be 4.7:1 and 3.9:1 respectively [Heinemeyer and Schmidt, 1983]. Low light grown cells contain a large proportion of variable complexes. The average ratio determined for the variable complexes should therefore approximate the ratio of the low light cells. This is clearly not the case for the above data. Because the pigment ratios of antenna complexes from *Rps. acidophila* have never been the subject of a thorough analytical study, it was decided to extend the present work to include these complexes.

The carotenoids of *Rps. acidophila*, strain 7050, have an interesting biosynthetic pathway which is partly controlled by the light intensity (Fig. 5.4). The carotenoid compositions of low and high light grown cells, determined by Heinemeyer and Schmidt (1983) are presented in Table 5.4. The unusual feature is the presence of carotenoid glucosides which account for over half of the total carotenoid in low light grown cells. These were first reported by Schmidt et al. (1971). A reduction of the light intensity induces the synthesis of Type II B800-850, and B800-820 complexes and the preferential synthesis of *cis*-rhodopinal glucoside. A striking change in the colour of the cells from orange to purple is then observed.



**Fig. 5.4** The biosynthetic pathway of carotenoids in *Rps. acidophila*. Block arrows show pathways which are preferentially stimulated under low light growth conditions. [Heinemeyer and Schmidt, 1983].

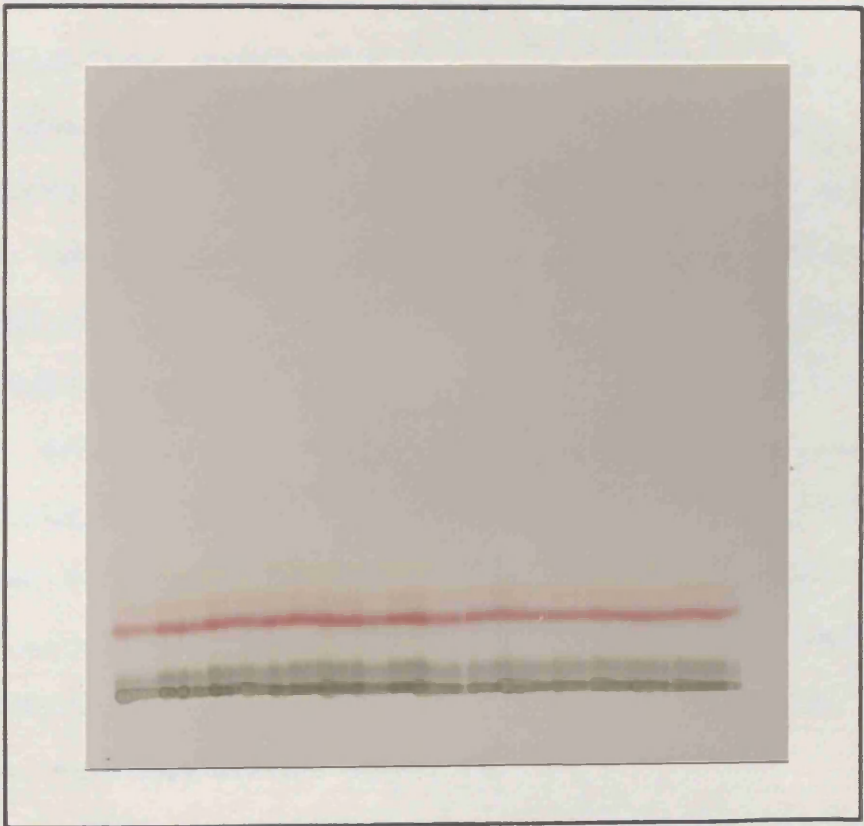
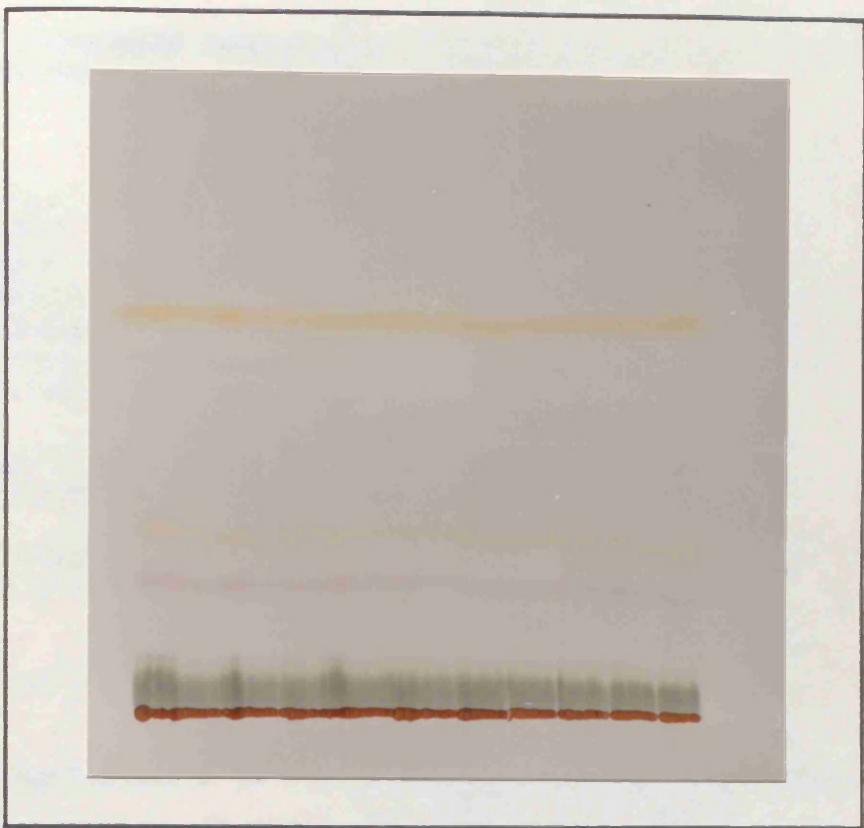


Fig. 5.5 Top: silica TLC of total pigment extract of the B800-820 complexes from low light grown *Rps. acidophila*, strain 7050; Bottom: TLC of carotenoid peracetates formed from the glucosides recovered from the above chromatogram.

**Table 5.4** Carotenoid compositions of HL and LL grown *Rps. acidophila*, strain 7050 [Heinemeyer and Schmidt, 1983]

	HL	LL
lycopene	5	1
lycopenal	1	0.5
rhodopin	25	10
rhodopinal	5	7
anhydrorhodovibrinal	<1	1
spirilloxanthin group <sup>1</sup>	4	3
glucosides	58	78
rhodopin glucoside	20	13
rhodopinal glucoside	38	65
total rhodopin	45	23
total rhodopinal	43	72

<sup>1</sup> anhydrorhodovibrin, rhodovibrin and hydroxyspirilloxanthin

#### 5.5(ii) Identification of the carotenoids from the B800-850 Type II, and B800-820 complexes from *Rps. acidophila*, strain 7050

A thin-layer chromatogram of a total pigment extract of the B800-820 complexes from the low light grown *Rps. acidophila*, strain 7050, is pictured in Fig. 5.5 (top). The normal spirilloxanthin-series carotenoid, lycopene was identified just below the solvent front, underneath which are the two, hardly visible bands of anhydrorhodovibrin and spirilloxanthin. For absorption spectra of these carotenoids see Appendix C. More strongly adsorbed are the orange carotenoid, rhodopin, and the more purple carotenoid rhodopinal. The identity of rhodopinal was confirmed by reducing the chromophore-conjugated aldehyde group to its alcohol with sodium borohydride. The rounded, aldehyde spectrum was rapidly converted to the triple-peaked spectrum of rhodopinol with a concomitant, large hypsochromic shift (Fig. 5.6).

The strongly, polar carotenoid glucosides remained at the origin of the TLC plate. The high concentration of rhodopinal glucoside present in the glucoside band provides the deep red colour. When rhodopinal and its glucoside are bound in the native antenna complexes a

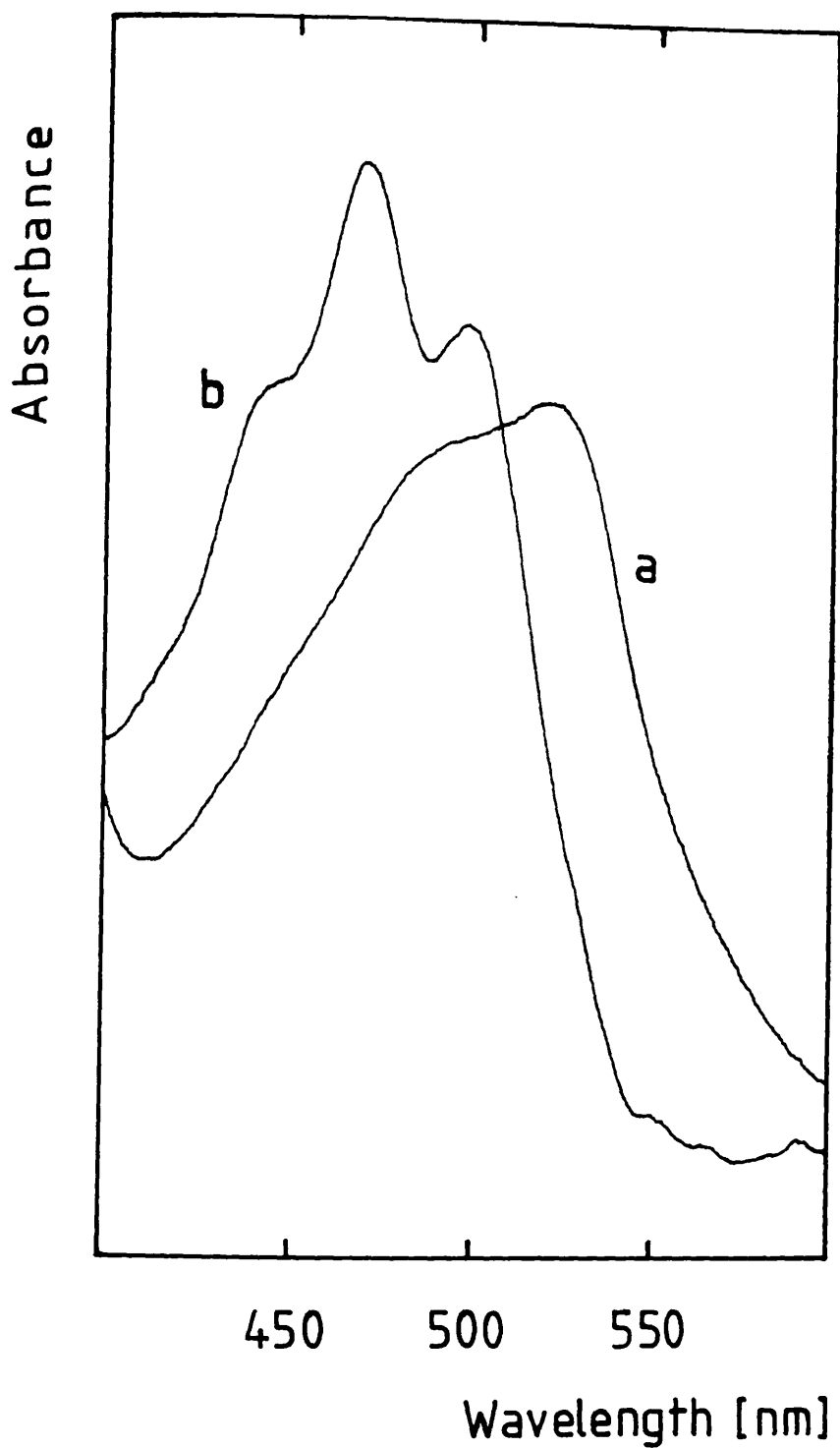
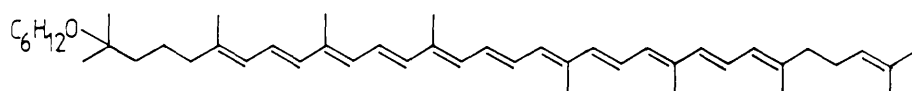


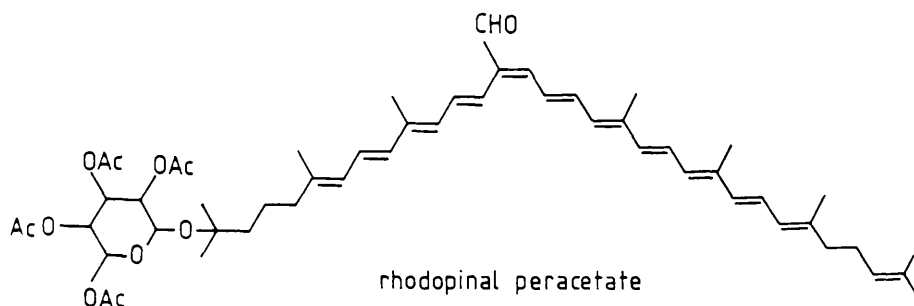
Fig. 5.6 Absorption spectra of (a) cis-rhodopinal and (b) cis-rhodopinal after reduction to cis-rhodopinol. Note the increase in vibronic persistence, the blue shift and the absorbance increase.

further bathochromic shift occurs, giving the cells their characteristic deep purple colour.

The carotenoid glucosides were scraped off the chromatogram and acetylated, converting them to their less polar peracetates. The structures of rhodopin glucoside and rhodopinal peracetate are shown below:



rhodopin  $\beta$ -D-glucoside



rhodopinal peracetate

The carotenoid peracetates were chromatographed in the same solvent system as used previously (Fig. 5.5, bottom). The electronic absorption spectra of the two orange carotenoid bands were very similar (Fig. 5.7). The upper band, which was present in greater amount, had an absorption maximum 2nm lower than the lower band, and it exhibited a stronger cis-peak (not shown). It was therefore concluded that the upper (Neo A) and lower (Neo U) bands were the cis- and trans-isomers of rhodopin peracetate respectively. (It should be noted that the relative positions of cis- and trans-isomers on silica TLC are carotenoid-type dependent and should therefore not be used to assign an isomeric

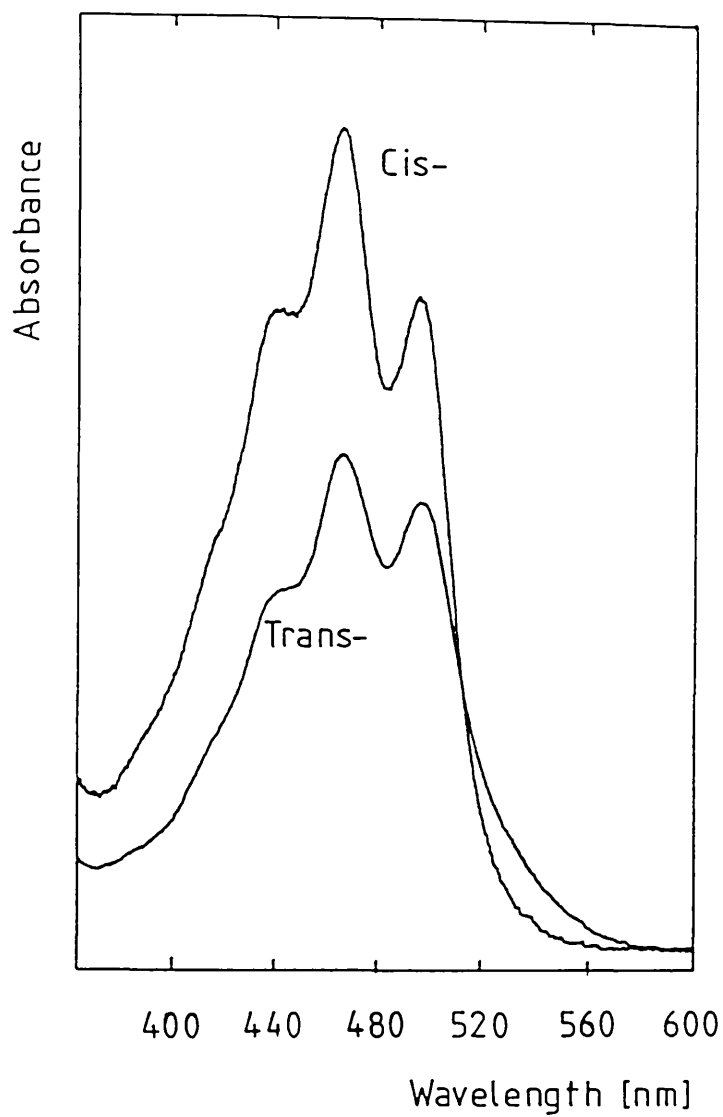


Fig. 5.7 Absorption spectra of the carotenoid peracetates identified as cis- and trans-isomers of rhodopin peracetate.

configuration to a carotenoid without knowledge of the behaviour of the carotenoids on that particular chromatographic system.) The lower, major, red band was identified as *cis*- $\beta$ ,D-rhodopinal peracetate. It has the same absorption spectrum as *cis*- $\beta$ , D-rhodopinal glucoside.

#### 5.5(iii) Carotenoid compositions and BChl-to-carotenoid ratios of B800-850 Type II, and B800-820 complexes from *Rps. acidophila*, strain 7050

The accurate determination of carotenoid compositions and BChl-to-carotenoid ratios for these complexes is extremely difficult, because of the problem of obtaining an accurate value for the absorption coefficient of *cis*-rhodopinal and its glucoside. As they are major carotenoids in these complexes the value of their absorption coefficients will strongly influence the final pigment ratio.

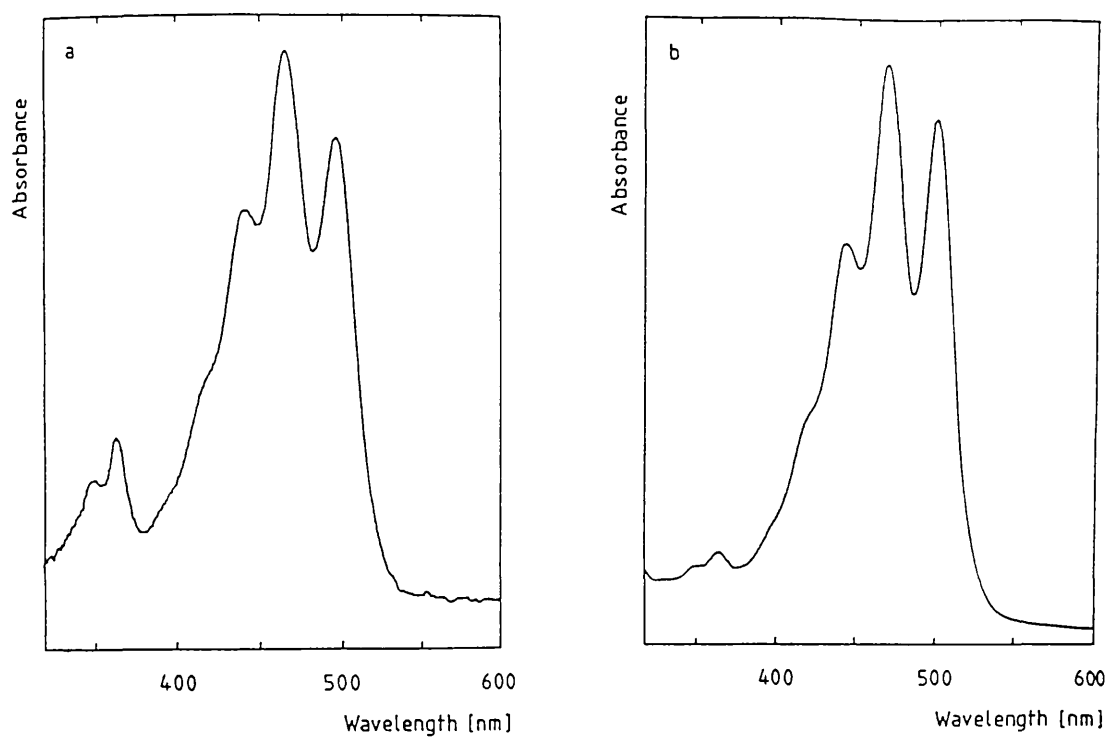
Absorption coefficients are usually determined gravimetrically, by slowly crystallising the pure carotenoid from a solvent, weighing it, making it to a known concentration in a chosen solvent and then by measuring its absorption maximum. The crystallisation is repeated from several different solvents and the absorption coefficients are expected to correlate. Unfortunately, *cis*-rhodopinal does not crystallise [Aasen and Liaaen Jensen, 1967; Schmidt et al., 1971] and it is difficult to free the carotenoid of solvated organic solvent molecules. These add an unknown weight making the true absorption coefficient difficult to determine accurately. An  $\epsilon_{1\text{cm}}^{1\%}$  value of 2300 has been estimated [Aasen and Liaaen-Jensen, 1967] but this must be used with caution (K. Schmidt, personal communication).

An attempt was made to reassess this absorption coefficient by an alternative method. Using the  $\epsilon_{1\text{cm}}^{1\%}$  value for all-trans-rhodopin of 3100 it was hoped that a coefficient for *cis*-rhodopinal could be determined in two steps: by quantitatively reducing *cis*-rhodopinal to

cis-rhodopinol, and then by quantitative isomerisation of cis-rhodopinol to trans-rhodopinol which also has an absorption coefficient of 3100. By measuring the change in the absorbance it was hoped that a back calculation would give a coefficient for cis-rhodopinol.

At 500nm the average absorbance increase after the reduction reaction was 26.0% with a sample standard deviation of 3.9% (n=5). Although the isomerisation reaction with iodine worked (see Fig. 5.8), the subsequent separation and quantitation of the isomers on silica TLC gave inconsistent data so an accurate absorbance change could not be determined. This was mainly because of incomplete recovery of the polar carotenoids from silica gel. Despite this an absorption coefficient could be calculated for trans-rhodopinol, ignoring the effect of isomerisation. The  $\epsilon_{1\text{cm}}^{1\%}$  value of 3100 was reduced by 26% to give a value of 2294 which is equivalent to a millimolar absorption coefficient at 500nm of  $127\text{cm}^{-1}$ . This is very similar to the value for the cis-isomer at 500nm calculated from the published coefficient ( $123\text{mM}^{-1}.\text{cm}^{-1}$ ). Because cis-isomers have lower absorption coefficients than the trans-forms, this represents the highest possible value for the coefficient of cis-rhodopinol (i.e. the value if the cis- and trans-isomers have identical coefficients).

Despite the uncertainty of the rhodopinol coefficient the BChl-to-carotenoid ratios were determined for *Rps. acidophila*, strain 7050, complexes using the published coefficient. The percentage carotenoid compositions are presented in Table 5.5. The average carotenoid  $\epsilon_{500\text{nm}}$  values were calculated to be  $135$  and  $140\text{mM}^{-1}.\text{cm}^{-1}$  for the B800-850 Type II and B800-820 complexes respectively. The ratios determined for the B800-820 complexes were: 3.12, 2.92, 2.98, 3.48, 3.66, 3.21, 2.92, 3.88, 3.86, 3.86, 3.92, 3.84, 3.91, 3.71, 3.51, 3.47 and 3.49. These give an arithmetic mean of 3.51, a sample standard deviation of 0.36 and



**Fig. 5.8** Absorption spectra of cis-rhodopinal(a) and its isomerisation product, trans-rhodopinal (b).

95% confidence limits of 3.33-3.69. The ratios determined for the B800-850 Type II complexes were: 2.66, 2.50, 2.55, 2.60, 2.69, 2.54, 2.72, 2.87 and 2.83, giving a mean of 2.66, standard deviation of 0.13 and 95% confidence limits of 2.38-2.98.

Because of difficulties in obtaining accurate ratio measurements for these complexes it was decided to determine the BChl-to-carotenoid ratios for other complexes from *Rps. acidophila* which do not contain rhodopinal. It has been reported that when strain 7750 is grown at 20-23°C it synthesises a B800-820 complex which is red in colour [Brunisholz et al., 1987; R. Brunisholz, personal communication] and which is therefore probably free of rhodopinal glucoside. Strain 7750 was grown under these conditions and the above reports were substantiated (see chapter three). The carotenoid composition of this complex, which is reported for the first time, and the composition of the B800-850 Type I complexes from high light grown *Rps. acidophila*, strain 7050, are presented in Table 5.6.

The average absorption coefficient for the total carotenoid from the B800-850 complexes was calculated to be  $133\text{mM}^{-1}\text{cm}^{-1}$  and the measured ratios were: 2.11, 2.16, 2.14, 2.13, 2.14 and 2.10. These give an arithmetic mean of 2.13, sample standard deviation of 0.02 and 95% confidence limits of 2.11-2.15. If the true ratio is 2:1 then a small systematic error must be present because the confidence interval does not encompass this value. The error is probably in the average absorption coefficient calculated for the total carotenoid. The average coefficient for the total carotenoid of the B800-820 complexes was  $134\text{mM}^{-1}\text{cm}^{-1}$  and the ratios were calculated to be: 2.17, 2.11, 2.19, 1.94, 1.95, 1.72 and 1.79, giving a mean of 1.98, standard deviation of 0.18 and 95% confidence limits of 1.83-2.17. These data suggest that the ratios for both complexes is 2:1.

**Table 5.5: Carotenoid compositions of the B800-820 and the B800-850 Type II antenna complexes of *Rps. acidophila*, strain 7050**

	B800-850 II	B800-820
% lycopene	27.0	36.1
% anhydrorhodovibrin	tr	tr
% rhodopin	9.5	2.7
% rhodopinal	-	7.2
% rhodopin glucoside	7.4	10.3
% rhodopinal glucoside	56.0	44.3

**Table 5.6: Carotenoid compositions of the B800-850 Type I complexes from *Rps. acidophila*, strain 7050 and the B800-820 complexes from *Rps. acidophila*, strain 7750**

	HL 7050	LT 7750
	B800-850 I	B800-820
% lycopene	15.9	30.2
% anhydrorhodovibrin	3.6	≤1
% spirilloxanthin	8.5	≤1
% rhodopin	32.2	65.4
% rhodopin glucoside	40.0	3.1

## 5.6 Summary Discussion of BChl-to-Carotenoid Ratio Determinations and Results of Linear Dichroism and Picosecond Energy Transfer Measurements on B800-850 Complexes from *Rps. palustris*

By determining the ratio of BChl to carotenoid for the B800-850 complexes from *Rb. sphaeroides* the method used for pigment quantitation in this chapter was shown to be consistent with the methods used in the previous chapter. A BChl-to-carotenoid ratio for the B875 complexes from *Rb. sphaeroides* was determined to be 1.06:1 which agrees well with the previously published values of 1:1.

The ratio for the B800-850 Type II complexes from *Chr. vinosum* was determined by Thornber (1970) to be 3.3:1, using an unreliable method and an incorrect carotenoid composition. It should be noted that the Type II complexes used by Thornber were obtained from low light grown cells rather than the high temperature grown cells used in this study. The ratios determined here for both the Types I and II complexes suggest that the true ratio is 2:1.

Cogdell et al. (1983) determined the BChl-to-carotenoid ratios of the B800-850 Type II complexes, and B800-820 complexes from *Rps. acidophila*, strain 7050, to be nearly 3:1. The difficulties in obtaining accurate ratio measurements for the rhodopinal-containing complexes has already been documented. The ratios were determined to be 2.66 for the B800-850 Type II complexes and 3.51 for the B800-820 complexes. Comparison of the data with the standard errors of all of the ratio determinations presented in this chapter (Table 5.7) indicates that the precision of these ratio determinations was, however, no less than for the other measurements. From an attempt to reassess the absorption coefficient of cis-rhodopinal, it appears that the published coefficient for this carotenoid is overestimated, introducing a systematic error which makes the ratios too high. Direct comparison

between the ratios of these two complexes is however valid, and the data suggests that the B800-820 complexes contains one more BChl molecule per carotenoid than the B800-850 Type II complexes. To see what the absorption coefficient of cis-rhodopinal would have to be, to obtain ratios of 3:1 for the B800-820 complexes and 2:1 for the B800-850 Type II complexes, the data were back-calculated. For the B800-820 complexes the average absorption coefficient of the total carotenoid, at 500nm in acetone/methanol, would have to be  $109\text{mM}^{-1}.\text{cm}^{-1}$  and the millimolar absorption coefficient for cis-rhodopinal would need to be  $75\text{cm}^{-1}$ . Similarly, for the B800-850 Type II complexes the average carotenoid millimolar absorption coefficient would have to be  $102\text{cm}^{-1}$  and the value for cis-rhodopinal would need to be  $61\text{cm}^{-1}$ . There is obviously a discrepancy between these data but this could easily be explained by the difficulties in determining the carotenoid compositions for these complexes and because the composition data was collected from single analyses. Averaging the calculated values gives a required absorption coefficient for cis-rhodopinal of  $68\text{mM}^{-1}.\text{cm}^{-1}$ . The attempted reassessment of this coefficient estimated the absorption coefficient of trans-rhodopinal to be  $127\text{mM}^{-1}.\text{cm}^{-1}$ . Accepting this value, a decrease in extinction during trans-cis isomerisation would need to be 46% to bring the ratios of the above complexes to whole numbers. This is within the range which could be expected for cis-trans isomerisations [Schweiter et al., 1969]. The evidence therefore does indicate that the ratios for the low light variable complexes are too high and that it is feasible that the true ratio for the B800-850 Type II complexes from *Rps. acidophila*, strain 7050 is 2:1 and that the ratio for the 800-820 complexes is 3:1.

From the data presented here the BChl-to-carotenoid ratios for the B800-850 Type I complexes from *Rps. acidophila*, strain 7050, and the

B800-820 complexes from strain 7750 are probably 2:1. The result for the B800-850 Type I complexes is consistent with the other data presented in this study. The results for the B800-820 complexes from strain 7750, however, contradict the current belief that all B800-820 complexes have ratios of 3:1.

The BChl-to-carotenoid ratios of the B800-850 complexes from *Rps. palustris* have not previously been determined. In the literature the variable complexes are designated B800-850 Type I complexes and are grouped with others estimated to have BChl-to-carotenoid ratios of 3:1 [Thorner, 1987]. From the data presented in this chapter it is proposed that the ratio for the HL B800-850 complexes from *Rps. palustris*, strain French, is 2:1 and that the ratio for the LL B800-850 complexes is 3:1. This data appears to corroborate some recent linear dichroism and picosecond absorption spectroscopy measurements performed on the antenna complexes from high and low light grown *Rps. palustris*, strain French.

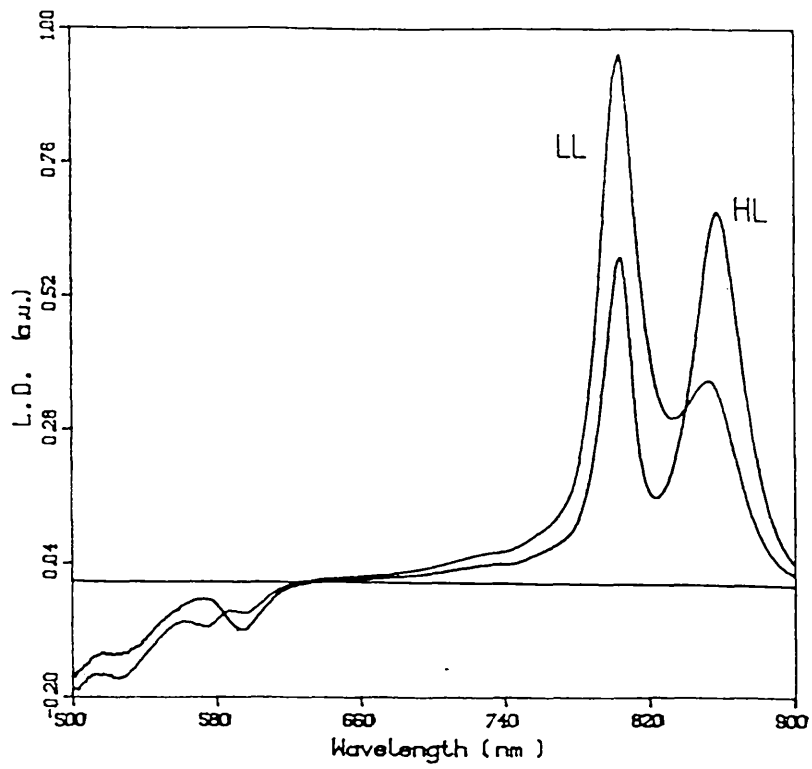
Preliminary linear dichroism measurements (F van Mourik, Department of Biophysics, The Free University, Amsterdam) further support the presence of an additional third BChl component in the low light B800-850 complexes from *Rps. palustris*. The high light B800-850 linear dichroism spectra (Fig. 5.9) have a negative linear dichroism in the Q<sub>x</sub> region with a peak at about 570nm and a trough at about 590nm. These correspond to absorption by the Q<sub>x</sub> dipoles of the BChl monomers and the BChl dimers in the complexes respectively.

The linear dichroism spectrum of the LL B800-850 complexes has a third band which can only be explained by the presence of a third BChl chromophore with a different Q<sub>x</sub> dipole orientation.

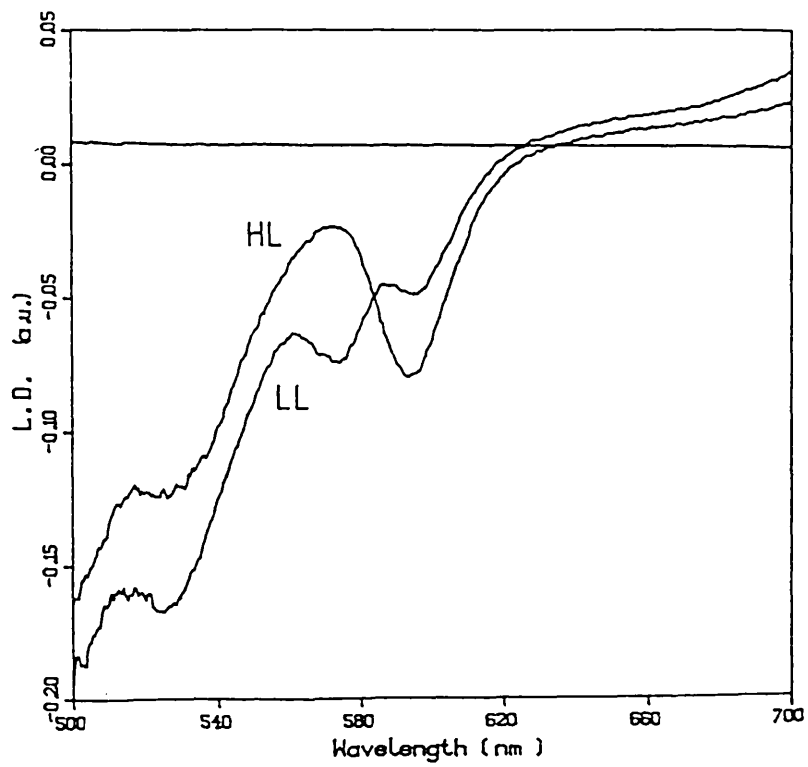
Preliminary picosecond energy transfer kinetics measurements on

Fig. 5.9 Linear dichroism spectra of B800-850 antenna complexes from high and low light grown *Rps. palustris* cells. The spectra of the two complexes are clearly different in the BChl Q<sub>x</sub> band absorption region (bottom).

Linear Dichroism



Linear Dichroism

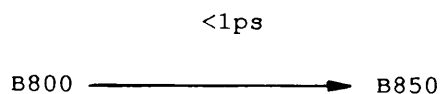


membranes and B800-850 antenna complexes from low and high light grown *Rps. palustris*, strain French, cells further support the existence of a third BChl pigment in the low light complexes. The picosecond measurements were performed by V. Sundström, University of Umeå, Sweden. At room temperature with open reaction centres, transfer from the B800 monomer to the B850 dimer in the high light membranes and complexes was shown to be very rapid with a time constant of  $<1\text{ps}$ . This is similar to measurements on other species e.g. *Rps. acidophila* [Bergström et al., 1988]. The transfer time between BChl 850, and BChl 875 in the B875 complexes was determined to be 15-20ps in membranes from both high and low light grown cells. This is the time taken for the energy to equilibrate over the B850 chromophores, and transfer and equilibrate over the B875 chromophores. The total trapping time from the B800-850 complexes to the reaction centres was 50-60ps in membranes from both the high light and low light grown cells.

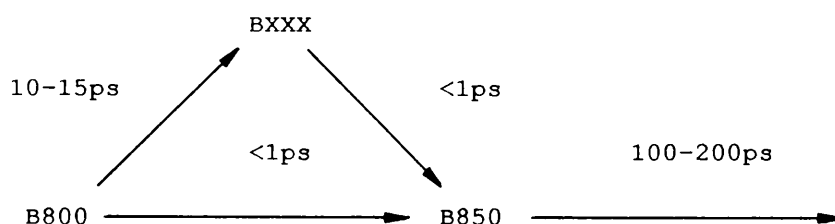
When the energy transfer kinetics are probed at 800nm, the decay of the B800 excited state can be monitored as the energy is transferred to B850. Fluorescence measurements on the low light membranes and B800-850 complexes have determined the rate of energy transfer out of B800 to be  $<<1\text{ps}$ ; significantly faster than for the high light grown cells. But in addition, in the LL B800-850 complexes and membranes a second time constant for energy transfer from B800 to an acceptor (probably B850) of 10-15ps was also measured. This suggests that there is an intermediate pigment absorbing at around 800nm according to the following scheme:



In the high light B800-850 complexes the energy transfer is simply:



According to the above scheme, however, the presence of the additional pigment increases the total transfer time to B850 which does not seem to confer an advantage. But if the direct route of energy transfer is also available, the scheme for transfer in the low light complexes would be more like the following:



The measurements estimated the quenching of the B850 in the isolated antenna to have a time constant of 100-200ps. In the LL complexes the overall rate with which energy leaves the B800 chromophore ( $k$ ) is equal to the sum of the rates of the direct ( $k_1$ ) and indirect ( $k_2$ ) pathways to B850 i.e.  $k = k_1 + k_2$ . Assuming that  $k_1$  is the same for both the HL and LL complexes, the faster rate of energy transfer out of B800 in the LL complexes must be due to the additional pathway with rate constant  $k_2$ .  $k_2$  could be higher than  $k_1$  because of the favourable spectral overlap between B800 and BXXX. As the indirect path of energy transfer is slower, BXXX does not improve the efficiency of energy transfer between B800 and B850. The transfer time from B800 to B850 in the HL complex is already so fast that further increases in efficiency would seem to be unnecessary. In such a position BXXX would act as an additional light-harvesting pigment, increasing the overall light-harvesting capability

of the complex.

The transfer time from BXXX to B850 is similar to the transfer time between B850 and the B875 chromophore of the B875 complex (15-20ps). This suggests that the additional pigment may be less intimately associated with the normal B800 and B850 chromophores. Perhaps it is bound by its own antenna polypeptides as a satellite complex which is synthesised under low light conditions and which associates with the existing HL complex. i.e. Fig. 5.10. Or perhaps an entirely new complex which accommodates the additional pigment is synthesised. i.e. (Fig. 5.11). A summary of the BChl-to-carotenoid ratio determinations from this chapter is presented in Table 5.7.

**Table 5.7: Summary of BChl-to-carotenoid ratios**

complex	n	molar ratio		95% confidence limits
		$\bar{x}$	SE	
<i>Rb. sphaeroides</i> B875	6	1.08	0.05	0.92-1.20
<i>Rps. palustris</i> B800-850 LL	25	3.05	0.05	2.90-3.10
B800-850 HL	10	1.98	0.06	1.84-2.11
<i>Chr. vinosum</i> B800-850 Type I	4	2.06	0.10	1.73-2.39
B800-850 Type II	4	2.07	0.28	1.78-2.36
<i>Rps. acidophila</i> B800-850 Type I	6	2.13	0.01	2.11-2.15
strain 7050 B800-850 Type II	9	2.66*	0.04	2.38-2.94
B800-820	17	3.51*	0.09	3.33-3.69
strain 7750 B800-820	8	2.00	0.07	1.83-2.17

$\bar{x}$  = arithmetic mean

SE = standard error

n = sample size

\* = these data are probably subject to systematic error so the true values are probably lower

Fig. 5.10

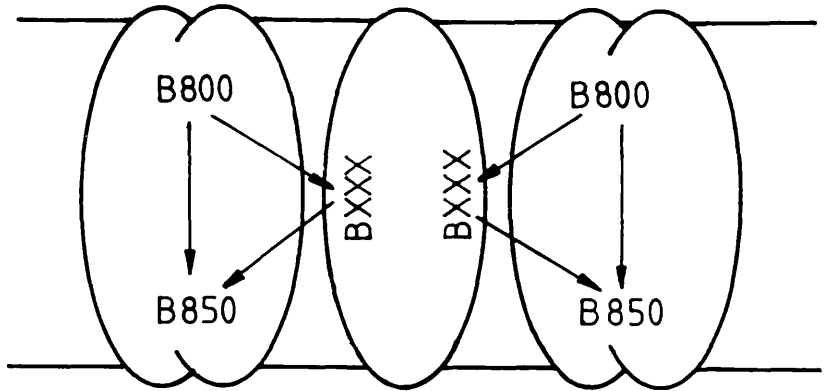


Fig. 5.11

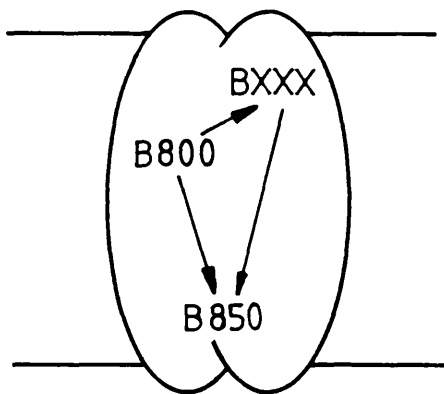


Fig. 5.10 and Fig. 5.11 Diagrams depicting the possible arrangement of the chromophores in the LL B800-850 antenna complexes of *Rps. palustris*, strain French.

CHAPTER SIX: Isolation and Primary Sequencing of the Light-Harvesting Polypeptides From Low and High Light Grown *Rps. palustris*, strain French.

## 6.1 Introduction

One of the central issues pertaining to the function of the light-harvesting antenna complexes of purple bacteria is the relationship between antenna structure and the position and shape of the near-infrared absorption spectrum. The antenna complexes are arranged within the photosynthetic unit so that BChl molecules with Qy dipoles absorbing at the highest wavelength are positioned most closely to the reaction centre. BChl-BChl, singlet-singlet energy transfer, which is mediated by the Qy dipoles is directed towards the BChls absorbing at the highest wavelengths, and is therefore directed towards the reaction centre. It is the interaction of the BChls with their environment which determines the position of the Qy band absorption maxima (section 1.7(iii)). Light-harvesting function is therefore directly related to pigment-protein interactions

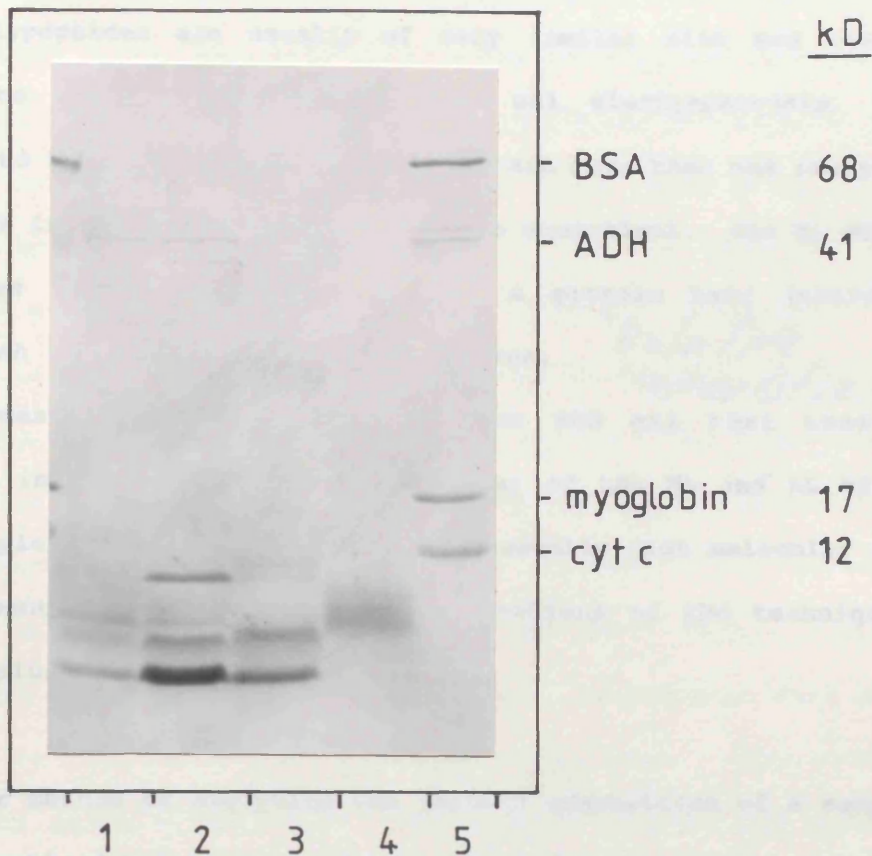
The B800-850 light-harvesting complexes from *Rhodospseudomonas palustris*, strain French, have several unusual features. When the cells are grown under high light intensities, the complexes have a normal, Type I absorption spectrum, like that of *Rb. sphaeroides*. However, when the cells are grown under low light the 850nm absorption band is greatly reduced in intensity, and the spectrum has the characteristics of Type II antenna complexes (chapter three). These complexes are therefore useful for investigating the relationship between the structure and absorption spectra of antenna complexes.

It has already been established that the pigment composition of the HL and LL B800-850 complexes is different (chapter five). The BChl-to-carotenoid ratio of the B800-850 complexes from high light grown cells was determined to be 2:1, but the ratio of the complexes from low light grown cells was determined to be 3:1. Linear dichroism studies and picosecond kinetics experiments suggest that the LL complexes contain an

additional BChl chromophore, absorbing at 800nm and with a different orientation to the other BChls. To investigate whether there is also a difference in the compositions of the antenna apoproteins, a programme to characterise the polypeptides from the HL and LL B800-850 complexes was initiated. The results of this study are presented in this chapter.

## **6.2 SDS Polyacrylamide Gel Electrophoresis**

An SDS polyacrylamide gel of membranes and antenna complexes isolated from high and low light grown *Rps. palustris*, strain French, cells is presented in Fig. 6.1. The photosynthetic membranes prepared from the low light grown cells (lane 1) resolved into three clear bands and a number of other faint bands, in the low molecular weight region of the gel which corresponds to the antenna complexes. Comparison of the protein bands separated from HL and LL B800-850 complexes demonstrate that differences in polypeptide composition do exist. Four distinct bands were resolved in the HL B800-850 complex gel lane (lane 2). An unusual feature of this gel lane is the presence of a protein band of rather high molecular weight for an antenna protein (uppermost). Because the gel is an acrylamide gradient gel the protein mobility is not linear with the logarithm of the protein molecular weight. The molecular weights of the antenna polypeptides cannot therefore be estimated from the gel other than to say that they are less than 12kD (i.e. less than the MW of the cytochrome c marker). This high molecular weight band appears to be a minor component of the LL B800-850 complexes. Above this in the LL B800-850 complex gel lane is a second faint high molecular weight protein band. Because antenna complexes are small hydrophobic proteins they sometimes form aggregates. It is possible then that the high molecular weight protein bands could be aggregates of existing polypeptides. However, the B800-850-



**Fig. 6.1** SDS polyacrylamide gel showing the protein compositions of photosynthetic membranes and antenna complexes from *Rps. palustris*, strain French. Lane 1: membranes from low light grown cells, lane 2: HL B800-850 complexes, lane 3: LL B800-850 complexes, lane 4: B875 complexes, lane 5: standards.

polypeptide from *Rc. gelatinosus*, with 69 amino acids, has an unusually high molecular weight [R A Brunisholz, unpublished], so the bands may correspond to individual polypeptides.

The two lower bands in the HL B800-850 complex gel lane roughly correspond to two bands in the LL B800-850 complex gel lane. Because antenna polypeptides are usually of very similar size and therefore difficult to resolve by polyacrylamide gel electrophoresis, it is impossible to tell whether these bands contain more than one protein, or if the bands in the HL and LL complexes are equivalent. The HL B800-850 complex does however appear to contain a protein band (third from bottom) which is absent from the LL complexes.

In summary it is evident from the SDS gel that there are differences in the polypeptide compositions of the HL and LL B800-850 antenna complexes, and that proteins of unusually high molecular weight may be present. But because of the limitations of the technique, no further conclusions can be drawn.

Another method of analysing the protein composition of a sample is to use recently-developed liquid chromatography systems. These have many advantages over gel electrophoresis, not least the ease with which separated proteins can be collected for further analysis. Samples of antenna protein must be prepared before analysis by liquid chromatography.

### 6.3 Isolation of Antenna Protein

Freeze-dried antenna complexes and cells were extracted into a dichloromethane/methanol/ammonium acetate buffer (section 2.9(i)) and separated from other components by sephadex LH60 gel permeation chromatography. A typical LH60-column elution profile is presented in

Fig. 6.2. The first protein peak to elute contains the relatively large, L and M reaction centre proteins (the H subunit is not extracted). This is followed by the antenna polypeptide fraction, a large pigment and lipid peak, and finally a small phospholipid peak [Brunisholz et al., 1985]. Elution profiles of extracts from high and low light grown cells, separated on a larger LH60 column, are presented in Fig. 6.3. The relatively greater proportion of reaction centre protein to antenna complex protein in the high light grown cells is further evidence for the relative expansion of the B800-850 complex component of the photosynthetic unit under low light conditions.

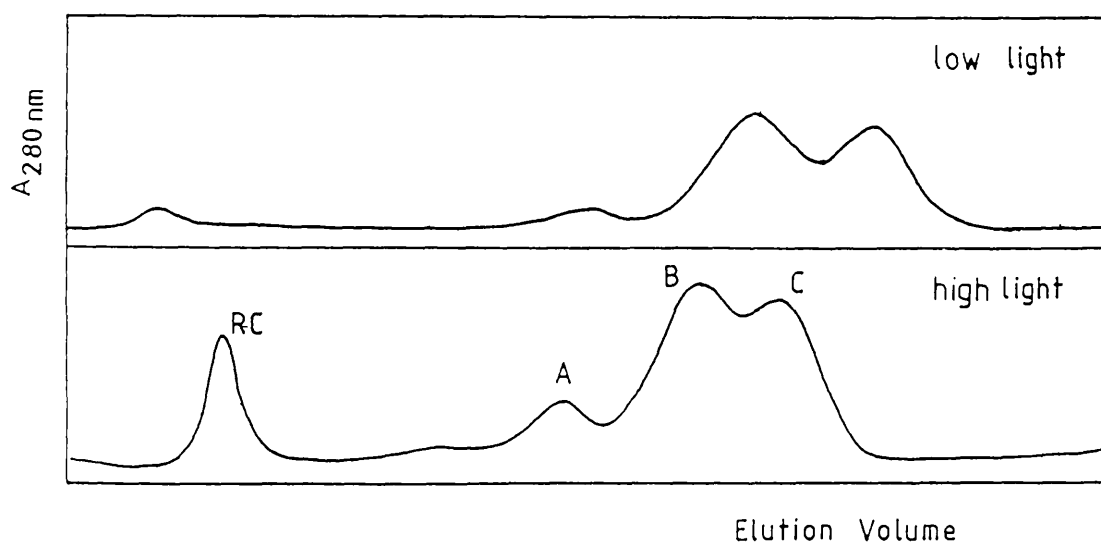
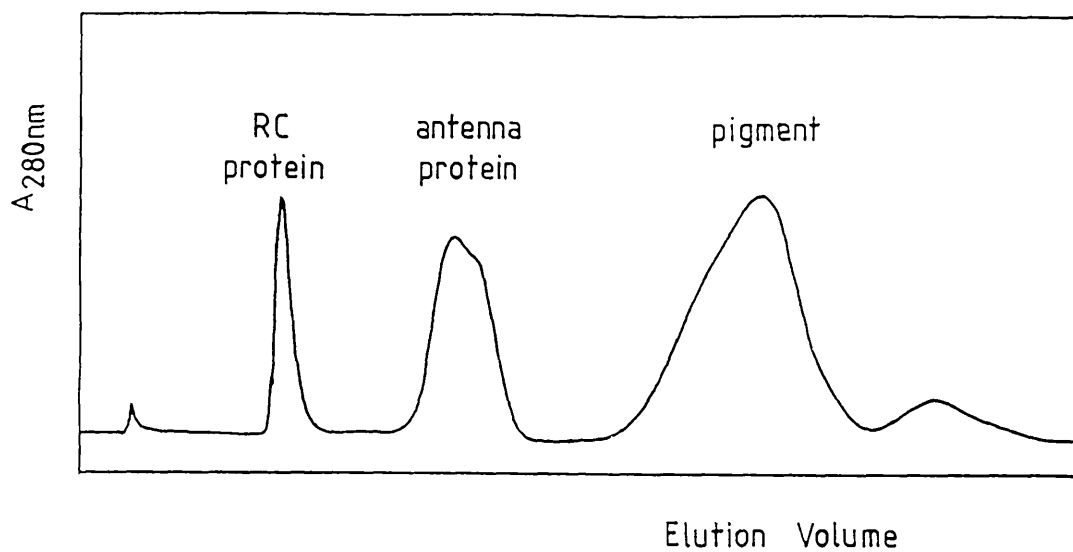
On the larger column the antenna polypeptide fraction was partially resolved into three peaks, labelled A, B and C. The high molecular weight protein peak (A) was partially resolved from fractions B and C. In the examples chosen, protein peak A appears to be present in relatively larger amounts in the high light grown cells. In other examples this is not as clear but on balance the evidence does suggest that peak A is associated with high light grown cells. This correlates with the SDS polyacrylamide gel. The antenna protein and individual fractions A, B and C were collected for further analysis.

#### **6.4 Separation of Antenna Protein into $\alpha$ - and $\beta$ -polypeptides**

Peaks A, B and C collected from the LH60 columns were further characterised by DEAE-cellulose anion-exchange chromatography. This method is able to separate the two classes of antenna polypeptides, designated  $\alpha$  and  $\beta$  (section 1.7(ii)) [Brunisholz et al., 1981].  $\alpha$ -polypeptides pass straight through the exchanger matrix but  $\beta$ -polypeptides bind. These can be eluted by the addition of 5% acetic acid to the dichloromethane/methanol/ammonium acetate buffer. DEAE-cellulose elution profiles for LH60 column peaks A, B and C are

Fig. 6.2 Elution profile of an organic solvent extract of protein from high light grown *Rps. palustris*, separated on a sephadex LH60 gel permeation chromatography column (60 x 1.5cm).

Fig. 6.3 Elution profiles of organic solvent extracts of protein from high and low light grown *Rps. palustris*, separated on a sephadex LH60 column (150 x 2.5cm).

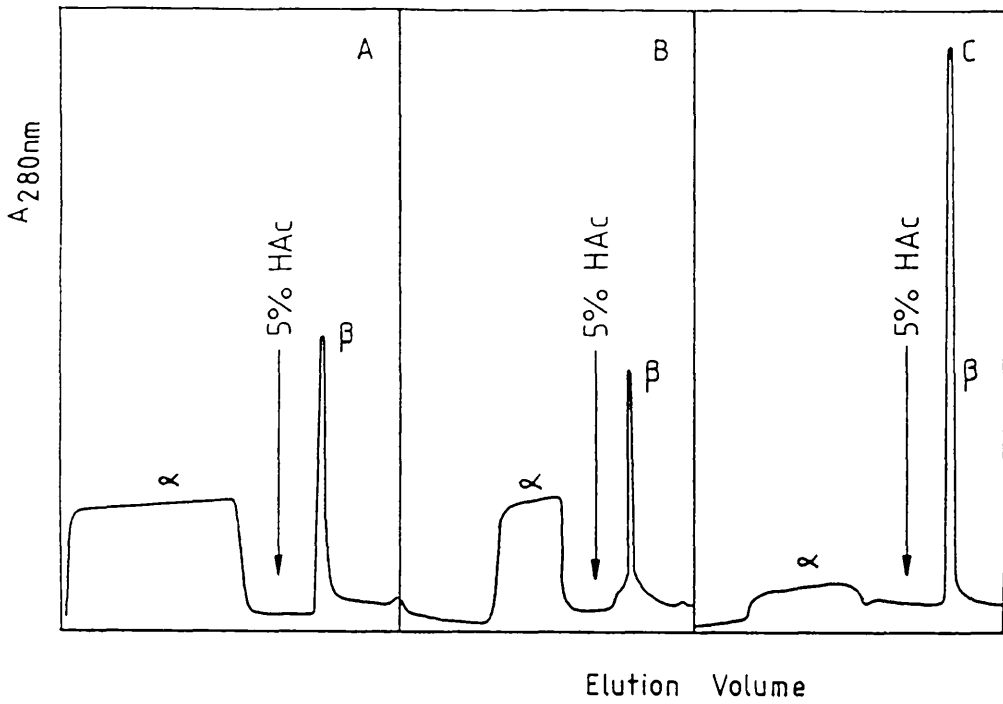


presented in Fig. 6.4. Because the absorbance coefficients of the  $\alpha$ - and  $\beta$ -polypeptides at 280nm are unknown the stoichiometry of  $\alpha$ - and  $\beta$ -polypeptides in each fraction cannot be determined. However, it is apparent that fraction A contains relatively more  $\alpha$ -polypeptide and less  $\beta$ -polypeptide than fraction C. And fraction B lies somewhere in between these. The  $\alpha$ -polypeptide fraction from peak A of the LH60 column was purified by DEAE-cellulose chromatography, collected, precipitated and then lyophilised for amino acid analysis.

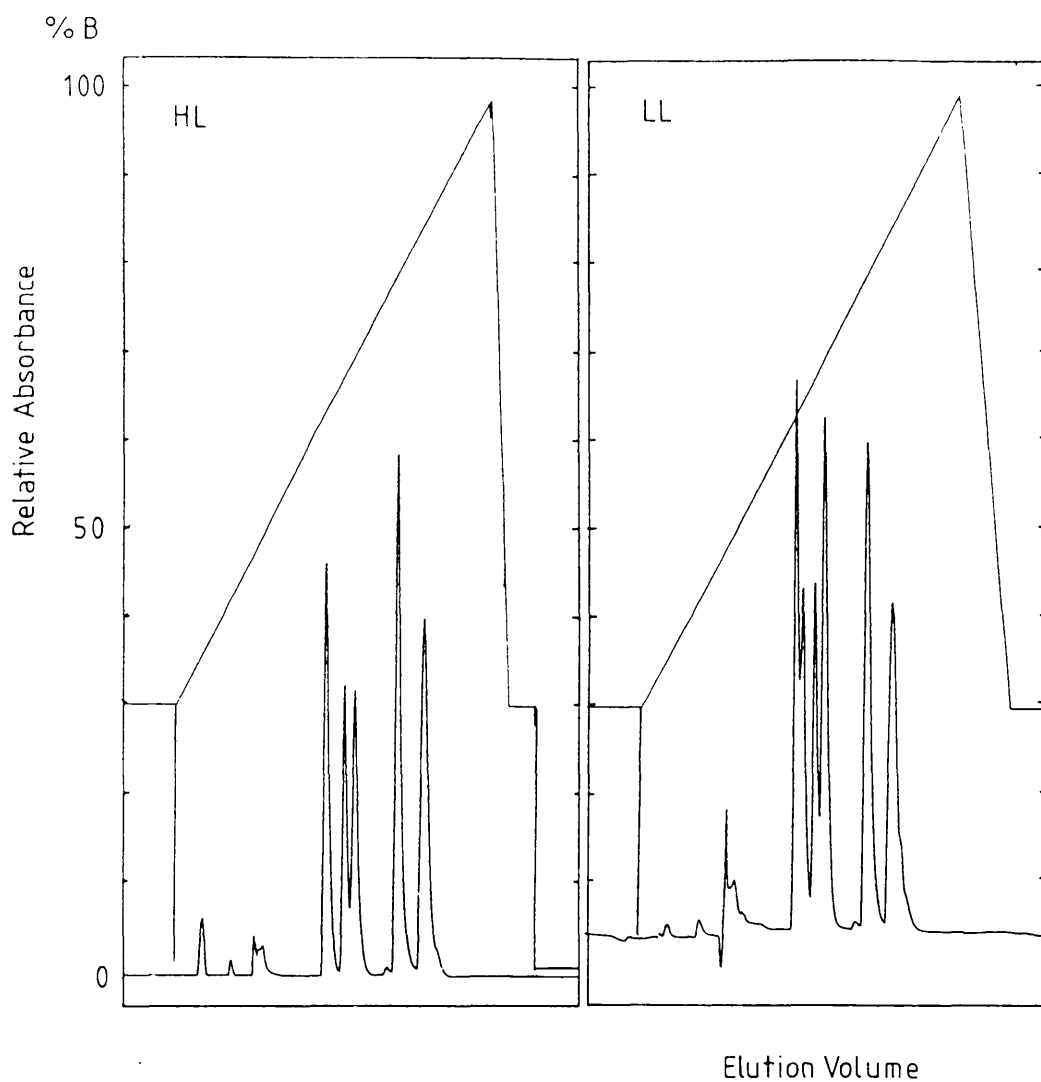
### 6.5 Liquid Chromatography of Antenna Polypeptides

LH60 column protein extracts of high and low light grown *Rps. palustris* cells were separated by reversed phase liquid chromatography on a C<sub>8</sub> pro RPC HR 10/10 column (Pharmacia), using either an FPLC pump system, or an LKB HPLC system. Initial data suggested that high light grown *Rps. palustris*, strain French, cells contain five antenna polypeptides and that low light grown cells contain six polypeptides (Fig. 6.5). The peaks were identified by chromatographing extracts of individual antenna complexes and their separated  $\alpha$ - and  $\beta$ -protein fractions (Figs 6.6a-d). Fig. 6.6a is an FPLC chromatogram of a protein extract of the LL B875 complexes from *Rps. palustris*, strain French. The retention times of the two most intense peaks correspond to the retention times of the two peaks which are eluted last in the chromatograms of Fig. 6.5. These are therefore identified as being B875 complex polypeptides. The cluster of four small peaks in Fig. 6.6a correspond to the cluster of four peaks in the LL chromatogram of Fig. 6.5. These are therefore probably the B800-850 complex polypeptides, which are present as contaminants in the B875 complex preparation.

Fig. 6.6b is a chromatogram of an  $\alpha$ -polypeptide fraction a low light grown, whole cell antenna extract. This chromatogram suggests



**Fig. 6.4** Elution profiles of LH60-column protein fractions A, B and C separated by DEAE-cellulose anion-exchange chromatography.  $\alpha$ -polypeptides pass through the column.  $\beta$ -polypeptides bind and are eluted later by the addition of buffer containing 5% glacial acetic acid.



**Fig. 6.5** FPLC chromatograms of protein extracts from high and low light grown cells. Solvent system: 30-100% B over 30min (A = water, 0.1% trifluoroacetic acid, B = acetonitrile, 0.1% TFA).

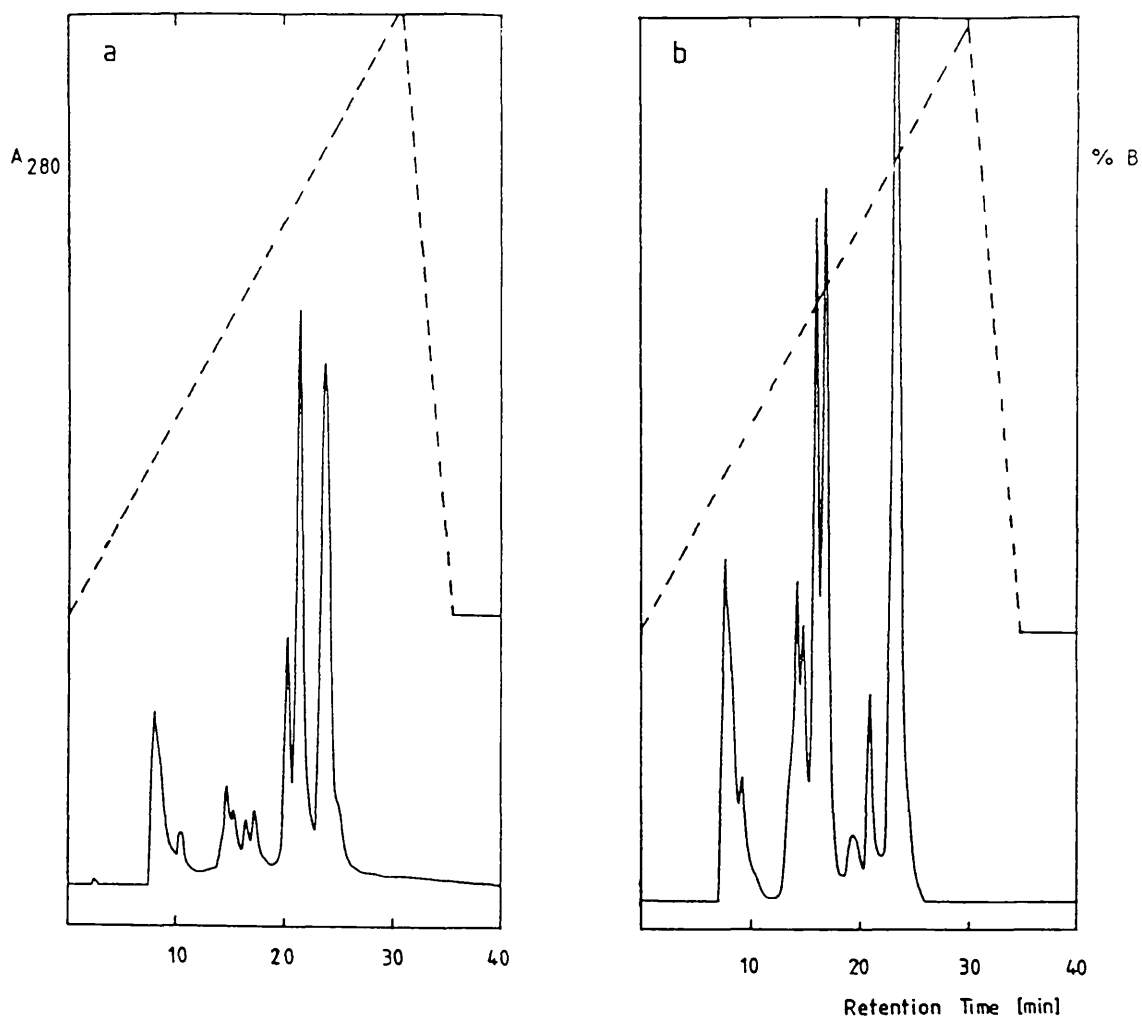
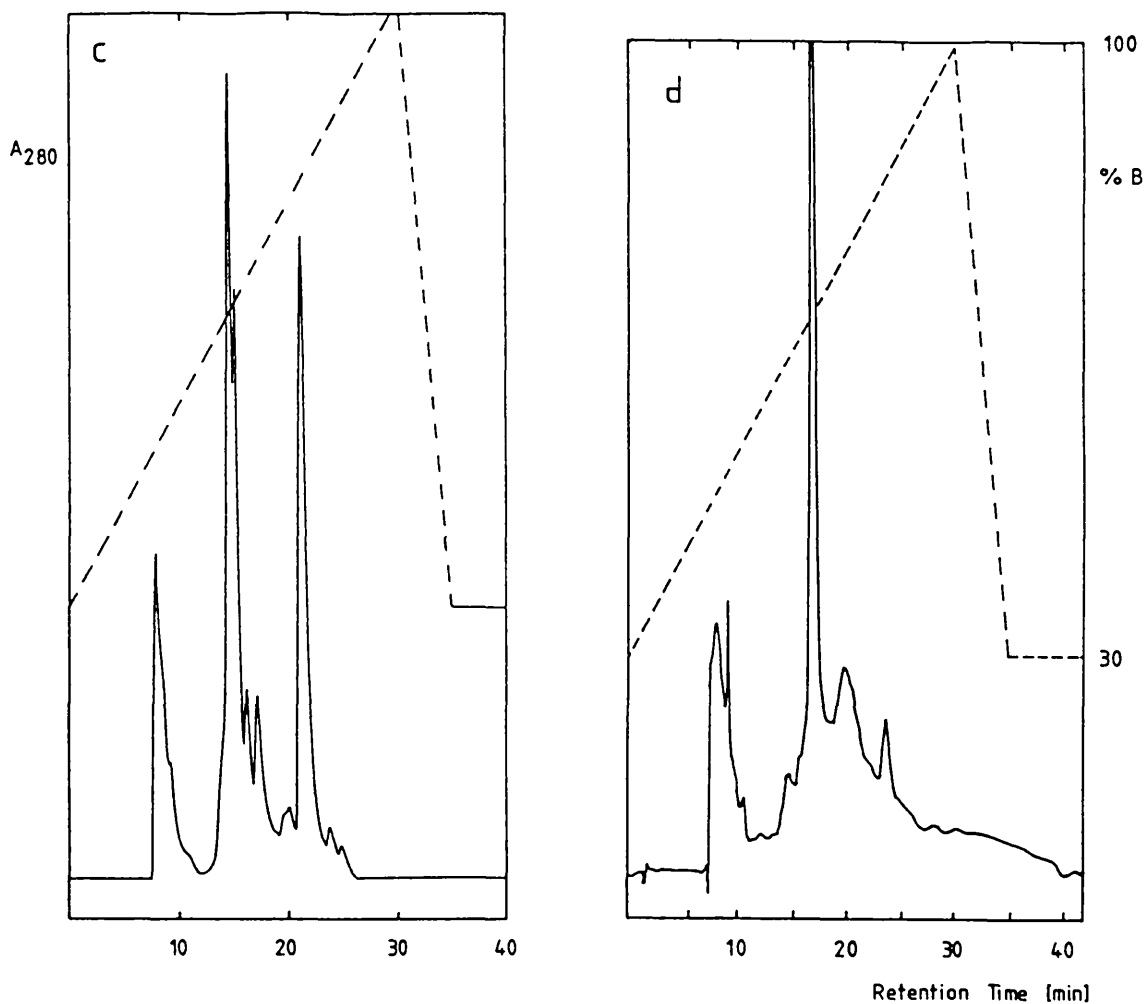


Fig. 6.6 FPLC chromatograms of various protein extracts from *Rps. palustris*. Solvent system as Fig. 6.5. (a) extract of B875 antenna complexes, (b) whole cell  $\alpha$ -polypeptide protein fraction. *continued overleaf...*

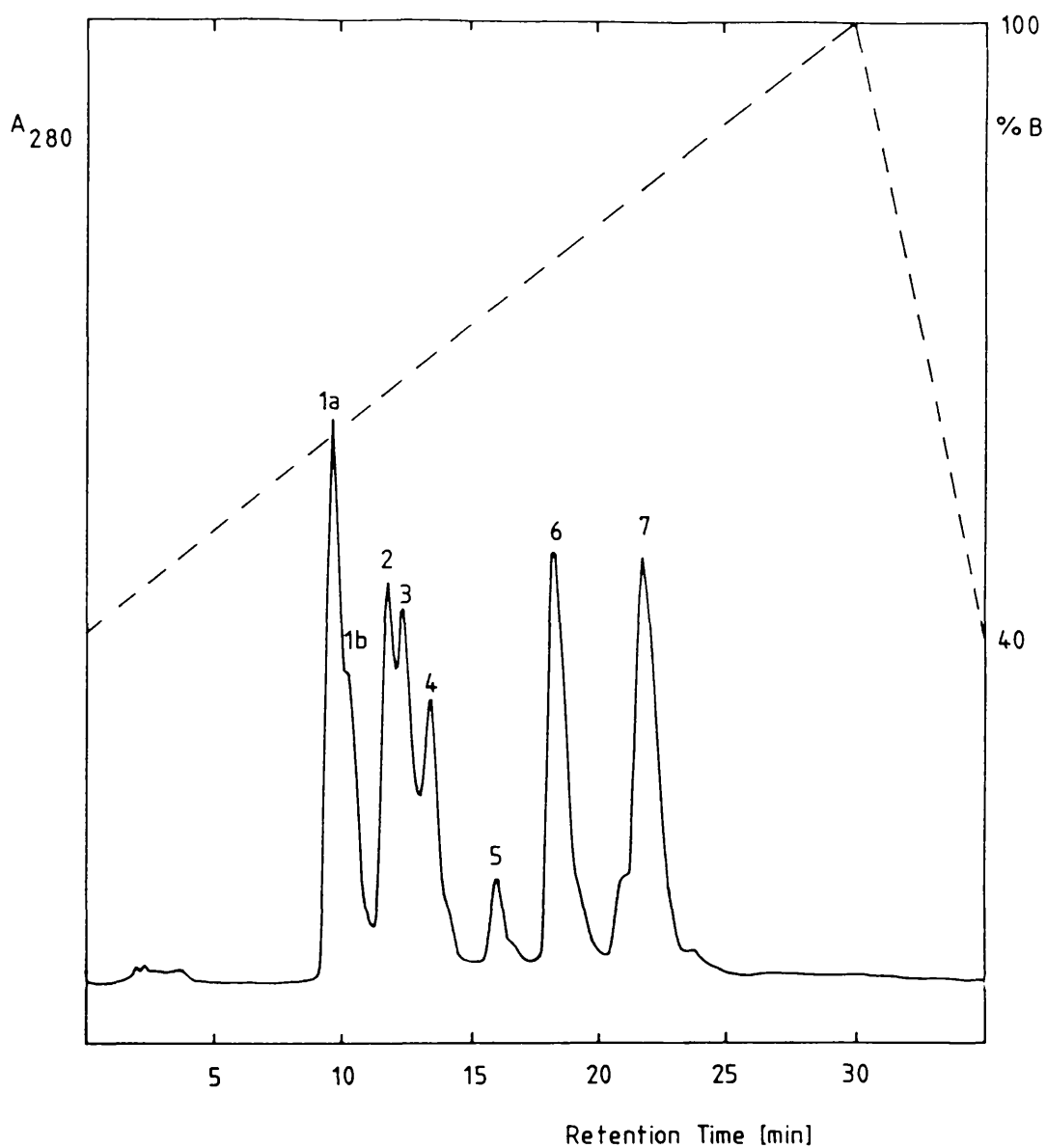


**Fig. 6.6** FPLC chromatograms of various protein extracts from *Rps. palustris*. Solvent system as Fig. 6.5. (c) Fraction C from sephadex LH60 chromatography, (d) Fraction A from sephadex LH60 column chromatography.

that of the two B875 polypeptide peaks the first to elute is a  $\beta$ -polypeptide and the second to elute is an  $\alpha$ -polypeptide. In the LL B800-850 polypeptide cluster, the first two peaks to elute appear to be  $\beta$ -polypeptides and the last two appear to be  $\alpha$ -polypeptides. Fig. 6.6c is a chromatogram of a  $\beta$ -polypeptide fraction of a low light grown, whole cell antenna extract. This chromatogram complements and corroborates the conclusions drawn from chromatogram b.

Combining the data the peaks in the chromatogram of the total antenna protein extract from low light grown cells can therefore, in order of increasing retention, be ascribed the identities: B800-850- $\beta$ , B800-850- $\beta$ , B800-850- $\alpha$ , B800-850- $\alpha$ , B875- $\beta$  and B875- $\alpha$ . By comparing the retention times the peaks in the chromatogram of the high light grown cell extract can be designated: B800-850- $\beta$ , B800-850- $\alpha$ , B800-850- $\alpha$ , B875- $\beta$  and B875- $\alpha$  polypeptides. Fig. 6.6d is a chromatogram of peak A from the LH60 column. The retention time of the main peak identifies this polypeptide as the second B800-850- $\alpha$  polypeptide in Fig. 6.5. From Fig. 6.5 this polypeptide does not appear to be more closely associated with the high light grown cells than with the low light grown cells which was suggested by the SDS gel electrophoresis and the LH60 column chromatography.

Fig. 6.7 is a chromatogram of an antenna protein extract from low light grown cells, separated by reversed phase HPLC. The resolution of the HPLC system is an improvement on the resolution of the FPLC system, although the solvent systems used were very similar. By systematically collecting the individual peaks, parts of the peaks and shoulders, followed by amino acid analysis and sequencing studies, nine different antenna polypeptides have been isolated from the low light grown cells. This is quite unique amongst antenna complexes from purple bacteria. With a few exceptions antenna complexes are reported to contain a single



**Fig. 6.7** .HPLC chromatogram of a cell protein extract of low light grown *Rps. palustris*. Solvent system: A = water, 0.1% TFA, B = acetonitrile, 0.1% TFA. Peak 1: B800-850- $\beta$  polypeptides, peak 2: B800-850- $\alpha_1$ , peak 3: B800-850- $\alpha_2$ , peak 4 800-850- $\alpha_3$  and - $\alpha_4$ , peaks 5 and 6: B875- $\beta$ , peak 7 B875- $\alpha$

$\alpha$ -polypeptide and a single  $\beta$ -polypeptide which aggregate to form the functional antenna complex. The exceptions are three species which are known to contain  $\gamma$ -polypeptides, and the B800-820 complex from *Rps. acidophila*, strain 7750, which contains an additional  $\beta$ -polypeptide (section 1.7(iv)).

Peak 1 of Fig. 6.7 was shown to contain three different B800-850 complex  $\beta$ -polypeptides. Peaks 2 and 3 contain single  $\alpha$ -polypeptides (B800-850- $\alpha_1$  and - $\alpha_2$ ) and two  $\alpha$ -polypeptides were isolated from peak 4 (B800-850- $\alpha_3$  and - $\alpha_4$ ). Amino acid sequencing of polypeptides isolated from peaks 5 and 6 showed that the two peaks contain the same B875- $\beta$  polypeptide. The B875- $\alpha$  polypeptide was isolated from peak 7.

Analysis and sequencing of protein extracts from high light grown cells has shown that all of the antenna polypeptides isolated from low light grown cells are also present in high light grown cells. However it is apparent from the chromatograms that the stoichiometries of the polypeptides are different in the two cases. This will be discussed in conjunction with information obtained from the sequence data later in the chapter.

## **6.6 Amino Acid Composition Analysis of Antenna Polypeptides**

Amino acid composition analysis is a necessary complement to the amino acid sequencing of a protein; the two sets of data should match. The procedure for obtaining the amino acid composition of a protein will be briefly described for the B800-850- $\alpha_4$  antenna polypeptide. For details of the method see section 2.9 (iv). The protein was first cleaved into its constituent amino acids by acid hydrolysis. The amount of each amino acid was then assayed using the ninhydrin colorimetric method in an automated amino acid analyser. An elution profile of the derivatised amino acids, separated on a cation exchange resin is

A<sub>440</sub> nm

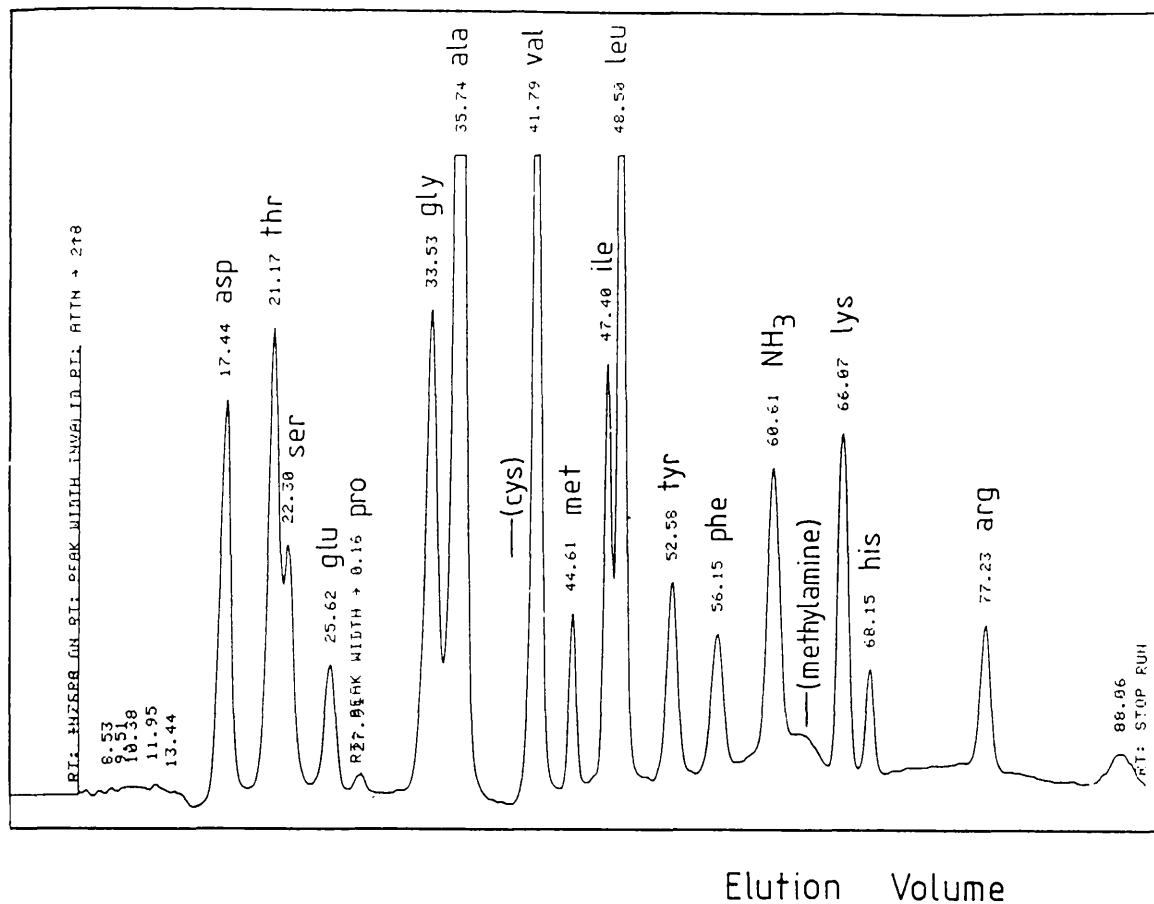


Fig. 6.8 Amino acid elution profile of hydrolysed B800-850- $\alpha_4$  antenna polypeptide, separated on a divinyl benzene resin column in an automatic amino acid analyser.

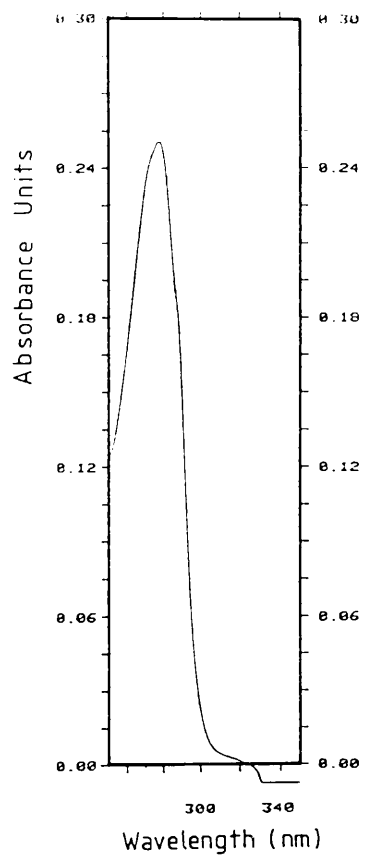
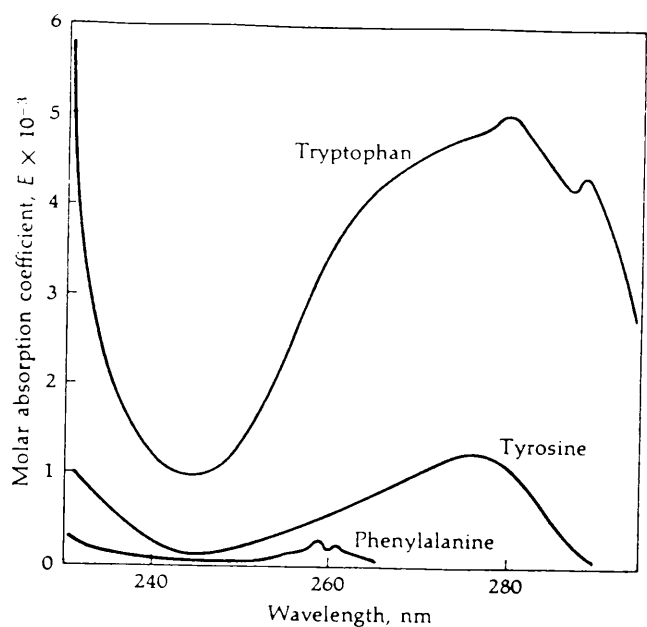
presented in Fig. 6.8. The amino acids are eluted in the order of most acidic to most basic. Each peak of the chromatogram is labelled with its retention time in minutes.

For accurate determination of the amino acid composition of a protein, analyses are performed on samples which have been hydrolysed for different lengths of time (e.g. 24, 48 and 72h). This is because leucine and valine are hydrolysed more slowly than the other amino acids so the amount detected increases with increasing hydrolysis time. And in addition the amino acids serine, threonine, cysteine and tyrosine are partially decomposed by acid hydrolysis. The amount of these amino acids present at zero time hydrolysis can be extrapolated from a plot of the amount of amino acid versus hydrolysis time. Multiple amino acid analyses were not performed for the proteins described here, but the analyses can be roughly corrected for losses by multiplying the amounts determined by the following percentages: serine 15%, threonine 6%, cysteine 4% and tyrosine 10% [Needleman, 1970].

As the absorbance area of the chromatogram peaks is proportional to the amount of amino acid, the amino acids can be quantitated by reference to a chromatogram of a 10nmol standard amino acid mixture. The imino acid proline forms a yellow complex with ninhydrin (the others form blue complexes) which is quantitated at 570nm. This explains why the proline peak at 440nm is very small. Tryptophan is absent from the chromatogram because it is almost totally decomposed during the protein hydrolysis. The amount of tryptophan can be determined using alkaline hydrolysis instead but this was not performed for this study. The presence of tryptophan in a protein can be detected from its UV absorption spectrum. The absorption spectrum of tryptophan has a small peak at 289nm (Fig. 6.9). This appears as a slight shoulder in tryptophan-containing proteins (Fig. 6.10). The chromatogram in Fig.

Fig. 6.9 UV absorption spectra of aromatic amino acids.

Fig 6.10 UV absorption spectrum of LL B800-850- $\alpha_4$  polypeptide. The presence of a shoulder at 289nm indicates the presence of tryptophan residues in the protein.



6.8 demonstrates the absence of cysteine residues in the protein. Antenna polypeptides from purple bacteria do not contain covalent cystine bridges.

The amino acid composition of the B800-850- $\alpha_4$  polypeptide is given in Table 6.1. The estimated numbers of amino acid residues have been corrected for decomposition of serine, threonine and tyrosine.

Table 6.1 Amino acid analysis data from LH60-column, peak A  $\alpha$ -polypeptide

amino acid	nmol*	nmol/2.65	estimated no.
asp	9.33	3.7	4
thr	11.50	4.6	5
ser	5.75	2.3	2
glu	2.98	1.2	1
gly	11.67	4.7	5
ala	29.70	11.9	12
val	18.29	7.3	8
met	2.63	1.1	1
ile	6.96	2.8	3
leu	15.56	6.2	6
tyr	4.75	1.9	2
phe	3.36	1.3	1
lys	7.34	2.9	3
his	1.83	0.7	1
arg	3.24	1.3	1
pro	16.50	6.6	6
			<u>61 + trp</u>

\* corrections included for serine, threonine and tyrosine

## 6.7 N-Terminal Amino Acid Sequence Analysis

### 6.6(i) Introduction

Automated sequential Edman degradation was performed on protein samples (0.5-1mg) collected after separation by liquid chromatography. The thiazolinone amino acid derivatives were collected from the sequenator and converted into PTH-amino acid derivatives (section

2.9(v)). The PTH-amino acids were identified by reversed phase HPLC on two different chromatographic systems: polar and nonpolar. Chromatograms of a standard PTH-amino acid mixture chromatographed in the two solvent systems are presented in Figs 6.11 and 6.12. Also included are chromatograms of the PTH-amino acid derivatives from positions 1 and 2 of the B800-850- $\alpha_4$  polypeptide.

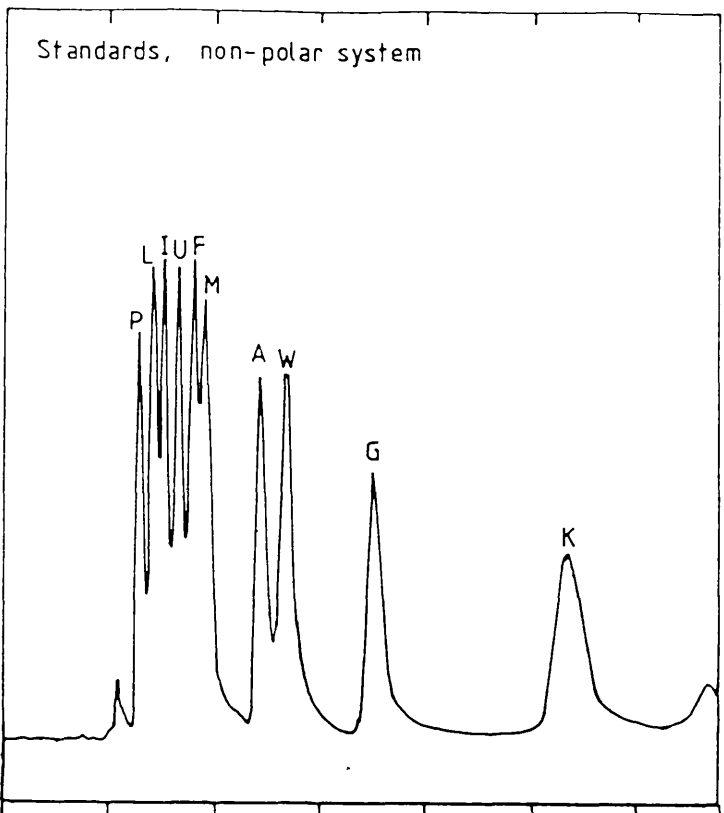
The number of amino acid residues which can be determined in a single sequencing run depends strongly on the purity of the sample. If protein impurities are present the HPLC chromatograms will exhibit multiple peaks which makes analysis of the required sequence difficult. When the protein is of high purity a single sequencing run usually allows the identification of 30-50 amino acids. The number is limited because at each cycle a small percentage of the N-terminal amino acids will not be cleaved. This means that in the next cycle a small percentage of contaminating derivatives will be formed. These show up on the HPLC chromatograms as background. The background increases with each cycle until it becomes impossible to accurately assess which of the peaks is the derivative required. To circumvent this the proteins can be fragmented by enzymic cleavage and the fragments separated by molecular sieve chromatography. The required fragments can then be individually sequenced to complete the missing data. C-terminal amino acid analysis by carboxypeptidase digestion is also required to confirm the C-terminal end of a protein. This is usually only needed for the last few residues and so it can be performed manually.

#### **6.6(ii) B875 antenna polypeptides**

Only the N-terminal amino acid sequences of the B875 complex polypeptides of *Rps. palustris*, strain French, have so far been determined. These are:

Fig. 6.11 HPLC chromatograms of a PTH-amino acid standard mixture, and the PTH amino acid from position 1 of the LL B800-850- $\alpha_4$  polypeptide sequence, separated on the nonpolar HPLC system.

A<sub>269</sub>



A<sub>269</sub>

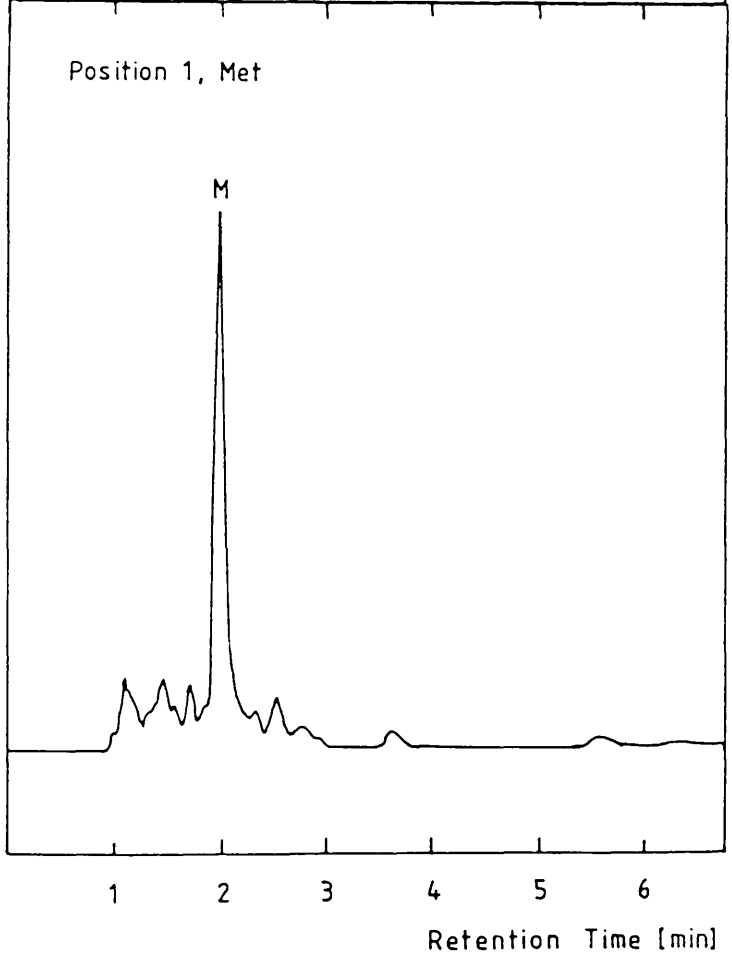
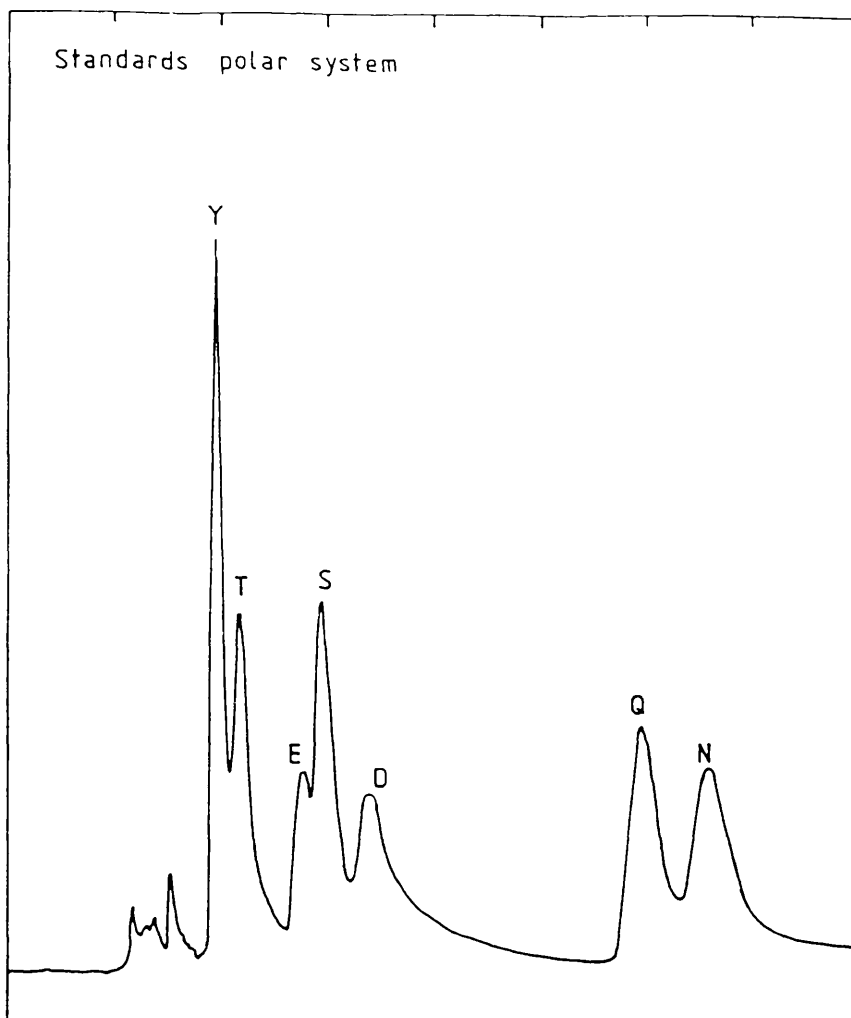
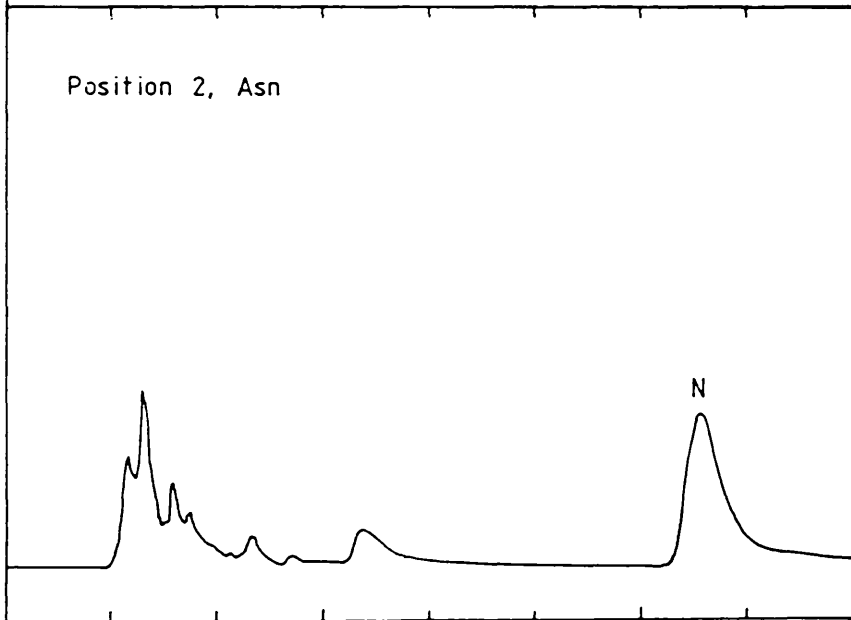


Fig. 6.12 HPLC chromatograms of a PTH-amino acid standard mixture, and the PTH amino acid from position 2 of the LL B800-850- $\alpha_4$  polypeptide sequence, separated on the polar HPLC system.

A<sub>269</sub>



A<sub>269</sub>



1

2

3

4

5

6

7

Retention Time [min]

$\alpha$       N<sub>f</sub>met-trp-arg-ile-trp-leu-leu...  
 $\beta$       asp-gly-ser-ile-ser-gly-leu-ser...

The N-terminal methionine residue of the  $\alpha$ -polypeptide is formylated. Methionine is a common N-terminal residue in bacterial proteins. N-formyl methionine residues indicate the presence of transcription initiation sites on the bacterial chromosome.

### 6.6(iii) B800-850- $\alpha$ complexes

The partial amino acid sequences of the B800-850- $\alpha$  antenna polypeptides from *Rps. palustris*, strain French, are presented in Fig. 6.13. Polypeptides  $\alpha_1$ ,  $\alpha_2$  and  $\alpha_3$  have been sequenced to 49 residues. From their amino acid analyses a further 2-4 C-terminal residues are expected. Polypeptide  $\alpha_4$  has been sequenced to 56 amino acids. The amino acid analysis predicted that this protein contains 61 residues plus any tryptophan residues. As there are 3 known Trp residues in the sequence the total number of amino acids may be more than 64.

The sequence homologies of the four B800-850- $\alpha$  polypeptides are very high:

<u>polypeptides</u>	<u>% sequence homology</u>
$\alpha_1/\alpha_2$	76
$\alpha_1/\alpha_3$	94
$\alpha_1/\alpha_4$	84
$\alpha_2/\alpha_3$	76
$\alpha_2/\alpha_4$	67
$\alpha_3/\alpha_4$	90

This suggests that these polypeptides diverged at a late stage in the evolution of the bacterium. Some of the amino acid exchanges in the  $\alpha$ -polypeptide sequences are for similar amino acids. e.g. serine for threonine, alanine for glycine or valine, valine for isoleucine, phenylalanine for tyrosine.

Fig. 6.13: Partial amino acid sequences of the B800-850- $\alpha$  light-harvesting polypeptides of *Rps. palustris*, strain French. Regions of inhomology are boxed.

	1	2	3	4	5	6	7	8	9	10	11	12	13	14	15	16	17
$\alpha_1$	met	asn	gln	ala	arg	ile	trp	thr	val	val	lys	pro	thr	val	gly	leu	pro
$\alpha_2$	met	asn	gln	gly	arg	ile	trp	thr	val	val	lys	pro	thr	val	gly	leu	pro
$\alpha_3$	met	asn	gln	gly	arg	ile	trp	thr	val	val	lys	pro	thr	val	gly	leu	pro
$\alpha_4$	met	asn	gln	gly	arg	ile	trp	thr	val	val	asn	pro	gly	val	gly	leu	pro
	18	19	20	21	22	23	24	25	26	27	28	29	30	31	32	33	34
$\alpha_1$	leu	leu	leu	gly	ser	val	thr	val	ile	ala	ile	leu	val	his	phe	ala	val
$\alpha_2$	leu	leu	leu	gly	ser	val	ala	ile	met	val	phe	leu	val	his	phe	ala	val
$\alpha_3$	leu	leu	leu	gly	ser	val	thr	val	ile	ala	ile	leu	val	his	phe	ala	val
$\alpha_4$	leu	leu	leu	gly	ser	val	thr	val	ile	ala	ile	leu	val	his	tyr	ala	val
	35	36	37	38	39	40	41	42	43	44	45	46	47	48	49	50	
$\alpha_1$	leu	ser	his	thr	thr	trp	phe	ser	lys	tyr	trp	asn	gly	pro	ala	...	
$\alpha_2$	leu	thr	his	thr	thr	xxx	val	ala	lys	phe	met	asn	gly	lys	ala	...	
$\alpha_3$	leu	ser	asn	thr	thr	trp	phe	ser	lys	tyr	trp	asn	gly	lys	ala	...	
$\alpha_4$	leu	ser	asn	thr	thr	trp	phe	ser	lys	tyr	trp	asn	gly	ala	thr	val	
	51	52	53	54	55	56											
$\alpha_4$	ala	ala	pro	ala	ala	ala	...										

**Fig. 6.14:** Comparison of the amino acid sequences of *Rps. palustris*, strain French, B800-850- $\alpha_4$  polypeptide with B800-850- $\alpha$  polypeptides from other species. Regions of homology are boxed.

*Rps. acidophila*, strain 7750, B800-850- $\alpha$

*Rb. sphaeroides* B800-850- $\alpha$

*Rb. capsulatus* B800-850- $\alpha$

*Rps. palustris*, strain French, B800-850- $\alpha_4$

1	2	3	4	5	6	7	8	9	10	11	12	13	14	15	16	17
met	asn	gln	gly	lys	ile	trp	thr	val	val	asn	pro	ala	ile	gly	ile	pro
met	thr	asn	gly	lys	ile	trp	leu	val	val	lys	pro	thr	val	gly	val	pro
met	asn	asn	ala	lys	ile	trp	thr	val	val	lys	pro	ser	thr	gly	ile	pro
met	asn	gln	gly	arg	ile	trp	thr	val	val	asn	pro	gly	val	gly	leu	pro
18	19	20	21	22	23	24	25	26	27	28	29	30	31	32	33	34
ala	leu	leu	gly	ser	val	thr	val	ile	ala	ile	leu	val	his	leu	ala	ile
leu	phe	leu	ser	ala	ala	phe	ile	ala	ser	val	val	ile	his	ala	ala	val
leu	ile	leu	gly	ala	val	ala	val	ala	ala	leu	ile	val	his	ala	gly	leu
leu	leu	leu	gly	ser	val	thr	val	ile	ala	ile	leu	val	his	tyr	ala	val
35	36	37	38	39	40	41	42	43	44	45	46	47	48	49	50	51
leu	ser	his	thr	thr	trp	phe	pro	ala	tyr	trp	gln	gly	gly	val	lys	lys
leu	thr	thr	thr	thr	trp	leu	pro	ala	tyr	tyr	gln	gly	ser	ala	ala	val
leu	thr	asn	thr	thr	trp	phe	ala	asn	tyr	trp	asn	gly	asn	pro	met	ala
leu	ser	asn	thr	thr	trp	phe	pro	lys	tyr	trp	asn	gly	ala	thr	val	ala
52	53	54	55	56	57	58	59	60								
ala-ala																
ala-ala-glu																
thr-val-val									ala-val-ala-pro-ala-gln							
ala-pro-ala									ala...							

Until the three-dimensional structures of antenna complexes have been determined the binding sites of the pigments, and the conformations of the polypeptides will remain uncertain. However, some information can be derived from analysis of the amino acid sequences.

Asparagine, histidine and glutamine amino acids are capable of forming co-ordinate bonds with BChl molecules. Raman spectroscopy has implicated histidine residues as the fifth ligands of the BChl dimers which form the B875 and B850 chromophores of antenna complexes (section 1.7(ii)). By comparing the amino acid sequences of many antenna complex polypeptides, Zuber (1985; 1987) has proposed that BChl dimers bind to two histidine residues, one on the  $\alpha$ -polypeptide and one on the  $\beta$ -polypeptide. The primary sequences of  $\alpha$ -polypeptides from several species, including the B800-850- $\alpha_4$  polypeptide from *Rps. palustris*, strain French, are presented in Fig. 6.14. The histidine residue at position 31 is postulated to be the  $\alpha$ -polypeptide binding site for the BChl dimer. All of the B800-850- $\alpha$  polypeptides from *Rps. palustris* contain a histidine in this position. In the previous chapter evidence was presented for the presence of an additional BChl chromophore in the LL B800-850 complexes of this species. The sequences in Fig. 6.13 suggest four possible binding sites for the extra chromophore at positions 2, 3, 37 and 46. Comparison with  $\alpha$ -polypeptides from other species shows that these possible binding sites are not exclusive to the polypeptides of *Rps. palustris*. It is worth noting that at position 37 the B800-850- $\alpha_1$  and - $\alpha_2$  polypeptides have histidine residues whereas the B800-850- $\alpha_3$  and - $\alpha_4$  polypeptides have asparagine residues. The sequence homologies between two  $\alpha$ -polypeptides from *R. palustris* and  $\alpha$ -polypeptides from other species have been calculated below:

% homology with *Rps. palustris*  
B800-850  $\alpha$ -polypeptides

		$\alpha_1$	$\alpha_4$
<i>Rps. acidophila</i>	7750 B800-820	63	67
	B800-850	59	59
	7050 B800-820	73	76
	B800-850	78	84
<i>Rb. sphaeroides</i>	B800-850	49	54
<i>Rb. capsulatus</i>	B800-850	39	41

Of these species it appears as though *Rps. palustris* is most closely related to *Rps. acidophila*, strain 7050. In Fig. 6.14 regions of homology between the polypeptides of the different species have been boxed. Regions of homology are often correlated with regions of functional importance on the basis that mutations of functionally important amino acids are usually deleterious. It is not only the point of ligation between the BChls and proteins which is important. The polypeptides are believed to play important roles in "fine tuning" the wavelengths at which BChl absorbs. Aromatic amino acids in the vicinity of the BChl dimer have been implicated for this role. Reference to Fig. 6.14 shows that aromatic residues are commonly found at positions 7, 40, 41, 44 and 45. The C-terminal aromatic amino acids which are positioned outwith the photosynthetic membrane (see later) may fold back and interact with the BChl dimer at the membrane surface. The B800-850- $\alpha$  polypeptides of *Rps. palustris* also contain aromatic amino acids at these C-terminal positions. The B800-850- $\alpha_2$  polypeptide is slightly different to the others in this region as two of the aromatic residues at positions 41 and 45 are absent, and Tyr<sub>44</sub> is exchanged for Phe<sub>44</sub>. One notable feature of the polypeptides from *Rps. palustris* is the presence of aromatic residues near the proposed binding site of the BChl dimer, at position 32. This appears to be unique amongst B800-850- $\alpha$  antenna polypeptides but other species do contain aromatic residues in the equivalent position of core antenna complex polypeptides. The most obvious feature of the B800-850- $\alpha_4$  polypeptide is the presence of an

alanine-rich C-terminal tail which is absent from the other polypeptides. This will be discussed in more detail later in the chapter.

#### 6.7(iv) B800-850- $\beta$ polypeptides

Peak 1 in Fig. 6.7 was found to contain three B800-850- $\beta$  polypeptides. Their sequences are illustrated in Fig. 6.15. B800-850- $\beta_1$  and  $\beta_2$  polypeptides are 94% homologous having only three amino acid differences. The  $\beta_1$  polypeptide has in addition an extra N-terminal amino acid, methionine. The B800-850- $\beta_3$  polypeptide is several residues shorter than the others, and contains a cluster of inhomology at the N-terminal (asp-lys-thr-leu). It is still 87% homologous to the B800-850- $\beta_2$  polypeptide though.

The histidine residue at position 40 is the proposed binding site for one of the dimer BChls (Figs. 6.15 and 6.16). Conserved histidine residues are also found at position 22. It has been proposed that these histidine residues are the sites at which the B800 monomer BChls are bound in B800-850 complexes [Zuber, 1986]. However, this has been disputed by resonance Raman studies [Robert and Lutz, 1985]. In total, the B800-850- $\beta$  polypeptides from *Rps. palustris*, strain French, contain four histidine residues (assuming that position 52 of the B800-850- $\beta_1$  polypeptide is also a histidine) at positions 22, 24, 40 and 52.  $\beta$ -polypeptides from most other species only contain histidine residues at positions 22 and 40. The additional histidine residues at positions 24 and 52 are therefore possible binding sites for the additional chromophore in the LL complexes. The only other organism known to have extra histidines at these positions is *Rps. acidophila*, strain 7050 [Brunisholz et al., 1987]. Two of the  $\beta$ -polypeptides contain asparagine residues at position 6 which could possibly interact with the BChl

Fig. 6.15: Partial amino acid sequences of the B800-850- $\beta_1$  polypeptides from *Rps. palustris*. Regions of inhomology are boxed.

	1	2	3	4	5	6	7	8	9	10	11	12	13	14	15	16	17
$\beta_1$	met	val	asp	asp	pro	asn	lys	val	trp	pro	thr	gly	leu	thr	ile	ala	glu
$\beta_2$		ala	asp	asp	pro	asn	lys	val	trp	pro	thr	gly	leu	thr	ile	ala	glu
$\beta_3$							asp	lys	thr	leu	thr	gly	leu	thr	val	glu	glu
	18	19	20	21	22	23	24	25	26	27	28	29	30	31	32	33	34
$\beta_1$	ser	glu	glu	leu	his	lys	his	val	ile	asp	gly	ser	arg	ile	phe	val	ala
$\beta_2$	ser	glu	glu	leu	his	lys	his	val	ile	asp	gly	thr	arg	ile	phe	gly	ala
$\beta_3$	ser	glu	glu	leu	his	lys	his	val	ile	asp	gly	thr	arg	ile	phe	gly	ala
	35	36	37	38	39	40	41	42	43	44	45	46	47	48	49	50	51
$\beta_1$	ile	ala	ile	val	ala	his	phe	leu	ala	tyr	val	tyr	ser	pro	trp	...	
$\beta_2$	ile	ala	ile	val	ala	his	phe	leu	ala	tyr	val	tyr	ser	pro	trp	leu	xxx
$\beta_3$	ile	ala	ile	val	ala	his	phe	leu	ala	tyr	val	tyr	ser	pro	trp	leu	xxx
	52																
$\beta_1$	his	...															
$\beta_2$	his	...															
$\beta_3$	his	...															

**Fig. 6.16:** Comparison of the amino acid sequences of  $\beta$ -polypeptides from a variety of species. Regions of homology are boxed.

*Rps. acidophila*, strain 7750, B800-850- $\beta$   
*Rb. sphaeroides* B800-850- $\beta$   
*Rb. capsulatus* B800-850- $\beta$   
*Rps. palustris*, strain French, B800-850- $\beta_1$

1	2	3	4	5	6	7	8	9	10	11	12	13	14	15	16	17
												ala-thr	leu-thr	ala-glu	gln	
thr	asp	asp	leu	asn	lys	val	trp	pro	ser	gly	leu	thr	val	ala	glu	
	fmet	thr	asp	asp	lys	ala	gly	pro	ser	gly	leu	ser	leu	lys	glu	
met	val	asp	asp	pro	asn	lys	val	trp	pro	thr	gly	leu	thr	ile	ala	glu
18	19	20	21	22	23	24	25	26	27	28	29	30	31	32	33	34
ser	glu	glu	leu	his	lys	tyr	val	ile	asp	gly	thr	arg	val	phe	leu	gly
ala	glu	glu	val	his	lys	gln	leu	ile	leu	gly	thr	arg	val	phe	gly	gly
ala	glu	glu	ile	his	ser	tyr	leu	ile	asp	gly	thr	arg	val	phe	gly	ala
ser	glu	glu	lys	his	lys	his	val	ile	asp	gly	ser	arg	ile	phe	val	ala
35	36	37	38	39	40	41	42	43	44	45	46	47	48	49	50	51
leu	ala	leu	val	ala	his	phe	leu	ala	phe	ser	ala	thr	pro	trp	leu	his
met	ala	leu	ile	ala	his	phe	leu	ala	ala	ala	ala	thr	pro	trp	leu	gly
met	ala	leu	val	ala	his	ile	leu	ser	ala	ile	ala	thr	pro	trp	leu	gly
ile	ala	ile	val	ala	his	phe	leu	ala	tyr	val	tyr	ser	pro	trp	..	



*palustris*, strain French, lie in the membrane, hydropathy plots have been drawn using two different hydropathy scales. Hydropathy values for the two indexes used are listed below. The values are for the Von Heijne hydropathy scale [Von Heijne, 1981] and the (Kyte and Doolittle scale) [Kyte and Doolittle, 1982]: Ala -4.2 (1.8), Asp 31.0 (-3.5), Glu 24.7 (-3.5), Phe -14.2 (2.8), Gly 0.0 (-0.4), His 14.3 (-3.2), Ile -10.5 (4.5), Lys 17.6 (-3.9), Leu -10.1 (3.8), Met -11.3 (1.9), Asn 10.2 (-3.5), Pro 13.9 (-1.6), Gln 10.1 (-3.5), Arg 47.3 (-4.5), Ser 6.3 (-0.8), Thr 3.8 (-0.7), Val -8.4 (4.2), Trp -8.4 (-0.9), Tyr 4.7 (-1.3).

Note that the two scales have been determined with opposite signs. The Von Heijne plots have therefore been reversed to allow easier comparison between the two. The hydropathy values are based on the change in free energy associated with the transfer of an amino acid from a hydrophobic to a hydrophilic environment, with experimental and theoretical corrections. The hydropathy plots were smoothed by calculating a moving average (or a moving total) with a window of seven amino acids.

In its native environment the hydrophobicity of a stretch of protein is determined not just by its amino acid content, but also by its co-operative binding with other regions of protein. Different hydropathy scales are based on different experimental evidence and theoretical assumptions, so some will fit a particular protein well and others won't. A less empirical approach for estimating the position of a transmembrane domain of a protein has been suggested by Eisenberg et al. (1984). They have devised a hydropathy scale to specifically analyse transmembrane helices. A 21-residue window is run along the entire protein sequence, calculating the mean hydrophobicity for each window. For the antenna polypeptides investigated here, the window with the highest mean hydrophobicity was selected as the best candidate for

the transmembrane domain. In practice, other "selection procedures" were first followed to determine whether the protein is capable of forming a transmembrane  $\alpha$ -helix. The selected domains are enclosed by the dashed lines on the hydrophobicity plots in Figs 6.17 and 6.18.

The general patterns of the Von Heijne, and Kyte and Doolittle hydropathy plots in Fig. 6.17 are similar except for the N-terminal region. Using the method of Eisenberg et al. it was estimated that the transmembrane domain of the B800-850- $\alpha_4$  polypeptide includes residues 15-35. This correlates better with the Von Heijne plot (A). At the C-terminal region of the protein the alanine-rich tail which is specific to the B800-850- $\alpha_4$  polypeptide is shown to be hydrophobic. Analysis of the amino acid compositions of known regions of  $\alpha$ -helix has enabled a list of those residues most commonly found in these structures to be compiled [Chou et al., 1978]:

Description	Amino Acids
Strong helix formers	Met, Ala, Glu, Leu
Helix formers	Ile, Trp, Lys, Val, Phe, Gln
Weak helix formers	His, Asp
Indifferent	Arg, Thr, Ser, Cys
Weak helix breakers	Asn, Tyr
Strong helix breakers	Pro, Gly

As alanine residues are classified as strong  $\alpha$ -helix formers, it seems likely that the hydrophobic tail of the B800-850- $\alpha_4$  polypeptide turns and inserts back into the membrane as a short helix. The B800-850- $\alpha$  polypeptide of *Rc. gelatinosus*, which has 69 amino acids, contains a similar alanine-rich C-terminal domain (R A Brunisholz, unpublished).

From the postulated positioning of the  $\alpha$ -polypeptides in the membrane, the His/Asn<sub>37</sub> residues are located just at the periplasmic surface of the membrane. His<sub>31</sub> is located in the middle of the periplasmic membrane leaflet. Of those amino acids of the B800-850- $\alpha_1$  polypeptide which have so far been sequenced, 31 of them are classified

Fig. 6.17 Hydropathy plots of the B800-850- $\alpha_4$  polypeptide using the Von Heijne (1981) [A], and Kyte and Doolittle (1982) [B] hydropathy indexes. The numbers on the central axes refer to the sequenced amino acid residue number. The dotted lines mark the boundary of the hydrophobic membrane-spanning region which was estimated by the method of Eisenberg et al. (1984).

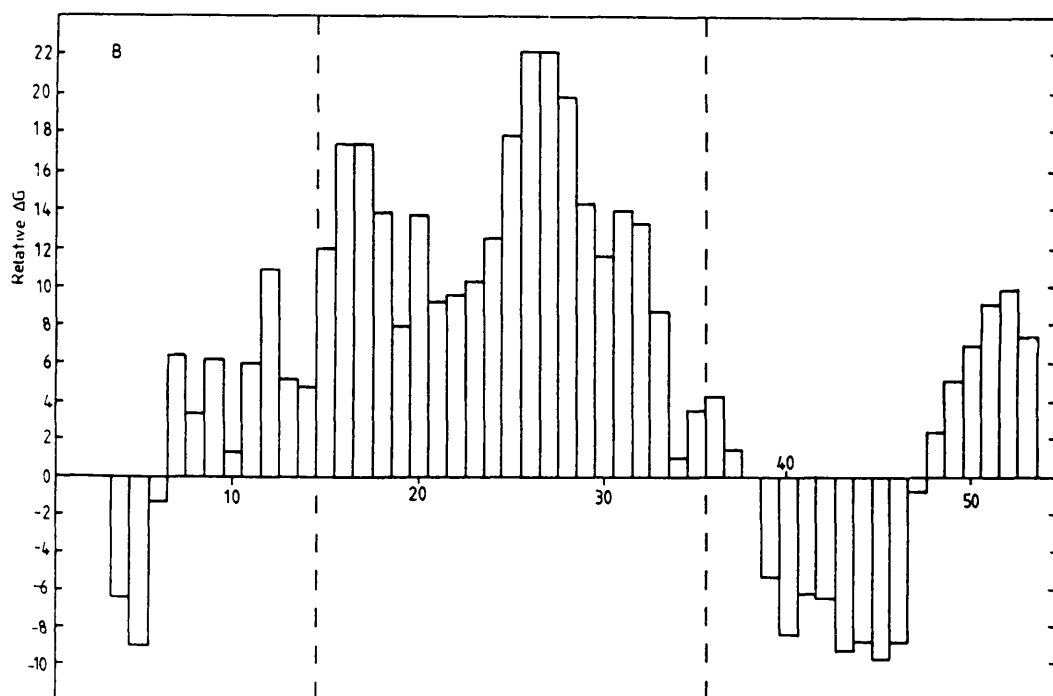
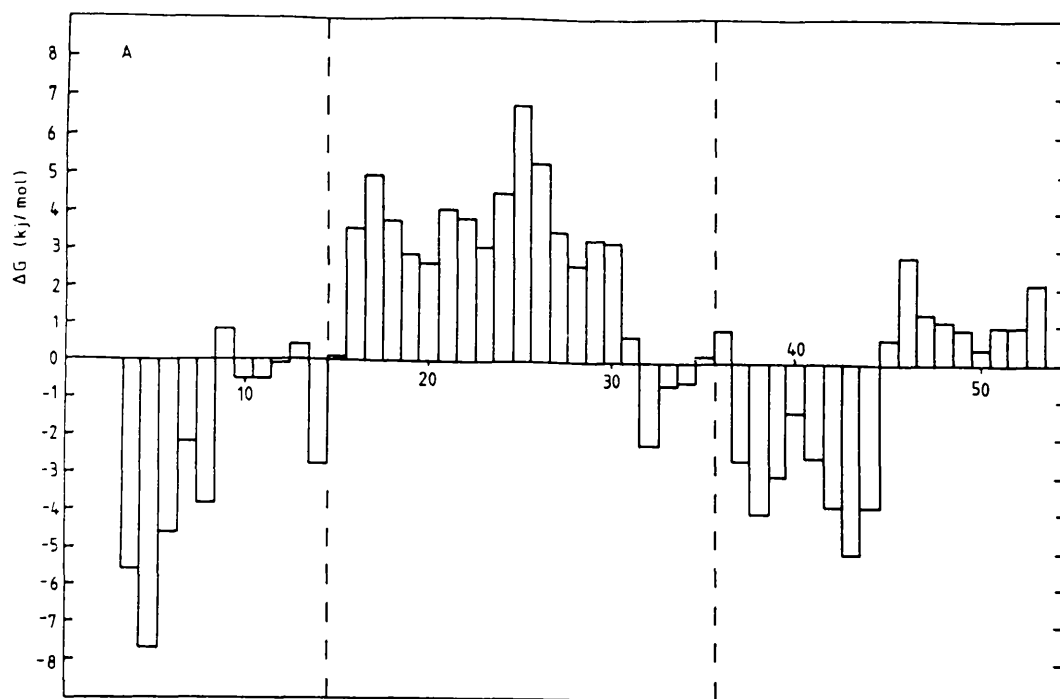
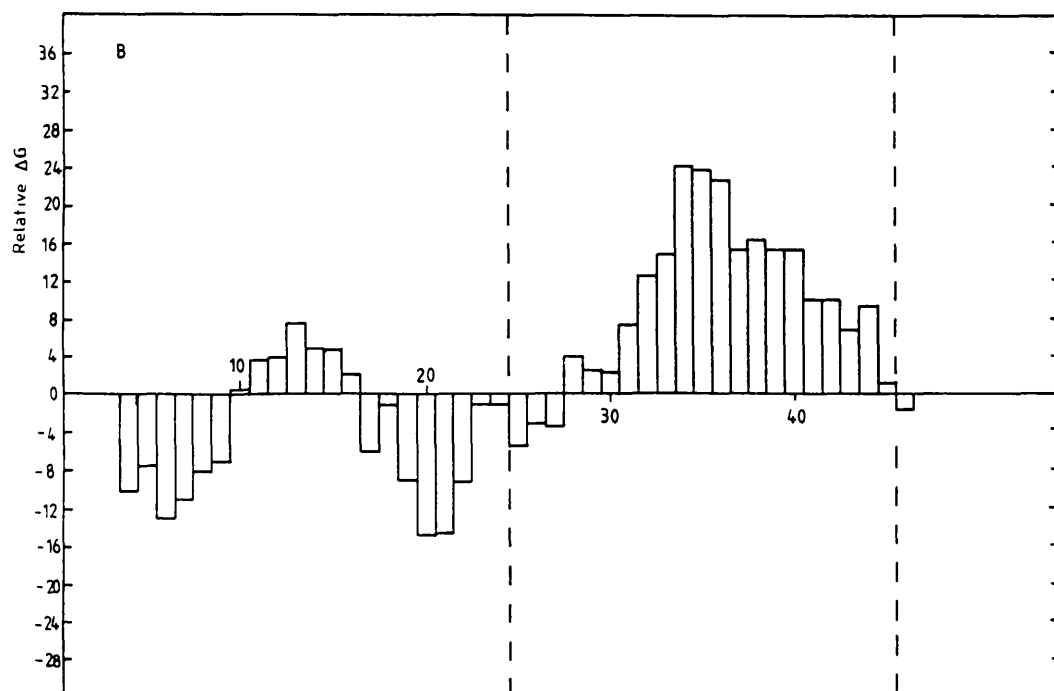
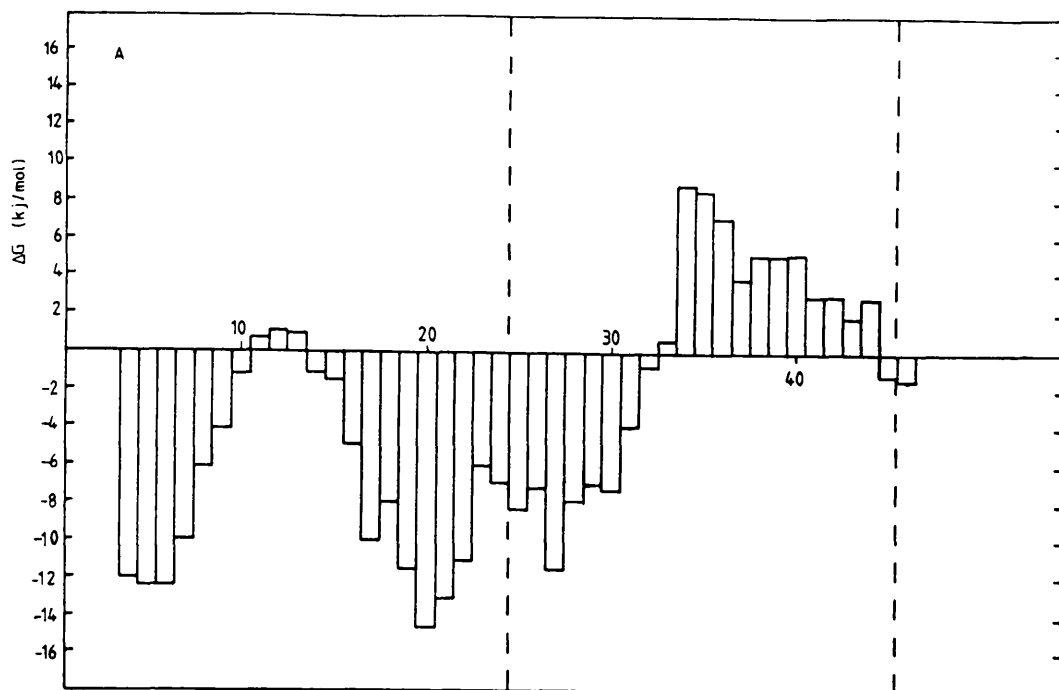


Fig. 6.18 Hydropathy plots of the B800-850- $\beta_1$  polypeptide using the Von Heijne (1981) [A], and Kyte and Doolittle (1982) [B] hydropathy indexes. The numbers on the central axes refer to the sequenced amino acid residue number. The dotted lines mark the boundary of the hydrophobic membrane-spanning region which was estimated by the method of Eisenberg et al. (1984).



as  $\alpha$ -helix forming residues and 9 are  $\alpha$ -helix breakers. This correlates with the high  $\alpha$ -helical content proposed for the antenna complex polypeptides of purple bacteria.

The hydropathy plots of the B800-850- $\beta_1$  polypeptide (Fig. 6.18) are again similar in shape but this time the Kyte and Doolittle scale (B) seems to correlate better with the transmembrane region estimated by the method of Eisenberg et al. This domain spans residues 25-45. This is closer to the C-terminal than the transmembrane domain of the  $\alpha$ -polypeptide, suggesting a longer N-terminal region and a shorter C-terminal region. The N-terminal domain seems to have a slightly hydrophobic middle region centred around residues 10-16. Perhaps this corresponds to a small hydrophobic fold in the protein, or a point of interaction with similar regions in other  $\beta$ -polypeptides. This may help to bind the complex together. The presence of two strong helix breakers in this region (proline and glycine) indicates that this region is unlikely to be a short stretch of  $\alpha$ -helix itself.

With the estimated transmembrane regions of  $\alpha$ - and  $\beta$ -polypeptides aligned, the histidine residues at positions 31 ( $\alpha$ ) and 40 ( $\beta$ ) which are thought to bind the BChl 850 dimer, are on the same helical turn and are therefore in close proximity.

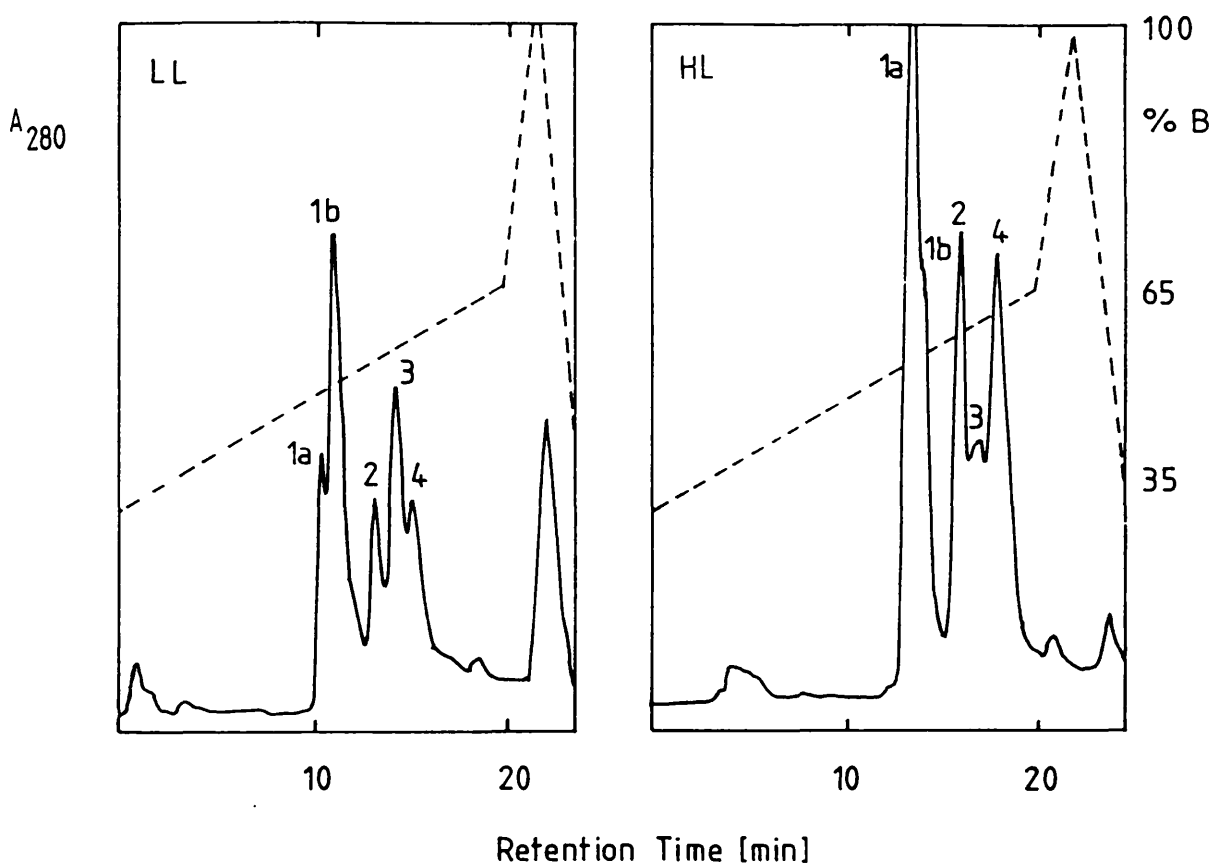
### **6.9 Stoichiometry of the Polypeptides in the B800-850 Complexes From High Light and Low Light Grown Cells**

To further our understanding of the structures of the B800-850 antenna complexes from low and high light grown cells, the next aim must be to determine the stoichiometry of the polypeptides in these complexes. SDS polyacrylamide gels and preliminary FPLC data suggested differences between the LL and HL complex polypeptide compositions.

Further liquid chromatography and sequencing data have shown that both the HL and LL grown cells contain the same antenna polypeptides. However the stoichiometry of the polypeptides in the B800-850 complexes appears to be different. HPLC chromatograms of extracts of isolated HL and LL complexes are shown in Fig. 6.19. The B800-850- $\beta$  polypeptides are represented by peak 1 as before. From the FPLC traces the peak appears to have two components, labelled 1a and 1b. LL B800-850 complexes contain predominantly peak 1a whereas the reverse is true for the HL complexes. The relationship between the two peaks and the three  $\beta$ -polypeptides is not yet clear.

The  $\alpha$ -polypeptides were isolated from FPLC peaks 2, 3 and 4. (Peak 4 contains a mixture of polypeptides  $-\alpha_3$  and  $-\alpha_4$ ). Again, a difference in the stoichiometry of the HL and LL B800-850 complexes is indicated. In the low light complexes the B800-850- $\alpha_2$  peak (peak 3) polypeptide is present in a large amount whereas it is a small peak in the HL complex.

The relative absorption coefficients of the polypeptides can be roughly estimated from the numbers of tryptophan and tyrosine amino acids in their sequences. At 280nm the absorption coefficient of tryptophan is about four times greater than that of tyrosine (Fig. 6.9). From the partial sequences so far obtained the B800-850- $\alpha_1$  and  $-\alpha_3$  polypeptides contain 1 tyrosine and 3 tryptophan residues. The B800-850- $\alpha_4$  polypeptide contains 3 tryptophan and 2 tyrosine residues and the B800-850- $\alpha_2$  polypeptide contains 2 tryptophan residues (assuming that position 40 is also Trp). The absorbance coefficient of B800-850- $\alpha_2$  should therefore be roughly half of the coefficients of the others. This would suggest that the relative amounts of protein present in peaks 2, 3 and 4 of Fig. 6.19<sup>(LL)</sup> is roughly the same. i.e. assuming that peak 4 is comprised of equal amounts of B800-850- $\alpha_3$  and  $-\alpha_4$  polypeptides (for which there is no evidence yet), the stoichiometry can be speculated to



**Fig. 6.19** HPLC chromatograms of LL and HL B800-850 antenna complex protein extracts. Solvent system and numbering as Fig. 6.7.

be  $\alpha_1:\alpha_2:\alpha_3:\alpha_4$ , 2:6:1:1. From the HPLC trace of the HL B800-850 complex the stoichiometry of the  $\alpha$ -polypeptides can be speculated to be 2:2:1:1. However it is important to stress that liquid chromatography of proteins is capricious. Multiple injections of the same sample can give slightly different elution profiles. A single peak may split into two or more peaks, or develop a shoulder or disappear entirely, which makes interpretation of the data difficult. The FPLC chromatograms included here are however representative of the total data obtained and the evidence does suggest a relatively greater proportion of B800-850- $\alpha_2$  polypeptide in the low light cells. This would explain the previous suggestion that there is relatively more B800-850- $\alpha_4$  polypeptide in the high light grown cells.

In chapter three it was described how low light grown cells actually contain a mixture of the extreme LL and HL spectral forms of the B800-850 antenna complexes. As a consequence of this it is not possible to say whether the HL and LL B800-850 complexes contain different polypeptides or whether they contain the same polypeptides but in a different stoichiometry. This can be determined by liquid chromatographic analysis of antenna complexes which comprise only the extreme spectral forms. These can be prepared by DEAE-cellulose anion exchange chromatography.

### 6.10 Summary

In summary low light grown *Rps. palustris*, strain French, contains at least nine different antenna polypeptides. Two of these comprise the B875 complex  $\alpha/\beta$ -polypeptide pair. There are four B800-850- $\alpha$  polypeptides and three B800-850- $\beta$  polypeptides. The four  $\alpha$ - and three  $\beta$ -polypeptides are highly homologous. Two of the  $\beta$ -polypeptides contain about 52-54 amino acids and the third is five amino acids shorter at the

N-terminal and has a four-residue N-terminal cluster of inhomology. The unusual feature of these polypeptides is the presence of at least one more histidine amino acid than is normally found in  $\beta$ -polypeptides. B800-850- $\alpha_1$ , - $\alpha_2$  and - $\alpha_3$  are probably also 52-54 amino acids long. B800-850- $\alpha_4$  has an additional alanine rich, C-terminal stretch about 10-12 amino acids long. This may turn back and insert into the membrane as an  $\alpha$ -helix. A notable feature of all of the B800-850 antenna polypeptides from *Rps. palustris*, strain French, is the presence of extra amino acids which are capable of binding BChl in comparison with those of other species

The stoichiometries of the polypeptides in the B800-850 complexes from low and high light grown cells are still uncertain, although from FPLC traces it appears that the LL complexes contain relatively more B800-850- $\alpha_2$  polypeptide. The chromatograms also suggest that lowering the light intensity induces a  $\beta$ -polypeptide exchange in the complex.

CHAPTER SEVEN: Determination of the Singlet-Singlet, Carotenoid to BChl, Energy Transfer Efficiencies of Antenna Complexes from *Rps. palustris*, *Chr. vinosum* and *Rps. acidophila*

## 7.1 Introduction

In some species of purple bacteria a change in the conditions of cell culture can alter the spectral form of antenna complexes which are incorporated into the photosynthetic membrane. Whenever the physiology of an organism is modulated in response to its environment the question arises, how do these changes benefit the organism? The function of antenna complexes is of course to absorb sunlight and transfer the energy efficiently to the reaction centre. It is likely then that changes to the antenna complex composition of the membranes serve to alter the efficiency of the light-harvesting process. Part of this process is the transfer of energy from carotenoid to BChl. In this chapter measurements of the efficiency of energy transfer from carotenoid to BChl will be described for antenna complexes which are specifically regulated by light intensity or temperature.

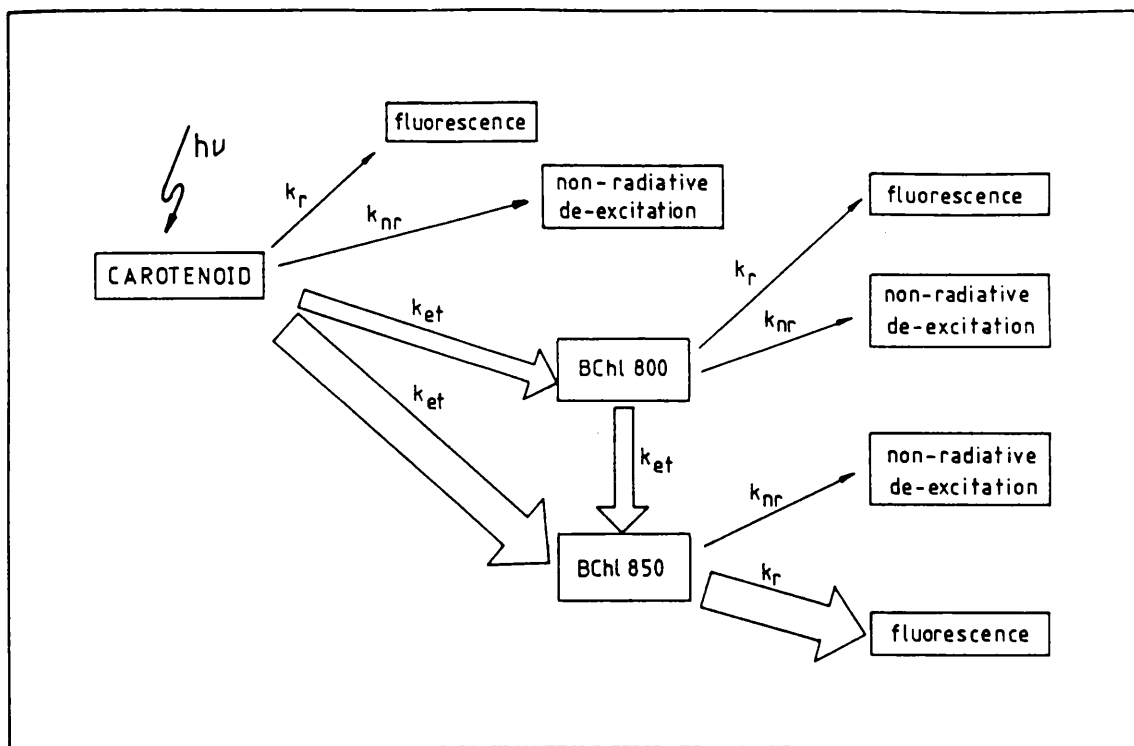
In chapter three the synthesis of B800-850 Types I and II complexes and B800-820 complexes in response to different culture conditions was described. A summary of the antenna complexes isolated from different strains, grown under various light and temperature regimes is presented in Table 7.1 below. It should be remembered that B800-850 Type II complexes may be a mixture of Type I complexes and B800-820 complexes.

Table 7.1

species	LL/30°C	HL/30°C	HL/40°C	HL/20°C
<i>Rps. palustris</i> , French	B800-850 LL	B800-850 HL	nd	nd
<i>Chr. vinosum</i> , D	B800-850 II B800-820	B800-850 I	B800-850 II B800-820 ?	nd nd
<i>Rps. acidophila</i> , 7050	B800-850 II B800-820	B800-850 I	nd	nd
7750	B800-850 I	B800-850 I	nd	B800-820

The synthesis of new complexes in response to a reduction in light intensity has led to the suggestion that they somehow enhance the efficiency of the light-harvesting process. B800-820 antenna complexes add an extra tier to the photosynthetic unit which enhances photon collection by increasing the overall amount of antenna and by improving its directed funnelling capability (section 1.7(iii)). A third function for the low light complexes was suggested by Angerhofer et al. (1986) when they determined the efficiency of energy transfer from carotenoid to BChl in the B800-820, and B800-850 Types I and II complexes from *Rps. acidophila*, strain 7050. They concluded that the efficiencies were 50-55% for the HL B800-850 Type I complexes and 70-75% for the LL B800-850 Type II, and B800-820 complexes. This introduces the idea that variable complexes synthesised by low light grown cells are inherently more efficient at harvesting energy. It should be noted that the *Chromatium* cells used to obtain the B800-850 Type II complexes were not cultured under low light intensities as described by Thornber (1970) but were cultured at the usual high light intensity, and at 40°C.

Under constant illumination at normal light intensities, the distribution of excitation energy within a population of pigment molecules can be calculated by measuring the relative intensities of fluorescence emission from each pigment type (see section 1.8). Disregarding internal energy conversions (e.g. triplet formation, BChl Soret-Qx-Qy energy transitions) the excitation/de-excitation processes in an isolated B800-850 complex can be described by Fig. 7.1. By exciting at the wavelengths at which carotenoids absorb light, and by measuring the intensity of fluorescence emitted from the B850 chromophore Qy band, the efficiency of energy transfer between the two can be calculated. The exact route of energy transfer from carotenoid to the B850 dimer is still uncertain. Kramer et al. (1984a) proposed



**Fig. 7.1** Deexcitation processes in the B800-850 antenna complexes of purple bacteria. The open arrows represent the pathway of energy transfer from carotenoid to the Qy energy level of BChl during energy transfer efficiency measurements on B800-850 antenna complexes. The pathway is based on the data presented by Kramer et al., (1984a) which suggests that one third of the excitation energy is transferred from carotenoid to B800 and that the remainder goes directly to B850.

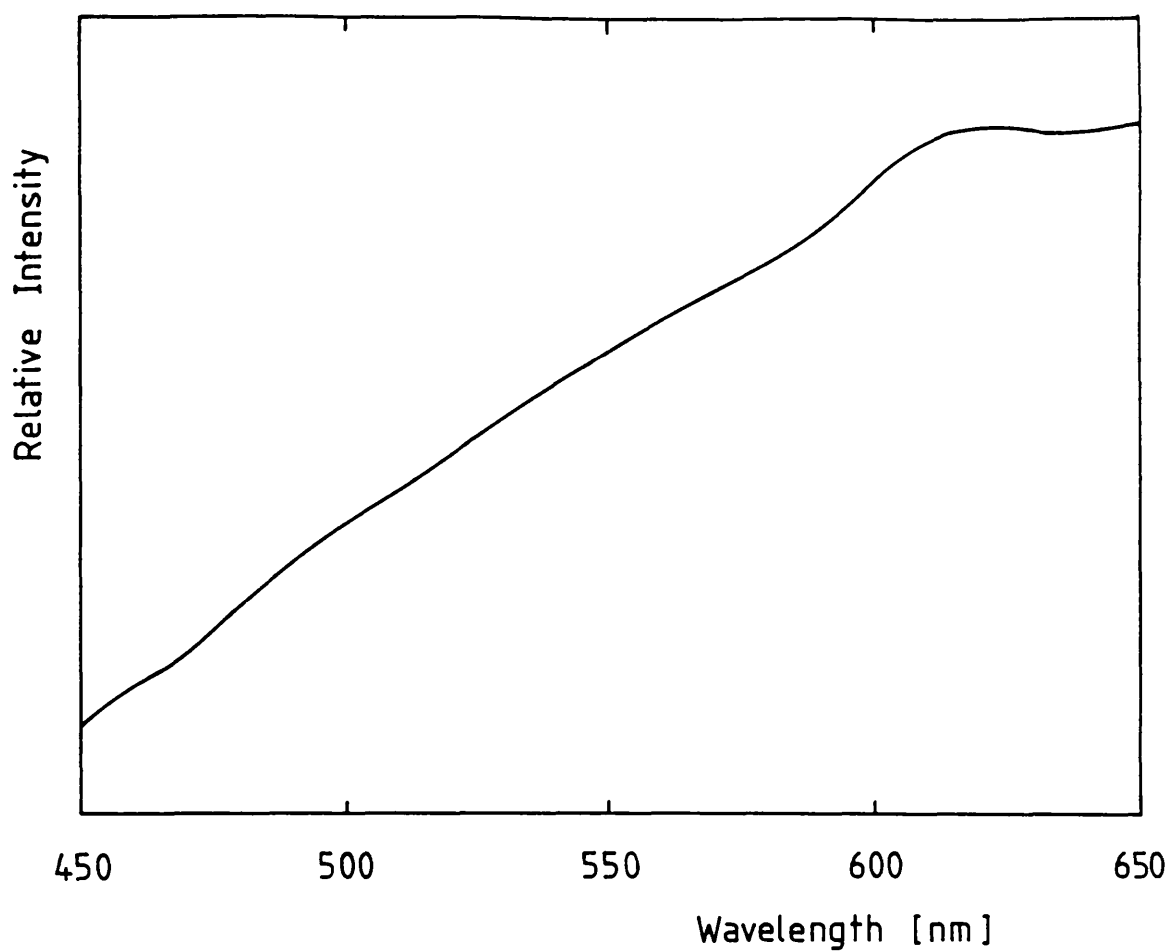


Fig. 7.2 A spectrum of the relative emission intensity of the excitation light source used in the energy transfer efficiency measurements.

that the B800-850 complexes from *Rb. sphaeroides* contain two discrete pools of carotenoid; the one pool transferring its excitation (one third of the total) to the B800 monomer, and the other pool transferring the remaining two thirds of the excitation to the B850 dimer. Kramer et al. (1984a) also measured the fluorescence emission from the Q<sub>y</sub> band of the B850 chromophore in *Rb. sphaeroides* and showed that the intensity is approximately the same irrespective of whether the excitation wavelength is 800nm or 850nm. This indicates that the energy transfer between the monomer and the dimer is highly efficient.

To calculate the quantum efficiency of energy transfer, the fluorescence excitation and absorption spectra were normalised at the Q<sub>x</sub> band of BChl. The assumption was therefore made that the efficiency of energy transfer from the Q<sub>x</sub> to the Q<sub>y</sub> dipoles is 100%.

## 7.2 Results and Discussion

A spectrum of the exciting-lamp emission intensity is shown in Fig. 7.2. Fluorescence excitation spectra of LL *Rps. palustris* B800-850 complexes, before and after correction for variation in the lamp emission intensity, are shown in Fig. 7.3. Examples of the fluorescence emission/absorption spectra plotted during the calculation of the efficiency measurements are presented in Figs 7.4-7.6.

The final carotenoid-to-BChl energy transfer measurements are tabulated for each of the three carotenoid vibrational bands (except for the B875 complexes from *Rps. palustris* which have a rounded spectrum) in Tables 7.2-7.6. The carotenoid vibrational bands are labelled according to the energy levels involved in the electronic transition from the ground state. To excite an electron into the redmost vibronic band the electron moves from the ground state (0) to the first vibronic band (0) of the first optically allowed excited state, 1Bu. Therefore

Fig. 7.3 Fluorescence excitation spectra of B800-850 complexes from low light grown cells before (  $\Delta$  ) and after (  $\circ$  ) correction for variation in the excitation lamp emission intensity.

Fig. 7.4 Fractional absorption spectrum (  $\Delta$  ) and normalised fluorescence excitation spectrum (  $\circ$  ) of B800-850 complexes from low light grown *Rps. palustris* cells.

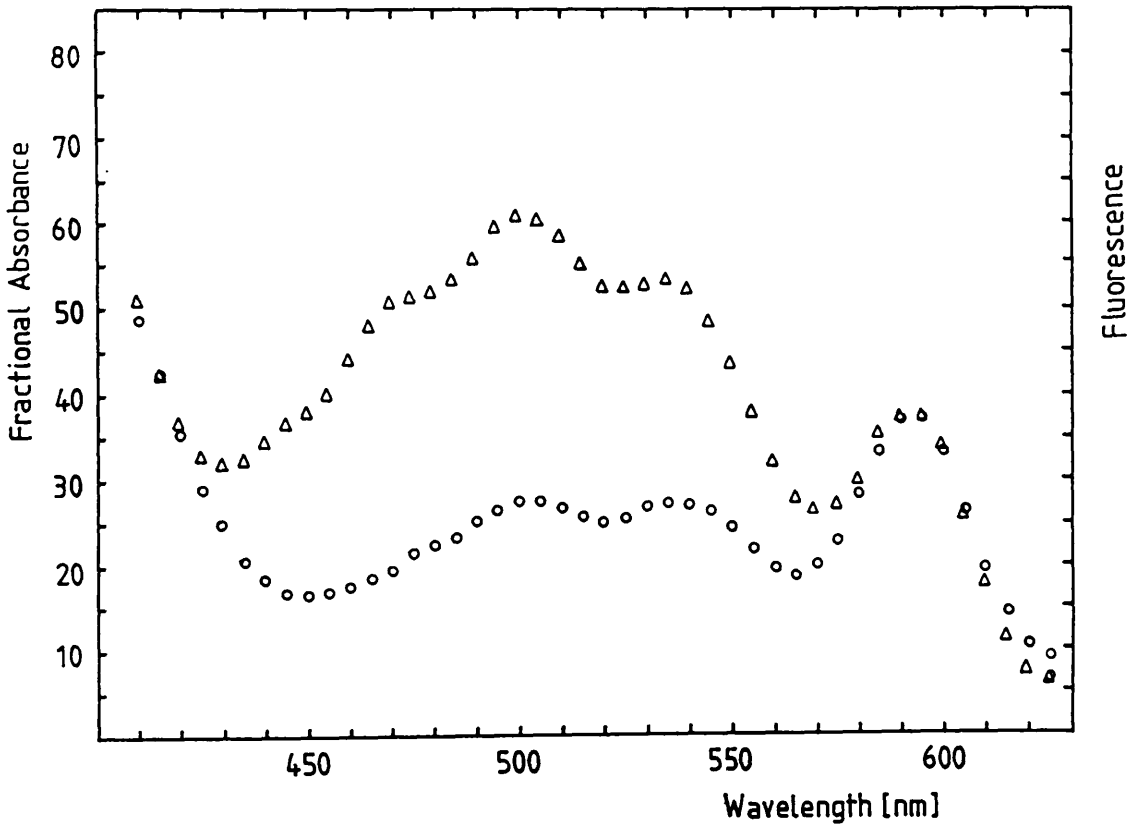
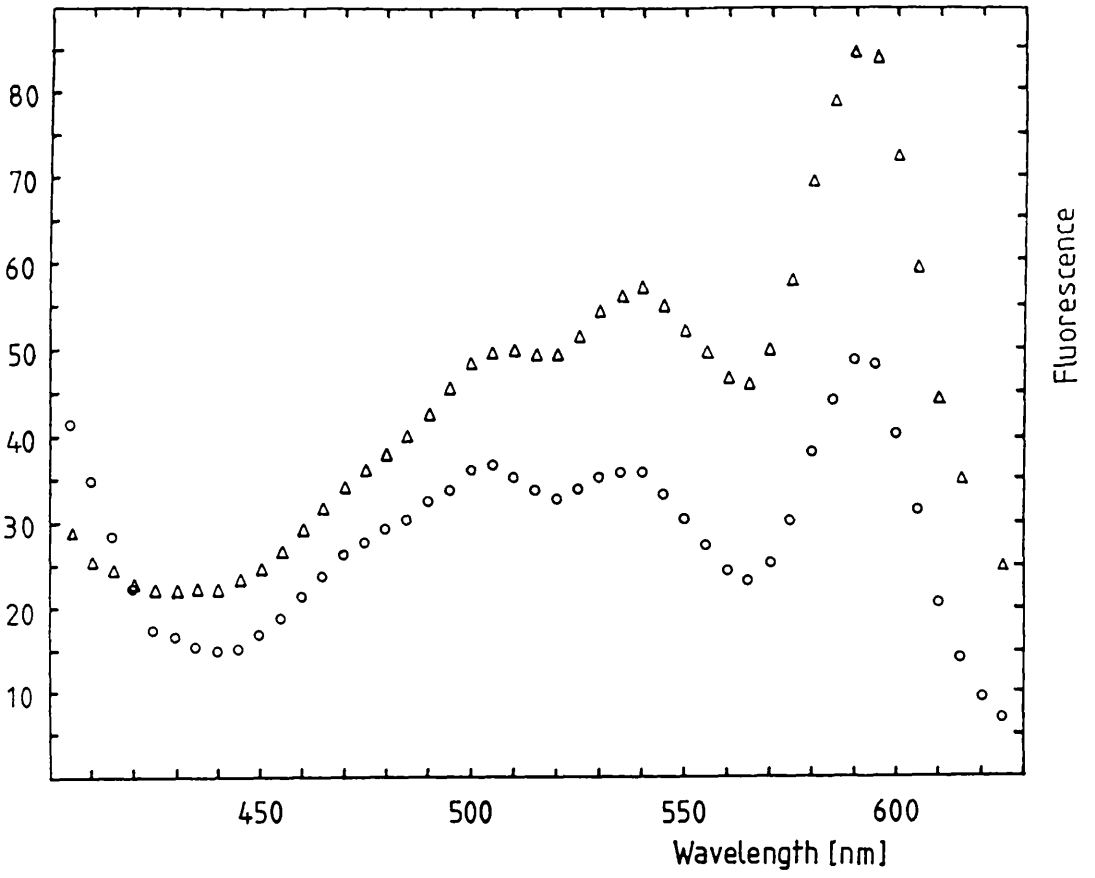
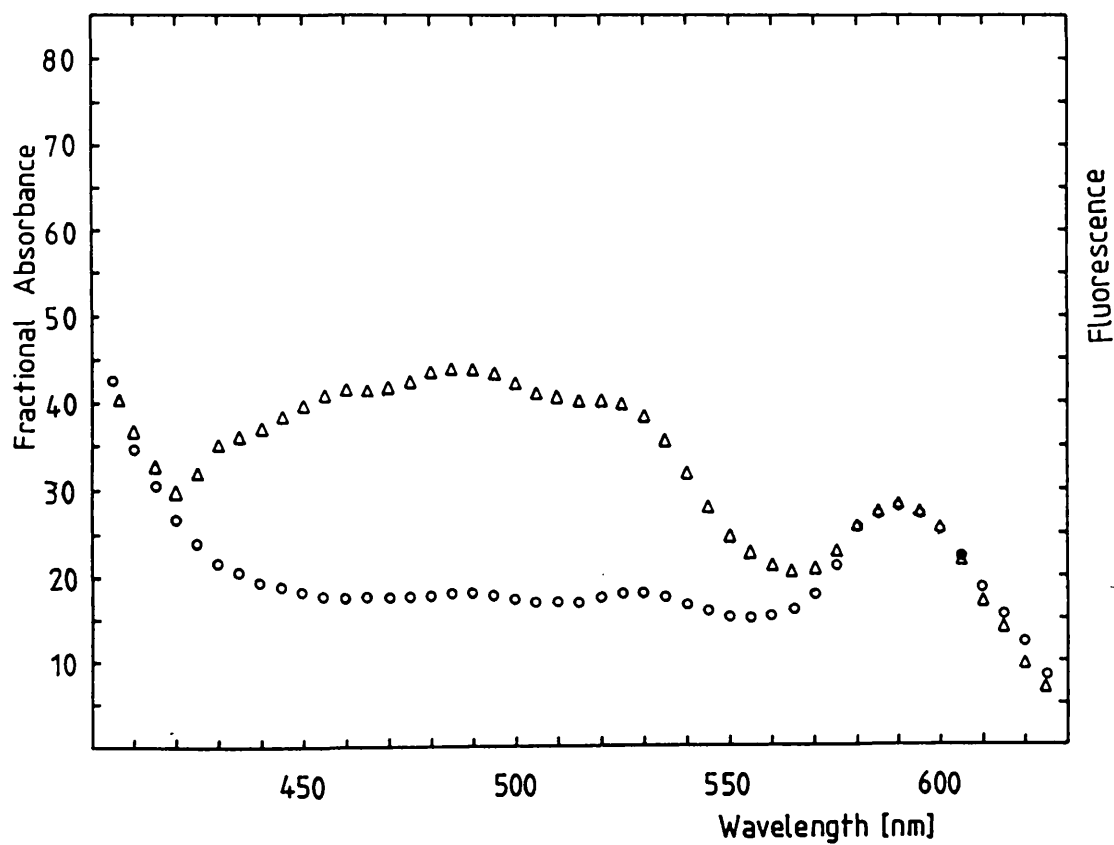
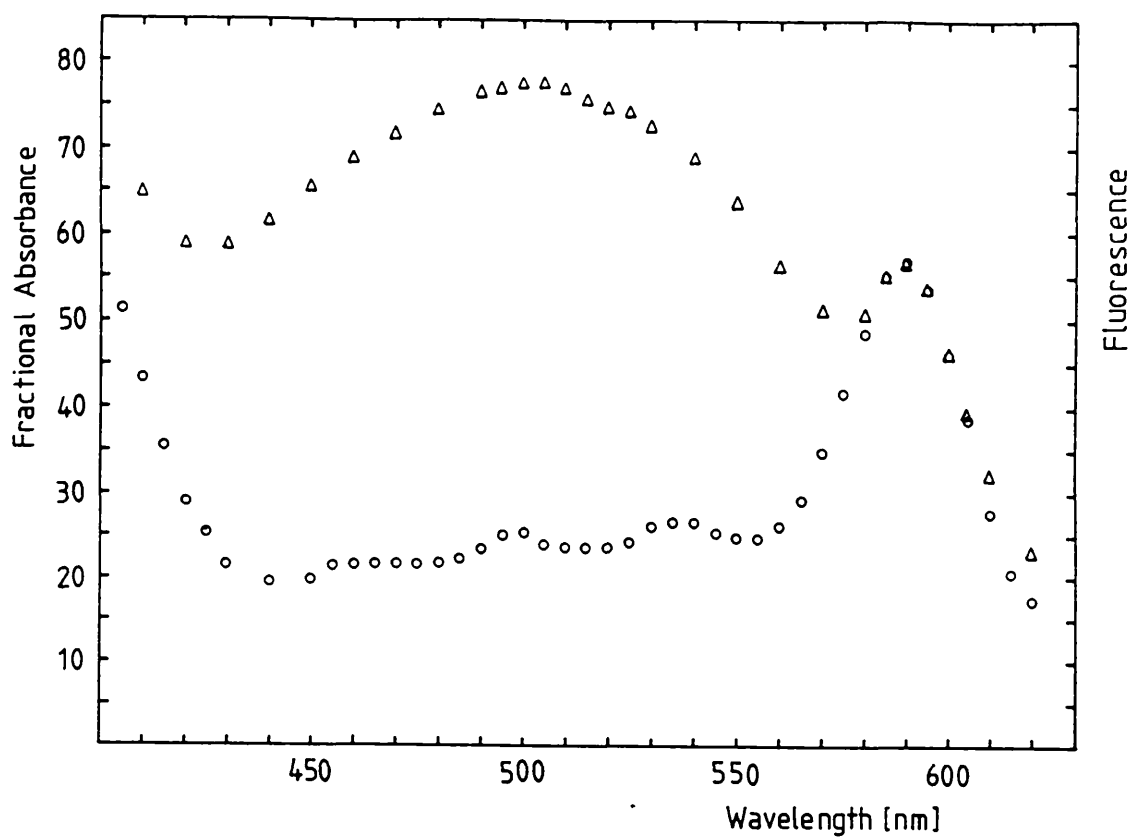


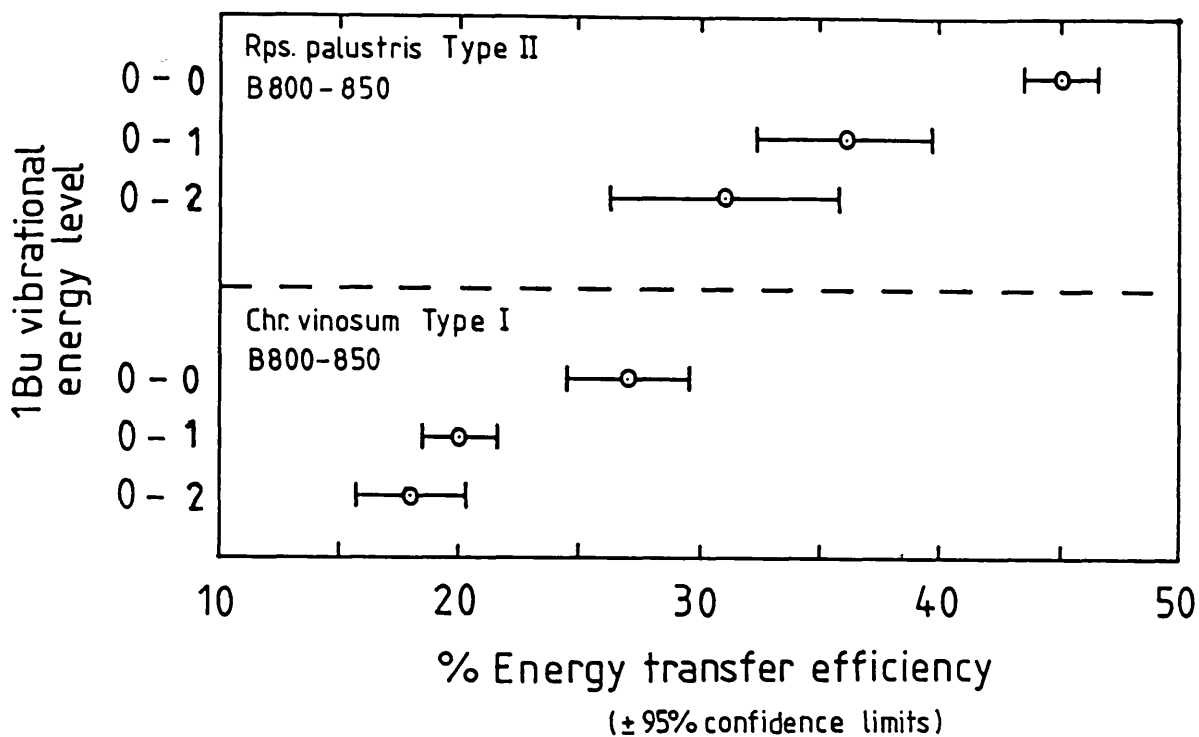
Fig. 7.5 Fractional absorption spectrum (  $\Delta$  ) and normalised fluorescence emission spectrum (  $\bigcirc$  ) of 875 antenna complexes from high light grown *Rps. palustris*.

Fig. 7.6 Fractional absorption spectrum (  $\Delta$  ) and normalised fluorescence emission spectrum (  $\bigcirc$  ) of B800-850 complexes from 40°C grown *Chr. vinosum* cells.



the redmost carotenoid band is called the 0-0 band, the middle band is called the 0-1 band, and the highest energy vibrational band is the 0-2 band (Fig. 1.15). With the exception of the B800-820 complexes from *Rps. acidophila*, strain 7750, measurements were performed on different preparations of the same complex type to determine whether the efficiency is dependent on the preparation. t-tests were performed between the data sets for the different preparations, measured at vibrational band 0-1. The efficiency of energy transfer did not vary significantly between different preparations of the same complex. The calculated t values, and significance levels (p) are quoted beneath the 0-1 columns of the tables. If the significance level is  $<0.05$  (i.e. 5%) a difference between the two sets of data is accepted. The lower the value of p, the less likely is an assumption of significance to be incorrect (i.e. if  $p=0.001$  there is a 0.1% chance of the assumption of statistical difference being incorrect).

Comparison of the energy transfer efficiencies measured at each of the three carotenoid absorption bands shows a clear trend in all of the complexes tested. Without exception the lowest efficiencies were measured for the carotenoid vibrational bands 0-2, and the highest for bands 0-0. One-way analysis of variance was used to determine whether the differences between these bands are statistically significant. The F ratios and their corresponding significance values (p) are also presented in the data tables. In each case it was found that there is significant wavelength-dependence of the energy transfer efficiency. If for each measurement, the efficiencies at bands 0-1 and 0-2 are normalised against the efficiency at band 0-0, the average efficiencies are calculated to be  $74 \pm 7\%$ ,  $84 \pm 8\%$  and  $100\%$  ( $\bar{x} \pm \text{SE}$ ) for bands 0-2, 0-1 and 0-0 respectively. Plots of energy transfer efficiency measured at each carotenoid vibrational band are presented in Fig 7.7 for two



**Fig. 7.7** Plots describing the energy transfer efficiencies of two typical antenna complexes measured at the carotenoid vibrational bands 0-2, 0-1 and 0-0 (0-0 is the redmost band). Where there is no overlap of error bars, the differences in the plotted mean values are not attributed to random error.

typical complexes.

**Table 7.2:** Carotenoid-to-BChl energy transfer efficiencies of the B800-820 complexes from *Rps. acidophila*, strain 7750

	% efficiency		
	0-2	0-1	0-0
	60	60	74
	64	72	78
$\bar{x}$	62	70	76
s	3	2	3

F=19.8

p=0.025-0.01

0-2, 0-1 and 0-0 represent the excitation wavelengths corresponding to the three carotenoid vibrational bands. 0-0 is the redmost band and 0-2 is the band of shortest wavelength.  $\bar{x}$  = arithmetic mean, s = sample standard deviation, F = variance ratio, p = significance level of variance ratio.

**Table 7.3:** Carotenoid-to-Bchl energy transfer efficiencies of the B800-850 complexes from LL *Rps. palustris*

	% efficiency		
	0-2	0-1	0-0
prep a	22	28	47
	33	39	45
	49*	55*	64*
	32	36	42
prep b	-	35	44
	31	38	46
	35	40	46
	32	37	45
$\bar{x}$	31	36	45
s	5	4	2
$t_{a/b}$		1.05	
p		0.34	
F=6.72			
p <0.01			

\* values omitted from data analysis

**Table 7.4:** Carotenoid-to-BChl energy transfer efficiencies of the HL B800-850 complexes from *Rps. palustris*

% efficiency			
	0-2	0-1	0-0
	30	35	42
	31	37	45
	34	39	46
	27	31	39
$\bar{x}$	31	36	43
s	3	3	3
F=14.55			
p=0.001			

**Table 7.5:** Carotenoid-to-BChl energy transfer efficiencies of 30°C *Chr. vinosum* B800-850 Type I complexes

% efficiency			
	0-2	0-1	0-0
prep a	18	21	27
	18	21	25
	14	18	23
	15	19	24
	15	20	27
	14	18	24
prep b	22	24	33
	21	24	32
	22	20	28
	18	19	30
$\bar{x}$	18	20	27
s	3	2	3
$t_{a/b}$		1.79	
p		0.11	
F=27.5			
p <0.005			

**Table 7.6: Carotenoid-to-BChl energy transfer efficiencies of 40°C *Chr. vinosum* B800-850 Type II complexes**

% efficiency			
	0-2	0-1	0-0
prep a	36	35	39
	38	36	40
	24	25	31
	24	27	31
	25	27	32
prep b	23	30	31
	26	29	34
	21	25	29
	18	25	32
$\bar{x}$	26	29	32
s	7	4	4
t <sub>a/b</sub>		1.04	
p		0.4-0.2	
F=6.72			
p <0.01			

Unless a wavelength-dependent systematic error is present in the measurements, these results should be assumed to be genuine. A systematic error could have arisen when the fluorescence excitation spectrum was corrected for the variation in the exciting-lamp intensity with wavelength. However, the fluorescence spectrometer was periodically wavelength-calibrated, new exciting-lamp emission spectra were recorded immediately before running each set of fluorescence excitation spectra, and baseline spectra were recorded after every run. Apart from a possible malfunction of the measuring equipment, no other sources of systematic error are apparent.

The efficiency of energy transfer from carotenoid to BChl has previously been measured for antenna complexes prepared from *Rps. sphaeroides* [Cogdell et al., 1981; Hipkins et al., 1981] and *Rps. acidophila* [Angerhofer et al., 1986], using essentially the same method as described here. In both reports the energy transfer efficiencies

were determined at three excitation wavelengths in the carotenoid region, but no significant differences between them were established. There have, however, been two reports where the energy transfer efficiency, measured at the vibronic bands, decreases from the long-wavelength band to the short-wavelength band. Van Reil et al. (1983) measured the laser excitation profile of  $\beta$ -carotene fluorescence and found that the long wavelength vibronic transition induces a higher excitation intensity. And recent observations of carotenoid fluorescence in which the fluorescence excitation, and absorption spectra are compared clearly shows this trend too [T Gillbro and R J Cogdell, unpublished]. Further evidence is provided by the plots of the normalised fluorescence excitation, and absorption spectra of the B875 complexes from *Rps. palustris* (Fig. 7.5). The absorption spectrum of this complex in the carotenoid region is rounded, with little fine structure. The fluorescence excitation spectrum, however, shows three peaks which possibly correspond to the three carotenoid vibrational energy states. Because the positions of the 0-0 and 0-2 vibrational bands of the absorption spectrum are not clearly defined, their efficiencies have not been calculated. Reference to the spectra does however suggest that the greatest efficiency is measured at the longest-wavelength absorbing band. If the efficiency were independent of the excitation wavelength, the fluorescence excitation spectrum would be expected to resemble the shape of the absorption spectrum.

The actual mechanism of energy transfer from carotenoid to BChl is still uncertain. Explanations for the wavelength-dependence of the energy transfer efficiency will therefore be discussed in two parts: on the assumption that the energy transfer operates by the Förster mechanism and then on the assumption that transfer operates by the Dexter electron-exchange mechanism.

If Förster transfer operates, the dependence of the energy transfer efficiency on excitation into different vibrational energy levels is difficult to explain. In Förster transfer vibrational coupling is weak so thermal relaxation is completed before energy transfer occurs. The results could be explained if at each of the wavelengths at which the efficiencies were measured, there was a preferential excitement of different carotenoids, so that the efficiency of energy transfer is really carotenoid-type dependent and not vibronic band dependent. The carotenoid absorption spectrum of a wild-type antenna complex is actually an average of several individual carotenoid absorption spectra, each with a different absorption maximum. When the efficiencies are measured at different excitation wavelengths, the proportion of excitation absorbed by each type of carotenoid will vary. The Förster equation includes a term for the overlap integral of the donor fluorescence emission spectrum and the acceptor absorption spectrum. The greater the overlap, the greater is the energy transfer efficiency. Different carotenoids absorbing at different wavelengths may therefore have different overlap integrals. However, from the observation of carotenoid fluorescence emission spectra obtained by Gillbro and Cogdell (unpublished), this explanation seems unlikely. The fluorescence emission band is so broad that small shifts will not significantly affect the overlap integral.

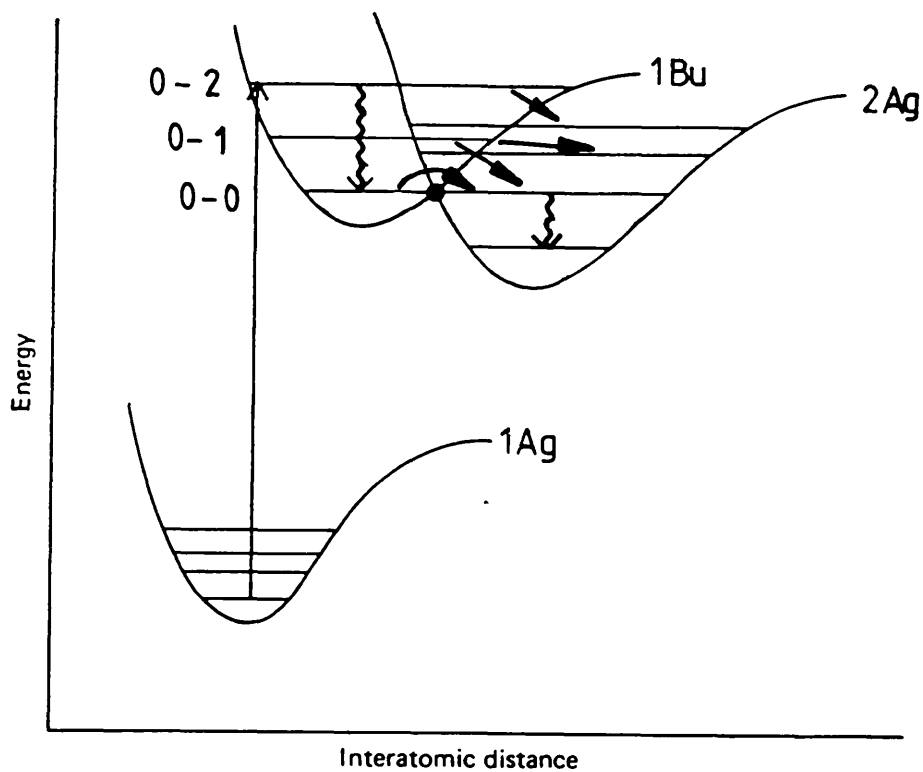
A second possible explanation is that the energy transfer efficiency is carotenoid-type dependent because different carotenoids have different *in vitro* fluorescence quantum yields (the rate of Förster transfer is proportional to donor fluorescence yields). This has recently been demonstrated by Gillbro and Cogdell (unpublished) with quantum yield measurements of  $6 \times 10^{-5}$  for  $\beta$ -carotene and  $3 \times 10^{-5}$  for spheroidenone, in carbon disulphide. Perhaps the shape of the

Fluorescence in  
wild model

fluorescence excitation spectrum in Fig. 7.5 can be explained by one particular carotenoid in the complex transferring energy inherently more efficiently than the others so that it is highlighted in the spectrum.

If the Dexter mechanism operates to transfer energy from carotenoid to BChl, the explanation of the carotenoid-type dependence of energy transfer efficiency on the overlap integral of the donor emission and acceptor absorption spectra can also be used, because the Dexter electron-exchange equation also contains an expression for this. With electron-exchange however, there is an alternative, more likely explanation (H. Frank, personal communication). This mechanism requires strong coupling between the donor emission, and acceptor absorption vibrational bands. Energy transfer can therefore occur before thermal relaxation of the donor vibrational states is complete. (i.e. electron exchange can take place from energetically discrete vibrational bands). An explanation of the above data requires that the rate of energy transfer from the lowest donor vibronic band to the ground state BChl is more efficient than that from the higher bands. The energetic positioning of the carotenoid 1Bu vibronic states and the BChl ground state may mean that energy transfer between the carotenoid 0-0 vibrational bands and the BChl is more favourable than energy transfer from the other vibronic bands i.e. the coupling may be stronger. This may be mediated by the 2Ag energy state of the carotenoid. It is known that the 2Ag energy state lies below the 1Bu state although its actual position is uncertain. The possible pathways of energy transfer between these states are described by the Morse curves in Fig. 7.8.

If the energy transfer efficiency between the 2Ag state and the ground state BChl is independent of the vibronic energy state a stronger coupling between the 0-0 1Bu vibrational energy level and a vibronic band of the 2Ag state could explain the higher energy transfer



**Fig. 7.8** Morse curves depicting energy transfer between the 1Bu and 2Ag energy states of carotenoids. The position of the 2Ag state is still unknown so this diagram is only an approximate representation.

efficiency. Alternatively the efficiency of energy transfer between the 1Bu and 2Ag states may be independent of the vibronic state so that the data could be explained by a stronger coupling between the lowest vibronic band of the 2Ag state and the ground state BChl.

Until the existence of the Dexter mechanism is further substantiated, and the position of the 2Ag energy level is known, this will remain speculation. The arguments which favour the Dexter electron-exchange mechanism over the Förster mechanism are detailed in section 1.8.

### 7.3 Summary

A summary of the carotenoid-to-BChl energy transfer efficiencies is presented in Table 7.7. The energy transfer efficiency for the B800-820 complexes from *Rps. acidophila*, strain 7750, was determined to be approximately 70% measured at the carotenoid absorption maximum. This agrees very well with the 70-75% efficiency measured for the B800-820 complexes from strain 7050. The carotenoid compositions of these two complexes are entirely different so this is perhaps further evidence that the energy transfer efficiency is not strongly dependent on the carotenoid type.

The efficiency measured for the B875 complexes from *Rps. palustris* is  $29\% \pm 1$  ( $\pm$  SE). This is consistent with the previously determined value of  $34 \pm 10\%$  for this complex at 3°C [Dawkins, D., PhD Thesis, Glasgow University]. The data presented here were recorded at room temperature but as BChl fluorescence is temperature independent the results should be comparable [Angerhofer et al., 1986].

t-tests indicate that there is no statistical difference between the energy transfer efficiencies of the LL and HL B800-850 complexes prepared from *Rps. palustris*, when measured at any of the three

absorption bands ( $p < 0.05$ ). The energy transfer efficiencies measured at the carotenoid absorption maxima were 36% for both the HL and LL B800-850 complexes.

The efficiencies for the B800-850 complexes of 30°C and 40°C grown *Chr. vinosum*, measured at each of the carotenoid vibrational bands, were however shown to be statistically different with a certainty of greater than 99.5%. Their respective efficiencies measured at the carotenoid absorption maxima were determined to be  $20 \pm 1\%$  and  $29 \pm 1\%$ . The B800-850 Type II complexes from *Chr. vinosum* are therefore approximately 45% more efficient at transferring energy than the Type I complexes. The B800-820, and B800-850 Type II complexes from *Rps. acidophila*, strain 7050, were determined to have an efficiency approximately 36% higher than the Type I complexes. When the energy transfer efficiencies were measured for the complexes from *Rps. acidophila* it could not be determined whether the difference in the efficiencies for the LL and HL complexes was due to the distinct difference in carotenoid compositions of the complexes, or whether it was due to specific differences in the carotenoid-BChl-protein interactions. For *Chr. vinosum*, there is no ambiguity in the interpretation of the data because the carotenoid compositions of the Types I and II complexes are similar.

Antenna complexes from purple bacteria show considerable variation in the efficiency with which energy is transferred from carotenoid to BChl. The energy transfer efficiency for the B800-850 complexes from *Rb. sphaeroides* is about 100% [Cogdell, et al., 1981] whereas the energy transfer efficiency of the B890 complexes from *R. rubrum* is 30% [Goodheer, 1959]. The processes which compete for the excitation energy received by the carotenoid are described for a B800-850 complex in Fig. 7.1. The efficiency of energy transfer between B800 and B850 is very high [Kramer et al., 1984a]. In solution carotenoids have very low

fluorescence yields and very short non-radiative lifetimes [Cogdell and Gillbro, unpublished; van Grondelle, 1985]. Chlorophyll molecules in solution have relatively high fluorescence yields and low non-radiative lifetimes. In those antenna complexes with low energy transfer efficiencies, only a small proportion of the energy is probably lost through non-radiative de-excitation of BChl, or carotenoid fluorescence. The high rate of non-radiative de-excitation of carotenoids is probably the source of much of the lost energy. For the energy transfer pathway to BChl to compete with carotenoid non-radiative de-excitation the interaction between the BChl and carotenoid molecules must be favourable for energy transfer. The basis of the wide range of carotenoid-to-BChl energy transfer efficiencies of antenna complexes is therefore mainly a consequence of differences in the relative positioning of donor and acceptor molecules.

**Table 7.7:** Summary table of carotenoid-to-BChl percent energy transfer efficiencies of antenna complexes measured at the excitation wavelengths corresponding to the carotenoid vibrational bands 0-2, 0-1 and 0-0

Complex		0-2			0-1			0-0		
		n	$\bar{x}$	SE	n	$\bar{x}$	SE	n	$\bar{x}$	SE
<i>Rps. acidophila</i>	B800-820	2	62	2	2	70	1	2	76	2
strain 7750										
<i>Rps. palustris</i>	LL B800-850 I	7	31	2	8	36	2	8	45	1
	HL B800-850 II	4	31	1	4	36	2	4	43	2
	B880		-		4	29	1		-	
<i>Chr. vinosum</i>	30°C B800-850 I	10	18	1	10	20	1	10	27	1
	40°C B800-850 I	9	26	2	9	29	1	9	32	1

**CHAPTER EIGHT: Crystallisation of the B800-850 Complexes From Low  
Light Grown *Rhodopseudomonas palustris*, strain French**

The structural characterisation of the B800-850 antenna complexes from *Rps. palustris*, strain French, has been a continuing theme throughout this thesis. By analysing the primary structures of the antenna polypeptides it has been possible to speculate about which pigment-protein interactions may be responsible for the red-shift of the near-infrared absorption bands displayed by the *in vivo* BChl pigments. However, until the three-dimensional structures of antenna complexes have been determined this will remain speculation. The only way currently available to determine protein structures to atomic resolution requires the formation of protein crystals and subsequent x-ray diffraction analysis. A prerequisite for this is highly ordered crystals of about 0.5mm in diameter.

Many water-soluble proteins have been successfully crystallised [McPherson, 1982] but the crystallisation of membrane proteins is a new science and has additional problems associated with it. The principles and methods for crystallising proteins will be briefly discussed below. This will be followed by a discussion of the special problems inherent in the crystallisation of membrane proteins, and the results of preliminary crystallisation trials on the B800-850 complexes from *Rps. palustris*.

Crystallisation is the ordered formation of a solid by precipitation of a dissolved compound. The change in state between the solute and solid during the formation of a crystal is an equilibrium process. A fully solvated molecule lies at a potential energy minimum so that crystallisation is not a spontaneous process. It must be initiated and maintained by inducing incomplete solvation of the protein. This upsets the equilibrium and the proteins aggregate through free energy minimisation, maximising the number of attractive

interactions and minimising the number of dispersive interactions. If precipitation occurs too quickly an amorphous precipitate will result. For the formation of ordered crystals the system must be brought slowly to supersaturation.

Precipitation of proteins can be induced by the addition of organic solvents, polyethylene glycol or salts such as ammonium sulphate. The latter two are most commonly used for the crystallisation of proteins. Precipitation with salts (salting out) in simple terms, is due to solvation of the salt by water molecules in preference to solvation of the protein so that incomplete protein solvation results [Scopes, 1982; Chang, 1982; Green and Hughes, 1955; McPherson, 1982]. The mechanism of polyethylene glycol precipitation is less well understood but it probably also acts by competing with the protein for water [McPherson, 1976; 1982]. The solubility of a protein is also determined by other factors. Proteins tend to be least soluble at pH's equivalent to their isoelectric points and solubility increases with temperature. The strategy of crystallisation is to bring the protein solution slowly to supersaturation by altering combinations of the precipitant type, precipitant concentration, pH and temperature.

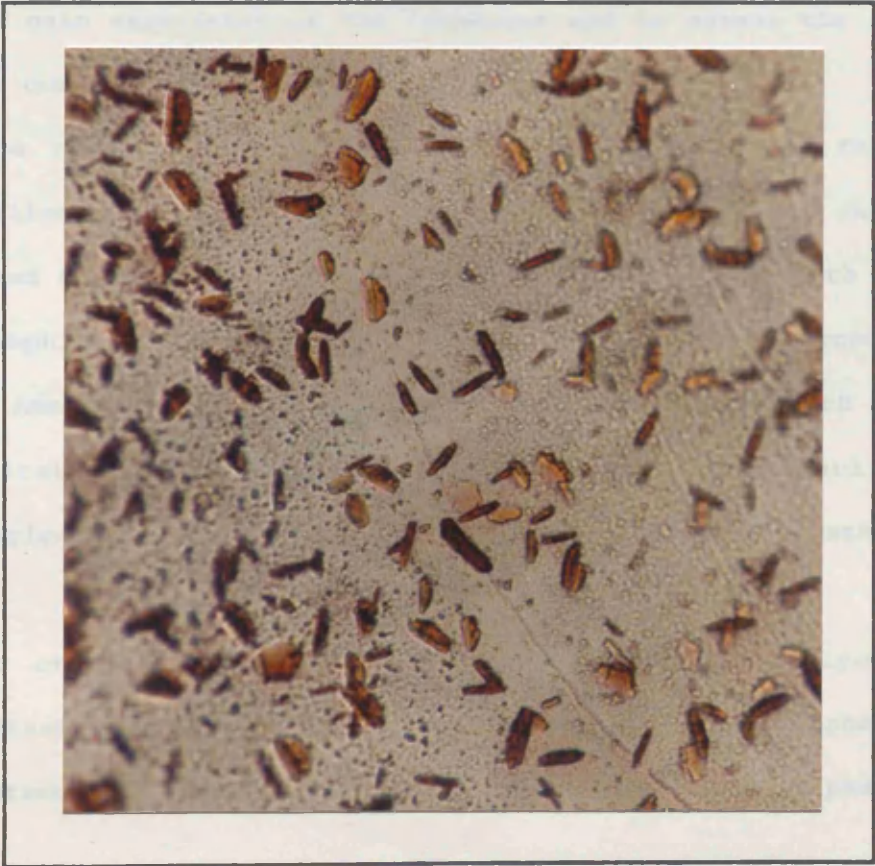
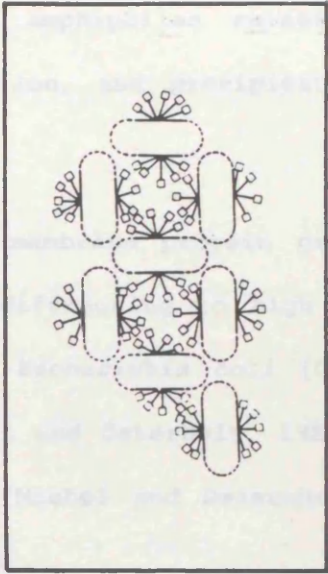
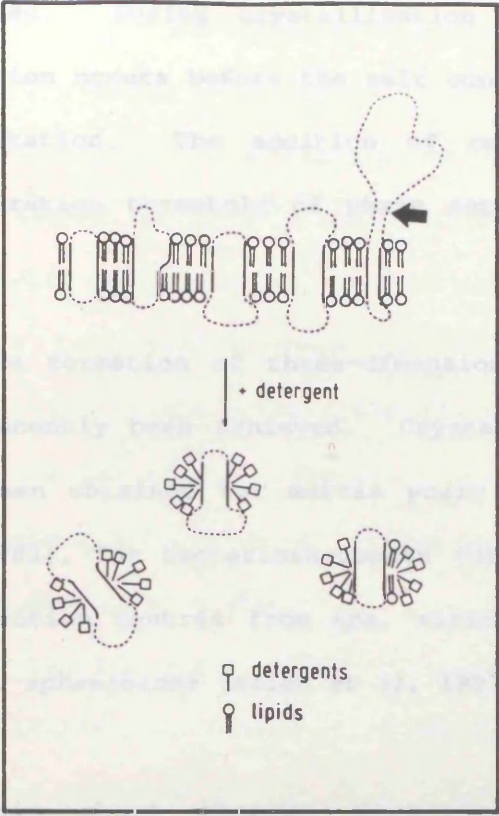
One method of crystallisation which allows considerable control over these variables is the "sandwich box" vapour diffusion method (section 2.11(ii)). The starting material is pipetted into a well on a depression slide which is suspended above a reservoir of ammonium sulphate (or polyethylene glycol) solution. The lid of the sandwich box is then sealed to provide an isolated environment. The concentration of ammonium sulphate in the sample is chosen to be below the solubility minimum of the protein. The concentration of ammonium sulphate in the reservoir is higher so that water evaporates and diffuses from the sample into the reservoir. The concentration of salt in the sample gradually increases and protein precipitation is induced.

The problem with crystallising integral membrane proteins is that they are amphipathic and require detergents to prevent their nonspecific aggregation in aqueous media [Tanford and Reynolds, 1976]. Detergents are lipids which contain polar and nonpolar regions [Helenius and Simons, 1975]. Under the right conditions, during detergent solubilisation of membrane proteins the detergent molecules effectively replace the phospholipids which interact with the hydrophobic regions of the proteins, forming micelles containing a single protein unit. The hydrophobic tails of the detergents interact with the hydrophobic regions of the protein, and the polar end groups of the detergents form polar interactions with the aqueous medium [Michel, 1983] (Fig. 8.1). Crystallisation from the protein-detergent micelles is then possible.

The shape of the detergent molecules are important for the packing of the proteins into ordered crystals. Protein crystals are mainly stabilised by polar interactions so if the detergent molecules used are too large they will obscure the polar regions of the protein and prevent crystal formation. Small detergents are therefore favoured. The type of protein-detergent packing envisaged for three-dimensional crystals of membrane proteins is depicted in Fig. 8.1. However because proteins have sculptured surfaces the surface of the protein-detergent micelle will be uneven and this will disturb the crystalline packing order. To circumvent this, small amphiphilic molecules are added to the detergent-containing buffer, which partially replace the detergent molecules in some regions and effectively smooth the surface of the protein micelle and so improve the chances of ordered crystal formation. The small amphiphiles also overcome the problem of phase separation during crystallisation. In the absence of small amphiphiles, high concentrations of salts force detergents out of solution into a detergent-rich phase, leaving a major aqueous detergent-poor phase. The

Fig. 8.1 Left: diagram depicting proposed arrangements of detergent-solvated membrane proteins. The hydrophobic tails of the detergents associate with membrane-spanning hydrophobic regions of the proteins. Right: proposed packing of protein-detergent micelles during crystal formation. (From Michel, 1980.)

Fig. 8.2 Crystals of the B800-850 light-harvesting complexes from low light grown *Rps. palustris*, strain French.



hydrophobic antenna proteins move into the detergent-rich phase and are denatured. During crystallisation without small amphiphiles phase separation occurs before the salt concentration is high enough to cause precipitation. The addition of small amphiphiles raises the salt concentration threshold of phase separation, and precipitation occurs first.

The formation of three-dimensional membrane protein crystals has only recently been achieved. Crystals diffracting to high resolution have been obtained for matrix porin of *Escherichia coli* [Garavito et al., 1983], for bacteriorhodopsin [Michel and Osterhelt, 1980] and for the reaction centres from *Rps. viridis* [Michel and Deisenhofer, 1986] and *Rb. sphaeroides* [Allen et al, 1987a,b].

This short chapter describes the results of preliminary crystallisation trials using B800-850 complexes from low light grown *Rps. palustris*. Approximately forty individual trials were performed, to both gain experience of the technique and to assess the suitability of this complex for further trials.

One of the more successful detergents used so far for the crystallisation of antenna complexes is dimethyldecylamine oxide (DDAO). For these trials 1% (v/v) DDAO was used in conjunction with one of the small amphiphiles, heptane-1,2,3-triol or benzamidinium hydrochloride (3% w/v). Ammonium sulphate and polyethylene glycol were both used to precipitate the protein-detergent micelles. The results of the polyethylene glycol 4000 crystallisation trials are presented in Table 8.1.

No crystals were obtained using polyethylene glycol as the precipitant. In the first trials using ammonium sulphate as the precipitant (set A) the concentration of ammonium sulphate in the

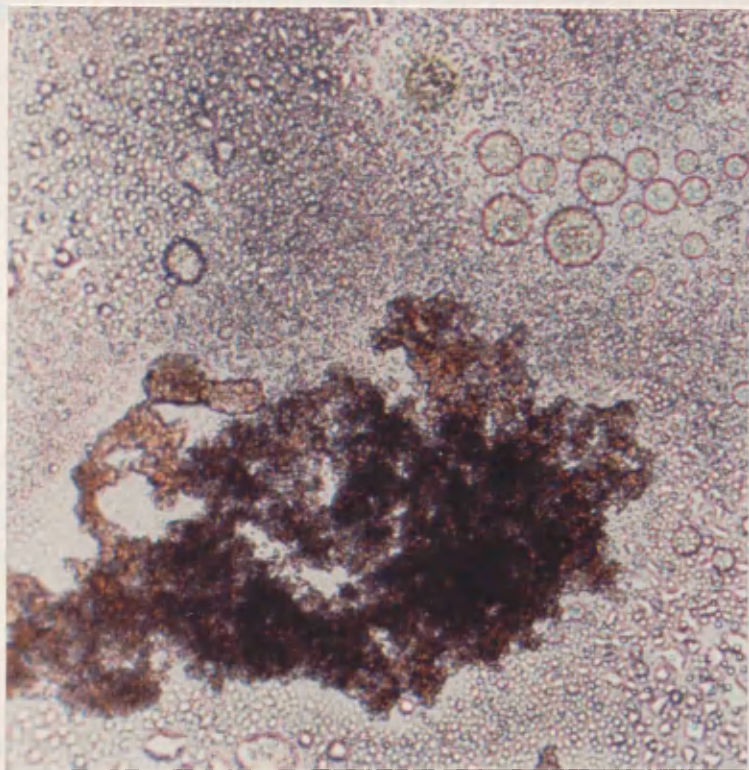
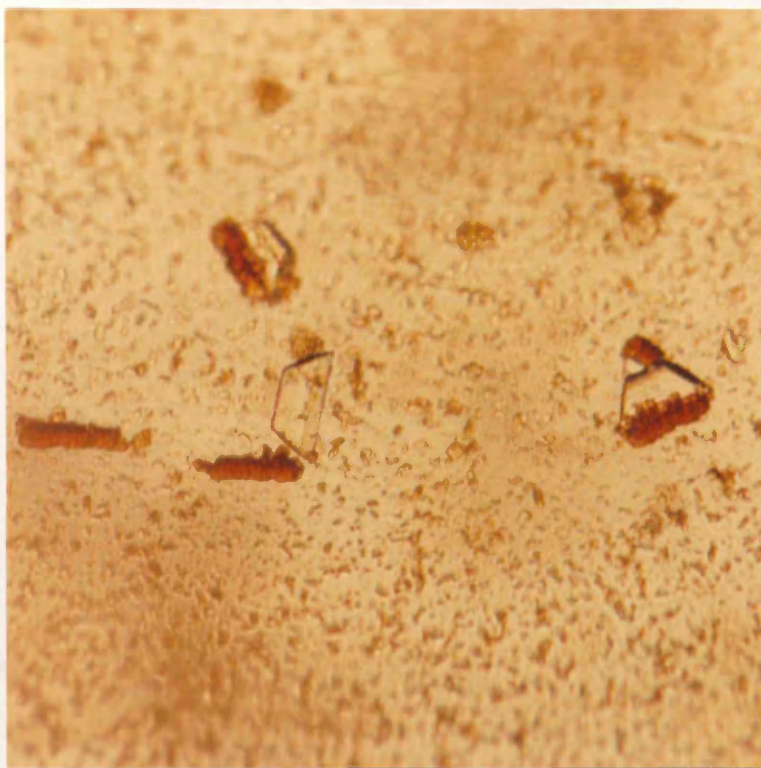
antenna preparation was varied and both benzamidine hydrochloride and heptane-triol small amphiphiles were tried. The only successful crystallisations were those using benzamidine hydrochloride, and ammonium sulphate concentrations of 2.2-2.6M.

A second set of crystallisation trials (set B) was conducted using benzamidine hydrochloride, concentrations of ammonium sulphate of 2.4, 2.5 and 2.6M, and a range of pH's from pH 6.0-10.6 (Table 8.3). Crystals were formed within the pH range 8.8-9.9 although they were too small (<0.2mm wide) to use for X-ray crystallography. A photograph of the crystals growing at pH 8.8 and an ammonium sulphate concentration of 2.6M is presented in Fig. 8.2.

During the first ammonium sulphate trials crystals of benzamidine hydrochloride were formed at an ammonium sulphate concentration of 2.2M. These are pictured in Fig. 8.3. Some antenna crystals and benzamidine hydrochloride crystals appear to grow together. In many of the trials phase separation occurred before crystallisation. Fig. 8.4 shows the typical result of phase separation. There is a mass of denatured protein surrounded by a detergent-poor aqueous phase. In all of the unsuccessful trials the presence of yellow membrane lipid globules was noted. Although during these trials crystals of sufficient dimensions for X-ray crystallography were not produced, it has demonstrated that crystals of the LL B800-850 complexes from *Rps. palustris* can be grown, and suggests that it would be worthwhile proceeding with this work.

Fig. 8.3 Crystals of the LL B800-850 complexes from *Rps. palustris* with crystals of the small amphiphile, benzamidine hydrochloride (clear crystals).

Fig. 8.4 Photograph depicting the result of phase separation before protein crystallisation occurs. A large aggregate of denatured protein forms, surrounded by an aqueous, detergent-poor phase. Note the presence of lipid-like globules, probably comprising membrane lipids which have not been replaced by detergent.



**Table 8.1 Summary of polyethylene glycol 4000 crystallisation trials**

% PEG in reservoir	results
12	ps
18	ps
22	ps
24	ps
26	ps

ps = phase separation

Constant conditions: 1% DDAO, pH 9.5, heptane-triol 3%, 20°C, 9%  
PEG/20mM MgCl<sub>2</sub> in sample well

**Table 8.2 Summary of ammonium sulphate crystallisation trials, set A**

[AmSO <sub>4</sub> ] in reservoir	constant conditions	
	A	B
1.8	ps	ps
2.0	ps	ps
2.2	ps, BH crystals, small antenna crystals	ps
2.4	ps small antenna crystals	ps
2.6	ps small antenna crystals	ps
2.8	-	ps
3.0	-	ps

Constant conditions: A 1% DDAO, pH 9.5, benzamidine hydrochloride 3%,  
20°C, KHPO<sub>4</sub> in sample well 0.9M.

B 1% DDAO, pH 9.5, heptane-triol 3%, 20°C, KHPO<sub>4</sub>  
in sample well 0.9M

ps = phase separation

BH = Benzamidine hydrochloride

**Table 8.3** Summary of ammonium sulphate trials, set B

pH	[AmSO <sub>4</sub> ] in reservoir		
	2.4	2.5	2.6
10.6	ps	ps	ps
9.9	ps	ps	v. small crystals
9.5	ps	small flat crystals	small irregular crystals
8.8	ps	ps	slow growing, well formed, small crystals
8.0	ps	ps	ps
7.5	ps	ps	ps
6.7	ps	ps	ps
6.0	ps	ps	ps

constants: 1% DDAO, benzamidine hydrochloride 3%, 20°C, KHPO<sub>4</sub> in sample well 0.9M.

**Chapter Nine: Summary Discussion**

The capture of light energy to drive growth and furnish the metabolism which is essential for the maintenance of plant life ranks among the most complex of the biochemical processes. If we are to understand the principles of photosynthetic function it is constructive to investigate the simplest photosynthetic systems, even though they are of little economic importance.

An investigation into the structure and function of the light-harvesting antenna complexes of purple bacteria requires the isolation of pure antenna preparations. The isolation procedures and spectral characterisation of some of the antenna complexes described in this thesis were discussed in chapter three. The determination of the ratios of BChl-to-carotenoid for the B800-850 antenna complexes from *Rb. sphaeroides* and the B890 complexes from *R. rubrum* were described in chapter four. Despite being the most thoroughly investigated antenna complexes, the ratio of BChl to carotenoid of the B800-850 complexes from *Rb. sphaeroides* was still a subject of controversy. In an attempt to settle the controversy this ratio was re-determined by three different methods. Two of these have previously been used to investigate pigment ratios. The third method, using reversed phase HPLC for the separation and quantitation of pigments from purple bacteria, was developed. The main difficulty in developing a quantitative HPLC system for the pigments was handling the large difference in polarity between the hydrocarbon carotenoids and the relatively polar BChl, without compromising their solubility. Particular attention was given to ensuring that all of the pigments in the extracts were completely dissolved before injection. BChl losses could not be completely eliminated but they were consistent and therefore quantifiable. This system is considerably quicker, more precise and gives greater resolution than the alternative method of pigment analysis by thin-layer

chromatography. All three of the methods used to determine the ratio of the B800-850 complexes, which combined totalled 23 individual determinations, gave BChl-to-carotenoid ratios of 2:1, contradicting the widely accepted value of 3:1. The ratio of the B890 complexes from *R. rubrum* was also determined to be 2:1, in agreement with the accepted value.

A literature review indicated that some of the published BChl-to-carotenoid ratios were measured rather quickly to accompany other data, and that a careful systematic study of the ratios of a variety of complexes would be useful. A new method using simultaneous equations, which allowed the concentrations of the carotenoid and BChl to be determined without their separation, proved to be quick and reliable. The BChl-to-carotenoid ratios, measured for 11 different antenna complexes will be presented later in this chapter.

A theme which runs throughout this thesis is the characterisation of the B800-850 antenna complexes from *Rps. palustris*, strain French. This particular strain has unusual spectral properties. When the cells are grown under high light intensities (the normal conditions for laboratory cultures) the near-infrared absorption spectrum of the B800-850 antenna complexes is very similar to that of other purple bacteria cultured under the same conditions. The 850nm absorption band is more intense than the 800nm absorption band. When the light intensity is lowered the form of the near-infrared absorption changes; the 850nm band is greatly reduced in intensity and the 800nm band increases in intensity (Fig. 3.7).

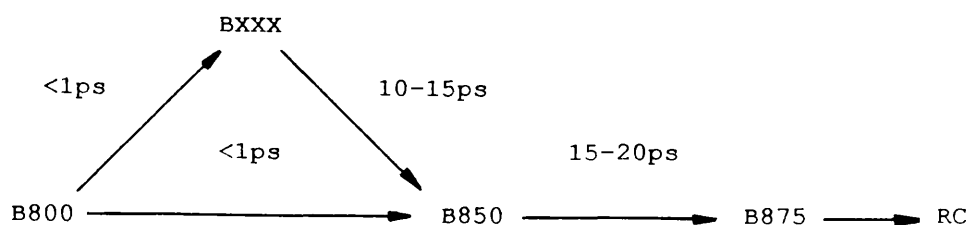
In organic solvent the near-infrared absorption band of BChl absorbs at about 770nm. The bathochromic wavelength shifts of the *in vivo* BChl molecules is believed to be due to interactions of the BChl molecules with their environment. The ability of antenna complexes to

absorb at different wavelengths is of functional importance because it forms the mechanism by which energy transfer is directed towards the reaction centre. The changes in the near-infrared absorption spectra of *Rps. palustris*, strain French, in response to changes in light intensity indicate that the environments of the BChls in the high and low light grown cells are different. By characterising the structural differences it is hoped that the correlation between structure and the near-infrared spectra, and hence function can be defined.

Anion exchange chromatography of B800-850 antenna complexes isolated from low light grown cells demonstrated that although the low light extreme spectral form dominates in the B800-850 complexes isolated from low light grown cells a small proportion of complexes with a high light spectral form are also present.

The BChl-to-carotenoid ratios were determined for the HL and LL B800-850 complexes from *Rps. palustris* (chapter five). The results unexpectedly gave ratios of 2:1 for the high light complexes and 3:1 for the low light complexes. From this data it was uncertain whether there is more BChl or less carotenoid in the low light complexes. However, subsequent linear dichroism measurements detected the presence of an additional BChl component in the LL complexes with a different Qx band orientation to the other BChls. Evidence for the existence of an extra BChl chromophore in the LL complexes has also been provided by picosecond fluorescence kinetics measurements. In the LL complexes the transfer of energy from the B800 chromophore to the B850 chromophore occurs at two different rates suggesting that there are two pathways. The one pathway is present in both the HL and LL complexes. This has a transfer rate of 1ps. In the LL complexes a second pathway occurs via an intermediate BChl molecule absorbing at around 800nm. This has a transfer time of 10-15ps. A scheme for the transfer of energy within

the photosynthetic unit of low light grown cells has therefore been proposed:



The extent to which the two pathways between the B800 and B850 chromophores operate has not yet been determined. But if all of the energy were to pass through the additional pigment, the result would be an overall increase of 10-15ps in the total trapping time. The total trapping time was found to be 50-60ps for both the LL and HL complexes, so it is probable that the pathways operate simultaneously. The extra BChl chromophore obviously doesn't accelerate the transfer of energy from B800 to B850 so its role must be to act as an additional light-harvesting pigment.

The polypeptide compositions of the LL and HL B800-850 antenna complexes from *Rps. palustris*, strain French, were investigated in chapter six. In total nine different antenna polypeptides were isolated. Two of these were identified as B875- $\alpha/\beta$  polypeptide pair from the core antenna complexes. The N-terminal amino acid sequences of these polypeptides were determined. Seven of the antenna polypeptides were found to be components of the B800-850 complexes. Four of these were classified as  $\alpha$ -polypeptides and the other three were classified as  $\beta$ -polypeptides. It is still uncertain whether all of these polypeptides are present in both the HL and LL B800-850 complexes. It may be that the HL and LL complexes contain different polypeptides, or they may contain the same polypeptides but in a different stoichiometry.

Analysis of the polypeptide compositions by liquid chromatography and SDS polyacrylamide gel electrophoresis has demonstrated differences in the stoichiometry of the HL and LL complex polypeptides, although the extent of the differences remains unclear. The liquid chromatography chromatograms suggest that a  $\beta$ -polypeptide exchange occurs between the two complexes and that the B800-850- $\alpha_2$  polypeptide is present in relatively larger amounts in the LL complexes. The stoichiometries of the polypeptides have been roughly estimated from the chromatograms to be  $\alpha_1:\alpha_2:\alpha_3:\alpha_4$ , 2:2:1:1 for the HL B800-850 complexes and 2:6:1:1 for the LL complexes. SDS polyacrylamide gels suggest that polypeptide B800-850- $\alpha_4$  is present predominantly in the high light grown cells.

Both the four  $\alpha$ -polypeptides and the three  $\beta$ -polypeptides are highly homologous. The amino acid sequences of their C-terminals have not yet been confirmed so the total numbers of amino acids in the complete sequences are unknown. However it is estimated that the B800-850- $\alpha_1$ , - $\alpha_2$  and - $\alpha_3$  polypeptides are 52-54 amino acids long and that the B800-850- $\alpha_4$  polypeptide is about ten residues longer. The  $\alpha_4$ -polypeptide possesses an unusual alanine-rich C-terminal tail. A similar sequence has been found in the B800-850- $\alpha$  polypeptide of *Rc. gelatinosus* [R. Brunisholz, personal communication].

From hydropathy plots it is proposed that this tail region turns and reinserts into the photosynthetic membrane as a short stretch of  $\alpha$ -helix. Hydropathy measurements have also been used to estimate that residues 15-35 of the  $\alpha$ -polypeptides lie within the hydrophobic interior of the membrane.

Two of the  $\beta$ -polypeptides are 52-54 amino acids long, and only differ at three amino acid positions. The third is about six residues shorter at the N-terminal. It is estimated that residues 25-45 of the  $\beta$ -polypeptides lie across the photosynthetic membrane, giving longer C-

terminal stretches and shorter N-terminal stretches than the  $\alpha$ -polypeptides.

The  $\alpha$ - and  $\beta$ - polypeptides contain histidine residues at positions 31 and 40 respectively which are thought to bind the chromophore dimer BChls. Aromatic amino acid residues in the C-terminal domain of the proteins have been implicated in the red-shift interactions with the dimer. The binding site of the BChl monomer is unknown.

The efficiency of energy transfer from carotenoid to BChl in the HL and LL B800-850 complexes from *Rps. palustris*, strain French, was also measured. The efficiencies were found to be 36% for both complexes when measured at the absorption maximum of the carotenoid. The structural differences described above are therefore not for the purpose of improving the efficiency of energy transfer from the carotenoid to the BChl.

Carotenoid-to-BChl energy transfer efficiency measurements were also performed on several other antenna complexes. The efficiency of the B800-820 antenna complexes from *Rps. acidophila*, strain 7750, was determined to be 70%, the same as the published efficiency for the B800-820 complexes from strain 7050. Because strain 7050 does not contain the purple carotenoid rhodopinal, this indicates that the greater efficiency of energy transfer found for the B800-820 and B800-850 Type II complexes from strain 7050, compared to the Type I B800-850 complexes, cannot be explained by the difference in carotenoid composition but must be due to differences in the arrangement of the pigments. The carotenoid-to-BChl energy transfer efficiency measurements on the Type I and Type II B800-850 antenna complexes from *Chr. vinosum*, strain D, indicated that the energy transfer efficiency is approximately 45% higher in the Type II complexes. This is similar to the 36% higher energy transfer efficiency reported for the Type II B800-

850 complexes from *Rps. acidophila*, strain 7050, compared to the high light Type I complexes. This provides further evidence that the improvement in efficiency noted in the variable light-harvesting complexes of *Rps. acidophila*, strain 7050, in response to a reduction in light intensity (i.e. the formation of B800-850 Type II, and B800-820 antenna complexes) is not due to the notable change in the carotenoid composition. The carotenoid compositions of the two B800-850 complexes from *Chr. vinosum* used in this study were shown to have very similar carotenoid compositions and yet their efficiencies were significantly different. It should be stressed again here that the Type II antenna complexes may actually be mixtures of a normal Type I complexes and another component such as B800-820 complexes, which have not been separated by any of the methods so far employed.

The carotenoid-to-Bchl energy transfer efficiencies were measured in all cases at the three vibrational absorption bands of the carotenoid. A surprising finding was that in all of the complexes analysed, without exception the lowest efficiencies were measured for the shortest wavelength-absorbing carotenoid vibrational band and the highest efficiencies were measured for the longest wavelength-absorbing band. The difference was shown to be significant. This is contrary to the report of Hipkins *et al.* who found no significant difference in the energy transfer efficiencies measured at the different vibrational bands. On average the lowest, and middle absorption bands were determined to be 74% and 84% less efficient at transferring energy to BChl than the highest wavelength-absorbing carotenoid absorption band. Van Reil *et al.* (1983) have previously reported that a higher excitation intensity was measured for the long wavelength carotenoid absorption band. Very recently, comparisons of carotenoid fluorescence excitation and absorption spectra of carotenoids indicate that the efficiency of energy transfer from carotenoid to BChl is excitation-wavelength

dependent in the manner described above [Gillbro and Cogdell, unpublished]. This observation is perhaps best explained by the existence of stronger coupling between the lowest vibrational band of the carotenoids first excited singlet state and the ground state of the BChl acceptor, which implies a Dexter electron-exchange mechanism of energy transfer between the two. This may be mediated through the optically forbidden  $2A_g$  state of the carotenoid.

*Rps. acidophila*, strain 7750, was cultured at low temperature following a report that it synthesises a B800-820 antenna complex without the presence of the carotenoid cis-rhodopinal. The report was confirmed but it was also noted that the amount of B800-850 complexes present in the cells was only about 5% of the amount of B800-820 complexes. This is an unusual finding because B800-820 complexes are envisaged as peripheral antennas which complement the existing B800-850 complexes when the cells grown under low light. It is the first report of a purple bacterium containing B800-820 complexes almost exclusively as the variable light-harvesting component.

Finally the B800-850 complexes isolated from low light grown *Rps. palustris* cells were crystallised in preparation for analysis for x-ray crystallography. Although the crystals were not large enough for crystallographic analysis it demonstrated that they have the potential to grow and that with more work the three-dimensional structure of this most unusual light-harvesting antenna complex may eventually be determined.

The antenna complexes of purple bacteria are frequently categorised on the basis of their near-infrared absorption spectra, their BChl-to-carotenoid ratios, their polypeptide compositions and their CD spectra. An example from Thornber (1986) is shown in Table 9.1. I propose that

this classification system should now be rearranged on the basis of the BChl-to-carotenoid ratios and polypeptide analyses presented in this thesis, and on polypeptide composition data published elsewhere. In the table from Thornber (1986) the quantitative measurements have not been performed on all of the species. Some of the species are categorised by other characteristics in common with other species, so perhaps some caution should be encouraged. In the proposed classification system, the low light B800-850 complexes from *Rps. palustris*, strain French, are considered separate from the B800-850 Type II antenna complexes. In other species Type II complexes are always associated with a B800-820 complex. There is no evidence for a B800-820 component in low light grown *Rps. palustris*, strain French. The low light B800-850 antenna complexes from *Rps. palustris*, strain French, have been called Type III complexes to reflect this. The asterisks alongside of the species names refer to those complexes for which BChl-to-carotenoid ratios were determined in this thesis.

**Table 9.1** Thornber et al

Comparison of the Major Antenna Caroteno-Chlorophyll-Proteins in Purple Bacteria*					
Antenna type	B890-protein class		B800-850-protein class		
	B890-protein	B875-protein	Type I	Type II	B800-820-protein
Examples of bacteria containing antenna type	<i>Rsp. rubrum</i> <i>C. vinosum</i> <i>Rps. acidophila</i> ? <i>Rps. viridis</i>	<i>Rps. palustris</i> <i>Rps. capsulata</i> <i>Rps. sphaeroides</i> <i>Rps. gelatinosa</i>  <i>Rps. acidophila</i> 7750 and 7050 (high light grown)			<i>C. vinosum</i> <i>Rps. acidophila</i> 7050 (low-light grown)
BChl a: carotenoid	2:1	2:2	3:1	3:1	3:1
No. of polypeptides in isolated complex	2	2	2 or 3	2	2
No. of amino acid residues in polypeptides	52 and 54	52-58 and 47-48	54-60 and 52	~ 50-65	~ 50-65
Intensity of CD spectrum of long wavelength band*	Strong	Weak	Strong	Strong	Strong

\*The quantitative data are based on analysis of complexes isolated from only a few of the species given as examples.

\*All spectra indicate BChl dimer present in the band.

Table 9.2 Core Complexes

	B1015	B890	B875
	<i>Rps. viridis</i>	<i>R. rubrum</i> * <i>Chr. vinosum</i> * <i>Rps. acidophila</i>	<i>Rb. sphaeroides</i> * <i>Rb. capsulatus</i> <i>Rc. gelatinosus</i> <i>Rps. palustris</i> *
BChl:carot ratio	2:1	2:1	1:1
polypeptide composition	$\alpha, \beta, \gamma$	$\alpha, \beta$	$\alpha, \beta$
CD: intensity of long- wavelength band	strong	strong	weak

\* species for which BChl-to-carotenoid ratio data is presented in this thesis

Table 9.3    Peripheral Antenna Complexes

	B800-850 Type I			B800-850 Type II		B800-850 Type III		B800-820	
	<i>Rb. sphaeroides</i> *	<i>Rb. capsulatus</i>	<i>Rps. palustris</i> , strain French*	<i>Chr. vinosum</i> *	<i>Rps. acidophila</i> , strain 7050*	<i>Rps. palustris</i> , str. French*	<i>Rps. acidophila</i> , str. 7750*	<i>Rps. acidophila</i> , str. 7050*	
BChl:carot ratio	2:1	2:1	2:1	2:1	3:1	2:1	3:1		
polypeptide composition	$\alpha, \beta$	$\alpha, \beta, \gamma$	$\alpha_4, \beta_3?$	$\alpha, \beta$	$\alpha_4, \beta_3?$	$\alpha, \beta_2$	$\alpha, \beta$		
CD: intensity of long- wavelength band	strong	strong	strong	strong	nd	nd	strong		

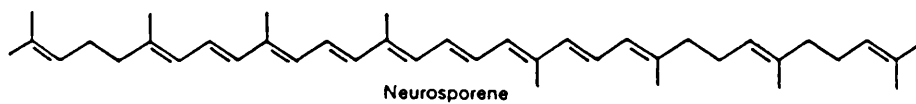
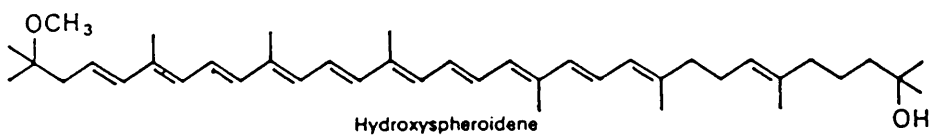
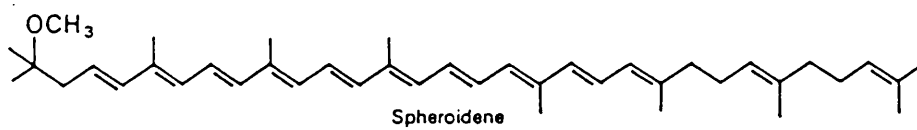
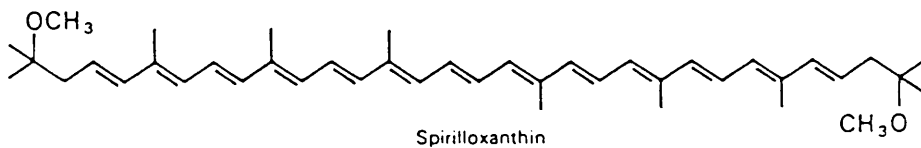
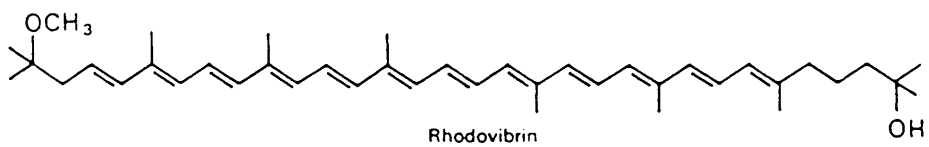
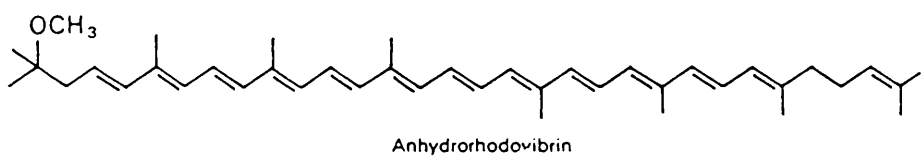
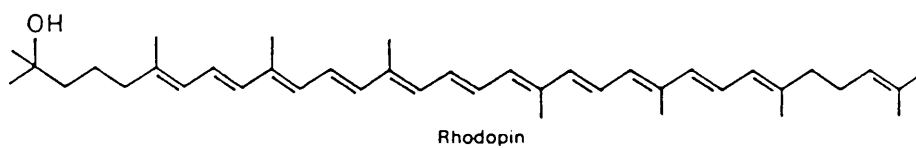
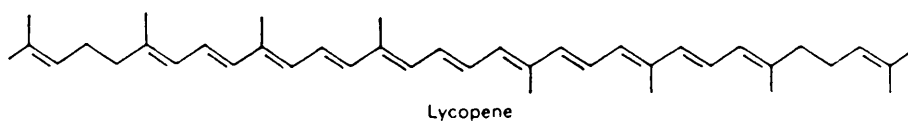
\* species for which Bchl-to-carotenoid ratio data is presented in this thesis

## **APPENDIXES**

**APPENDIX A: SEMI-SYSTEMATIC NAMES OF CAROTENOIDS**

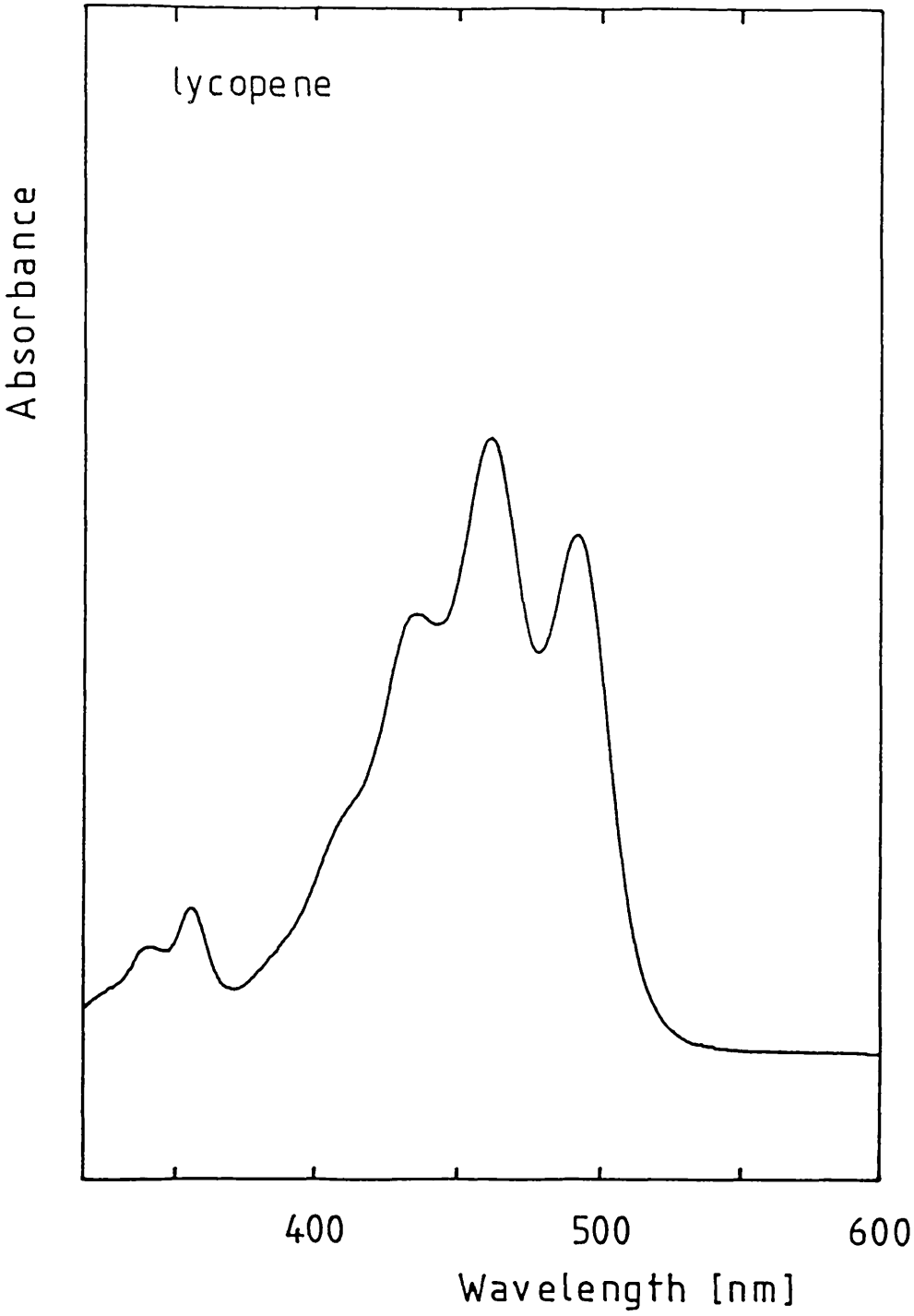
<u>Common Name</u>	<u>Semi-systematic name</u>
anhydrorhodovibrin	1-methoxy-2-hydro-3,4-dehydrolycopene
chloroxanthin	1-hydroxy-1,2,7',8'-tetrahydrolycopene
lycopene	lycopene
lycoxanthin	3-hydroxylycopene
monodemethyated	hydroxyspirilloxanthin spirilloxanthin
neurosporene	7,8-dihydrolycopene
phytoene	7,8,11,12,7',8',11',12'-octahydrolycopene
phytofluene	7,8,11,12,7',8'-hexahydrolycopene
rhodopin	1-hydroxy-1,2-dihydrolycopene
rhodovibrin	1-methoxy-1'-hydroxy-1,2,1',2'-tetra- hydro-3,4-dehydrolycopene
spheroidene	1-methoxy-1,2,7',8'-tetrahydro-3,4- dehydrolycopene
spheroidenone	1-methoxy-2-keto-7',8'-dihydro-3,4- dehydrolycopene
spirilloxanthin	1,1'-dimethoxy-1,2,1',2'-tetrahydro- 3,4,3',4'-dehydrolycopene

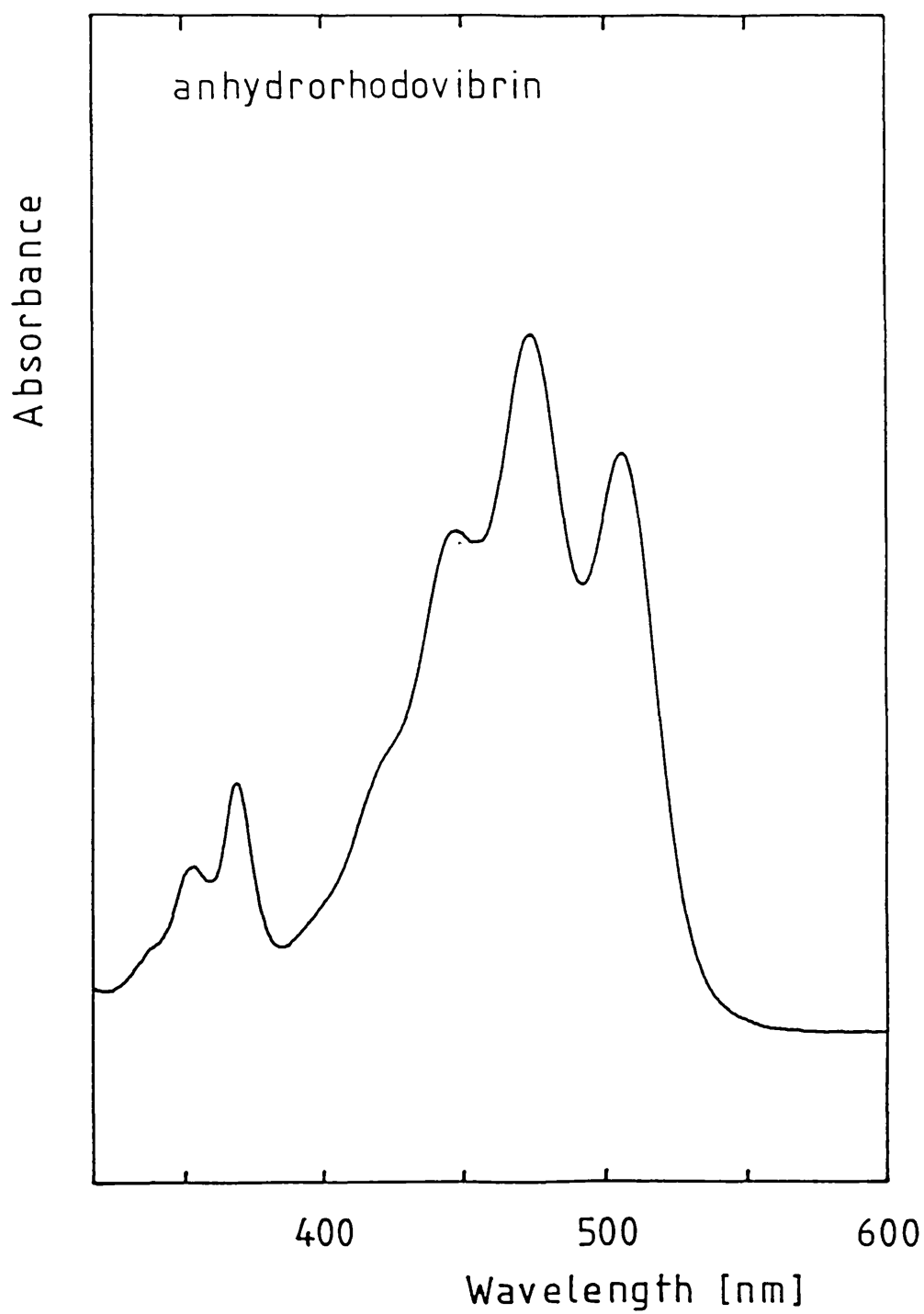
**APPENDIX B: CHEMICAL STRUCTURES OF CAROTENOIDS**

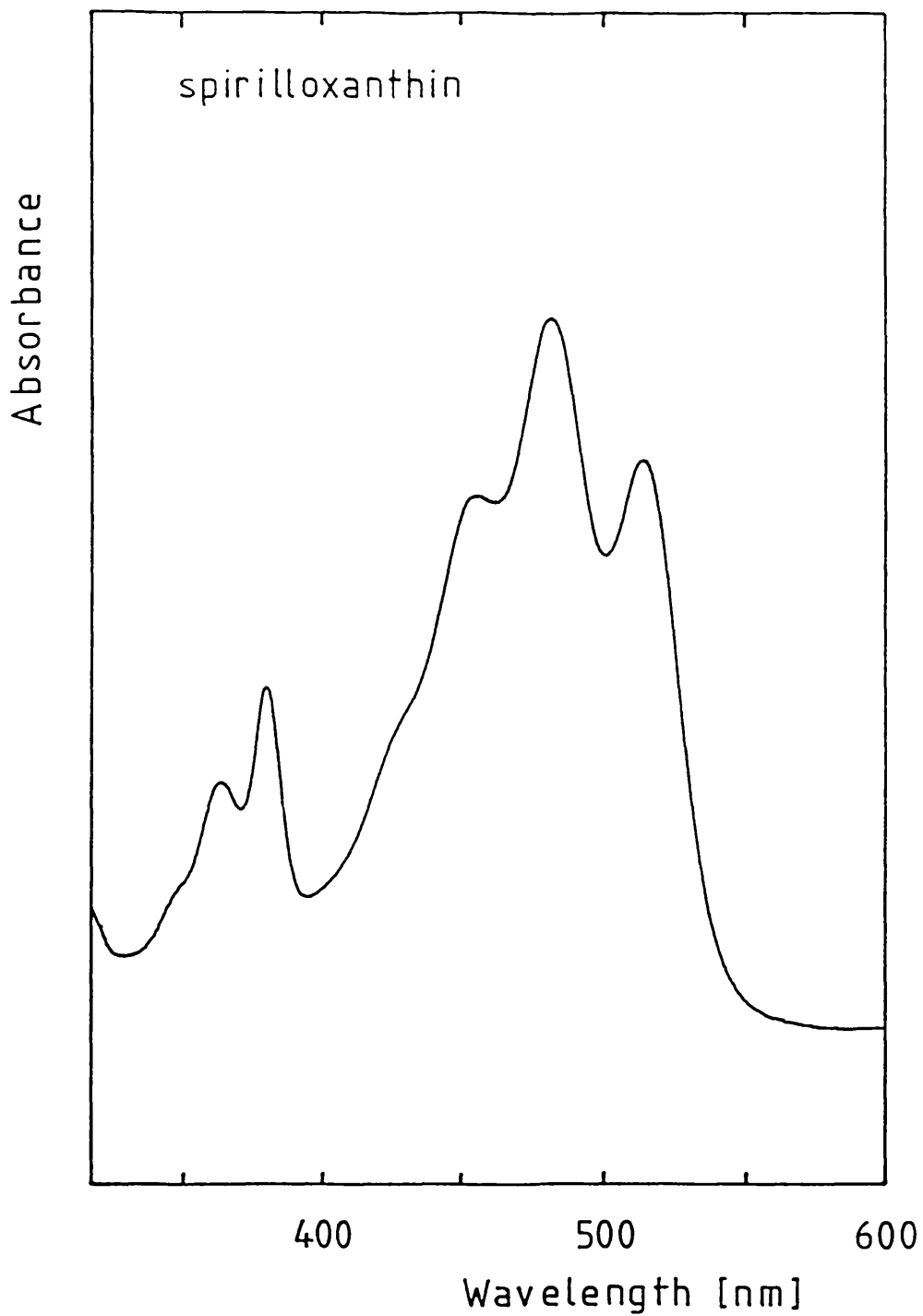


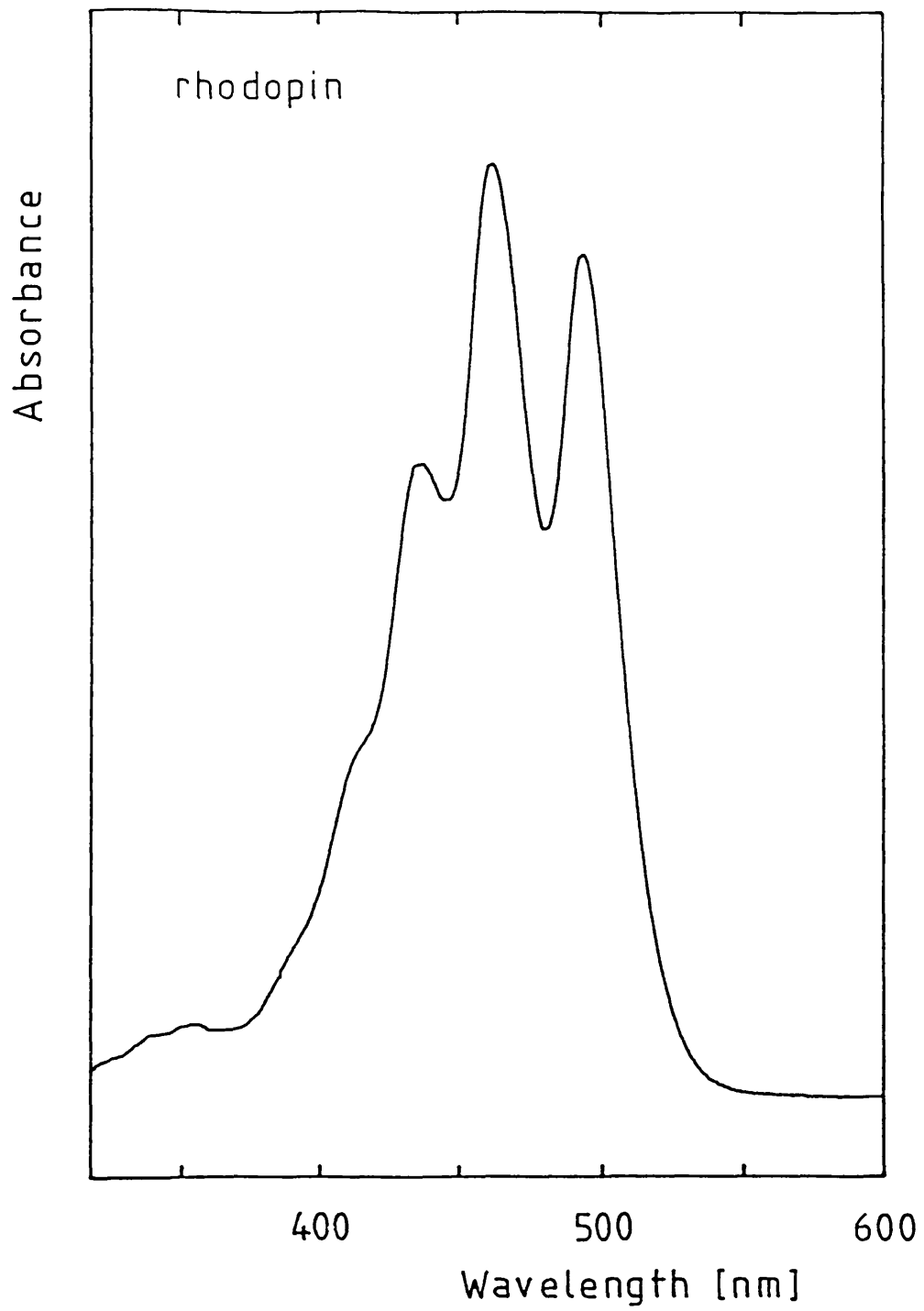
APPENDIX C: ABSORPTION SPECTRA OF SPIRILLOXANTHIN SERIES

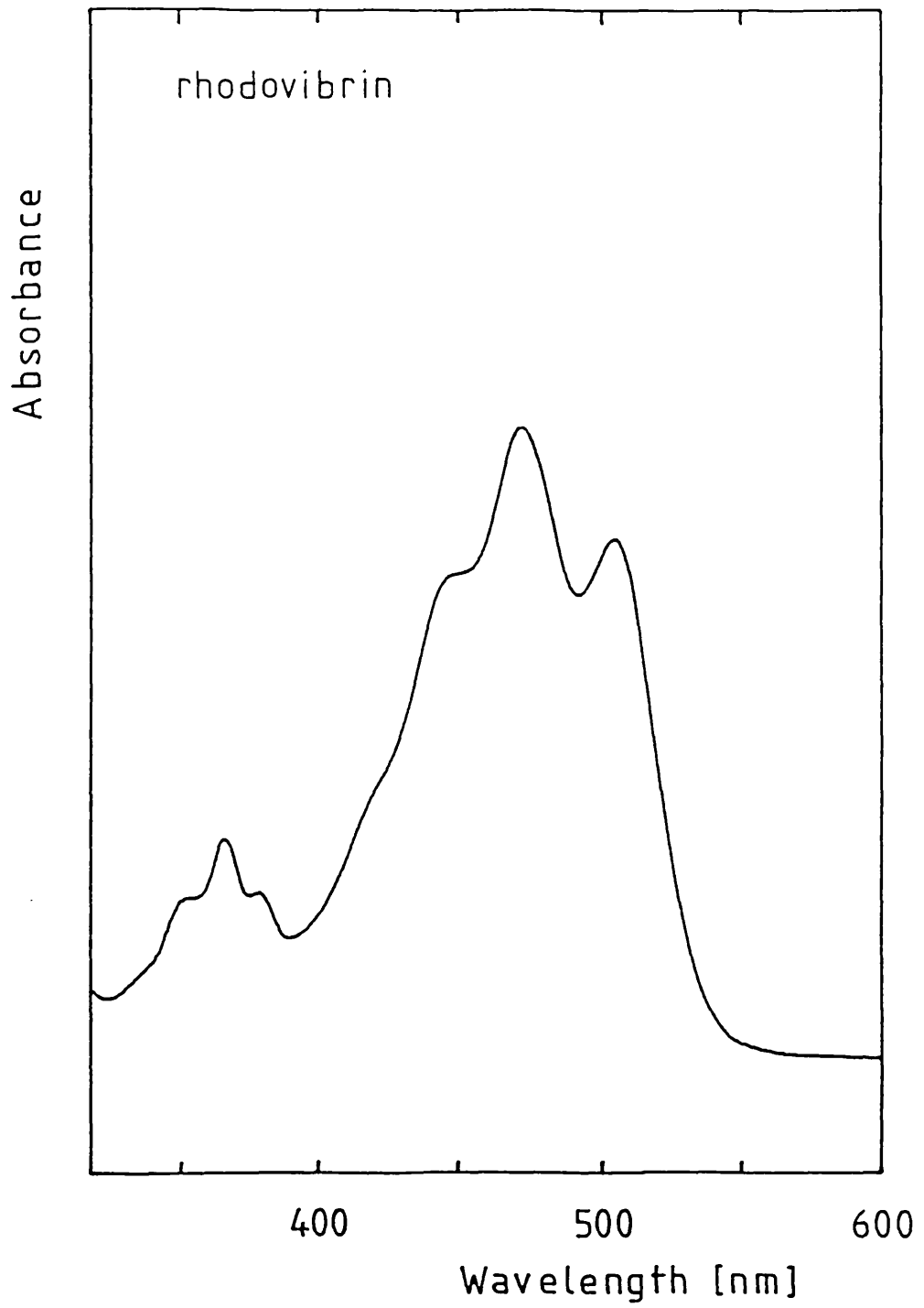
CAROTENOIDS RECORDED IN LIGHT PETROLEUM 40-60°C bp.











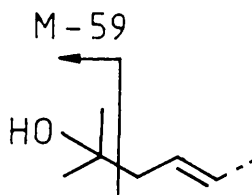
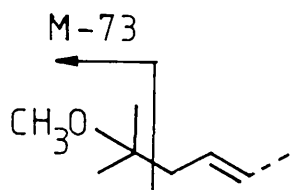
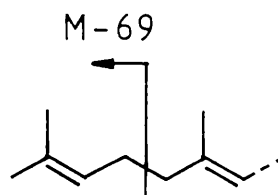
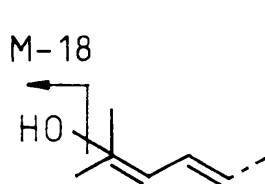
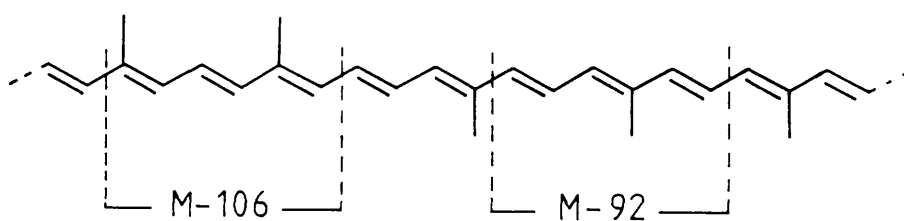
#### APPENDIX D: MASS SPECTRA OF SPIRILLOXANTHIN SERIES CAROTENOIDS

A mass spectrometer is an instrument that produces ions and then separates them according to their mass-to-charge (m/e) ratio [Millard, 1978]. Mass spectroscopy of carotenoids has been reviewed by Schweiter et al. (1969) and Enzell et al. (1969). The carotenoid sample is vapourised and bombarded with electrons of predetermined energy. When the energy of the electron beam exceeds the ionisation potential of part of the molecule, an electron is eliminated from that region of the molecule, forming a molecular ion. Fragmentation of the molecule occurs in a pattern which is characteristic of the structure of the parent molecule. The fragment ions are then accelerated along an evacuated tube. The ions are deflected from their original course by a magnetic field. The mass-to-charge ratio of the ion is calculated from the equation:

$$m/e = H^2 R^2 / 2V$$

where H is the strength of the magnetic field, R is the radius of the circular path and V is the ion-accelerating voltage. The fragment ions therefore follow a different trajectory according to their m/e ratios. At any one time the ions of a single m/e ratio are accelerated through a fixed slit and into a detector. By changing the strength of the applied magnetic field, the ion fragment intensity for each m/e ratio is recorded with time. In advanced instruments an average of several scans is calculated. A mass spectrum of ion intensity versus m/e ratio is then plotted.

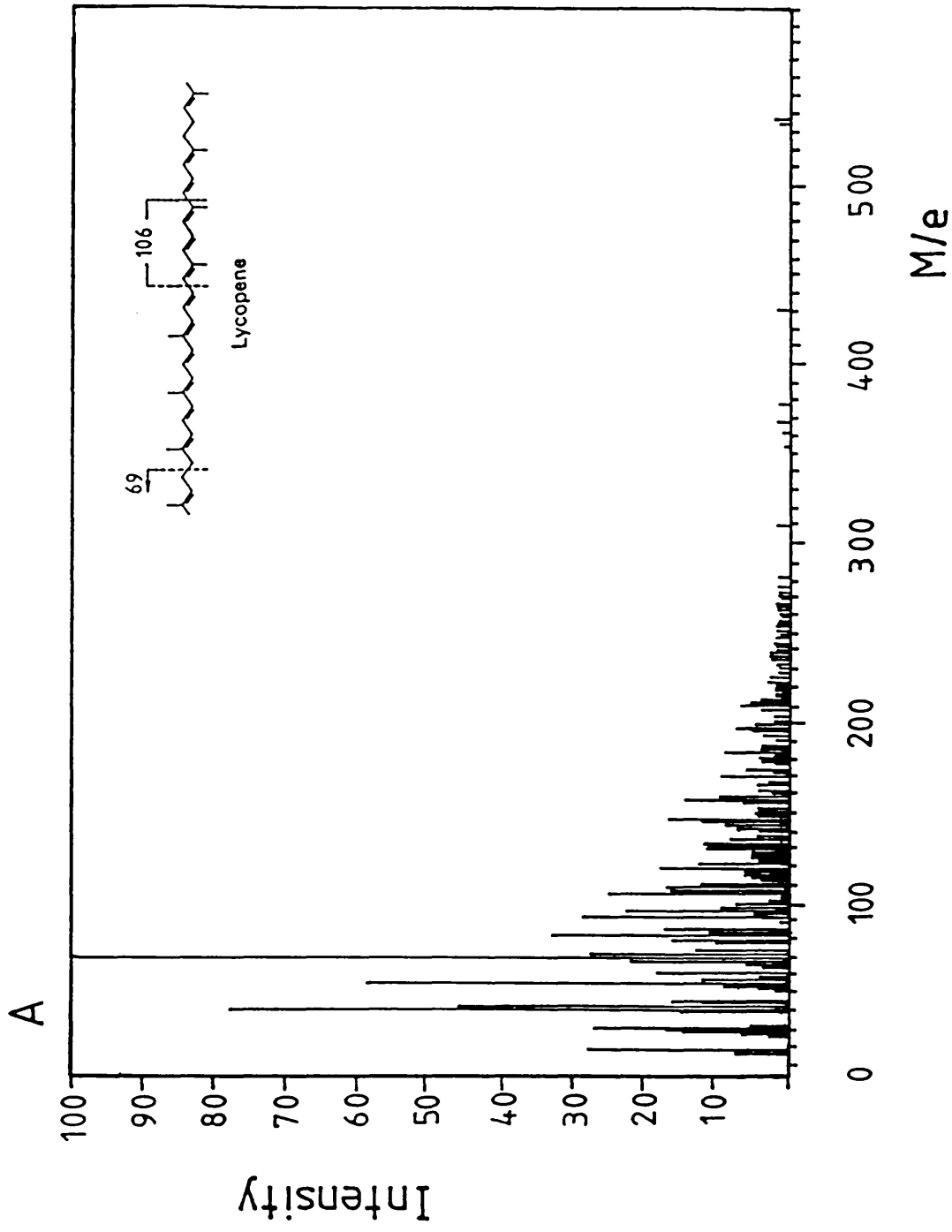
All carotenoids with three or more conjugated double bonds yield M-92 and M-106 fragment ions by elimination of regions of the chromophore which correspond to the molecular compositions of toluene and xylene respectively. The origins of the main diagnostic fragment ion losses are shown below.

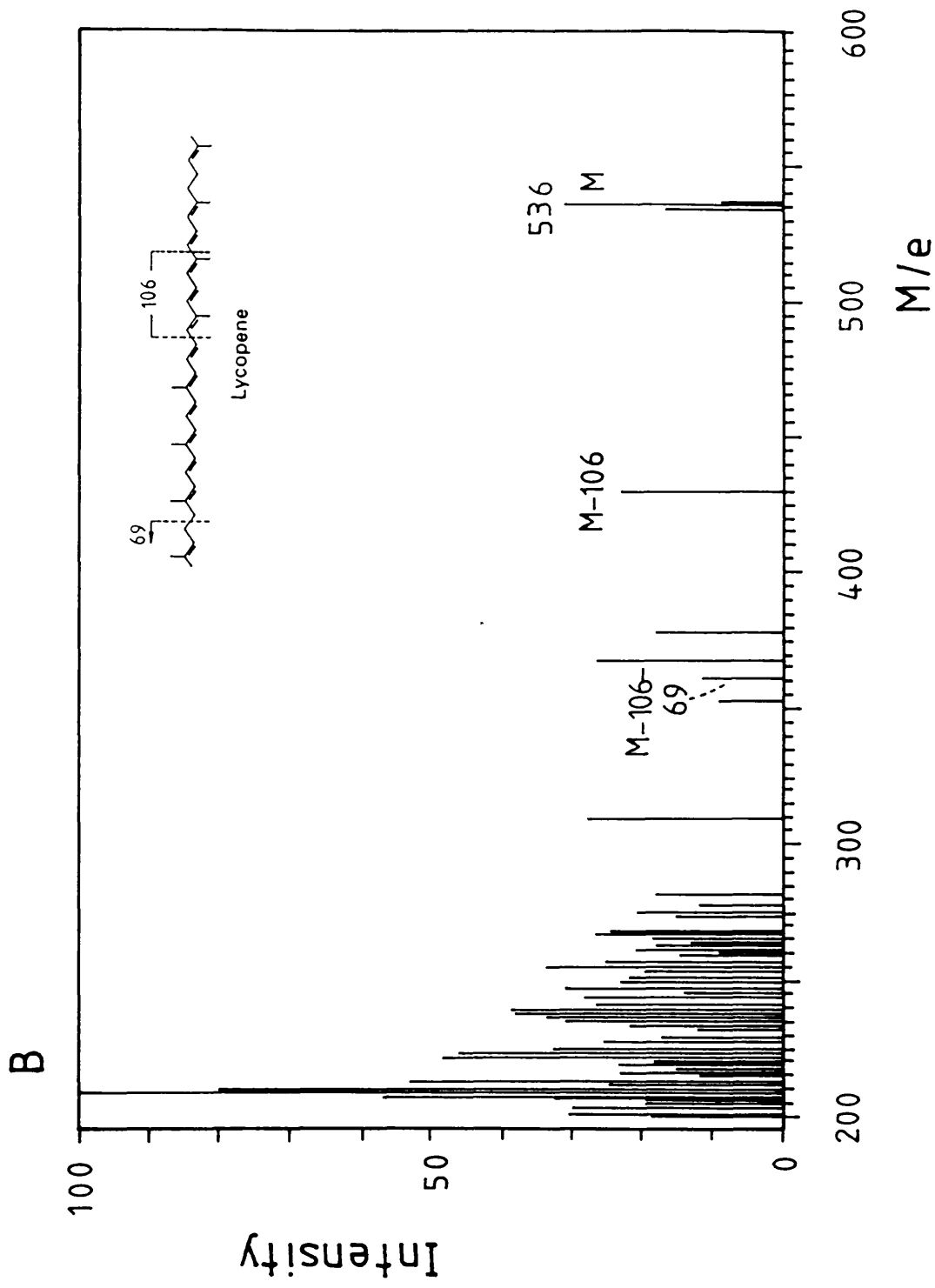


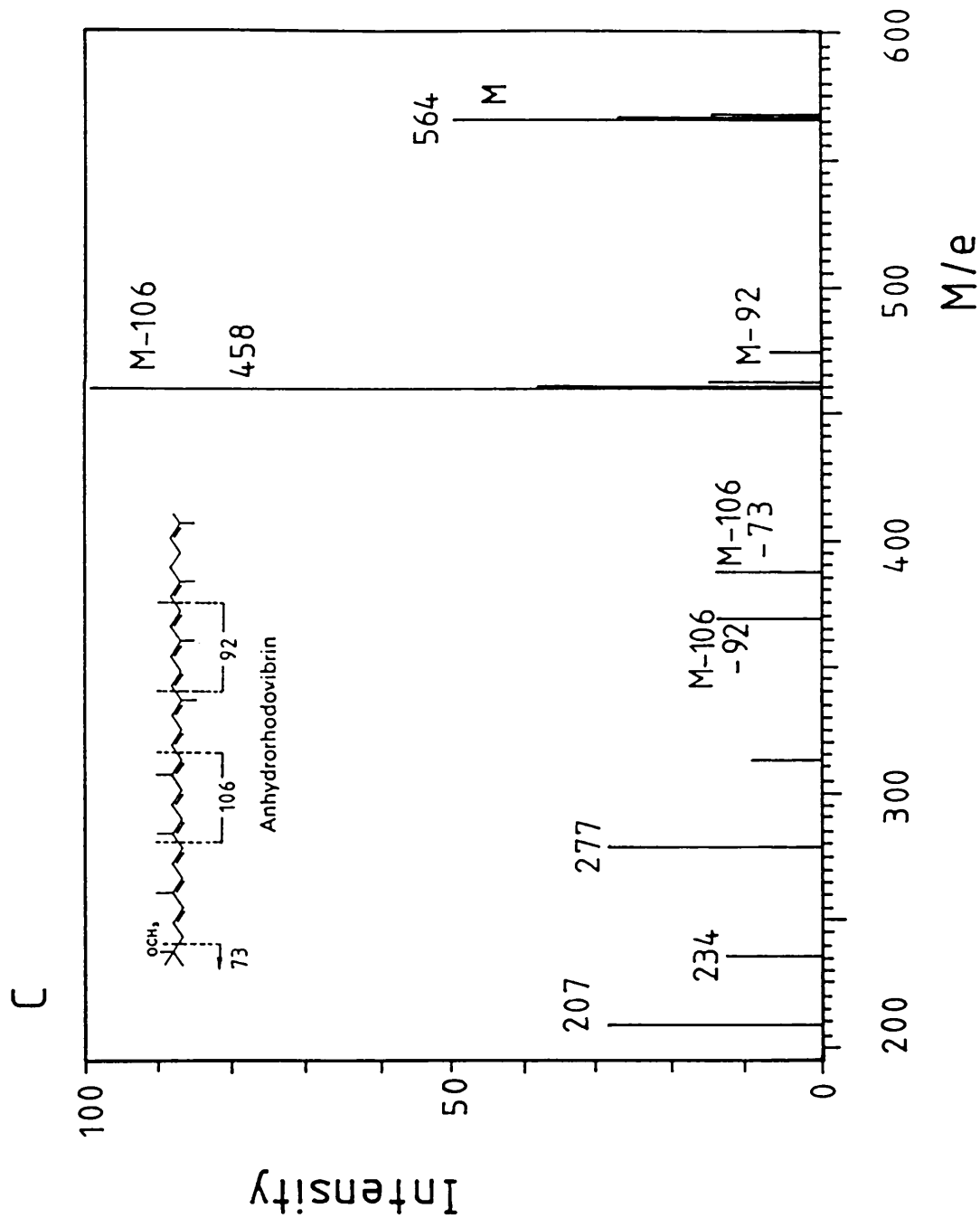
Mass spectra usually contain fragment ions which have eliminated more than one region of the molecule e.g. M-106-32. A complete mass spectrum of lycopene is shown in Spectrum A. The molecular ion of lycopene is at m/e 536 but this, and the important diagnostic fragment ions, are typically weak. It is therefore usual to present only an upper, partial mass spectrum. In spectrum B the molecular ion at m/e 536 is now evident along with the M-106 and M-106-92 peaks. Partial mass spectra of the remaining spirilloxanthin-series carotenoids are presented in Spectra C-F.

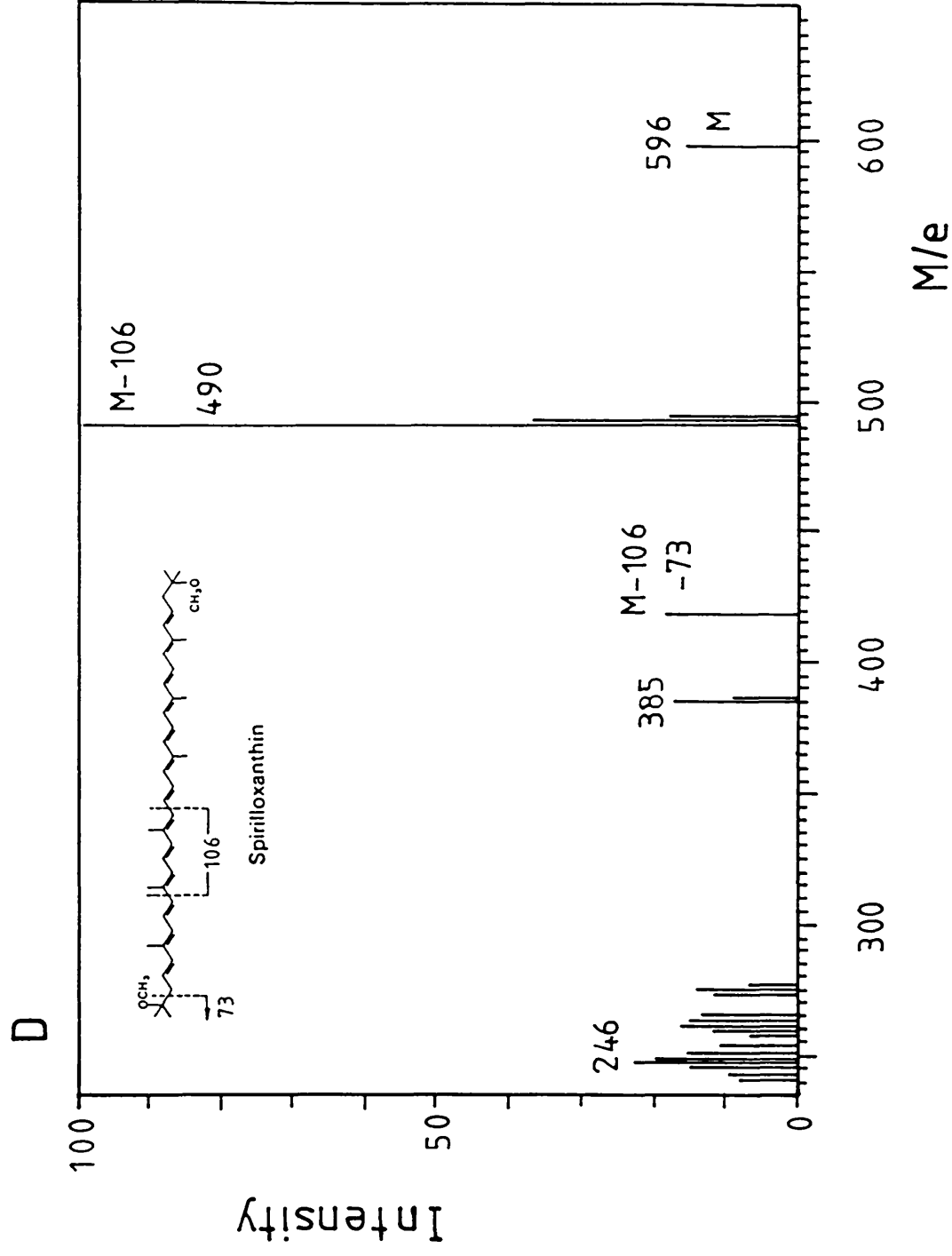
Because the intensities of the peaks in the upper spectral region are rather low for carotenoids, quality spectra of these molecules are difficult to obtain. The spectra presented are adequate to confirm the identities of the carotenoids isolated from *Rps. palustris* but they do

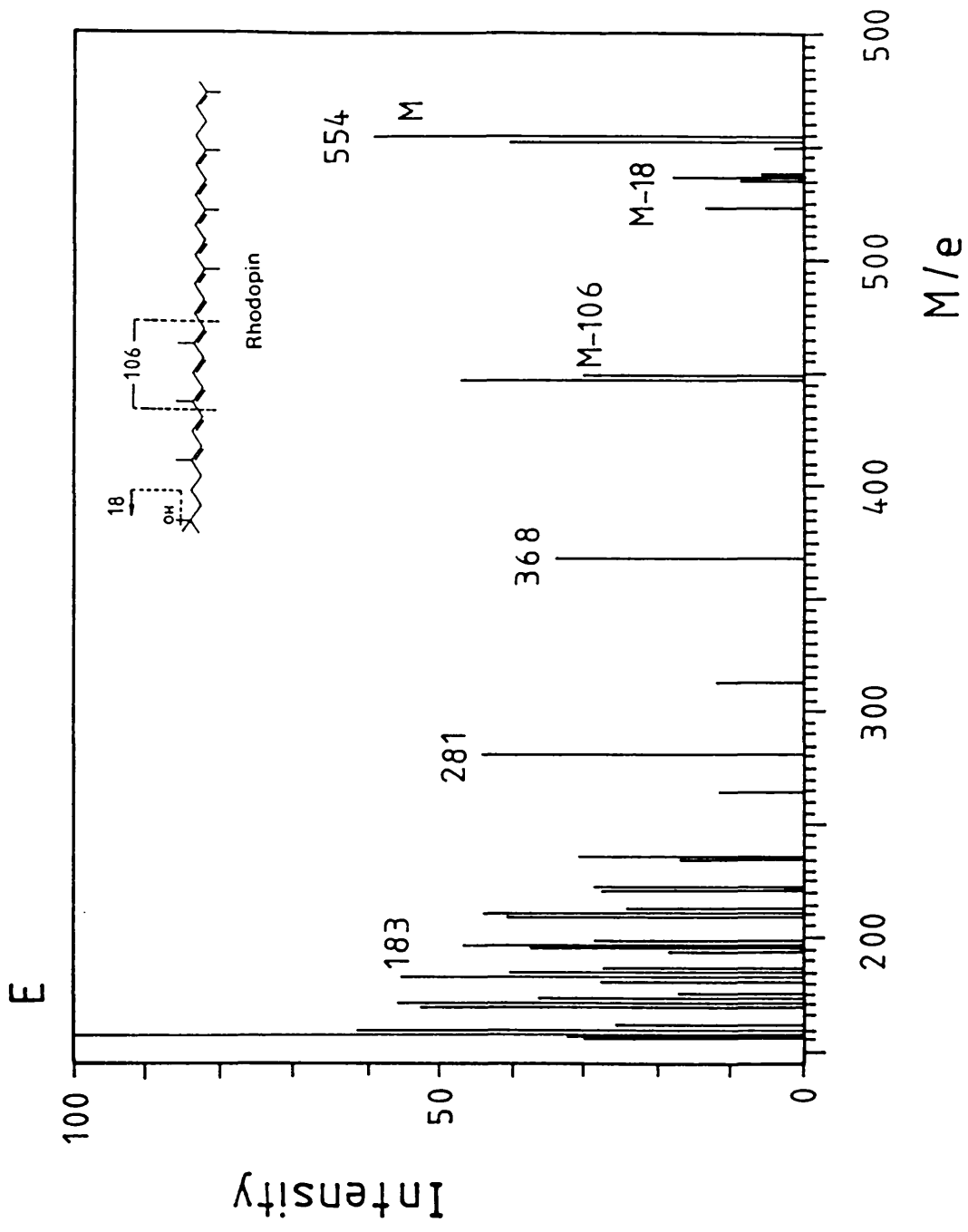
not show the full complement of peaks which can be obtained. The spectrum of rhodovibrin shows the presence of an impurity which eliminates fragment ions in the region  $M/e$  500-580. The spectrum is still sufficient however to determine the molecular weight and the presence of a methoxy substituent.

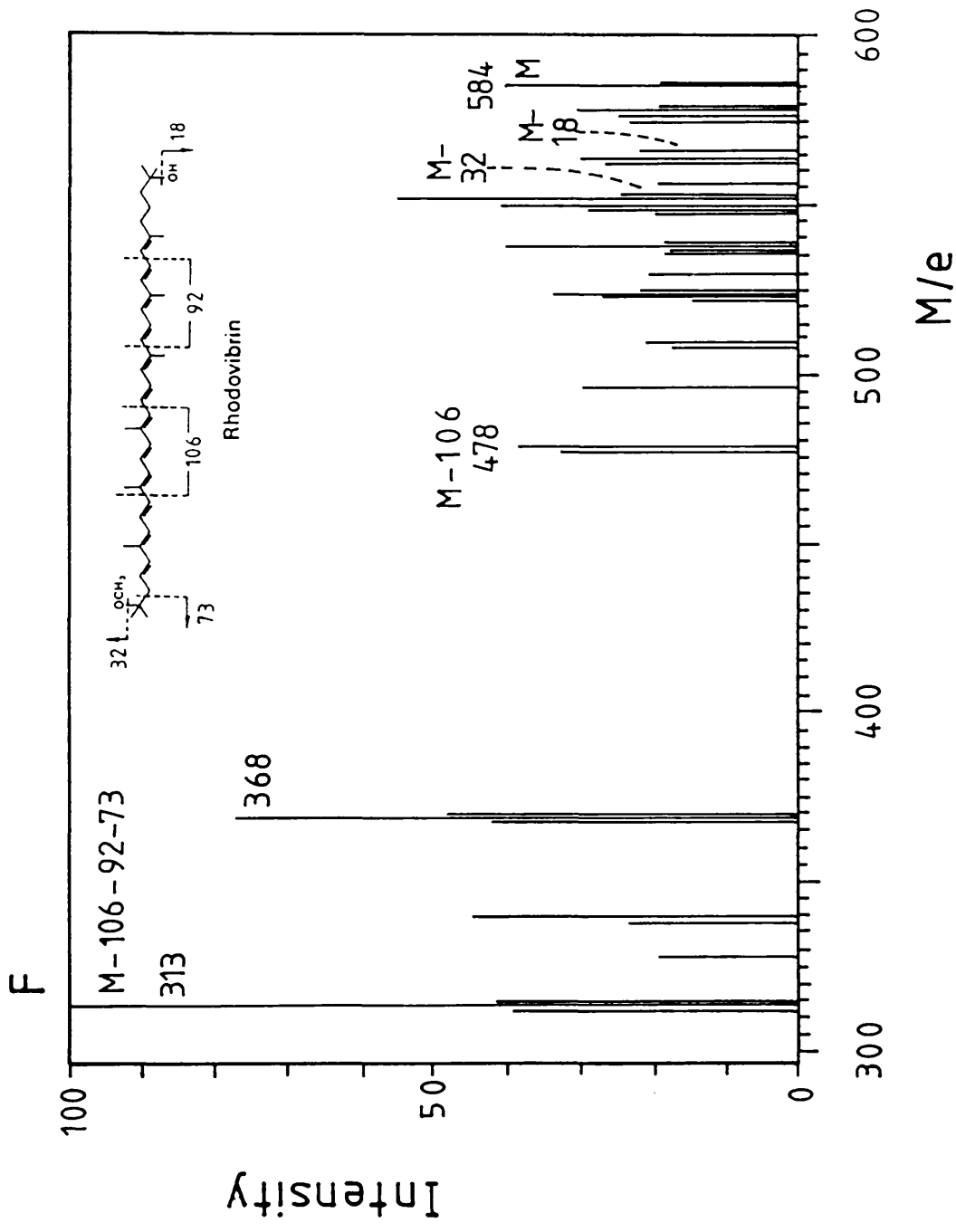












**APPENDIX E: COMPOSITIONS OF GROWTH MEDIA**

Succinate medium for *Rb. sphaeroides*, *Rps. palustris*, *R. rubrum* and *Rc. gelatinosus*

	per litre
Concentrated base	20ml
1M dipotassium hydrogen orthophosphate	10ml
1M potassium dihydrogen orthophosphate	10ml
10% ammonium sulphate	5ml
growth factors	1ml
casamino acids	1g

growth factors	per 100ml
biotin	0.002g
sodium hydrogen carbonate	0.05g
water	100ml
nicotinic acid	0.1g
aneurine hydrochloride	0.05g
4-aminobenzoic acid	0.1g

concentrated base	per litre
nitriiloacetic acid	10g
magnesium sulphate	14.45g
calcium chloride	3.4g
ammonium molybdate	0.00925g
ferrous sulphate	0.099g
nicotinic acid	0.05g
aneurine hydrochloride	0.025g
biotin	0.005g
metos 44	50ml

metos 44	mg per 100ml
EDTA	250
zinc sulphate	1095
manganous sulphate	154
copper sulphate	39.2
cobaltous nitrate	24.8
ferrous sulphate	500
disodium tetraborate	17.7
concentrated sulphuric acid	2 drops

Medium for Chr. vinosum

solution 1	1 litre
solution 2	1 litre
solution 3	8 ml

Adjust final pH to 7.8

<b>solution 1</b>	<b>g/l</b>
sodium chloride	60
potassium dihydrogen orthophosphate	1
dipotassium hydrogen orthophosphate	1
ammonium chloride	2
calcium chloride	0.25
magnesium chloride	1

<b>solution 2</b>	<b>g/l</b>
sodium thiosulphate	6
sodium hydrogen carbonate	8

<b>solution 3</b>	<b>g/l</b>
ferrous sulphate	1.6
EDTA	3

Store in cold room

Medium for Rps. acidophila

	<b>per litre</b>
potassium dihydrogen orthophosphate	1g
magnesium sulphate	0.4g
sodium chloride	0.4g
sodium succinate	1.5g
calcium chloride	0.05g
ammonium chloride	0.5g
ferric citrate solution	5ml
trace element solution	10ml

Adjust to pH 5.2

<u>Electrolyte</u>	g/l
TRIS	3
sodium dodecyl sulphate	1
glycine	14.6

<u>Boiling solution</u>	per 50ml
50mM TRIS	0.3025
2% sodium dodecyl sulphate	1
10% glycerol	5
2% mercaptoethanol	1
0.1% bromophenol blue	0.05

<u>Gel stain</u>	
isopropanol	625ml
acetic acid	250ml
coomassie blue	1g
distilled water	1625ml

<u>Gel destain</u>	
methanol	1l
glacial acetic acid	1l
distilled water	8l

#### Polyacrylamide gel preparation

6% acrylamide stacking gel	
stacking gel buffer	1.25ml
acrylamide stock	0.75ml
distilled water	3.0ml
10% ammonium persulphate	40 l
TEMED	5 l

resolving gel	1l .5%	18%
running gel buffer	4.9ml	4.9ml
acrylamide stock	5.6ml	9.0ml
65% sucrose	1.5ml	5.4ml
20% sodium chloride	0.49ml	0.49ml
distilled water	7.5ml	-
10% ammonium persulphate	31.5 l	31.5 l
TEMED	3.0 l	3.0 l

**ferric citrate solution**

ferric citrate	100mg
boiling water	100ml

**trace elements solution**

g/l

EDTA	0.5
ferrous sulphate	0.01
manganous chloride	0.003
boric acid	0.03
cobalt chloride	0.02
calcium chloride	0.001
nickel chloride	0.002
sodium molybdate	0.003

Adjust pH to 3.4

Agar culture medium

yeast extract	0.3g
casamino acids	0.2g
agar	1.5g
tap water	100ml

**APPENDIX F: COMPOSITIONS OF SOLUTIONS FOR POLYACRYLAMIDE GEL ELECTROPHORESIS**Acrylamide stock

g/100ml

30% acrylamide	39
0.8% bis-acrylamide	1

Running gel buffer

g/250ml

TRIS	45.3
Sodium dodecyl sulphate	1

Adjust to pH 8.8

Stacking gel buffer

g/250ml

0.5M TRIS	15.1
0.4% sodium dodecyl sulphate	1

## APPENDIX G: COMPOSITIONS OF BUFFERS AND OTHER SOLUTIONS

<u>MES/KCl buffer</u>	g/l
20mM 2[N-Morpholino]ethanesulphonic acid	3.9
0.1M KCl	7.4

Adjust to pH 6.8

### Tannin assay solutions

tannin reagent:	1M HCl	196ml
	tannic acid	20g
	phenol	4ml

heat to 80°C, filter and store in a cold room.

gum arabic:	acacia	0.2%
-------------	--------	------

**REFERENCES**

- Aagard, J. and Sistom, W.R. (1972) **Control of synthesis of reaction centre BChl in photosynthetic bacteria** Photochem. Photobiol. 15, 209-225.
- Aasen, A.J. and Liaaen Jensen, S. (1967) **The carotenoids of the Thiiorhodaceae 7. Cross-conjugated carotenals** Acta Chem. Scand. 21, 2185-2204.
- Ackers, G.K. (1975) **Molecular Sieve Methods of Analysis**, in "The Proteins" (Neurath, H. and Hill, R.L. eds) Academic Press, pp 2-92.
- Allen, J.P., Feher, G., Yeates, T.O., Komiya, H. and Rees, D.C. (1987a) **Structure of the reaction centre from Rb. sphaeroides R-26: the cofactors** Proc. Natl. Acad. Sci. USA 84, 5730-5734.
- Allen, J.P., Feher, G., Yeates, T.O., Komiya, H. and Rees, D.C. (1987b) **Structure of the reaction centre from Rb. sphaeroides: the protein subunits** Proc. Natl. Acad. Sci. USA 84, 6162-6166.
- Allen, J.P., Feher, G., Yeates, T.O., Komiya, H. and Rees, D.C. (1988) In "The Photosynthetic Bacterial Reaction Centre" NATO ASI Series A: Life Sciences, (Breton, J. and Vermeglio, A. eds) pp. 5-72 Plenum Press, New York.
- Amesz, J. (1978) **Fluorescence and energy transfer** In "The Photosynthetic Bacteria" (Clayton, R.K. and Sistrom, W.R. eds) Plenum Press, New York.
- Amesz, J. and Vasmel, H. (1986) **Fluorescence properties of photosynthetic bacteria** In "Light Emission by Plants and Bacteria", Academic Press, New York.
- Angerhofer, A., Cogdell, R.J. and Hipkins, M.H. (1986) **A spectral characterisation of the light-harvesting pigment-protein complexes from Rps. acidophila** Biochim. Biophys. Acta 848, 333-341.
- Barnes, J.E. and Waring, A.J. (1970) "Pocket Programmable Calculators in Biochemistry", John Wiley and Sons.
- Benson, J.R. (1975) **Some recent advances in amino acid analysis** In "Instrumentation in Amino Acid Sequence Analysis" (Perham, R.N. ed.) Academic Press.
- Bergström, H., Sundström, V., van Grondelle, R., Gillbro, T. and Cogdell, R.J. (1988) **Energy transfer dynamics of isolated B800-850 and B800-820 pigment-protein complexes of Rb. sphaeroides and Rps. acidophila** Biochim. Biophys. Acta 936, 90-98.
- Birge, R.R., Bennet, J.A., Pierce, B.M. and Thomas, T.M. (1986) **Two photon spectroscopy of protein bound chromophores** J. Am. Chem. Soc. 100, 1533-1539.
- Bissig, I., Brunisholz, R.A., Suter, F., Cogdell, R.J. and Zuber, H. (1988) **The complete amino acid sequences of the B800-850 antenna polypeptides from Rps. acidophila, strain 7750.** Z. Naturforsch 43c, 77-83.

- Bogorad, L. (1965) **Chlorophyll biosynthesis** In, "Chemistry and Biochemistry of Plant Pigments" (Goodwin, T.W., ed.) pp. 29-74 Academic Press.
- Bolt, J.D., Sauer, K., Shiozawa, J.A. and Drews, G. (1981) **Linear and circular dichroism of membranes from *Rps. capsulatus*** Biochim. Biophys. Acta 635, 535-541.
- Borisov, A. Yu., Gadonas, R.A., Danjeličius, R.V., Piskarskas, A.S. and Razjivin, A.P. (1977) **Minor component B-905 of light-harvesting antenna in *Rsp. rubrum* chromatophores and the mechanism of singlet-singlet annihilation as studied by difference selective picosecond spectroscopy** FEBS Lett. 138, 25-28.
- Bose, S.K. (1963) in "Bacterial Photosynthesis" (Gest, H., San Pietro, A. and Vernon, L.F., eds.), Antioch Press, Yellow Springs, Ohio.
- Breton, J. and Navedryk, E. (1984) **Transmembrane orientation of  $\alpha$ -helices and organisation of Chl in photosynthetic pigment-protein complexes** FEBS Lett 176, 335-359.
- Britton, G. (1985) **General Carotenoid Methods** Meths. Enzymol. 111, 113-149.
- Britton, G. and Goodwin, T.W. (1971) **Biosynthesis of carotenoids** Meths. Enzymol. 18C, 654-701.
- Britton, G., Barry, P. and Young, A.J. (1987) Proc. Brit. Crop Protection Conf. Weeds 3, 1015-1022.
- Broglie, R.M., Hunter, C.N., Delepelaire, P., Niederman, R.A., Chua, N. and Clayton, R.K. (1980) **Isolation and characterisation of the pigment-protein complexes of *Rps. sphaeroides* by lithium dodecylsulphate/polyacrylamide gel electrophoresis** Proc. Natl. Acad. Sci. USA 77, 87-91.
- Brown, J.S. (1972) **Forms of chlorophyll in vivo** Ann. Rev. Plant Physiol. 23, 73-86.
- Brown, S.B. (1980) "Introduction to Spectroscopy for Biochemists" Academic Press.
- Brunisholz, R.A. and Zuber, H. (1987) **Primary structure analyses of bacterial antenna polypeptides** In "Photosynthetic Light-harvesting Systems" Proc. Int. Workshop, Freising, FRG. (Scheer, H. and Schneider, S. eds), Walter De Gruyter, Berlin.
- Brunisholz, R.A., Cuendet, P.A., Theiler, R. and Zuber, H. (1981) **The complete amino acid sequence of the single light harvesting protein from chromatophores of *Rhodospirillum rubrum* G9<sup>+</sup>** FEBS Lett. 129, 150-154.
- Brunisholz, R.A., Suter, F. and Zuber, H. (1984) **The light-harvesting polypeptides of *Rhodospirillum rubrum*** Hoppe-Seyler's Z. Physiol. Chem. 365, 675-688.
- Brunisholz, R.A., Jay, F., Suter, F. and Zuber, H. (1985) **The light-harvesting polypeptides of *Rhodopseudomonas viridis*** Biol. Chem. Hoppe-Seyler 366, 87-98.

- Brunisholz, R.A., Zuber, H., Valentine, J., Lindsay, J.G., Woolley, K.J. and Cogdell, R.J. (1986) **The membrane location of the B890 complex from *Rhodospirillum rubrum* and the effect of carotenoid on the conformation of its two apoproteins exposed at the cytoplasmic surface** Biochim. Biophys. Acta 849, 295-303.
- Brunisholz, R.A., Bissig, I., Niederer, E., Suter, F. and Zuber, H. (1987) **Structural studies on the light-harvesting polypeptides of *Rps. acidophila*** In "Progress in Photosynthesis Research II" (Biggins, J., ed.) Martinus Nijhoff, The Netherlands.
- Buchanan, R.E. and Gibbons, N. (eds) (1974) "Bergey's Manual of Determinative Bacteriology", 8th edition, Baltimore: Williams and Wilkins.
- Chadwick, B.W., Frank, H.A., Chaoying, Z., and Taremi, S.S. (1987) **Singlet energy transfer in photosynthetic bacteria: Absorption and fluorescence excitation of B800-850 complexes** In "Progr. Photosynth. Res. vol. I (Biggins, J. ed.) Martinus Nijhoff, The Netherlands.
- Chang, R. (1981) **Physical Chemistry with Applications to Biological Systems** 2nd ed. MacMillan Press.
- Clayton, R.K. (1966) **Spectroscopic analysis of bacteriochlorophylls in vivo** Photochem. Photobiol. 5, 669-677.
- Clayton, R.K. (1978) **Physicochemical mechanisms in reaction centres of photosynthetic bacteria** In "The Photosynthetic Bacteria" (Clayton, R.K. and Sistrom, W.R. eds) Plenum Press, New York.
- Clayton, R.K. (1980) "Photosynthesis: physical mechanisms and chemical patterns" IUPAB biophysics series;4, Cambridge University Press.
- Clayton, R.K. and Clayton, B.J. (1972) **Relations between pigments and proteins in photosynthetic membranes of *Rhodopseudomonas sphaeroides*** Biochim. Biophys. Acta 283, 492-504.
- Cogdell, R.J. (1986) **Light-harvesting complexes in the purple photosynthetic bacteria** In "Photosynthesis III: Photosynthetic Membranes and Light-Harvesting Systems" (Staehelin, L.A. and Arntzen, C.J. eds) Encyclopedia of Plant Physiology, New Series, vol. 19.
- Cogdell, R.J. and Crofts, A.R. (1978) **Analysis of the pigment content of an antenna complex from three strains of *Rps. sphaeroides*** Biochim. Biophys. Acta. 502, 409-406.
- Cogdell, R.J. and Thornber, J.P. (1979) in "Chlorophyll Organisation and Energy Transfer in Photosynthesis", Ciba Foundation Symposium 61, Excerpta Medica, Elsevier, Amsterdam.
- Cogdell, R.J. and Scheer, H. (1985) **Circular dichroism of light-harvesting complexes from purple photosynthetic bacteria** Photochem. Photobiol. 42, 669-689.
- Cogdell, R.J. and Frank, H. (1987) **How carotenoids function in photosynthesis** Biochim. Biophys. Acta 895, 63-79.

- Cogdell, R.J., Parson, W.W., and Kerr, M.A. (1976) **The type, amount, location and energy transfer properties of the carotenoid in reaction centres from *Rhodopseudomonas sphaeroides***
- Cogdell, R.J., Hipkins, M.F., MacDonald, W. and Truscott, G.T. (1981) **Energy transfer between the carotenoid and the BChl within the B800-850 light-harvesting pigment-protein complex of *Rps. sphaeroides*** Biochim. Biophys. Acta 634, 191-202.
- Cogdell, R.J., Lindsay, J.G., Valentine, J. and Durant, I. (1982) **A further characterisation of the B890 light-harvesting pigment-protein complexes from *Rps. rubrum* strain S1** FEBS Lett. 150, 151-154.
- Cogdell, R.J., Durant, I., Valentine, J., Lindsay, J.G. and Schmidt, K. (1983) **The isolation and partial characterisation of the light-harvesting pigment-protein complement of *Rps. acidophila*** Biochim. Biophys. Acta 722, 427-432.
- Cogdell, R.J., Woolley, K.J., Dawkins, D.J. and Lindsay, J.G. (1986) In "Microbial Energy Transduction, Current Communications in Molecular Biology" (Youvan, D.C. and Daldal, F., eds.) pp. 47-51, Cold-Spring Harbor Symposium, Cold-Spring Harbor, New York.
- Cohen-Bazire, G., Sistrom, W.R. and Stanier, R.Y. (1957) **Kinetic studies of pigment synthesis by non-sulfur purple bacteria** J. Cell Comp. Physiol. 49, 25-68.
- Cornette, J.L., Cease, K.B., Margalit, H., Spouge, J.L., Berzofsky, J.A. and DeLisi, C. (1987) **Hydrophobicity scale and computational techniques for detecting amphipathic structures in proteins** J. Mol. Biol. 195, 659-685.
- Cotton, T.M., Loach, P.A., Katz, J.J. and Ballschmiter, K. (1978) **Studies of Chl-Chl and Chl-ligand interactions by visible absorption and infra red spectroscopy at low temperatures** Photochem. Photobiol. 27, 735-749.
- Cowan, D.O. and Drisko, R.L. (1976) "Elements of Organic Photochemistry", Plenum Press, New York.
- Dawkins, D.J. (1988) "Isolation and Characterisation of Reaction Centre-Antenna Conjugates From a Range of BChl a-Containing Species of Purple Bacteria" PhD Thesis, Glasgow University.
- Dawkins, D.J., Ferguson, L.A. and Cogdell, R.J. (1988) **The structure of the "core" of the purple bacterial photosynthetic unit** In "Photosynthetic Light-harvesting Systems" (Scheer, H. and Schneider, S., eds) Walter de Gruyter and Co, Berlin and New York.
- Davidson, E. and Cogdell, R.J. (1981) **Reconstitution of carotenoids into the light-harvesting pigment-protein complexes from the carotenoidless mutant *Rps. sphaeroides* R26** Biochim. Biophys. Acta 635, 295-303.
- Davies, B.H. (1965) in "Chemistry and Biochemistry of Plant Pigments" (Goodwin, T.W., ed.) Academic Press, New York.
- Davies, D.R. and Segal, D.M. (1971) **Protein Crystallization: microtechniques involving vapour diffusion** Meths. Enzymol. 22, 266.

- Deisenhofer, J. and Michel, H. (1985) in "Antennas and Reaction Centres of Photosynthetic Bacteria (Michel-Beyerle, M.E., ed.), Springer-Verlag, Berlin.
- Deisenhofer, J., Epp, O., Miki, K., Huber, R. and Michel, H. (1984) **X-ray structure analysis of a membrane protein complex.** J. Mol. Biol. 180, 385-398.
- Deisenhofer, J., Michel, H. and Huber, R. (1985) **The structural basis of photosynthetic light-reactions** Trends Biochem. Sci. 10, 243-248.
- Dexter, D.L. (1953) **Theory of sensitized luminescence in solids** J. Chem. Phys. 21, 836-850.
- Dirks, G., Moore, A.L., Moore, T.A., and Gust, D. (1980) **Light absorption and energy transfer in polyene-porphyrin esters** Photochem. Photobiol. 32, 277-280.
- Drews, G. (1978) **Structure and development of the membrane system of photosynthetic bacteria** Curr. Topics Bioenerg. 8, 161-207.
- Drews, G. (1985) **Structure and Functional Organization of light-harvesting complexes and photochemical reaction centres in membranes of photosynthetic bacteria** Microbiol. Rev. 49, 59-70.
- Drews, G. and Oelze, J. (1981) **Organization and differentiation of membranes of phototrophic bacteria** Adv. Microbiol. Physiol. 22, 1-92
- Dunlap, G.E., Gentleman, S. and Lowney, L.I. (1978) **Use of trifluoroacetic acid in the separation of opioid peptides by reversed phase high performance liquid chromatography** J. Chromat. 160, 191.
- Dutton, P.L. (1986) **Energy transduction in anoxygenic photosynthesis** in "Photosynthesis III" (Staehelin, L.A. and Arntzen, C.J. eds) Encyclopedia of Plant Physiology vol. 19, Springer-Verlag.
- Duysens, L.M.N. (1951) **Transfer of light energy within the pigment systems present in photosynthesising cells** Nature 168, 548-550.
- Edman, P. (1970) **Sequence Determination**, in "Protein Sequence Determination, Molecular Biology, Biochemistry and Biophysics 8" (Needleman, S.B. ed.), Chapman and Hall.
- Edman, P. and Beg, G. (1967) **A Protein Sequenator** Eur. J. Biochem. 1, 80-91.
- Eimhjellen, K.E. and Liaaen-Jensen, S. (1964) **Biosynthesis of carotenoids in *Rps. gelatinosus*** Biochim. Biophys. Acta. 82, 21-40.
- Eisenberg, D., Schwarz, D., Kamoromy, M. and Wall, R. (1984) **Analysis of membrane and surface protein sequences with the hydrophobic moment plot** J. Mol. Biol. 179, 125-142.
- Englehardt, H., Baumeister, W. and Saxton, W.O. (1983) **Electron microscopy of photosynthetic membranes containing bacteriochlorophyll a** Arch. microbiol. 135, 169-175.
- Enzell, C.R. (1969) **Mass spectrometric studies of carotenoids** Pure and Appl. Chem. 20, 497-515.

- Everleigh, J.W. and Winter, G.D. (1970) **Amino Acid Composition Determination** in "Protein Sequence Determination, Molecular Biology, Biochemistry and Biophysics 8" (Needleman, S.B. ed.), Chapman and Hall.
- Feick, R. and Drews, G. (1978) **Isolation and characterisation of light-harvesting protein complexes from *Rps. capsulata*** Biochim. Biophys. Acta 501, 499-513.
- Fenna, R.E. and Matthews, B.W. (1975) **Chlorophyll arrangement in a bacteriochlorophyll protein from *Chlorobium*** Nature 258, 573-577.
- Fenna, R.E., Ten Eyck, L.F., and Matthews, B.W. (1977) **Atomic coordinates for the chlorophyll core of a BChl *a*-protein from green photosynthetic bacteria** Biophys. Res. Commun. 75, 751-756.
- Firsow, N.J. and Drews, G. (1977) **Differentiation of the intracytoplasmic membrane of *Rps. palustris* induced by variations in oxygen partial pressure or light intensity** Arch. microbiol. 115,, 299-306.
- Floodgate, G.D. (1962) Microbiol. Rev. 26, 277-291.
- Forster, Th. (1948) Ann. Phys. 2, 55-75.
- Forster, Th. (1965) In "Modern Quantum Chemistry" vol 3 (Sinnaroglu, O., ed.) Academic Press.
- French, C.S. (1940) **The pigment-protein compound in photosynthetic bacteria** J. gen. Physiol. 23, 469-494.
- French, C.S. and Milner, W. (1955) **Disintegration of bacteria and small particles by high pressure extrusion** Meths. Enzymol. 1, 64-67.
- Frenkel, A.W. and Nelson, R.A. (1971) **Bacterial chromatophores** Meths. Enzymol. 23, 256-268.
- Fuller, R.C. (1978) **Photosynthetic carbon metabolism in the green and purple bacteria** in, "The Photosynthetic Bacteria" (Clayton, R.K. and Sistrom, W.R. eds) Plenum Press, New York.
- Gabellini, N., Bowyer, J.R., Hurt, E., Melandri, B.A. and Hauska, G. (1982) **A cytochrome *bc*<sub>1</sub> complex with ubiquinol-cytochrome *c*<sub>2</sub> oxidoreductase activity from *Rps. sphaeroides* GA** Eur. J. Biochem. 126, 105-111.
- Garavito, R.M., Jenkins, J., Jansonius, J.N., Karlsson, R. and Rosenbusch, J.P. (1983) **X-ray diffraction analysis of matrix porin, an integral membrane protein from *E. coli* outer membrane** J. Mol. Biol. 164, 313.
- Garcia, A., Vernon, L.P. and Hilton, M. (1966) **Properties of subchromatophore particles obtained by treatment with Triton X-100** Biochem. 5, 2399-2407.
- Gilliland, G.L. and Davies, D.R. (1984) **Protein crystallisation: The growth of large-scale single crystals** Meths. Enzymol. 104, 370-381.



- Hayashi, H. and Morita, S. (1980) **Near infrared spectra of light-harvesting BChl-protein complexes from *Chromatium vinosum***. J. Biochem, 88, 1251-1258.
- Hayashi, H., Miyao, M. and Morita, S. (1982a) **Absorption and fluorescence spectra of light-harvesting BChl-protein complexes from *Rps. palustris* in the near infrared region** J. Biochem. 91, 1017-1027.
- Hayashi, H., Nozawa, T., Hatno, M. and Morita, S. (1982b) **Circular dichroism of BChl *a* in light-harvesting BChl-protein complexes from *Rps. palustris*** J. Biochem. 91, 1029-1038.
- Heinemeyer, E. and Schmidt, K. (1983) **Changes in carotenoid biosynthesis caused by variation of growth conditions in cultures of *Rps. acidophila*, strain 7050**. Arch. microbiol. 134, 217-221.
- Helenius, A. and Simons, K. (1975) **Solubilisation of membranes by detergents** Biochim. Biophys. Acta 415, 29-79.
- Helenius, A., McCaslin, D.R., Fries, E. and Tanford, C. (1981) **Properties of detergents** Meths. Enzymol. 56, 734-749.
- Henderson, R. and Unwin, P.N.T. (1975) **Three-dimensional model of purple membranes obtained by electron microscopy** Nature 257, 28-32.
- Hipkins, M.F., Cogdell, R.J., MacDonald, W. and Truscott, T.G. (1981) **Energy transfer between the carotenoid and the BChl within the B800-850 light-harvesting pigment-protein complex of *Rhodobacter sphaeroides* in "Photosynthesis I Photophysical Processes-membrane energisation (Akoyunoglo, G ed.) Babalan Int. Sci. Services, Philadelphia**.
- Holmqvist, O. (1979) **Evidence of discontinuity between the cytoplasmic and intracytoplasmic membranes in *Rps. sphaeroides*** FEMS Lett. 6, 37-40.
- Hunter, N. (1988) **Molecules of the green machine** New Scientist 118, 60-63.
- Imhoff, J.F. (1984) **Reassignment of the genus *Ectothiorhodospira* Pelsh 1936 to a new family, Ectothiorhodospiraceae amf. nov., and emended description of the Chromatiaceae Barendamm 1924**. Int. J. Syst. Bacteriol. 34, 338-339.
- Imhoff, J.F. (1988) **Anoxygenic phototrophic bacteria** in "Methods in Aquatic Biology" (Austin, B. ed.) John Wiley and Sons.
- Imhoff, J.F., Truper, H.G. and Pfennig, N. (1984) **Rearrangement of the species and genera of the phototrophic purple nonsulfur bacteria**. Int. J. Syst. Bacteriol. 34, 340-343.
- IUPAC-IUB Joint Commission in Biochemical Nomenclature (1984) Eur. J. Biochem. 138, 9-37.
- Jackson, J.B. and Crofts, A.R. (1969) **The high energy state in chromatophores from *Rps. sphaeroides*** FEBS Lett. 4, 185-189.

- Kannangara, C.G., Gough, S.P., Bruyant, P., Hooper, J.K., Kahn, A. and Von Weltstein, D. (1988) **tRNA<sup>Glu</sup> as a cofactor in s-aminolevulinate biosynthesis. Steps that regulate chlorophyll synthesis** Trends Biochem. Sci. 148, 139-143.
- Kaplan, S. and Arntzen, C.J. (1982) In "Photosynthesis" (Govindjee ed.) vol. I, Academic Press, New York.
- Katz, E. and Wassink, E.C. (1939) **Infrared absorption spectra of chlorophyllous pigments in living cells and in extracellular extracts** Enzymologia, 7 97.
- Katz, J.J., Shipman, L.L., Cotton, T.M. and Janson, T.R. (1977) In "The Porphyrins" (Dolphin, D. ed.) Academic Press.
- Katz, J.J., Strain, H.H., Harkness, A.L., Studier, M.H., Svec, W.A., Janson, T.R. and Cope, B.T. (1982) **Esterifying alcohols in the chlorophylls of purple photosynthetic bacteria. A new Chl, BChl (gg) all-trans-geranylgeranyl** J. Am. Chem. Soc. 94, 7938-7939.
- Kirmaier, C. and Holten, D. (1986) **Primary photochemistry of iron-depleted and zinc-reconstituted reaction centres from Rps. sphaeroides** Proc. Natl. Acad. Sci. 83, 6407-6411.
- Knox, R.S. (1975) **Theory and modeling of excitation, delocalisation and trapping** In "Bioenergetics of Photosynthesis" (Govindjee, ed.) Academic Press.
- Knox, R.S. (1977) In "Topics in Photosynthesis" vol 2. Barber, J. (ed.) Elsevier, Amsterdam.
- Knox, R.S. (1986) **Theory and modeling of excitation delocalisation and trapping** In "Photosynthesis III" Encyclopedia of Plant Physiology vol. 19 (Staehelin, L.A. and Arntzen, C.J. eds) Springer-verlag.
- Kramer, H.J.M., van Grondelle, R., Hunter, C. N., Westerhuis, W.H.J. and Ames, J. (1984a) **Pigment organization of the B800-850 antenna complex of Rhodospseudomonas sphaeroides** Biochim. Biophys. Acta. 765, 156-165.
- Kramer, H.J.M., Pennoyer, J.D., van Grondelle, R., Westerhuis, W.H.J., Niederman, R.A. and Ames, J. (1984b) **Low temperature optical properties and pigment organisation of the B875 light harvesting BChl-protein complex of purple photosynthetic bacteria** Biochim. Biophys. Acta 767, 335-344.
- Kunzler, A. and Pfennig, N. (1973) Arch. microbiol. 91, 83-86.
- Kyte, J. and Doolittle, R.F. (1982) **A simple method for displaying the hydropathic character of a protein** J. Mol. Biol. 157, 105-132.
- Laemmli, U.K. (1970) **Cleavage of structural proteins during the assembly of the head of bacteriophage T4** Nature 227, 680.
- Lascelles, J. (1968) **The bacterial photosynthetic apparatus** Adv. Microbiol. Physiol. 2, 1-42.
- Leigh, J.S. (1978) **EPR studies of primary events in bacterial photosynthesis** In "The Photosynthetic Bacteria" (Clayton, R.K. and Sistrom, W.R. eds) Plenum Press, New York. pp. 431-436.

- Lester, R.L. and Crane, F.L. (1959) **The natural occurrence of coenzyme Q and related compounds** J. Biol. Chem. 234, 2169-2175.
- Liaaen Jensen, S. (1963) **Carotenoids in photosynthetic bacteria** In "Bacterial Photosynthesis" (Gest, ... Vernon, L.P. and San Pietro, ... eds) Yellow Springs, Ohio, Antioch Press.
- Liaaen Jensen, S. (1965) **Biosynthesis and function of carotenoid pigments in microorganisms** Ann. Rev. Microbiol. 19, 163-179.
- Liaaen Jensen, S. (1978) **Chemistry of carotenoid pigments** In "The Photosynthetic Bacteria" (Clayton, R.K. and Sistrom, W.R. eds) Plenum Press, New York.
- Liaaen Jensen, J. and Jensen, A. (1971) **Quantitative determination of carotenoid in photosynthetic tissues** Meths. Enzymol. 23, 586-602.
- Liaaen Jensen, J., Cohen-Bazire, G., Nakayama, T.O.M. and Stanier, R.Y. (1958) **The path of carbon synthesis in a photosynthetic bacterium** Biochim. Biophys. Acta 29, 477-498.
- Liaaen Jensen, S., Cohen-Bazire, G. and Stanier, R.Y. (1961) **Biosynthesis of carotenoids in photosynthetic bacteria** Nature 192, 1168-1172.
- Liddell, P.A., Nemeth, G.A., Lehman, W.R., Joy, A.M., Moore, A.L., Bensasson, R.V., Moore, T.A. and Gust, D. (1982) **Mimicry of carotenoid function in photosynthesis: synthesis and photophysical properties of a carotenoid pyropheophorbide** Photochem. Photobiol. 36, 641-645.
- Loach, P.A., Sekurra, D.L., Hadsell, R.M., and Stemer, A. (1970) **Quantitative dissolution of the membrane and preparation of photoreceptor subunits from *Rps. sphaeroides*** Biochem. 9, 724.
- Lutz, M., Agagidis, I., Hervo, G., Cogdell, R.J. and Reiss-Husson, F. (1978) **On the state of carotenoid bound to reaction centres of photosynthetic bacteria: a resonance Raman study** Biochim. Biophys. Acta 503, 287-303.
- Malhotra, H.C., Britton, G. and Goodwin, T.W. (1969) **The identification of spheroidene and hydroxyspheroidene in diphenylamine-inhibited cultures of *Rhodospirillum rubrum*** Phytochem 8, 1047.
- McCormick, D. and Roach, A. (1987) "Measurement, Statistics and Computation. Analytical Chemistry by Open Learning", John Wiley and Sons.
- McDermott, J.C.B., Ben-Aziz, A., Singh, R.K., Britton, G. and Goodwin, T.W. (1973) **Recent studies of carotenoid biosynthesis in bacteria** Pure Appl. Chem. 35, 29-45.
- McElroy, J.D., Feher, G. and Mauzerall, D.C. (1969) **On the nature of the free radical formed during the primary process of bacterial photosynthesis** Biochim. Biophys. Acta 172, 180-183.
- McPherson, A. (1976) **Crystallisation of proteins from polyethylene glycol** J. Biol. Chem. 251, 6300-6303.

- McPherson, A. (1982) **Preparation and analysis of protein crystals** John Wiley and Sons, Inc.
- Mechler, B. and Oelze, J. (1978a) **Differentiation of the photosynthetic apparatus of *Chromatium vinosum*, strain D. I The influence of growth conditions** Arch. microbiol. 118, 91-97.
- Mechler, B. and Oelze, J. (1978b) **Differentiation of the photosynthetic apparatus of *Chromatium vinosum*, strain D. II Structural and functional differences** Arch. microbiol. 118, 99-108.
- Mechler, B. and Oelze, J. (1978c) **Differentiation of the photosynthetic apparatus of *Chromatium vinosum*, strain D. III Analysis of spectral alterations** Arch. microbiol. 118, 109-114.
- Mejbaum-Katzenellenbogen, S. and Drobyszczka, W.J. (1959) **New method for quantitative determination of serum proteins separated by paper electrophoresis** Clin. Chim. Acta 4, 515-522.
- Michel, H. (1983) **Crystallisation of membrane proteins** Trends Biochem. Sci. 8, 56-59.
- Michel, H. and Deisenhofer, J. (1986) **X-ray diffraction studies on a crystalline bacterial photosynthetic reaction centre**, in "Photosynthesis III: Photosynthetic Membranes and Light-harvesting Systems" Encyclopedia of Plant Physiology, New Series, vol. 19. (Staehelin, L.A. and Arntzen, C.J. eds).
- Michel, H. and Osterhelt, D. (1980) **Three-dimensional crystals of membrane proteins: bacteriorhodopsin** Proc. Natl. Acad. Sci. USA 77, 1283.
- Michel, H., Weyer, K.A., Gruenberg, H., Dunger, I., Osterhelt, D. and Lottspeich, F. (1986) **The "light" and "medium" subunits of the photosynthetic reaction centre from *Rps. viridis*: isolation of the genes, nucleotide and amino acid sequences** EMBO J. 5, 1149-1158.
- Millard, B.J. (1978) **"Quantitative Mass Spectroscopy"** Heyden and Son Ltd, London.
- Mitchell, P. (1961) **Coupling of phosphorylation to electron and hydrogen transfer by a chemi-osmotic type of mechanism** Nature 191, 144-148.
- Miyazaki, T. and Morita, S. (1981) **CD and absorption spectra of BChl types in *Chromatium vinosum* and *Rhodopseudomonas palustris*** Photosynthetica 156, 238-243.
- Monger, T.G. and Parson, W.W. (1977) **Singlet-triplet fusion in *Rhodopseudomonas chromatophores*- a probe of the organisation of the photosynthetic apparatus** Biochim. Biophys. Acta 460, 393-401.
- Moore, A.L., Dirks, G., Gust, D. and Moore, T.A. (1980) **Energy transfer from carotenoid polyenes to porphyrins: a light-harvesting antenna** Photochem. Photobiol. 32, 691-695.
- Moskalenko, A.A. and Erokhin, Yu. E. (1978) **Investigation light-harvesting complexes *Rps. sphaeroides*** FEBS Lett. 87, 254-256.

- Netzel, T.L., Rentzepis, P.M. and Leigh, J. (1973) **Picosecond kinetics of reaction centres containing BChl** Science 182, 238-241.
- Nicholls, D.G. (1982) "Bioenergetics- An Introduction to Chemiosmotic Theory", Academic Press.
- Niederman, R.A. and Gibson, K.D. (1978) **Isolation and physicochemical properties of membranes from purple photosynthetic bacteria** in "The Photosynthetic Bacteria" (Clayton, R.K. and Sistrom, W.R. eds) Plenum Press, New York.
- Norris, J.R., Uphaus, R.A., Crespi, H.L. and Katz, J.S. (1971) **Electron nuclear double resonance of BChl free radical in vitro and in vivo** Proc. Natl. Acad. Sci. USA 68, 625-628.
- Norris, J.R., Druyan, M.E. and Katz, J.J. (1973) **Electron Nuclear Double Resonance of bacteriochlorophyll free radical in vivo and in vitro** J. Am. Chem. Soc. 95, 1680-1682.
- Oelze, J. and Golecki, J.R. (1975) **Properties of reaction centre depleted membranes of Rhodospirillum rubrum** Arch. microbiol. 102, 59-64.
- Okamura, M.Y., Feher, G. and Nelson, N. (1982) In "Photosynthesis" vol. I (Govindjee ed.), Academic Press, New York.
- Ormerod, J.G. and Gest, H. (1962) **Hydrogen photosynthesis and alternative metabolic pathways in photosynthetic bacteria** Microbiol. Rev. 26, 51-66.
- Ormerod, J.G. and Sirevag, R. (1983) **Essential aspects of carbon metabolism** In "The Phototrophic Bacteria" (Ormerod, J.G. ed) Blackwell Scientific Publications.
- Parkes Loach, P., Sprinkle, J.R. and Loach, P.A. (1988) **Reconstitution of the B873 light-harvesting complex of Rsp. rubrum from separated  $\alpha$ - and  $\beta$ -polypeptides and BChl  $a$**  Biochem. 27, 2718-2727.
- Parson, W.W. and Holten, D. (1986) **Primary electron transfer reactions in photosynthetic bacteria: energetics and kinetics of transient states** In "Photosynthesis III: Photosynthetic Membranes and Light-harvesting Systems" (Staehelin, L.A. and Arntzen, C.J. eds) Encyclopedia of Plant Physiology, vol. 19, Springer-verlag.
- Pearlstein, R.M. (1987) In "Photosynthesis" Ames, J. (ed.) Elsevier Science Publishers pp. 299-315.
- Pearlstein, R.M. and Zuber, H. (1985) **Exciton state and energy transfer in bacterial membranes. The role of pigment-protein cyclic unit structures** In "Antennas and Reaction Centres of Photosynthetic Bacteria" Michel-Beyerle (ed.) Springer-Verlag Series in Chemical Physics, 42
- Perham, R.N. (ed) (1975) "Instrumentation in Amino Acid Sequence Analysis", Academic Press.
- Pfennig, N. (1977) **Phototrophic green and purple bacteria: a comparative systematic study.** Ann. Rev. Microbiol. 31, 275-290.

- Pfennig, N. (1969) *Rhodopseudomonas acidophila* sp. n., a new species of the budding nonsulphur purple bacteria J. Bacteriol. 99, 597-602.
- Picorel, R. and Gingras, G. (1988) Preparative isolation and characterisation of the B875 complex from *Rb. sphaeroides* 2.4.1 Biochem. Cell Biol. 66, 442-448.
- Picorel, R., Belanger, G. and Gingras, G. (1983) Antenna holochrome B880 of *Rsp. rubrum* S1. Pigment, phospholipid and polypeptide composition Biochemistry 22, 2491-2494.
- Prince, R.C. and Dutton, P.L. (1978) Protonation and reducing potential of the primary electron acceptor In "The Photosynthetic Bacteria" (Clayton, R.K. and Sistrom, W.R. eds) Plenum Press, New York. pp. 439-450.
- Radcliffe, C.W., Pennoyer, J.D., Broglie, R.M. and Niederman, R.A. (1984) Associations of pigment-proteins and phospholipids into specific domains in *Rps. sphaeroides* photosynthetic membranes as determined by lithium dodecyl sulphate/polyacrylamide gel electrophoresis In "Advances in Photosynthesis Research (Sybesma, C., ed), vol. II, pp. 215-220.
- Ragan, M.A. and Chapman, D.J. (1978) "A Biochemical Phylogeny of the Protists", Academic Press, New York.
- Razi-Naqvi, K (1980) The mechanism of singlet-singlet excitation energy transfer from carotenoids to chlorophyll Photochem. Photobiol. 31, 523.
- Razjivin, A.P., Danielus, R.V., Gadonas, R.A., Borisov, A. Yu. and Pisarkus, A.S. (1978) The study of excitation transfer between light-harvesting antenna and reaction centre in chromatophores from purple bacterium *R. rubrum* by selective picosecond spectroscopy FEBS Lett. 143, 40-44.
- Reed, D.W. (1970) Isolation and composition of a photosynthetic reaction centre complex from *Rps. sphaeroides* J. Biol. Chem. 244, 4936-4941.
- Reed, D.W. and Clayton, R.K. (1968) Isolation of a reaction centre fraction from *Rhodopseudomonas sphaeroides* Biochem. Biophys. Res. Comm. 30, 471.
- Reynolds, J.A. (1982) Interactions between proteins and amphiphiles in "Lipid-protein interactions" vol 2, Wiley and Sons pp. 183-224.
- Robert, B. and Lutz, M. (1985) Structures of antenna complexes of several *Rhodospirillales* from their resonance Raman spectra Biochim. Biophys. Acta 807, 10-23.
- Robertson, D.E. and Dutton, D.L. (1988) The nature and magnitude of the charge separation reactions of ubiquinone cytochrome  $c_2$  oxidoreductase Biochim. Biophys. Acta 935, 273-291.
- Sauer, K. (1975) Primary events and the trapping of energy In "Bioenergetics of Photosynthesis" (Govindjee ed.) pp. 115-181, Academic Press, New York.

- Sauer, K. and Austin, L.A. (1978) **BChl-protein complexes from the light-harvesting antenna of photosynthetic bacteria** Biochemistry 17, 2011-2019.
- Schachman, H.K., Pardee, A.B. and Stanier, R.Y. (1952) **Studies on the macromolecular organisation of microbial cells** Arch. Biochem. Biophys. 38, 245-60
- Scherz, A. and Parson, W.W. (1984) **Oligomers of bacteriochlorophyll and bacteriopheophytin with spectroscopic properties resembling those found in photosynthetic bacteria** Biochim. Biophys. Acta 766, 653.
- Scherz, A., Rosenbach, V. and Malkin, S. (1986) **Small oligomers of bacteriochlorophylls as in vitro models for the primary electron donors and light-harvesting pigments in purple photosynthetic bacteria** In "Antennas and Reaction Centres of Photosynthetic Bacteria", Michel-Beyerle, M.E. (ed.), Springer-Verlag, pp. 314-323.
- Schmidt, K. (1965) **Carotenoids of Thiorhodaceae IV the carotenoid composition of 25 pure isolates** Arch. microbiol. 52, 132.
- Schmidt, K. (1971) **Carotenoids of purple nonsulphur bacteria. Composition and biosynthesis of carotenoids of some strains of Rhodopseudomonas acidophila, Rhodospirillum tenue and Rhodocyclus purpureus** Arch. microbiol. 77, 231.
- Schmidt, K. (1978) **Biosynthesis of carotenoids** in "Bacterial Photosynthesis" (Clayton, R.K. and Sistrom, W.R., eds) Plenum Press, New York.
- Schmidt, K., Pfennig, N. and Liaaen-Jensen, S. (1965) **Carotenoids of the Thiorhodaceae IV. The carotenoid compositions of 25 pure isolates** Arch. microbiol. 52, 132.
- Schmidt, K., Francis, G.W. and Liaaen Jensen, S (1971) **Bacterial carotenoids XXXVI C<sub>43</sub>-carotenoid artefacts of cross-conjugated carotenals and new carotenoid glucosides from Athiorhodaceae** Acta. Chem. Scand. 25, 2476-2486.
- Schoch, S., Lempert, U., Wieschoff, H. and Scheer, H. (1978) **High performance liquid chromatography of tetrapyrrole pigments** J. Chromatography 157, 357-364.
- Schweiter, U., Englert, G., Rigassi, N. and Vetler, W. (1969) **Physical organic methods in carotenoid research** Pure Appl. Chem. 20, 365-496.
- Scopes, R. (1982) "Protein Purification: Principles and Practice", second edition, Springer-verlag.
- Sebban, P., Jolchine G. and Moya, I. (1984) **Spectra of fluorescence lifetime and intensity of Rps. sphaeroides at room and low temperature.. Comparison between the wild-type, the C71 reaction centre-less mutant and the B800-850 pigment-protein complex** Photochem. Photobiol. 39, 247-253.
- Segal, I.H. (1976) "Biochemical Calculations", second edition, John Wiley and Sons.

- Shiozawa, J.A., Welte, W., Hodapp, N. and Drews, F. (1982) **Studies on the size and composition of the isolated light-harvesting B800-8500 pigment-protein complex of *Rps. capsulatus*** Arch. Biochim. Biophys. 213, 473-485.
- Singh, R.K., Ben-Aziz, A., Britton, G. and Goodwin, T.W. (1973) **Biosynthesis of spheroidene and hydroxyspheroidene in *Rhodospseudomonas* species. Experiments with nicotine as an inhibitor** Biochem. J. 132, 649-652.
- Snyder, L.R. and Kirkland, J.J. (1979) "Introduction to Modern Liquid Chromatography", John Wiley and Sons.
- Song, P.S., Moore, T.A. and Sun, M. (1972) in "The Chemistry of Plant Pigments" Chichester, C.O. ed. pp 33-74 Academic Press, New York.
- Sprague, S.G. and Varga, A.R. (1986) **Topography, composition and assembly of photosynthetic membranes** In "Photosynthesis III: Photosynthetic Membranes and Light-harvesting Systems" Encyclopedia of Plant Physiology, New Series vol. 19 (Staehelin, L.A. and Arntzen, C.J. eds.).
- Stanier, R.Y., Adelberg, E.A. and Ingraham, J.L. (1976) In "General Microbiology", 4th edition, Macmillan Press, London.
- Stark, W., Kuhlbrandt, W., Wildhaber, H., Wehrli, E. and Muhlethaler, K. (1984) **The structure of the photoreceptor unit of *Rps. viridis*** EMBO J. 3, 777-783.
- Stryer, L. and Haughland, R.P. (1967) **Energy transfer: a spectroscopic ruler** Proc. Natl. Acad. Sci. USA 58, 719-726.
- Studier, F.W. (1973) **Analysis of bacteriophage T7 early RNAs and proteins on slab gels** J. Mol. Biol. 79, 237-248.
- Tadros, M.H., Suter, F., Drews, G. and Zuber, H. (1983) **The complete amino acid sequence of the large BChl-binding polypeptide from the light-harvesting complex (II) B800-850 of *Rps. capsulatus*** Eur. J. Biochem. 129, 533-536.
- Tanford, C. (1980) "The hydrophobic Effect: Formation of Micelles and Biological Membranes" 2nd ed. Wiley and Sons.
- Tanford, C. and Reynolds, J.A. (1976) **Characterization of membrane proteins in detergent solutions** Biochim. Biophys. Acta 457, 133-170.
- Theiler, R. and Zuber, H. (1984) **The light-harvesting polypeptides of *Rps. sphaeroides* R26.1** Hoppe Seyler's Z. Physiol. Chem. 365, 721-729.
- Theiler, R., Suter, F., Wiemken, V. and Zuber, H. (1984) **The light-harvesting polypeptides of *Rps. sphaeroides* R26.1** Hoppe-Seyler's Z. Physiol. Chem. 365, 703-719.
- Thornber, J.P. (1970) **Photochemical reactions of purple bacteria as revealed by studies of three spectrally different caroteno-BChl-protein complexes isolated from *Chr. vinosum* strain D** Biochemistry 9, 2688-2698.

- Thornber, J.P. (1987) **Biochemical characterisation and structure of pigment-proteins of photosynthetic organisms** in "Photosynthesis III: Photosynthetic Membranes and Light-harvesting Systems" (Staehelin, L.A. and Arntzen, C.J. eds) Encyclopedia of Plant Physiology, New Series, vol. 19, Springer-verlag.
- Thornber, J.P. , Trosper, T.L. and Strouse, C.E. (1978) **Bacterio-chlorophyll in vivo: relationship of spectral forms to specific membrane components** In "The Photosynthetic Bacteria" (Clayton, R.K. and Sistrom, W.R. eds) Plenum Press, New York.
- Thornber, J.P., Cogdell, R.J., Pierson, B.K., Seftor, R.E.B. (1983) **Pigment-protein complexes of purple photosynthetic bacteria** J. Cell Biol. 23, 159-169.
- Thornber, J.P., Cogdell, R.J., Seftor, R.E.B., Pierson, B.K. and Tobin, E.M. (1984) **Comparative biochemistry of chlorophyll-protein complexes** In "Advances in Photosynthesis Research" vol II Ciba Foundation p25 Sybesma, C. (ed.)
- Thrash, R.J., Fang H, L-B, and Leroi, G.E. (1979) **On the role of forbidden low-lying excited states of the light-harvesting carotenoids in energy transfer in photosynthesis** Photochem. Photobiol. 29, 1049-1050.
- Trüper, H.G. and Pfennig, N. (1978) **Taxonomy of the Rhodospirillales** In "The Photosynthetic Bacteria" (Clayton, R.K. and Sistrom, W.R. eds), Plenum Press, New York.
- Ueda, T., Morimoto, Y., Sato, M., Kakuno, T., Yamashita, J. and Horio, T. (1985) **Isolation, characterisation and comparison of a ubiquitous pigment-protein complex consisting of a reaction centre and light-harvesting BChl proteins present in photosynthetic bacteria** J. Biochem. 98, 1487-1498.
- Van der Rest, M. and Gingras, G. (1974) **The pigment complement of the photosynthetic reaction centre isolated from *R. rubrum*** J. Biol. Chem. 249, 6446-6453.
- van Gemerden, H. and Beeftink, H.H. (1983) **Ecology of phototrophic bacteria** In "The Phototrophic Bacteria: anaerobic life in the light" (Ormerod, J.G. ed.) Studies in Microbiology vol. 4, Blackwell Scientific Publications
- van Grondelle, R., Kramer, H.J.M. and Rijgersberg, C.P. (1982) **Energy transfer in the B800-850 complex of various mutants of *Rps. sphaeroides* and *Rps. capsulata*** Biochim. Biophys. Acta 682, 208-215.
- van Grondelle, R. (1985) **Excitation energy transfer, trapping and annihilation in photosynthetic systems** Biochim. Biophys. Acta 811, 147-195.
- Van Niel, C.B. (1947) **Studies on the pigments of the purple bacteria III. The yellow and red pigments of *Rps. sphaeroides*** Antonie van Leeuwenhoek J. Microbiol. Serol. 12, 156-166.
- Van Niel, C.B. (1967) **Education of a microbiologist: some reflections** Ann. Rev. Microbiol. 21, 1-30.

- Van Reil, M., Kleinen Hammaus, J., van de Ven, M., Verner, W. and Levine, Y.K. (1983) **Fluorescence excitation profiles of beta-carotene in solution and in lipid/water mixtures** Biochem. Biophys. Res. Comm. 113, 102.
- Von Heijne, G. (1981) **On the hydrophobic nature of signal sequences** Eur. J. Biochem. 116, 419-922.
- Vredenberg, W.W. and Ames, J. (1967) Brookhaven Symp. Biol. 19, 49-61
- Wacker, T., Gad'on, N., Becker, A., Mantele, W., Kreuz, W. Drews, G.R. and Welte, W. (1986) **Crystallisation and spectroscopic investigation with polarised light of the RC-B875 light-harvesting complexes of *Rps. palustris*** FEBS Lett. 197, 267-273.
- Wasielowski, M.R. and Kispert, L.D. (1986) **Direct measurement of the lowest excited singlet state lifetime of all-trans  $\beta$ -carotene and related carotenoids** Chem. Phys. Lett. 128, 238-243.
- Wassink, E.C., Katz, E. and Dorrestein, R. (1939) **Infra red absorption spectra of various strains of purple bacteria** Enzymologia 7, 113.
- Williams, J.C., Steiner, L.A., Feher, G. and Simon, M.I. (1983) **Primary structure of the L subunit of the reaction centre from *Rhodopseudomonas sphaeroides*** Proc. Natl. Acad. Sci. USA 81, 7303-7307.
- Woese, C.R. (1987) **Bacterial evolution** Microbiol. Rev. 51, 221-271.
- Woese, C.R., Gibson, J. and Fox, G.E. (1980) **Do genealogical patterns in purple photosynthetic bacteria reflect interspecific gene transfer?** Nature 283, 212-214.
- Yeates, T.D., Komiya, H., Rees, D.C., Allen, J.P. and Feher, G. (1987) **Structure of the reaction centre from *Rb. sphaeroides* R-26: membrane protein interactions** Proc. Natl. Acad. Sci. USA 84, 6438-6442.
- Youvan, D. and Ismail, S. (1985) **Light-harvesting II (B800-850 complex) structural genes from *Rhodopseudomonas sphaeroides*** Proc. Natl. Acad. Sci. USA 82, 58-62.
- Youvan, D., Bylina, E.J., Alberti, M. Begusch, H. and Hearst, J.E. (1984) **Nucleotide and deduced polypeptide sequences of the photosynthetic reaction centre B870 antenna and flanking polypeptides from *Rps. capsulatus*** Cell 37, 949-957.
- Zankel, K.L. (1978) **Energy transfer between antenna components and reaction centres** In "The Photosynthetic Bacteria" (Clayton, R.K. and Sistrom, W.R. eds) Plenum Press, New York.
- Zuber, H. (1985) **Yearly review: structure and function of light-harvesting complexes and their polypeptides** Photochem. Photobiol. 42, 821-844.
- Zuber, H. (1986) **Structure of light-harvesting antenna complexes of photosynthetic bacteria, cyanobacteria and red algae** Trends Biochem. Sci. 11, 414-419.

Zuber, H. (1987) **Structural principles of the antenna system of photosynthetic organisms** In "Progress in Photosynthesis Research" (Biggins, J. ed.) vol. II, Martinus Nijhoff Publishers, Dordrecht.

Zuber, H., Sidler, W., Fuglistaller, P., Brunisholz, R.A. and Theiler, R. (1985) **Structural studies on the light-harvesting polypeptides from cyanobacteria and bacteria** In, "Molecular Biology of the Photosynthetic Apparatus", Cold Spring Harbor Laboratories.

